The Development of Zinc Electrodes for Alkaline Rechargeable Batteries

Jinrong Michael Liu

2002

The Development of Zinc Electrodes for Alkaline Rechargeable Batteries

A thesis presented in partial fulfilment of the requirements
for the degree of Doctor of Philosophy
in Chemistry
At Massey University, Palmerston North
New Zealand

Jinrong Michael Liu

June 2002

Abstract

The cycle life of nickel zinc cells is determined by a number of parameters, several of which have been investigated. The results of these investigations have led to the development of experimental nickel zinc (Ni-Zn) cells with cycle life in excess of 1200 cycles at high rates of charge/discharge. These are superior to any other nickel zinc cells reported in the open literature.

It was found that gross zinc active mass diffusion was the most significant problem in Ni-Zn cells and is associated with zinc electrode shape change. The ready access of the electrolyte to the electrode assembly was the main cause for gross diffusion. It was proposed that the access of the electrolyte to the electrode assembly should be restricted.

It was identified that the reduction of zincate was a diffusion-controlled process and led to the growth of zinc dendrites. The addition of quaternary ammonium hydroxide to the electrolyte can efficiently inhibit the reduction of zincate. Among the quaternary ammonium hydroxides, tetrabutylammonium hydroxide saturated in the electrolyte was found to be the best for retarding the reduction of zincate.

Stainless steel wire was successfully adapted to replace the traditional Hg/HgO reference electrode as a simple pseudo-reference electrode for indicating the potentials of both nickel and zinc electrodes in a cell during cycling.

Sponge nickel is an important material used as the current collector to replace the conventional sintered nickel as the current collector used for Ni-Cd, Ni-MH and Ni-Zn cells. Using polymer sponge as a template, sponge nickel was successfully prepared in the laboratory with optimized procedures.

The cell structure was optimized with restriction of electrolyte to the electrode assembly. The electrode assembly was wound with nylon thread and then tightly enclosed in a plastic bag open at the top edges with minimal volume for the electrolyte. The bulk electrolyte was

separated from the electrode assembly. The discharge/charge efficiency of a cell with this optimized structure was over 70% for 500 cycles (Cell #5.4).

Addition of zinc stearate or calcium stearate to the zinc active mass to make it hydrophobic was a further effort to restrict the access and diffusion of the electrolyte to the zinc active mass. With the optimized cell structure, 18.9% (w/w) zinc stearate resulted in much prolonged cycle life (Cell #6.3). Over the first 400 cycles the capacity for Cell #6.3 only declined from 94% to 91%. The efficiency remained over 80% for 620 cycles.

Further modifications were made by using 18.9% (w/w) calcium stearate in place of zinc stearate, adding solid KOH into the zinc active mass and electroplating the brass mesh current collector with zinc prior to pasting further prolonged the cycle life of the cells (duplicate cells, Cells #6.4 and #6.5). Cell #6.4 showed a high, and even slightly increasing discharge capacity from 92% to 94% over the first 560 cycles. The discharge/charge efficiency remained over 84.9% for 720 cycles. During these 720 cycles there were 4 periods of overcharging of the cell due to equipment failure, but no long lasting effects were discernible. The result of Cell #6.5 is similar in nature to those for Cell #6.4. The discharge/charge efficiency of Cell #6.4 remained over 70.7 % for 1221 cycles while the discharge/charge efficiency of Cell #6.5 remained over 70.22 % for 1112 cycles. Cells #6.4 and #6.5 exhibit the most prolonged cycle life performance of any other nickel zinc battery described in the open literature.

This new capability was successfully scaled-up by the use of two units in a cell, each identical to Cells #6.4 and #6.5 except for their size and capacity. One such cell (Cell #7.4) had a cycle life approaching 550 cycles with efficiency over 70%, indicating the potential for further scale-up.

Some of these findings are embodied in NZ Provisional Patent Application (No: 510554). This application has progressed to an international PCT (Patent Cooperation Treaty) application.

ACKNOWLEDGEMENTS

It would be a long story to mention and acknowledge all of those who have contributed to the completion of this study.

First of all, I shall always be grateful to my supervisor, Dr Simon B. Hall, for his guidance, encouragement, support and understanding.

I would like to acknowledge those without whom the study would not have been commenced and completed.

To Assoc. Prof. Grapham Wright, Department of Chemistry, Auckland University, thanks for his interview to give me the knowledge on how to choose an appropriate supervisor for my study.

To Dr. John Harrison, Institute of Fundamental Science, Massey University, Albany Campus, who gave me the information and introduced Dr. Simon B. Hall while I was in Auckland.

To those in the Electronic Workshop, Institute of Fundamental Science, Massey University, who helped to construct the battery cycling systems.

To Dr. Simon Brown, for his permission to adapt his software for the battery cycling.

To Assoc. Prof. David Officer, for his generosity and financial support.

To Allen Charkey, the vice president of Evecel, who recognized and appreciated the result of this study and invited myself and Dr Simon Hall to visit Evercel.

To Rod McKenzie, who helped to analyze the concentration of zincate in the alkaline electrolyte.

To Colin Johnson, who recognized and appreciated the value of this study.

To Massey Scholarship Committee, who provided me with a doctoral scholarship for this study.

To Liu Yong Qiu, who helped with the photo process.

To Giovanna, who helped to check and correct the thesis.

I should acknowledge many others including Prof. Andrew Brodie, Assoc. Prof. Roger Reeves, Assoc. Prof. Len Blackwell, Assoc. Prof. David Harding, Assoc. Prof. Geoff Jameson and our electrochemisty group members, Emad, Justin, Anthony, Amy and Chen Houguang.

I am also indebted to my family: my wife Millie, my daughter Jennifer, my little boy Jason and my father in law, Yu Qinjang.

Table of Contents

List of Figures

List of Symbols

Symbol	Description	Unit
E^{o}	standard electrode potential	V
E_{cell}	cell voltage	V
$E_{cell,eoc}$	cell voltage at the end of charge	V
E_{neg}	negative electrode potential	V
E_{Ni}	nickel electrode potential	V
$E_{Ni,\ eoc}$	nickel electrode potential at the end of charge	V
$E_{Ni,\ eq}$	nickel electrode potential at equilibrium	V
E_{oc}	cell voltage at open circuit	V
E_{pos}	positive electrode potential	V
E_{Zn}	zinc electrode potential	V
$E_{Zn,\ eoc}$	zinc electrode potential at the end of charge	V
$E_{Zn,\ eq}$	zinc electrode potential at equilibrium	V
η_{Zn}	overpotential of the zinc electrode	V
η_{Ni}	overpotential of the nickel electrode	V

List of Abbreviations

A	current, ampere
AAS	Atomic Absorption Spectroscopy
Ag-Zn	silver zinc cells
3Cs	computers, camcorders, cell phones
CMC	carboxymethylcellulose
DOD	Depth of Discharge
EV	electric vehicle
HEV	hybrid electric vehicle
LSV	Linear Sweeping Voltammetry
MF	maintenance free
Ni-Zn	nickel zinc cells
Ni-MH	nickel metal hydride cells
Ni-Cd	nickel cadmium cells
Ni-Fe	nickel iron cells
M	mol/L
OCV	open circuit voltage
PEO	Polyethylene oxide
PTFE	polytetrafluoroethylene
RAM	rechargeable alkaline manganese
rpm	round per minute
SHE	standard hydrogen electrode
SLI	starting, lighting and ignition
SPE	solid polymer electrolyte
TEAH	tertraethylammonium hydroxide
TBAH	tetrabutylammonium hydroxide
TMAH	tetramethylammonium hydroxide
VRLA	valve regulated lead-acid batteries
Zn-air	zinc air cells
Zn-Br	zinc bromine cells

$Zn\text{-}MnO_2$	zinc manganese dioxide cells

Chapter one Introduction

1.1 Introduction

Batteries are electrochemical energy storage devices, which enable the stored chemical energy to be liberated and converted directly into electrical energy through electrochemical reactions. The first description of an electrochemical battery was given by Alessandro Volta in 1800. However, it was not until the 1830s with the introduction of telegraphic systems that reliable commercial batteries were developed [1].

Batteries, which are widely used in our daily life, can be divided into two major classes: primary and secondary batteries [2]. Primary batteries (which mainly comprise those known as dry batteries), because of the non-reversible electrochemical processes involved, cannot be recharged after the stored energy has been used up. Secondary or rechargeable batteries, which are widely used in automobiles (lead-acid battery) and cell phones (nickel-cadmium, nickel-metal hydride and lithium ion batteries), are rechargeable due to the reversible electrochemical processes in the batteries. There are two fundamental functions that all batteries fulfill.

i) Portable electric power sources

These range from small button cells used in electric watches or calculators to the widely used lead-acid batteries used for starting, lighting and ignition (SLI) in cars and other vehicles with internal combustion engines. In the past 25 years, advance in microelectronics technology has brought about a revolution in the electronics industry. Electronics-based consumer products, such as portable computers, camcorders, cell phones (the '3Cs') and other 'cordless' power tools, are now inexpensive and widely used in daily life [1]. Such electronic consumer products demand the evolution of portable power sources that can offer a high energy density and superior charge/discharge characteristics compared with those of traditional primary and secondary or rechargeable batteries. For example, a cell phone designed to fit in a shirt pocket requires a smaller suitably-designed battery pack but with no less energy capacity. Primary lithium batteries and secondary nickel-metal hydride (Ni-MH) and lithium ion batteries have been developed to meet such demand. Ni-MH

batteries are now widely available for many portable consumer products. Cell phone users have benefited from the recently developed rechargeable lithium ion batteries, which have made cell phones even smaller. Rechargeable alkaline zinc cells, such as nickel-zinc (Ni-Zn), zinc-manganese dioxide (Zn-MnO_2) batteries are under commercialization [1].

ii) Energy storage systems

Based on the ability of battery systems to store electrical energy supplied by external sources, batteries play an important role in energy storage systems and this is likely to increase for a variety of applications. These include: standby power systems for computer systems; orbiting satellites are equipped with batteries (typically nickel cadmium batteries) to store the electricity generated by solar cells, ensuring continuous power supplies to the apparatus when not in sunlight [1] and stand-alone wind turbine or solar cell systems usually incorporate battery energy storage systems to maintain a continuous power supply to the houses equipped with these renewable power systems [3].

The progressive exhaustion of oil supplies and concerns relating to environmental pollution in urban areas suggest that battery-powered electric vehicles might replace vehicles driven by internal combustion engines. Since batteries for electric vehicles must be transported as part of the vehicle load, they require high power and energy densities in addition to high efficiency and long cycle life. Rechargeable Ni-Zn batteries, may potentially fulfill some of these requirements with inexpensive and nontoxic materials, and are considered to be the most promising short-term solution for electric vehicle (EV) propulsion [1].

Ni-Zn batteries have been the focus of considerable research, since the secondary Ni-Cd, Ni-MH and Ni-Zn batteries utilize the same positive Ni electrode and alkaline electrolyte, while the rechargeable alkaline zinc batteries such as Zn-MnO_2, Ag-Zn, Zn-air and Ni-Zn batteries employ similar negative zinc electrodes and alkaline electrolytes. Furthermore, the components for a nickel zinc battery appear to be relative inexpensive and environmentally friendly with respect to production, utilization and eventual disposal. All secondary alkaline batteries with zinc electrodes, however, suffer from the same problems, zinc dendrite formation and zinc electrode shape change both of which cause poor cycle life. It is the

solution of these problems that has formed the focus of the present study.

Dendrite growth occurs when redeposition of zinc metal during recharging and overcharging of the zinc electrode take place at a collection of points on the electrode, rather than as an even distribution across the entire surface. The source of zinc material to produce the dendrites is not the precipitated zinc hydroxide, but the dissolved zinc in the electrolyte solution. Narrow needles, or dendrites of zinc metal grow from the electrode surface and eventually form an internal electrical short to the nickel electrode causing the battery to fail.

In addition to the zinc dendrites, the phenomenon of zinc electrode shape change also takes place. Shape change is a phenomenon whereby zinc hydroxide, formed during discharge, is partially dissolved in the electrolyte as zincate and redeposited during recharge in a location remote from where it originated. The zinc is lost preferentially from the edges of the zinc electrode during discharge, followed by redeposition in a more compact form at the electrode center during charging. This results in a gradual depletion of the active surface area of the electrode.

Prior to embarking on a detailed discussion of earlier work on nickel zinc batteries it is useful to provide a brief overview of other battery systems relevant to nickel zinc batteries, since appreciation of these fundamentals will assist description of the present work.

The following terms are widely used in battery technology and are used to assess the performance of primary or secondary batteries [2]:

i) *Energy Density* also known as *Specific Energy* is the ratio of the energy available from a cell or battery to its volume (Wh/L) or on a weight basis (Wh/kg). The energy density is related to the discharge rate. The higher the discharge rate, the lower the energy density.

ii) *Charge Rate* is the current applied to a secondary cell or battery to restore its capacity.

iii) *Discharge Rate* is usually expressed in amperes, at which electrical current is taken from the cell or battery.

iv) *Capacity* is the value of the output capability of a battery, expressed in Ah (Ampere hour). 1Ah = 3600 (coulombs).

v) *C Rate* is the discharge or charge current in amperes, expressed as a multiple of the rated capacity in ampere-hours, Ah.

$$I = M \times C_n \tag{1.1}$$

Where I = current, A

C = numerical value of rated capacity of a cell or battery (Ah).

n = C rate at which cell or battery was rated.

M = multiple or fraction of C (1/h)

For example, a 0.05C or C/20 discharge current for a battery rated at 5 Ah at the 0.2C or C/5 rate is 250 mA.

$I = M \times C_{0.2} = (0.05) \times (5) = 0.250$ A

vi) *Power Density,* also known as *Specific Power,* is the ratio of the power (in Watts, W) available from a battery to its weight (W/kg) or volume (W/L).

vii) *Depth of Discharge (DOD)* is the ratio of the quantity of electricity (usually in ampere-hours) removed from a cell or battery on discharge to its rated capacity.

viii) *Cycle Life* in a secondary storage battery, the number of cycles the battery may experience before its capacity falls to a point considered a failure.

ix) *Failure*, the condition in which a battery is unable to perform satisfactorily.

1.2 Primary batteries incorporating zinc electrodes

In 1866, the telegraphic engineer Georges-Lionel Leclanché proposed a very important battery system consisting of a zinc anode, a manganese dioxide cathode and an electrolyte of ammonium chloride and zinc chloride dissolved in water [4]. The Leclanché cell, also termed as the zinc-carbon cell, is still the most widely used of all primary batteries because

of its low cost, reliable performance and ready availability. Despite many advances and improvement to the Leclanché cell, the electrochemical system of the modern primary cell is fundamentally the same as that proposed by Leclanché. The cell forms the technical basis of the modern dry-cell industry. Zinc-carbon cells can be divided into two cell systems, classical Leclanché and zinc chloride cells.

1.2.1 Classical Leclanché cells

The important feature of the traditional Leclanché cell is that the electrolyte is coupled with the separator, which is associated with the cause for its long-standing problems. Figure 1.1 shows a diagram of this cell [2]. The electrolyte is a solution of ammonium chloride and zinc chloride. Flour-starch paste is usually employed as the separator. The cell may be written as

$$Zn\ (s)\ |\ ZnCl_2\ (aq),\ NH_4Cl\ (aq)\ |\ MnO_2\ (s),\ C\ (s) \tag{1.2}$$

The open circuit voltage (OCV) is in the range 1.55-1.74 V. During discharge zinc as the negative electrode is oxidized

$$Zn(s) \longrightarrow Zn^{2+}(aq) + 2e^- \tag{1.3}$$

and MnO_2 at the positive electrode is reduced

$$2MnO_2(s) + 2H_2O(aq) + 2e^- \longrightarrow 2MnO.OH(s) + 2OH^-(aq) \tag{1.4}$$

The long-standing problem with Leclanché dry cells is their propensity to leak after heavy or deep discharge, which arises from localized pitting corrosion of the zinc anode container. In order to inhibit this corrosion, zinc alloy anode container containing cadmium and lead is employed, coupled with the addition of corrosion inhibitors such as mercurous chloride in the flour-starch paste [2]. Cadmium, lead and mercury are toxic materials, but are effective

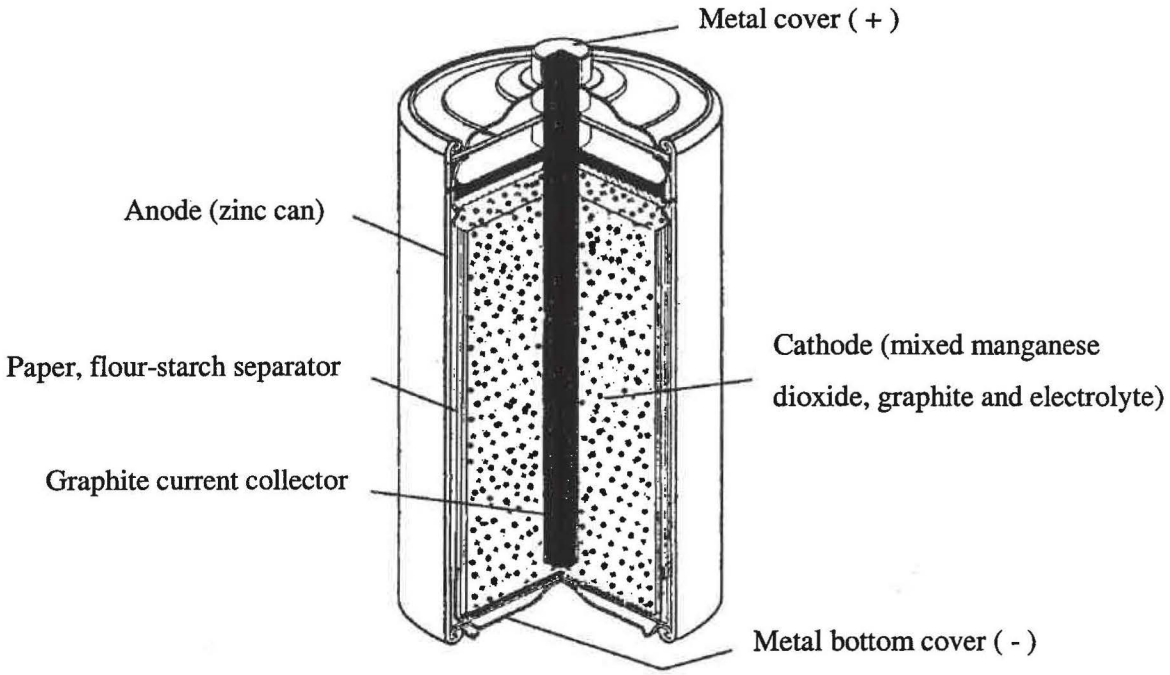

Fig. 1.1 Cross sectional diagram of a cylindrical Lechlanché cell with paste separator (redrawn from ref. [2]).

as corrosion inhibitors for metallic zinc. The inclusion of these materials has also been used in nickel zinc cells to retard the corrosion and suppress hydrogen evolution at the zinc electrode as will be discussed in Section 1.4. Employing an alloy anode container with the addition of corrosion inhibitors reduces the leakage to some degree, but is unable to completely prevent leakage.

The components of the electrolyte and the separator comprising of flour-starch paste were also important factors contributing to the leakage. The flour-starch paste separator contributed to the leakage by storage of a relatively large amount of aqueous electrolyte in the cell. The ammonium chloride in the electrolyte enhances the dissolution of the zinc discharge product [1], and hence accelerates the corrosion of the zinc container.

$$Zn^{2+}(aq) + 2OH^{-}(aq) + 2NH_4^{+}(aq) \longrightarrow Zn(NH_3)_2^{2+}(aq) + 2H_2O(aq) \qquad (1.5)$$

1.2.2 Zinc chloride cells

A major advance in Leclanché cells was the introduction of zinc chloride cells in which the ammonium chloride was completely replaced by zinc chloride and paper separators were employed to replace the flour starch paste separator. As a consequence, the leakage is no longer such a significant problem for zinc chloride cells.

Figure 1.2 shows a diagram of a commercial zinc chloride cell [2].
The cell is described by

$$Zn(s) \mid ZnCl_2(aq) \mid MnO_2(s), C(s) \qquad (1.6)$$

During discharge, zinc as the cell container is oxidized identically to reaction (1.3) and MnO_2 in the positive electrode is reduced similarly to reaction (1.4). In the absence of ammonium chloride in the electrolyte, zinc discharge product Zn^{2+} undergoes a series of reactions with formation of insoluble products:

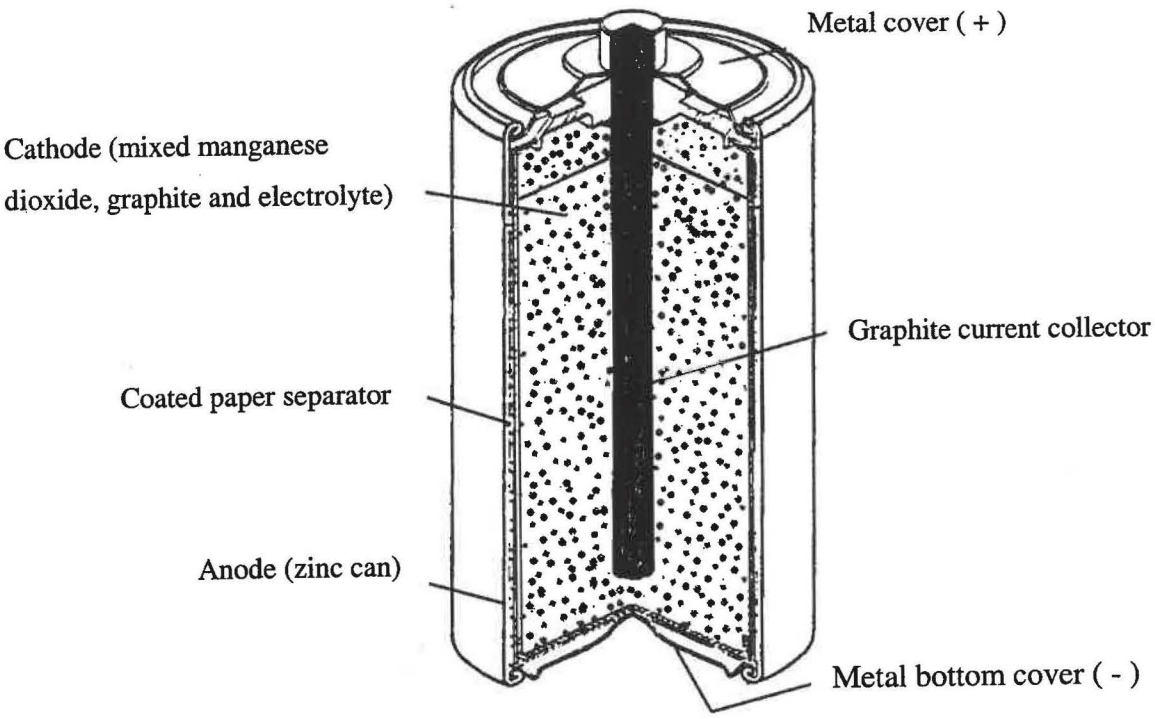

Fig. 1.2 Cross sectional diagram of a cylindrical zinc chloride cell with a paper separator (redrawn from ref. [2]).

$$Zn^{2+}(aq) + 2H_2O(aq) \longrightarrow Zn(OH)_2(s) + 2H^+(aq) \quad (1.7)$$

$$Zn^{2+}(aq) + 2OH^-(aq) \longrightarrow Zn(OH)_2(s) \quad (1.8)$$

$$H^+(aq) + OH^-(aq) \longrightarrow H_2O(aq) \quad (1.9)$$

where $OH^-(aq)$ arises from reaction (1.4).
Following this, hydration of zinc hydroxide takes place.

$$Zn(OH)_2(s) + nH_2O(aq) \longrightarrow Zn(OH)_2.nH_2O(s) \quad (1.10)$$

Because of the reactions (1.4), (1.7), (1.8) and (1.10) water is consumed with a tendency for the cell to dry out during discharge. Consequently, zinc chloride cells have a much greater resistance to electrolyte leakage. The resulting cells have a much wider range of operating temperature and a better service capacity at high current drain, at low temperatures and on continuous discharge. Because of the superior performance of zinc chloride cells, there is an increasing tendency to phase out the classical Leclanché formulation. The best zinc chloride cells, typically referred to as "extra heavy duty", have at least twice the energy density of even the best Leclanché cells [1].

1.2.3 Alkaline manganese cells

The alkaline manganese cell is the most important advance over the classical Leclanché and zinc chloride cells and meets the growing need for high-rate sources of electrical energy. The first alkaline manganese cells became available in 1960 [4]. In the alkaline manganese cell, the electrolyte is a concentrated solution of potassium hydroxide (about 30% w/w) with varying amounts of zincate, $Zn(OH)_4^{2-}$, afforded by adding ZnO that dissolves in the alkaline electrolyte through the reactions given below:

$$ZnO(s) + H_2O(aq) \longrightarrow Zn(OH)_2(s) \quad (1.11)$$

$$Zn(OH)_2(s) + 2OH^-(aq) \longrightarrow Zn(OH)_4^{2-}(aq) \quad (1.12)$$

Figure 1.3 shows a diagram of a cylindrical alkaline manganese cell [1]. The cell arrangement differs from that of the Leclanché and zinc chloride cells as shown in Figs. 1.1 and 1.2 respectively. This is especially the case for the anode, which consists of a cylinder of powdered zinc set in a gel electrolyte. Starch or cellulosic derivatives, polyacrylates, or ethylene maleic anhydride copolymers are used as gelling agents [2]. The median particle size of the zinc powder ranges from 150 to 250 μm [1].

The alkaline manganese cell has a much superior performance to either classical Leclanché or zinc chloride cells, especially at high rate. This is predominantly due to the larger surface area anode and the high conductivity of the alkaline electrolyte in comparison with those in the classical Leclanché and zinc chloride cells.

The cell may be written as

$$Zn(s)|\ KOH(aq)\ |\ MnO_2(s), C(s) \quad (1.13)$$

The open circuit voltage (OCV) is about 1.55V at room temperature. The overall cell reaction may be written as

$$Zn(s) + 2MnO_2(s) + 2H_2O(l) \longrightarrow 2MnO{\cdot}OH(s) + Zn(OH)_2(s) \quad (1.14)$$

During discharge, zinc is oxidized

$$Zn(s) + 2OH^-(aq) \longrightarrow Zn(OH)_2(s) + 2e^- \quad (1.15)$$

The discharge product $Zn(OH)_2(s)$ partially dissolves in the alkaline electrolyte to form zincate.

$$Zn(OH)_2(s) + 2OH^-(aq) \longrightarrow Zn(OH)_4^{2-}(aq) \quad (1.16)$$

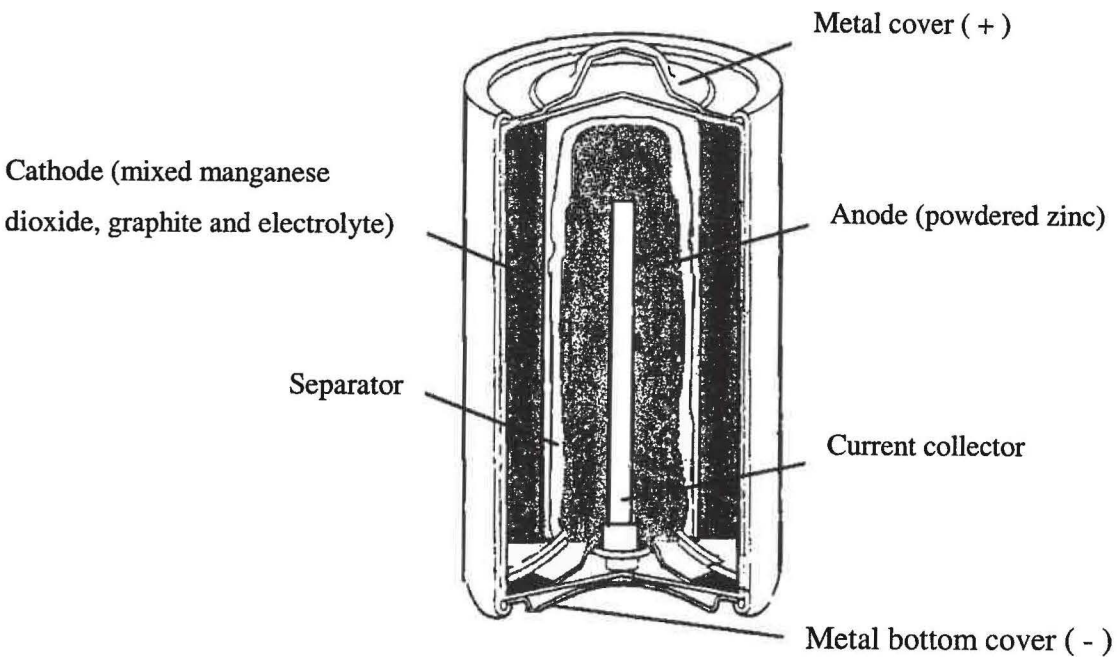

Fig. 1.3 Cross sectional diagram of a cylindrical alkaline manganese primary cell (redrawn from ref. [1]).

The alkaline manganese cell is relevant to the rechargeable Ni-Zn cells since the alkaline electrolyte is similar to that used in rechargeable nickel zinc cells and similar discharge reactions take place at the zinc electrode as will be discussed in Section 1.4.

The most important feature of the alkaline manganese system is that it forms the basis of the rechargeable Zn-MnO_2 battery system, which has the similar cell construction and is available as commercial product produced by Union Carbide and Rayovac [4].

The classical primary batteries based on zinc and manganese dioxide are now more than a century old but are still by far the most predominant primary cells with the largest production [1]. The strong market position of these cells is due to a combination of factors including low cost of materials and ease of manufacture, together with reliable performance characteristics, which are suitable for a wide range of practical applications.

1.3 Secondary or rechargeable batteries

1.3.1 Lead-acid batteries

The history of lead-acid cell commenced in 1860 with the construction of the first practical rechargeable cell by the French physicist, Gaston Planté [5]. The original cell consisted of two lead foils, separated by a linen cloth soaked in sulfuric acid. This system forms the basis of the most widely used secondary battery at the present time. About three hundred million lead-acid batteries are manufactured every year, ranging in size from 2 Wh cells to 100 Wh SLI batteries and to 4 - 100 MWh stationary load-leveling battery modules [1].

The lead-acid cell consists of a negative electrode of porous lead and a positive electrode of lead dioxide PbO_2, separated by a porous polymer separator and immersed in an aqueous solution of sulfuric acid (4.65 mol/L). The cell can be written as

$$Pb(s) \mid PbSO_4(s) \mid H_2SO_4(aq) \mid PbSO_4(s) \mid PbO_2(s) \mid Pb(s) \qquad (1.17)$$

The OCV is about 2.15 V at 25°C. The overall electrochemical process can be represented by the equation

$$Pb(s) + PbO_2(s) + 2H_2SO_4(aq) \rightleftharpoons 2PbSO_4(s) + 2H_2O(aq) \quad (1.18)$$

The lead acid battery is the most widely used of the rechargeable batteries because of its maturity and high performance over cost ratio, even though it has innate disadvantages. These include a low energy density by weight or by volume, poor low-temperature characteristics and the use of toxic electrode materials. Furthermore, deep discharge or full discharge may damage the battery. The lead acid battery differs from the nickel zinc battery in electrodes and electrolytes and the advances in lead acid battery technology may not assist solving the problems with nickel zinc batteries. The fields where lead acid batteries are utilized, however, may help identify where nickel zinc batteries have the potential to replace lead acid batteries, provided that the cycle life of nickel zinc batteries could be much prolonged.

Lead acid batteries are available in two versions, the shallow-cycle version and deep-cycle version. The shallow-cycle version is used for SLI in automobiles where a short burst of energy is drawn from the battery when needed. They are constructed of thin pasted plates with thin separators or retainer layers and short connector buses to minimize internal resistance. In contrast to the shallow-cycle version, the deep-cycle version is designed to be suitable for repeated full charge/discharge cycles at mild and low rates. Standby power lead acid batteries are required in many situations. Energy storage lead acid batteries are employed in many renewable energy applications to store the energy from solar cells or wind turbines [3]. Emergency power to light people to safety without panic is necessary for department stores, offices, factories, cinemas and other public places. Power stations, telephone exchanges, lighthouse and computer installations are other examples of the applications of standby power batteries. Lead acid batteries are also used in electric vehicle (EV) traction, where the batteries must be able to sustain deep discharge at effectively constant current.

In traditional lead-acid cells, the recharge reactions become less efficient as the cell approaches 85-90% state of charge, and the positive electrode begins to evolve oxygen and hydrogen gas is formed at the negative electrode, resulting in water loss. Many of the lead-acid batteries used in cars are of this type, which require the addition of water as maintenance. Distilled water is required since addition of contaminants may lead to problems. A typical example is the corrosion of lead by chloride [6].

Valve regulated lead-acid batteries (VRLA) are designed to promote the chemical recombination of the oxygen at the negative electrode to minimize water loss. The sulfuric acid is immobilized in a silica gel or absorbed in a porous glass separator with voids for oxygen transport. Oxygen gas diffuses from the positive electrode to the negative electrode and oxidizes the lead, preventing it from attaining the potential for hydrogen evolution.

Another development in lead-acid battery technology is the introduction of the "maintenance free" (MF) batteries, which are constructed of such materials as gelled electrolyte so that no substantial gas evolution occurs. Such batteries contain modified positive grid and strap alloys, incorporating calcium lead alloys to minimize hydrogen evolution.

Batteries used as standby power sources must be reliable for long life and low self-discharge. Such batteries employ Planté plates or tubular plates, or thick pasted plates formed on low antimony grids [1].

Over the past few years, a number of studies have been made of the use of lead-acid batteries for load levelling [1]. The service required is very similar to that of traction batteries except that the cycle efficiency is more important than energy density.

In recent years, the market for small portable lead-acid batteries has grown considerably [1]. Almost all of these portable batteries are of VRLA design. Both cylindrical and rectangular unit cells are made and assembled into multicell packs. Portable VRLA

batteries can operate in any orientation without acid leakage and find many applications, such as in electronic cash registers, alarm systems, emergency lighting units and minicomputers and terminals.

Despite these advances in lead-acid batteries, concerns on the toxic electrode materials from disposed batteries are growing, promoting the development of nickel zinc battery among the battery systems being developed with low toxicity and superior performance to lead acid batteries. There are reports of nickel zinc batteries being used in some fields where lead acid batteries would prevail, such as in electric scooters, fishing boats and electric vehicles [7].

1.3.2 Secondary alkaline batteries

Among the secondary alkaline batteries, which include nickel cadmium (Ni-Cd), nickel metal hydride (Ni-MH), nickel zinc (Ni-Zn), zinc silver oxide (Zn-AgO), zinc manganese dioxide (Zn-MnO_2) and nickel iron (Ni-Fe), Ni-Zn should be considered for the reasons below:

i) Any advances of zinc electrode technology in Ni-Zn cells will be applicable to Zn-AgO and Zn-MnO_2 cells;

ii) Advances in zinc electrodes could lead to replacement of cadmium electrodes in Ni-Cd batteries;

iii) Any modification or improvement in nickel electrodes for Ni-Zn batteries may be adapted in Ni-Cd, Ni-MH and Ni-Fe batteries; and

iv) Ni-Zn cells can potentially replace Ni-Cd cells that use toxic materials and Ni-MH cells that are relative expensive in a variety of applications, provided that the cycle life of Ni-Zn cells could be significantly prolonged.

The secondary alkaline battery industry has been dominated by Ni-Cd cells, other new systems including Ni-Zn, Ni-MH and the rechargeable alkaline manganese dioxide (Zn-MnO_2) cells, however, are making major inroads and may eventually displace the Ni-Cd cells, particularly if legislation enforces the removal of this system.

1.3.2.1 Ni-Cd batteries

About 1890 and in the subsequent years, Walderman Janger developed the alkaline Ni-Cd battery in Sweden [8]. Janger used potassium hydroxide as the electrolyte, nickel hydroxide as the positive active material and a mixture of cadmium and iron as the negative active material.

The fully charge cell can be written as

$$Cd(s) \mid KOH(aq) \mid NiO.OH(s) \mid Ni(s) \qquad (1.19)$$

The OCV is 1.35 V at room temperature and the overall cell reaction is typically written as

$$Cd(s) + 2NiO{\cdot}OH(s) + 2H_2O(l) \rightleftharpoons Cd(OH)_2(s) + 2Ni(OH)_2(s) \qquad (1.20)$$

The cell reactions are more complex than this due to the formation of a range of NiOOH species and a series of higher nickel oxides with differing degrees of hydration [1]. Figures 1.4 and 1.5 show two different Ni-Cd cells, prismatic and cylindrical cells [2], respectively.

It is important to note that the KOH does not participate in the main cell reaction, so that its concentration is virtually independent of the state of charge. As a consequence, neither the internal resistance nor the freezing point of the electrolyte is affected by the state of charge [8]. Depending on the construction, Ni-Cd cells have practical energy densities in the range 10-75 Wh/kg, a cycle life ranging from several hundreds for sealed cells to several thousands for vented cells.

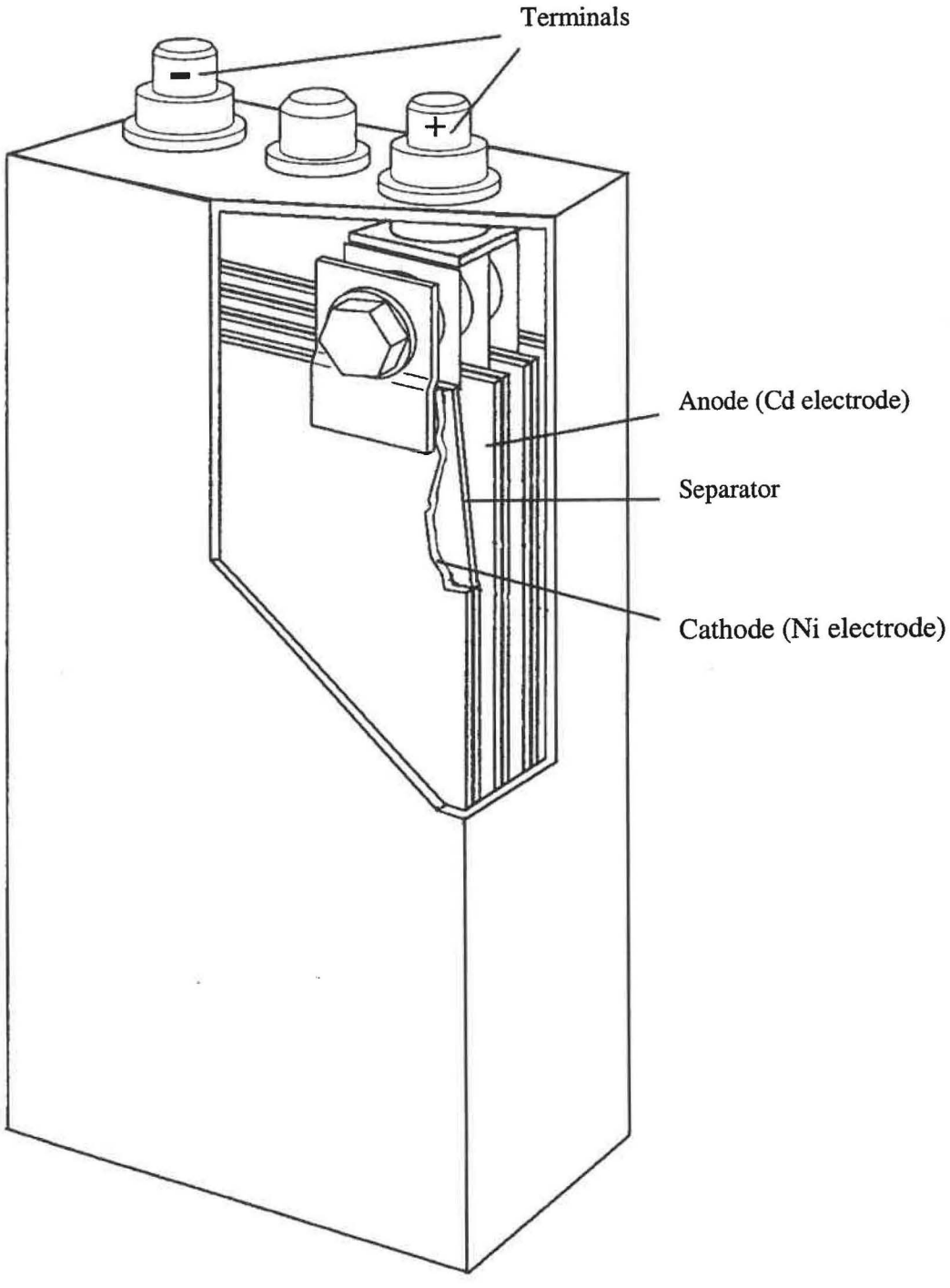

Fig. 1.4 Cross sectional diagram of a prismatic rechargeable Ni-Cd cell (redrawn from ref. [2]).

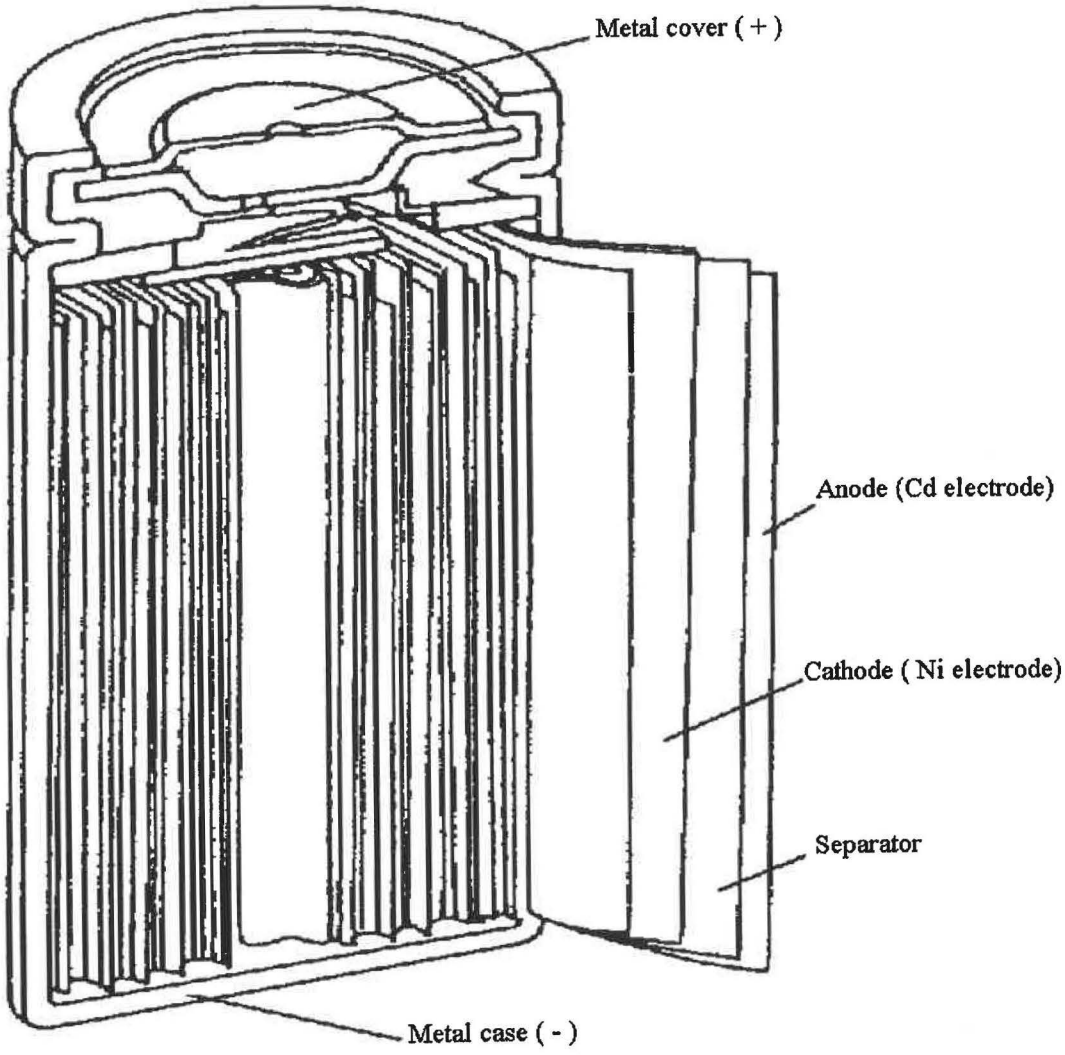

Fig. 1.5 Cross sectional diagram of a cylindrical rechargeable Ni-Cd cell (redrawn from ref. [2]).

The most important feature relevant to, but different from Ni-Zn cells is that the negative electrode active material $Cd(OH)_2$ is completely insoluble. This may account for the differences in cycle life performance between Ni-Cd cells and Ni-Zn cells. Cadmium dendrite growth and cadmium electrode shape change do not take place in Ni-Cd cells. In contrast to $Cd(OH)_2$, the negative electrode material of Ni-Zn cells as $Zn(OH)_2$ is highly soluble in alkaline electrolyte, ultimately contributing to zinc dendrites and zinc electrode shape change.

Since Ni-Cd cells have identical positive electrode and alkaline electrolyte to that used in Ni-Zn cells, Ni-Cd cells could be readily converted to Ni-Zn cells by replacing the Cd electrodes as shown in Figs. 1.4 and 1.5 with Zn electrodes provided that there was a breakthrough in zinc electrode technology. Conversely, the modification or improvement to nickel electrode technology in Ni-Cd cells can be applied to Ni-Zn cells.

The Ni-Cd system has been developed in a number of ways to produce a wide range of commercially important rechargeable systems. These include sealed maintenance-free cells with capacities of 10 mAh-15Ah, vented standby power units with capacities of over 1000 Ah and cranking batteries capable of delivery a peak current of 8000 A [1].

Ni-Cd cells are characterized by long cycle life, continuous overcharge capability, relatively high rates of discharge and charge, almost constant discharge voltage and the ability to operate at temperatures ranging from –40°C to +45°C [9]. However, the cost of cadmium is several times of that of lead and is unlikely to decrease. Cadmium is a rare element and is predominantly found in zinc ores (containing 0.2-0.3 per cent of cadmium). It is usually separated from the zinc by means of its greater volatility. The cost of Ni-Cd cell construction is more expensive than that of lead-acid cells, so that the overall capital cost of energy storage is over 10 times higher. Health risks associated with the manipulation of cadmium and environmental concerns associated with cell disposal will undoubtedly promote the development of other environmentally friendly systems, such as Ni-Zn, Ni-MH and the rechargeable $Zn\text{-}MnO_2$ systems.

1.3.2.2 Alkaline silver zinc batteries

The first silver-zinc battery system was developed in France by André in the late 1930s [1]. André overcame the problem of silver migration as $Ag(OH)_2^-$ and $Ag(OH)_3^{2-}$ to the zinc electrode by using cellophane membrane separators. The Ag-Zn system has the highest energy density of all rechargeable aqueous batteries [10]. Ag-Zn cells use the same zinc electrode and alkaline electrolyte as those used in Ni-Zn cells.

The fully charged cell may be written as

$$Zn(s) \mid KOH(aq) \mid Ag_2O(s) \mid Ag(s) \tag{1.21}$$

The cell reactions take place in two stages, first

$$2AgO(s) + Zn(s) + H_2O(aq) \rightleftharpoons Ag_2O(s) + Zn(OH)_2(s) \tag{1.22}$$

followed by

$$Ag_2O(s) + Zn(s) + H_2O(aq) \rightleftharpoons 2Ag(s) + Zn(OH)_2(s) \tag{1.23}$$

with cell potentials of 1.85 V and 1.59 V, respectively. The discharge reactions at the zinc anode are similar to those occurring in the alkaline primary Zn-MnO_2 and rechargeable Ni-Zn cells as in reactions (1.14) and (1.15).

Ag-Zn batteries are mainly used in military applications, such as aerospace, submarine and underwater weapon (particularly as used in torpedoes) applications. Yardney and Eagle Picher are two major Ag-Zn battery manufacturers in the USA. Figure 1.6 shows a Ag-Zn battery construction [4]. The main difference between the Ag-Zn and Ni-Zn systems lie in the positive electrodes. Ag-Zn cells as shown in Fig. 1.6 can be readily converted into Ni-Zn cells simply by replacing the silver electrodes with the advanced nickel electrodes used in Ni-Cd cells. This may account for Yardeny pioneering the development of Ni-Zn cells in the USA during the 1960s [4] as discussed in detail in Section 1.4. Similarly, Eagle Picher

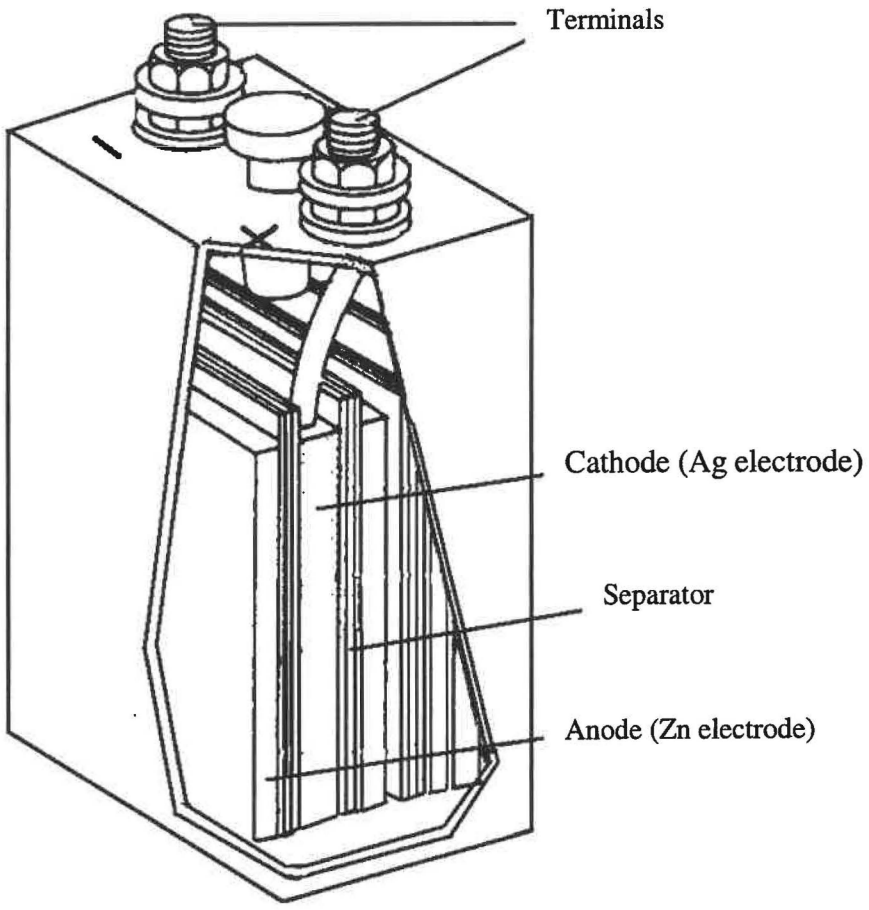

Fig. 1.6 Cross sectional diagram of a prismatic rechargeable Ag-Zn cell (redrawn from ref. [4]).

also offers a range of vented Ni-Zn batteries in the capacity range 2-35 Ah [4].

Ag-Zn and Ni-Zn batteries share the same problems arising from zinc electrodes: those of zinc dendrite growth and zinc electrode shape change. According to the information released by Eagle Picher[11], the cycle life of their Ag-Zn batteries is limited to 50-100 cycles. Consequently, it can be anticipated that any advances in zinc electrode technology in Ni-Zn cells may assist improving the cycle life performance of Ag-Zn cells.

1.3.2.3 Alkaline manganese batteries

The concept of rechargeable zinc manganese cells has been under consideration and investigation for many years. Attempts to recharge Leclanché or zinc chloride cells have been doomed to failure because of the innate irreversibility of the discharge reactions [1]. With the introduction of the alkaline manganese primary battery during the 1960s, it became feasible to produce a practical rechargeable Zn-MnO_2 system. The original design, dating from around 1975, closely adapts the design of the alkaline Zn-MnO_2 primary cell and retained its advantages of long shelf life, good current density and safety [12].

A potassium hydroxide solution of about 30% (w/w) is used as the electrolyte (similar to that used in Ni-Zn cells). The discharge reactions at the anode are similar to those occurring in the alkaline primary Zn-MnO_2 and rechargeable Ni-Zn cells as in reactions (1.15) and (1.16). The cell may be written as

$$Zn(s) \mid KOH(aq) \mid MnO_2(s), C(s) \qquad (1.24)$$

The cell reaction can be simply written as

$$Zn(s) + 2MnO_2(s) + 2H_2O(l) \rightleftharpoons Zn(OH)_2(s) + 2MnO.OH(s) \qquad (1.25)$$

The OCV is about 1.55V and the batteries are interchangeable in application with primary Zn-MnO_2 cells.

The reduction of MnO_2 in alkaline conditions is a complex process and follows a number of steps, which can be written formally as [1]:

$$MnO_2 \longrightarrow MnO_{1.5} \tag{1.26}$$

$$MnO_{1.5} \longrightarrow MnO_{1.33} \tag{1.27}$$

$$MnO_{1.33} \longrightarrow MnO \tag{1.28}$$

The last two stages are only possible at very low current drain. The discharge proceeds at the cathode by the movement of protons and electrons into the MnO_2 lattice. Provided that the reduction does not proceed below $MnO_{1.33}$, the reaction can be reversed and the cathode becomes rechargeable [2]. In practice, this means terminating the discharge at 1.1 V cell voltage.

In the late 1970s and 1980s, a major research program headed by Kirdech at the Technical University of Gratz, transformed the prospects of what have now become known as RAM cells [4]. These now have greatly improved capacity and reliable cycling behavior. Figure 1.7 is a cross sectional diagram of a RAM cell [1], which may be considered to be an inside-out construction of the alkaline primary Zn-MnO_2 cell (Fig. 1.3).

Unlike ordinary rechargeable cathodes with positive active material pasted onto a conducting current collector, the cathode in RAM cells uses electrolytically prepared manganese dioxide with 10% graphite formed into four ring-shaped pellets [1]. It may also include additives as catalysts for the recombination of hydrogen and inert powders to control porosity. The anode or negative electrode consists of zinc powder (rather than zinc active mass pasted onto a current collector) in a gelled KOH matrix (with organic inhibitors to reduce corrosion) wound on a central metallic current collector. A two or multilayer separator with a strong fibrous element in it is generally used to prevent internal short circuits by zinc dendrites formed during charge. The electrolyte is a concentrated solution

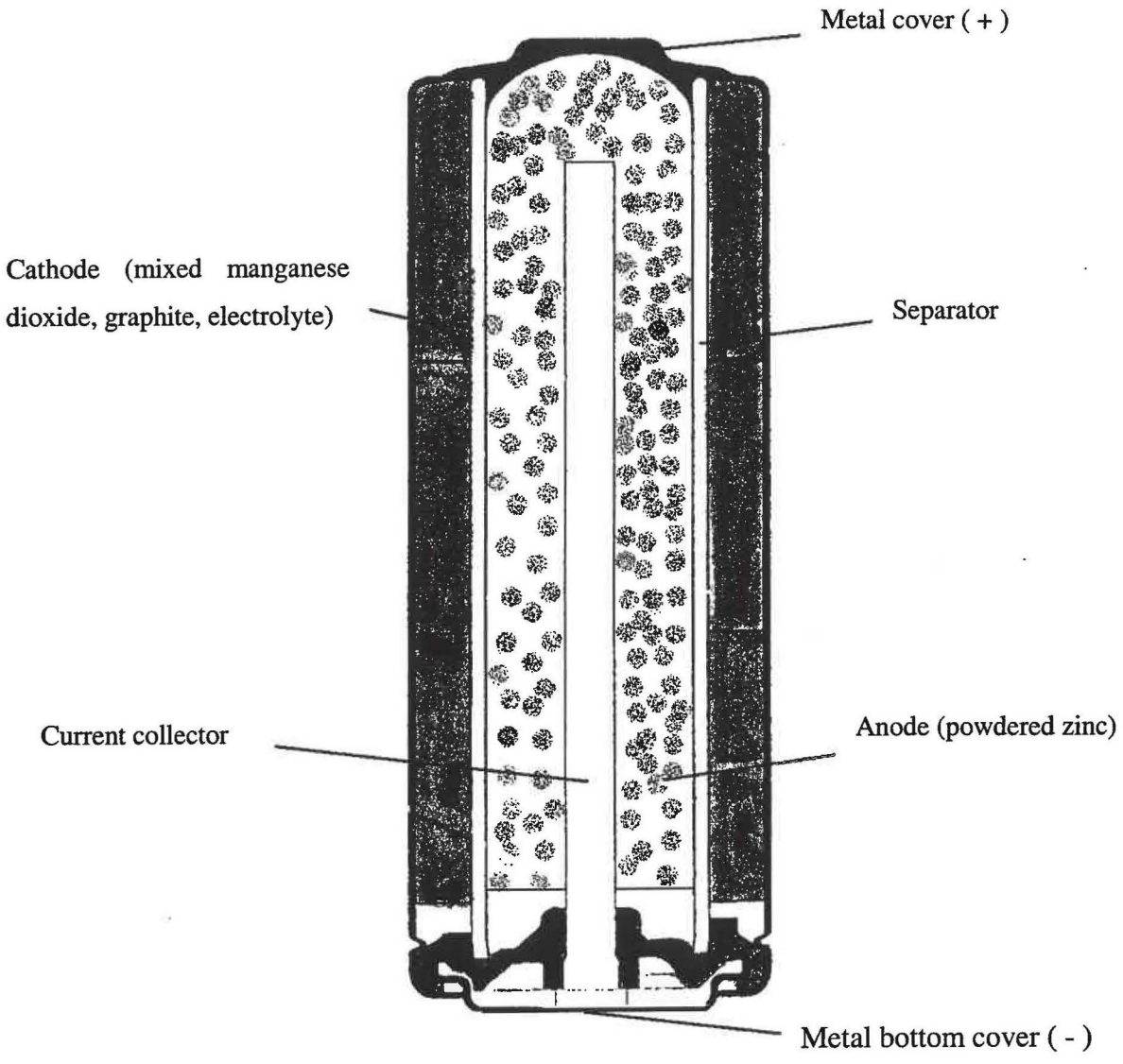

Fig. 1.7 Cross sectional diagram of a rechargeable alkaline manganese (RAM) cell (redrawn from ref. [1]).

of KOH with added ZnO to diminish the possibility of hydrogen formation during charge [1].

RAM cells are manufactured and shipped in a charged state and have an initial capacity of about 1.8 Ah at a 50 mA discharge rate. Cycling RAM cells produces a significant and progressive capacity loss, especially during deep discharge. The degree of capacity loss can be dismished if the discharge is terminated at high voltages. Under such partial discharge conditions, RAM cells can provide many hundreds of cycles with little capacity loss [1].

The high internal resistance of RAM cells limits the maximum continuous output current and also peak output current, in comparison with Ni-Cd, Ni-MH cells. The higher internal resistance is believed to be associated with the cell design as shown in Figs. 1.3 and 1.7. Provided that secondary Zn-MnO_2 cells could be assembled with structure similar to that for Ni-Cd or Ni-MH cells (Figs. 1.4 and 1.5) and with the appropriate current collectors for both electrodes, the internal resistance may well be reduced significantly.

The structure of RAM cells seems to be of unusual design for a rechargeable cell where the current collectors should be in intimate contact with the active mass. Furthermore, there should be a large surface area for both positive and negative electrodes to ensure low current density during charge, especially for cells with zinc anodes. These important features in rechargeable cells are absent in RAM cells.

Similarly to the situation in Ni-Zn cells, zinc dendrite growth during overcharge is another problem with secondary Zn-MnO_2 cells, which leads to internal short circuits. It is important to note that secondary Zn-MnO_2 cells do not suffer from the memory effect reported in Ni-Cd and Ni-MH systems and self-discharge rate is approximately 0.01% per day, which provides this system with a clear superiority over Ni-Cd and Ni-MH cells (0.05% and 5% respectively) [1].

Rayovac is the main producer of RAM cells in the USA. According to publicly released information, the cycle life of Rayovac RAM cells is about 25 cycles [13]. It can be anticipated that there remains scope for modification or improvement to rechargeable Zn-

MnO_2 cells and the advances in zinc electrode technology in Ni-Zn cells may well be applied to secondary Zn-MnO_2 systems.

1.3.2.4 Ni-MH batteries

Nickel metal hydride cells are interchangeable with Ni-Cd cells in most applications and are identical in structure as shown in Figs. 1.4 and 1.5. These employ the same positive nickel electrodes and the same electrolyte. In Ni-MH cells, hydrogen is absorbed in a metal alloy at the negative active material in place of cadmium. The replacement of cadmium not only increases the energy density, but also produces a more environmentally friendly power source without severe disposal problems [1].

The cell may be written as

$$MH(s) \mid KOH(aq) \mid NiO{\cdot}OH(s) \qquad (1.29)$$

As in the Ni-Cd cell, the electrolyte is concentrated potassium hydroxide solution (30% w/w). The OCV is in the range 1.32-1.35 V, similar to that of the Ni-Cd cells.

The overall reaction is

$$M(s) + Ni(OH)_2(s) \rightleftharpoons MH(s) + NiO.OH(s) \qquad (1.30)$$

A distinct feature of Ni-MH cells is that water is not consumed in the cell reaction and the electrolyte concentration is completely invariant during cycling. Hydrogen adsorption alloys were discovered in 1960s during research into magnetic materials [2]. These alloys can absorb several thousand times their own volume of hydrogen and usually consist of two metals, one of which absorbs hydrogen and a second of which acts as a catalyst for the dissociative absorption which precedes diffusion of hydrogen atoms into the lattice. The most important alloys are $ZrNi_2$ and $LaNi_5$ alloys. Due to the high cost of these hydrogen storage alloys, Ni-MH cells are considerably more expensive than Ni-Cd cells [1].

Self-discharge is the main problem with Ni-MH cells, with values of 4-5% per day not untypical [1]. This is caused by hydrogen reacting with the positive electrode. The hydrogen is from the desorption of hydrogen from the metal hydride. These reactions are shown below:

$$2MH(s) \longrightarrow H_2(g) + M(s) \tag{1.31}$$

$$H_2(g) + 2NiO.OH(s) \longrightarrow 2Ni(OH)_2(s) \tag{1.32}$$

The energy density of Ni-MH cells is highly dependent on discharge rate, but for comparable conditions it is 25% higher than an equivalent Ni-Cd cell [4].

In addition to the '3 Cs' (Camcorders, Cell phones and Computers), Ni-MH cells are replacing Ni-Cd cells in a wide variety of cordless electronic consumer products, communication equipment and other high rate long cycle life applications. This cell system is under active development for EV traction by Ovonic [4]. The thermal management and relatively high cost, however, are likely to be the key factors that may limit the development of Ni-MH technology for electric vehicles and standby power applications. Ni-Zn batteries, which are relatively inexpensive and environmentally friendly, have potential to replace Ni-Cd and Ni-MH systems for use in electric vehicles and standby power applications. Since identical electrolyte and positive electrodes are used in Ni-MH cells, Ni-MH cells can be readily converted to Ni-Zn cells by replacing the metal hydride electrodes with zinc electrodes provided that the cycle life of the zinc electrodes could be much prolonged.

1.4 Ni – Zn batteries

1.4.1 Introduction

The Ni-Zn battery system has been recognized for over 100 years. The first alkaline Ni-Zn cell was patented by Milhalovskii in 1899 [14]. The first serous attempt to develop Ni-Zn

batteries was in Ireland in the 1930s. The Drumm early Ni-Zn power source was used for railway traction on a regular passenger line in Ireland [15-17]. However, problems associated with the short cycle life of the zinc electrode prevented further commercial interest in this system.

In the late 1950s and early 1960s, the Ni–Zn battery was under development in the former USSR [18]. In the later 1960s, there was a resurgence of development efforts in the USA. After the oil embargo of 1973, infusion of government funds in the USA led to the major development programs on the Ni–Zn batteries for electric vehicle applications, which lasted for about ten years [18]. There was also a major development effort on vehicle batteries at The General Motors Corporation [18].

Using a combination of zinc and nickel electrodes, a battery with long cycle life and high energy density was envisioned. When subjected to cycling, the zinc electrode deteriorates and suffers from loss of capacity. The potential commercial market appears to be significant enough to perpetuate development efforts. The Ni-Zn battery is an attractive system for use in electric-powered equipment as well as electric vehicles and it has been recognized as a good choice for portable applications for the following reasons:

i) The Ni-Zn battery provides the lowest-cost, highest energy density option for alkaline rechargeable systems [19];

ii) Such system uses non-toxic and relatively inexpensive materials [2]; and

iii) The Ni-Zn battery affords good performance even under very low ambient temperatures (-20°C) [2].

Currently, development on this battery type is still in process to lengthen the cycle life of the zinc electrode.

A number of researchers have published review articles on the development of Ni-Zn

batteries.

James McBreen, who used to work at Yardney on Ag-Zn cells [20] and then joined General Motors Corporation for the battery programs on electric vehicles including Ni–Zn battery [21-24], has reviewed the research and development of Ni-Zn batteries from the 1980s to 1993 [18]. His conclusion was that the technical problems are still related to zinc electrode shape change and the disparity in charging efficiency between the positive and negative electrodes. This is particularly a challenge in large cells. The nickel-zinc combination offers considerable leeway in the choice of electrolyte, separator and charging method that may be used. The careful choice of these together with combinations of additives may yield batteries with adequate cycle life. If the technical problems can be overcome, Ni-Zn batteries could replace Ni-Cd batteries in high-power applications. However, Evercel's efforts [28-60] on development of sealed Ni-Zn batteries over the last 20 years were ignored in McBreen's review [18].

Jiri Jindra, who used to be involved in research and development of Ni-Cd batteries, shows his great interest in Ni-Zn batteries. In 1992, 1997 and 2000, he reviewed the progress of sealed Ni-Zn cells [25-27]. In his latest review covering 1996-1998 [27], Jiri Jindra concluded that no dramatic improvements stemming from research and development on cells were observed and presently, the cells of Energy Research Corporation [40] seem to be the best and most widely used.

In 1999, Energy Research Corporation, now FuelCell Energy, spun-off its Battery Divison to become Evercel. Evercel is the premier manufacturer of sealed Ni-Zn rechargeable batteries in the world. No other manufacturer of nickel-zinc batteries has announced the life and performance reported for Evercel's products [7]. In spite of Evercel being a "new" company spun off from Energy Research Corporation, its researchers have a long history of battery innovation. The Battery Divison of Energy Research Coporation had been actively pursuing advanced electrochemistry in the areas of rechargeable batteries, particularly the sealed Ni-Zn batteries, since the early 1970s when Allen Charkey joined Energy Research Corporation.

Charkey is the dominant contributor to the commercial development of Ni-Zn batteries [28-60]. His activity in development of Ni-Zn batteries stemmed from 1966 while at Yardney [61-68] that was a major company in the USA producing Ag-Zn batteries and pioneering the development of Ni-Zn batteries in USA in 1960s [4]. There, he was engaged in research and development of Ag-Zn and Ni-Zn batteries until joining Energy Research Corporation in 1972 [60-61].

As is normal in commercialization at an early stage, Evercel seems to have been hampered in its progress to full commercialization of sealed Ni-Zn batteries due to the unstable performance of their batteries. This is consistent with the latest review that no dramatic improvements have been observed in recent years [27].

The development of any new battery is time-consuming. In Ni-Zn batteries, failure is usually associated with two phenomena [69]:

i) Zn dendrite initiation and propagation caused by the deposition of $Zn(OH)_4^{2-}(aq)$ from the electrolyte during recharge, leading to cell shorting;

ii) Zn active material redistribution (shape change), causing gradual capacity loss.

The fundamental cause of Zn electrode shape change is not known with certainty, however, various mechanisms have been proposed for the explanation [69]:

i) Electrolyte flow or forced convection caused by osmotic pressure gradients in cells with ion exchange separators;

ii) Electrolyte concentration gradients caused by differences between the current density distribution during charging and that during discharging;

iii) Natural convection of the electrolyte caused by density gradient;

iv) Auto-catalytic Zn dissolution from the periphery or the outside edge of the Zn electrode;

v) Lower charge efficiency for the Zn deposition reaction at the electrode periphery caused by non-uniform OH^- ion concentration; and

vi) Oxidation of Zn by O_2 that has migrated from the nickel electrode (where it is evolved during charging) to the periphery of the Zn electrode.

It is believed that it is the high solubility of $[Zn(OH)_4]^{2-}$ ions in alkaline electrolyte, and the propensity for the formation of zincate-supersaturated electrolyte during discharging, that is strongly associated with the shape change process [69].

In attempts to solve these problems with Ni-Zn cells, research into the following remedial methods have been undertaken [25]:

i) Additives in the electrolyte to suppress the formation of zincate ions;

ii) Additives in the zinc electrode to suppress the shape change;

iii) Use of auxiliary electrodes for oxidation of H_2 in sealed cells;

iv) Additives to the zinc electrode to suppress the formation of dendrites;

v) Modification of charging regime;

vi) Development of improved separators to resist the penetration of dendrites and transport of zincates; and

vii) Adjustment of the proportion of active materials (e.g. large excesses of zinc).

The electrolyte, zinc active mass, cell structure and the separator are the factors that effect the life-time of Zn-Ni batteries. It is appropriate here to review the findings on such factors.

1.4.2 The solubility of zinc active materials

There is a dilemma for selection of electrolyte for use in Ni-Zn cells. The Ni electrode demands highly alkaline electrolyte for optimum performance, the ionic conductivity of the electrolyte improves with increasing OH^- concentration, and the solubility of zincate increases approximately with the square of OH^- concentration. Consequently, the cell performance will increase with higher KOH concentration whereas the cycle life of the cell will decrease [70].

The shape change of the zinc electrode is associated with the discharge products dissolved in the alkaline electrolyte during discharge. During discharge, metallic zinc is oxidized, forming $Zn(OH)_2$ as the main discharge product, which partially dissolves as $Zn(OH)_4^{2-}$ in the alkaline electrolyte. A possible mechanism for the dissolution of the discharge product is [71]:

$$Zn(s) + OH^-(aq) \longrightarrow Zn(OH)_{ad} \quad (1.33)$$

$$Zn(OH)^-_{ad} \longrightarrow Zn(OH)(s) + e^- \quad (1.34)$$

$$Zn(OH)(s) + OH^-(aq) \longrightarrow Zn(OH)_2(s) + e^- \quad (1.35)$$

$$Zn(OH)_2(s) + 2OH^-(aq) \longrightarrow Zn(OH)_4^{2-}(aq) \quad (1.36)$$

The amount of $Zn(OH)_2$ dissolved in the electrolyte is related to the concentration of zincate in the electrolyte. Reaction (1.36) is believed to be reversible with evidence that decreasing the OH^- concentration results in precipitation of $Zn(OH)_2$. It can be written here as

$$Zn(OH)_2(s) + 2OH^-(aq) \rightleftharpoons Zn(OH)_4^{2-}(aq) \quad (1.37)$$

The higher the concentration of zincate, the lower the amount of $Zn(OH)_2$ is dissolved in the electrolyte during discharge.

In order to suppress the dissolution of $Zn(OH)_2(s)$ from the Zn electrode during discharge associated with zinc electrode shape change, the electrolyte is usually saturated with ZnO(s) to increase the initial concentration of $Zn(OH)_4^{2-}(aq)$ in the electrolyte.

The concentration of $Zn(OH)_4^{2-}(aq)$ in electrolyte 'saturated with ZnO(s)' and the methods of dissolving this ZnO(s) in the alkaline electrolyte are usually unstated in articles found in the open literature. According to one article [72], the electrolyte super-saturated with zincate consisted of 100 mL of 31% (w/w) KOH with 'several grams of solid ZnO' dissolved in it. In another article [73], the electrolyte consisted of 8.6 mol/L KOH saturated with zincate prepared from reagent grade 80% KOH and ZnO with distilled deionized water. The concentration of zincate in the resulted solution was 5% (w/w) ZnO. In McBreen's review [18], the equilibrium solubility of ZnO is reported to be 53 g/L in 30% (w/w) KOH solution.

The dissolution of zinc active mass from the zinc electrode during cycling is usually identified as the cause for the formation of zincate-supersaturated electrolyte during discharge. In the present study, it will be established in Chapter 3 that the electrolytes reported by others were not truly saturated with respect to zincate. In this study, we will investigate the factors which influence the concentration of zincate in the electrolyte.

1.4.3 Additives to the zinc active mass

The inclusion of additives to the zinc electrode active mass is one of the approaches to eliminating the problems of zinc electrode shape change and dendrite growth.

The addition of $Ca(OH)_2$ to zinc electrodes has longed been recognized [74-76] and is covered in the patent literature [77-79]. The benefit is understood to arise from the reaction

of $Ca(OH)_2$ and zincate to form insoluble calcium zincate, maintaining much of the zinc active mass in a solid form. By the end of the 1980s, the most extensive work on the addition of $Ca(OH)_2$ to the zinc electrode was performed by General Motors [80-85]. A key finding of this work was that there is no suppression of the ZnO solubility at concentrations over 34% (w/w) KOH and the kinetics of calcium zincate formation is very slow at concentrations above 25% (w/w) KOH. The important aspects in applying this approach are the use of 20% (w/w) KOH, elimination of carbonate contamination of the electrolyte and the use of microporous separators. It is clear that the nickel electrode performance will be sacrificed with employment of these low concentration KOH electrolytes.

Cairns and co-workers in Lawrence Berkeley Laboratories performed extensive work investigating the effect of $Ca(OH)_2$ on the cycle life of Ni-Zn cells [69, 86, 87]. It was confirmed and recognized that the formation of calcium zincate was very slow in the electrolyte at high KOH concentrations (31% w/w) [69]. A prototype Ni-Zn battery with a KOH-KF electrolyte achieved >500 cycles at 100% depth-of-discharge, with >70% original capacity [86]. The anode was modified by addition of 25 mol% $Ca(OH)_2$. Despite this, the expected hexagonal Ca zincate crystals were not observed in the anodes after cycling in the alkaline-fluoride electrolyte.

Batteries with Zn anodes containing 0, 10, 25, and 40 mol% $Ca(OH)_2$ were fabricated and tested [69, 87]. The best performing cells tested were those with 25 mol % $Ca(OH)_2$ electrodes, which lost capacity at a rate of 0.13%/cycle, compared to 0.47%/cycle in Ca-free control cells. The 25 mol % $Ca(OH)_2$ electrodes retained their capacity beyond 150 deep discharge cycles, with indications that further Zn redistribution would occur very slowly. The electrodes with only 10% $Ca(OH)_2$ contained insufficient $Ca(OH)_2$ for complexation to make a marked improvement of cycle life. According to the results, the performance of the cells without $Ca(OH)_2$ in the zinc electrodes was superior to those with 40 mol% $Ca(OH)_2$. It is believed here, that these high concentrations of $Ca(OH)_2$ partially isolated the zinc active particles and caused high local current densities at the zinc electrode during charge, thereby enhancing zinc dendrite growth. 25 mol % $Ca(OH)_2$ was inadequate to convert all of the ZnO formed at the zinc electrode into calcium zincate. The effect of

$Ca(OH)_2$ seemed to be limited in 31 wt % KOH electrolyte and this may account for Cairns and co-workers changing to use of electrolytes with lower KOH concentrations [70].

Charkey performed similar work on the effect of $Ca(OH)_2$ while at Energy Research Corporation to that reported by Cairns at Lawrence Berkeley Laboratory, but with a greater focus on commercialization [33, 35, 40]. A reduced solubility zinc electrode and sealed cell design was patented by Charkey in 1995 [40]. The zinc electrode comprised a Zn active material, $Ca(OH)_2$ and a conductive matrix including a metallic oxide PbO or Bi_2O_3, CdO, Ga_2O_3, Tl_2O_3 which is more electropositive than Zn. The anode was incorporated into a secondary Ni-Zn battery using a low KOH concentration electrolyte. The Zn anode was split into assemblies separated by porous hydrophobic elements. A "roll-bonded" process for manufacturing plastic bonded nickel and zinc electrodes was also patented by Charkey [88]. The zinc electrode also contained $Ca(OH)_2$ and PbO.

Cells assembled with $Ca(OH)_2$ incorporated in the zinc electrodes demonstrated the ability to deliver over 60 Wh/kg at the one hour rate and more than 450 W/kg at a 12C rate [37]. Cycle life was improved to more than 600 cycles at 80% depth of discharge by using the patented reduced solubility zinc electrode and an improved sealed cell design [40]. More than 7000 charge/discharge cycles at 10% depth-of-discharge were also reported [40]. Large quantities of sealed prismatic cells were manufactured in Energy Research Corporation, including a 220 V battery for a hybrid electric vehicle (HEV) [89].

Ni-Zn cells with $Ca(OH)_2$ in the zinc electrode were further tested. Life cycle testing included discharge capacity and voltage performance as a function of cycling, charging characteristics as a function of cycling, the effect of overcharge on performance and cycle life, cell internal impedance as a function of cycling, and cycle life as a function of depth-of-discharge (DOD). The cells yielded more than 600 cycles at 80% DOD and 11,000 cycles at 10% DOD [34].

The development and progress in Ni-Zn batteries by Energy Research Corporation [33-60] resulted in the formation of Evercel in 1999. Since then, more work on commercial Ni-Zn

batteries has been performed [28-32]. The low temperature performance of Evercel Ni-Zn batteries has been reported [28]. These results suggest that the batteries can deliver more than 50% of their room temperature capacity at the C/3 discharge rate at –30°C. Moreover, the batteries retain their capacity during repetitive cycling. The failure mode of Evercel Ni-Zn batteries has also been identified [29]. The typical failure mechanism appears to be loss of electrolyte with a resulting increase in cell internal resistance and decreased electrical storage capacity.

Recently, it was found that zinc electrodes using calcium zincate prepared by chemical coprecipitation show better electrochemical performance than those using calcium zincate prepared by physical mixing of zinc oxide and calcium hydroxide [90].

In addition to $Ca(OH)_2$, the inclusion of polytetrafluoroethylene (PTFE) has long been recognized as an important additive to the active materials to form plastic-bonded zinc electrodes. While at Yardney in 1969, Charkey used PFTE (5% w/w) as a binder in the zinc electrode in his early Ni-Zn cells [66]. In 1974, he also used PFTE in the zinc electrodes for silver zinc cells [91]. At present, Evercel's commercial Ni-Zn batteries include PFTE as a binder in the calcium-zinc electrodes [88]. Cairns and co-workers also employed PTFE (4-6% w/w) in the zinc-calcium electrode as a binder [69, 86, 87].

A number of other additives have been employed in the zinc electrodes. Charkey found the benefit of addition of 5-30% w/w Portland cement to suppress the zinc electrode shape change and prolonged the cycle life of the Ni-Zn cells [49]. This presumably supplied a source of calcium for calcium zincate formation. A Ni-Zn battery with this anode gave good performance for 260 charge-discharge cycles before its capacity declined to 70% of its initial value. A comparison battery exhibited decline in performance after 100 cycles and failed after 150 cycles. A patent was attained covering this research [92]. Charkey also investigated the effect of $Ba(OH)_2$ and $Sr(OH)_2$ on the performance of zinc electrodes [25, 26]. $Ba(OH)_2$ or $Sr(OH)_2$ was not superior to $Ca(OH)_2$ as an additive to the zinc electrode. Other additives, such as PbO, Bi_2O_3, SnO, SnO_2, Ga_2O_3, In_2O_3 and CdO, in the zinc electrode to improve its electrical conductivity and to suppress hydrogen evolution have

also been reported to be beneficial to the performance of the zinc electrode. Charkey established the benefits of addition of CdO in the zinc active mass [53, 54]. Evercel's zinc calcium electrodes all contain these metal oxides [33, 38-39].

Cairns and co-workers added small amounts of PbO into the zinc active mass [69, 86, 87]. The addition of Bi_2O_3 [93-97] or metallic Bi powder [90] into the zinc active mass has been found beneficial to the zinc electrodes, suppressing hydrogen evolution and improving electrical conductivity of the zinc active mass.

1.4.4 Electrolytes with lower KOH concentration

Addition of $Ca(OH)_2$ into the zinc active mass alone is not sufficient to eliminate the zinc electrode shape change and zinc dendrite growth. $Ca(OH)_2$ must be employed with electrolyte of lower KOH concentration.

As mentioned previously, it is challenging to select an appropriate electrolyte concentration for use in Ni-Zn cells. The Ni electrode requires KOH electrolytes with high concentration for optimal performance. The ionic conductivity of the electrolyte and the cell power performance improves with increasing the KOH concentration. The solubility of the zinc active mass, however, increases approximately with the square of the KOH concentration. Therefore, the cell performance will improve with higher KOH concentration whilst the cell cycle life in contrast will improve with lower KOH concentration.

Ignoring the impaired performance of Ni electrode in the electrolyte with lower KOH concentrations, attempts have still been made by employing electrolytes with lower KOH concentrations. This has usually involved the use of supporting electrolytes such as K_3BO_3, K_3PO_4 and K_2CO_3.

In the early 1970s, Schneider *et al.* employed K_3BO_3 solution in the electrolyte in Ni-Zn cells [97]. This substantially reduced the solubility of zincate and consequently suppressed the formation of zinc dendrites. Eisenberg [98] recommended salts of a weak acid and a

strong base such as K_3BO_3, $NaBO_2$ or Na_3BO_3 for vented and sealed Ni-Zn cells. Later, he developed a series of mixed electrolytes for reducing zincate solubility. A typical electrolyte composition was 3 M KOH + 3 M K_3PO_4 [99]. Addition of up to 10% w/w of K_3PO_4 in the electrolyte was patented in Japan [100]. Jost *et al.* in 1969 patented an alkaline electrolyte containing carbonate for Ni-Zn cells [101]. In 1988, Cairns *et al.* in Lawrence Berkeley National Laboratory used the following two solutions in their cells [102].

i) 2.5M KOH + 2.5M K_2CO_3 + 0.5M LiOH

ii) 3.5M KOH + 3.3M KF

The solubility of ZnO in the electrolyte was decreased in each case.

Cairns *et al.* repeated the above work in collaboration with Energy Research Corporation by using the following solutions in 1.35 Ah cells [36, 103].

i) 2.5 M KOH + 2.5 M K_2CO_3 + 0.5 M LiOH

ii) 3.5 M KOH + 3.3 M KF

iii) 3.2 M KOH + 1.8 M KF + 1.8 M K_2CO_3

The moderately alkaline electrolyte (3.2 M KOH + 1.8 M KF + 1.8 M K_2CO_3) in 1.35 Ah cells provided over 500 deep-discharge cycles before reaching 60% of initial capacity. They concluded that the processes, which degraded Zn electrode performances, were not major problems in these cells and that it was the nickel electrode that limited the lifetime.

Cairns *et al.* investigated the effect of lower KOH concentration electrolyte together with addition of F^-, CO_3^{2-}, BO_3^{3-} and PO_4^{3-} on the performance of Ag-Zn cells containing calcium zincate electrodes [104]. It was found that all of the anion additives to KOH electrolytes resulted in lower cell capacities and shorter lifetimes, which could be attributed to the formation of soluble silver salts with the subsequent degradation of the Ag electrode performance. The authors failed to account for the formation of insoluble $Ca(OH)_2$ and CaF_2. They did not identify what the soluble Ag salts might be, a somewhat surprising assertion in any event since insoluble Ag salts would be expected to form in this alkaline electrolyte.

Evercel's commercial Ni-Zn batteries with calcium zincate electrodes are based upon low concentration KOH-KF-K_2CO_3 electrolyte systems (20% w/w KOH) [36]. It is expected that the $Ca(OH)_2$ will be converted into insoluble precipitates of $CaCO_3$ and CaF_2 in this electrolyte system. The assumption of the role of insoluble calcium zincate in decreasing the solubility of zinc active mass is consequently not likely to be appropriate in this lower KOH concentration electrolyte in the presence of F^- and CO_3^{2-}. However, the benefits from the presence of $Ca(OH)_2$ are demonstrable but must act by an alternative mechanism.

1.4.5 Further additives to the electrolyte

Further additives to the electrolyte have been used to prevent the corrosion of zinc electrode and suppress the zinc dendrites formation and growth. A electrolyte containing thiocyanate was patented in Japan in 1996 [105]. Here, thiocyanate was employed to inhibit the dissolution of Zn during discharge and provide long cycle life.

Shivkumar *et al.* studied the effect of V_2O_5 , ZnO, PbO and $(NH_4)_2CS$ on the reversibility of the redox couple [106]. ZnO and $(NH_4)_2CS$ can be used as electrolyte additives (10^{-2} - 10^{-3} M), because they reduce the zinc corrosion markedly, do not enhance passivation of the zinc electrode and increase the cycle life.

Tetraethylammonium bromide (10^{-4} M) was found to suppress the formation of zinc dendrites and shape change [107]. Quaternary ammonium salts have been used to suppress the zinc dendrite growth in Zn-Br batteries [108]. The effect of quaternary ammonium salts will be reported in this work (Chapter 4).

Fatty esters of sorbitan have been added to the electrolyte and the batteries exhibited slower rates of zinc dendrite and long cycle life [109]. Fatty esters are not stable in alkaline electrolyte and are likely to decompose into fatty acid salts. The beneficial use of fatty acid salts in the zinc active mass is explored in Chapter 6 in this thesis.

Potassium 1,3,5-phenyltrisulfonate has been used as an additive in the electrolyte and self-

discharge rates appear to be dramatically reduced [110]. Polyethylene oxide (PEO), has been used in electrolytes with 40-80% KOH (w/w) with the conversion into a solid polymer electrolyte (SPE) system [111]. The PEO-SPE is a gelled electrolyte which has a number of important characteristics. The convection caused by temperature gradient, density gradients and others is suppressed. The diffusion of $Zn(OH)_4^{2-}$ ions in the electrolyte associated with the zinc electrode shape change is also suppressed. Here, the self-discharge of Ni-Zn cells is reduced together with improved cycle life.

1.4.6 Effect of separators

The separators used in Ni-Zn cells is also an important factor, which effects the dendrite growth and shape change. Modification of the porous separators by filling with inorganic compounds has been reported by Charkey *et al.* [50, 56, 61, 64-65]. The separator system used in Evercel Ni-Zn batteries may also contribute to battery performance. Two layers of non-woven nylon material and several layers of a zinc migration barrier separator are employed [36].

Alexandre *et al.* employed a special separator consisting of a highly porous nickel membrane, which was inserted between two separators placed between the nickel and zinc electrodes in their 44 Ah Ni-Zn batteries [112]. This separator acted as a catalyst for the dissolution of zinc dendrites. This system achieved 500 cycles.

It was reported that the Ni-Zn batteries with specially arranged separators have long cycle life [113]. Here, the number of separators at the edges of the zinc electrodes is greater than that at the center. Anion-exchange membranes have also been used in Ni-Zn cells where cycle life reached 200 cycles before the cells failed [114].

1.4.7 Charging/discharging regime

The charging/discharging regime is another factor which influences the cycle life. It is interpreted here that the charging/discharging regime used by Cairns *et al.* was as important

to the high cycle life of the cells as the modifications to the electrolyte and zinc active mass [72, 103]. The regular cycle regime used by Cairns *et al.* for 1.32 Ah cells consisted of [70]:

i) Charging at 0.263 A for 5 hours;

ii) 10 minutes at open circuit;

iii) Discharging at 0.526 A for 2.5 hours; followed by

iv) 10 minutes at open circuit prior to the next cycle.

Unlike other cells with 10 mol % and 40 mol % $Ca(OH)_2$ in the zinc active mass, the 25 mol % $Ca(OH)_2$ electrodes exhibited above average and erratic overpotentials at the 0.263 A charging rate, so the charge rate was decreased by 24% to 0.200 A [70]. The above regimen for the 25 mol % $Ca(OH)_2$ electrode then consisted of:

i) Charging at 0.200 A until the proper number of Ah was passed (with a 1-5% overcharge) or until an upper voltage limit was reached (voltage limit not stated);

ii) 10 minutes at open circuit;

iii) Discharging at 0.526 A until either the cell voltage (1.0 V) or the zinc electrode potential exceeded specified values (1.0 V and –1.0 V vs. Hg/HgO, respectively), or until the 1.32 Ah designed capacity was reached; followed by

iv) 10 minutes at open circuit prior to the next cycle.

The above cycling was carried out with the further conditions that when the zinc electrode potential increased near the end of charge (indicating a depletion of the available ZnO), a reformation cycle was performed (full discharge at a low rate followed by recharge). As the

cycling was computer controlled, the overcharge of the zinc electrode could be avoided. However, such a cycling regimen is not practical in use.

The cycle regimen used to investigate low zinc solubility electrolytes was even more complicated [103]. This cycle regime was designed in attempt to avoid overcharge of the zinc electrode and to approach high cycle life. Such results indirectly indicate that cycle regimen is important for cycle life of Ni-Zn cells.

Vibration and pulsed charging have also been investigated to avoid zinc dendrites formation. The highest reported cycle life for a Ni-Zn cell is 1000 cycles for vibrating zinc electrodes [113]. The use of mechanical vibration is to fragment the fragile dendrite needles as they grow. This clearly is not an option for practical batteries.

It would seem that most of the investigations on Ni-Zn batteries have been carried out using a 'black box' approach for the selection of the additives or electrolyte, alteration of the conditions and then cycling the cells. Much more attention has been paid to the effect of additives or electrolyte on the cycle life, rather than on the mechanisms which are more important and essential to solve the problems with Ni-Zn batteries.

1.5 Scope of this study

The scope, aims and objectives of the present work may be succinctly identified. The locations of the accompanying results are indicated.

i) To examine the zinc electrode in alkaline electrolyte and explore the mechanisms of zinc dendrite formation and growth, and zinc electrode shape change (Chapter 3);

ii) To establish an experimental method to study the mechanisms of the effect of additives on the dendrite growth and shape change (Chapter 4);

iii) Based on these mechanistic findings, to determine the dominant aspects that affect

the cycle life of Ni-Zn cells (Chapter 4);

iv) To construct cells based on these findings and to perform charge/discharge testing of these cells (Chapter 5, 6, 7); and

v) To find a method of preparing sponge or foam Ni for use as the current collector for Ni electrode (Chapter 2).

It will be shown that these aims have been met and that nickel-zinc batteries of relatively simply construction can now be assembled that can survive 1000 deep-discharge cycles. These cycles are at high rates of charge and discharge and do not require complex cycle regimes.

Chapter Two Preparation of sponge nickel current collectors

2.1 Introduction

A fundamental goal in many secondary battery systems is the use of high surface area, low mass and low volume current collectors. Such current collectors must have high electrical conductivity and have both mechanical and chemical stability under the battery operation conditions. At present, sintered nickel plates are used as current collectors for the negative electrodes in Ni-Cd and Ni-MH cells and also for the nickel electrodes in Ni-Cd, Ni-MH and Ni-Zn cells. The preparation of sintered nickel plate is by thermal decomposition of $Ni(CO)_4$ at 800-1000°C. This is relatively difficult and costly to achieve on an industrial-scale and $Ni(CO)_4$ represents a significant safety hazard.

An alternative process using 'foam' or 'sponge' nickel was first commercially developed by Prof. Wang Jisan in the 777 Battery Company Ltd. in Jiangmen, Guangdong Province, P. R. China in the early 1990s. The current collector is referred to as either 'foam' or 'sponge' nickel since electroless and electroplating of nickel takes place on an organic polymer sponge template and consequently the nickel deposit takes the same shape as the polymer sponge. Sponge nickel with its large specific surface area, high stability in alkaline solutions and relative ease of production may provide a viable alternative to sintered nickel plates. Specific advantages of sponge nickel compared to sintered include:

i) Simple manufacture process;

ii) Less expensive components; and

iii) Lower density collector.

A variety of preparation methods for high surface area Ni electrodes exist [116-118]. Although Ni electroless and electroplating are involved in the preparation, but details have not been revealed about the important electroless plating procedures [119]. The existing manufacturing methods in P.R. China also remain as trade-secrets. According to the

information obtained from those who have been involved in the manufacturing process, the preparation of sponge nickel consists of three basic procedures:

i) Electroless plating of an organic polymer sponge sheet with nickel;

ii) Further nickel electroplating the nickel coated sponge sheet; and

iii) Treating the electroplated sponge in a hydrogen flame.

Initial electroless plating is necessary due to the non-conductive polymer sponge. During this process a uniform, but thin, metallic nickel coating is deposited throughout the sponge to make it conductive. In order to obtain a sufficiently thick and uniform nickel coating for mechanical strength and adequate electrical conduction, this conductive sponge must be subjected to further nickel electroplating. Following this, the nickel-coated sponge is burnt in a hydrogen flame to:

i) Remove the organic polymer template;

ii) Fuse the finely-divided electrodeposited nickel crystals to provide a contiguous mass; and

iii) Reduce surface nickel oxides to provide a 'bright' surface.

In this chapter the details for the development of a method for preparing sponge nickel using electroless plating combined with electroplating are presented.

2.2 Electroless plating of Nickel

Electroless plating has been used for many years for the deposition of metals on non-conducting substrates either to provide an initial coating for subsequent electroplating, or to provide the sole method for metal deposition. Typical non-conducting substrates include

plastics, glass, ceramics, wood and biological materials (leather, skin, bones etc.). The end-use of such coated materials range from electronics and moldings to ornamental purposes.

The electroless plating process is an autocatalytic deposition during which a uniform coating, usually metallic nickel is deposited onto the catalytic surfaces, regardless of the shape of the object to be plated. Prior to electroless plating, pre-treatment of the substrate may be required. In particular, the electroless plating of plastics usually involves etching and surface neutralization steps [120]. The process developed in this project consisted of cleaning, drying, catalyzing and accelerating, prior to electroless plating.

2.2.1 Selection of sponge template

Electroless plating provides an opportunity to provide a substantial coating of a metal, in this case nickel, onto a non-conducting template. Consequently, the presentation of the template dictates the final form of the metal artifact. In this case, the finished article must provide a porous surface with void volumes of appropriate size to accommodate the battery plate active mass. Furthermore, there should be a minimum of completely enclosed voids through the thickness of the foam template. Such enclosed voids will not host the active mass and will act to decrease the energy density (Wh/L) in the battery. These points are illustrated in Fig. 2.1.

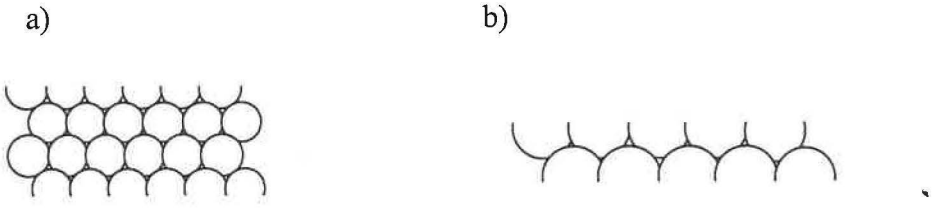

Fig. 2.1 Cross sectional schematic diagram of sponge templates where the solid lines indicate the polymeric material. a) An undeşirable sponge template for electroless plating where internal voids may not be coated with nickel or subsequently filled with active mass. b) An ideal sponge where nickel coating may take place and active mass may be introduced to fill all voids.

More importantly, if such hidden voids exist, then the electroless plating process will not occur throughout the complete thickness of the template. In the worst possible case that multiple layers of enclosed voids are present (Fig. 2.1a), then electroless plating will only take place on each face of the template and a mechanically robust nickel sponge will not remain after combustion of the polymeric material.

Many different polymer sponges were evaluated for use as templates. These ranged in thickness, size of pores and polymer types which included polyester, non-woven nylon cloth and polyurethane. The optimum material used in all subsequent work was a polyurethane foam (Para Rubber Ltd., Palmerston North, NZ) with a porosity similar to that for the commercial sponge nickel, cut into 2.1-2.3 mm thick sheets as used in air-conditioning filters. Here, the pores are bubbles cleaved by the cutting process. The foam is grown as 20-30 cm thick slabs and then cut with a sharp blade into whatever thickness slices are desired. The bubbles arise during the polymerization process from the entrapment of CO_2 gas. A further distinct advantage of this particular material is the high ratio of bubble diameter/bubble wall thickness. Typical bubbles have diameters of 0.7 mm while the thickness of the polyurethane walls is 50 μm. Consequently, not only is there relatively little polyurethane polymer to remove in the final heat treatment process, but also these thin walls when coated with nickel will lead to a low nickel mass per unit volume foam. Figure 2.2 is a photograph of the polymer sponge used as the template to prepare the sponge nickel.

2.2.2 Initial cleaning of sponge template

An initial cleaning step was found to improve the electroless plating process. This consisted of washing with commercial washing powder (Cold Water Surf, Diversey Lever, New Zealand) followed by copious rinsing with water. This removed fine particles of polyurethane formed during the cutting of the thin sheets from the original cast slab. Such particles tended to reside within the pores of the foam and if left *in situ* during electroless plating, the pores became filled with nickel granules and were not available for pasting of the active mass. In some cases 'grease spots' were also observed on the foam sheets as

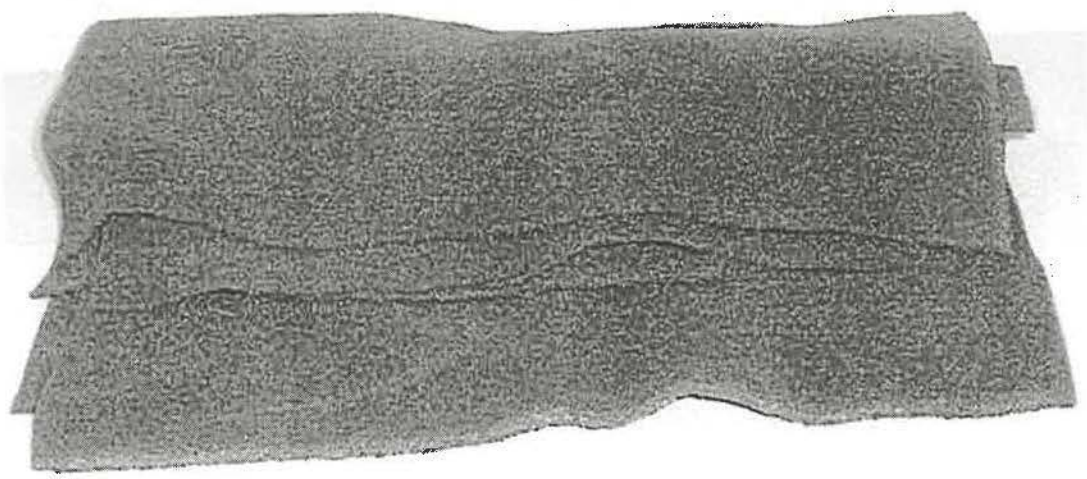

Fig. 2.2 Photograph of the polyurethane sponge.

delivered by the supplier. These presumably arose during the cutting process or subsequent handling. The washing adequately removed these hydrophobic spots.

2.2.3 Two-step catalyzing procedure

During the catalyzing step, metallic palladium particles were precipitated and absorbed onto the clean polyurethane sponge surface. These particles provided catalytic sites for initiation of the electroless plating process. Palladium is generally used as the catalyst and may be deposited in either a two-step or one-step procedure.

In the two-step catalyzing procedure, a piece of dry and clean sponge was immersed in an acidic (40 ml/L 36% HCl) solution of stannous chloride (10 g/L $SnCl_2.H_2O$) at 20-25°C for 3 minutes. During this time some stannous ions are absorbed onto the polyurethane. Gentle, but thorough, rinsing with water was used to remove excess stannous chloride. After that, the sponge was immersed in an acidic (10 mL/L 36 wt % HCl) palladium chloride solution (0.5-1 g/L $PdCl_2$), during which Pd^{2+} was reduced by the absorbed Sn^{2+} ions and precipitated onto the sponge surface as a thin layer of catalyst for nickel electroless deposition.

$$Pd^{2+}(aq) + Sn^{2+}(ads) \longrightarrow Pd^{0}(ads) + Sn^{4+}(aq) \qquad (2.1)$$

The need for washing before immersion in the palladium solution is important since the excess stannous chloride is detrimental for two reasons. First, if excess stannous chloride remains in the sponge then too much palladium will deposit as granules rather than as a thin film. Secondly, if the stannous chloride transfers into the palladium (II) solution, then large scale formation of metallic palladium particles will take place in the aqueous solution and will exhaust this relatively expensive reagent. Consequently, inadequate rinsing resulted in excessive consumption of the palladium (II) solution but did result in coating of the polyurethane with palladium. Conversely, excessive rinsing may remove the absorbed Sn^{2+} on the sponge surface, a problem that frequently resulted in poor coverage of the polyurethane by palladium. In this case, uniform nickel coating is unable to take place during nickel electroless plating.

After removal from the palladium chloride solution, the sponge must be subjected to thorough rinsing to remove excess palladium (II) to avoid introduction of palladium ions to the nickel electroless plating bath, where uncontrolled reduction of nickel could take place.

2.2.4 One-step Catalyzing process

In order to overcome the difficulties involved in the two-step procedure, an alternative one-step process, based upon that used in plastic electroless plating [120], was adapted and optimized for this project. Usually in a one-step process, the plastic object is placed in a specially prepared colloidal palladium solution. Then, colloidal particles of palladium metal are absorbed onto the plastic surface. After treatment to remove absorbed Sn^{2+} and Sn^{4+} ions, these colloidal palladium particles serve as catalyst centers for nickel electroless plating.

The colloidal palladium solution was prepared by mixing two pre-prepared solutions A and B. The composition of solution A is given below:

Component	Quantity
$PdCl_2$	1.0 g
$SnCl_2.2H_2O$	2.5 g
HCl (conc.)	100 mL
H_2O	400 mL

$PdCl_2$ was dissolved in 50 mL of HCl and then 400 mL of H_2O was added. A separate solution was prepared by dissolving the $SnCl_2.2H_2O$ in 50mL conc. HCl while heating until boiling, since this compound is difficult to dissolve in cold HCl. After cooling, a clear stannous chloride solution was obtained. The $SnCl_2$ solution was then added slowly to the $PdCl_2$ solution at 30°C with stirring. After 12 min stirring and maintaining at this temperature a colloidal palladium solution was formed.

$$Sn^{2+}(\text{excess}) + Pd^{2+}(aq) \longrightarrow Sn^{4+}(aq) + Pd(s)(Sn^{2+}_{ads}) \qquad (2.2)$$

Where Pd(s)(Sn^{2+}_{ads}) represents colloidal palladium cored with Sn^{2+}.

The composition of solution B is given below:

Component	Quantity
$Na_2 SnO_3.3H_2O$	7.0 g
$SnCl_2.2H_2O$	75.0 g
HCl (conc.)	200 mL

Solution B was prepared by first dissolving $SnCl_2.2H_2O$ in 200mL of conc. HCl by heating to the boiling point followed by dissolution of Na_2SnO_3. $3H_2O$ to form a clear solution.

At room temperature, all of solution B was added slowly into all of solution A with stirring and then water was added to make up to a total volume of 1000 mL. A stable colloidal palladium solution, dark green in colour, formed immediately. With time, this solution became brown in colour, but no less useful in adhering to the polyurethane foam.

The polyurethane sponge was immersed in the colloidal palladium solution for 3 minutes to permit the formation of an adsorbed layer of these colloidal particles on the surface of the polyurethane. The temperature was not critical and success was found over the temperature range 18-30°C. The palladium colloid contains excess stannous chloride together with stannic chloride and hydrochloric acid. The palladium particles in the colloid may well be coated with absorbed Sn^{2+} and Sn^{4+}. A further step is required to remove this layer since it appeared to hinder the electroless plating process.

In this washing step, the stannous and stannic ions adsorbed on palladium particles were removed to enhance or accelerate the activity of the palladium particles for the electroless plating. This was best achieved by dissolution in 2 M HCl at 45-55°C for 15-25 second.

The temperature and immersion times were critical for this step. Higher temperatures and/or longer immersion resulted in removal of the palladium particles from the sponge.

Lower temperatures and/or shorter immersion did not sufficiently dissolve the stannous and stannic chlorides. After immersion in the accelerating solution, the sponge was rinsed with water before placing into the electroless plating bath.

In comparison with the two-step catalyzing procedure described in section 2.2.3, it was easier and more reproducible to obtain a uniform nickel coating on the polyurethane sponge with this one-step catalyzing. This process was used in subsequent studies until a simple but more reliable catalyzing procedure was developed (Section 2.5).

2.2.5 Electroless plating of nickel

Solutions for the electroless plating of nickel usually contain a source of nickel (II), an aqueous reducing agent, such as hypophosphite and a complexing agent to ensure the solubility and stability of the nickel (II) at pH > 9. The most widely used solutions and conditions used for electroless plating of nickel are given below [120]:

Condition	Value
$NiSO_4.7H_2O$	20 g/L
$NaH_2PO_2.2H_2O$	30 g/L
$Na_3C_6H_5O_7.2H_2O$	10 g/L
NH_4Cl	30 g/L
pH	8.5 – 9.5
Temperature	40 – 45°C
Immersion time	5 – 10 min.

This widely-used electroless nickel plating solution and conditions were initially used. The rinsed catalyzed sponge was immersed in the electroless-plating bath while stirred until a uniform nickel coating was formed.

Among the compounds, $NiSO_4.7H_2O$ is the source of nickel (II), $Na_3C_6H_5O_7.2H_2O$ and NH_4Cl are the complexing agents and $NaH_2PO_2.2H_2O$ is the reducing agent.

$NiSO_4 . 7H_2O$ was dissolved in 500 mL of H_2O, then $Na_3C_6H_5O_7.2H_2O$ was added and dissolved in this solution, followed by NH_4Cl and $NaH_2PO_2 . 2H_2O$. Water was added to make the solution up to 1 L.

As the coated sponge is immersed in the solution, a series of reactions take place on the adsorbed palladium particles at the sponge surface. First, hypophosphite oxidizes with the production of adsorbed hydrogen

$$2H_2PO_2^-(aq) + 2OH^-(aq) \longrightarrow H_2O(aq) + 2HPO_3^{2-}(aq) + 2H(ads) \quad (2.3)$$

Addition of OH^- to ensure pH > 8.5 is necessary for the formation of reductive hydrogen atoms. The nickel ions are then reduced and precipitated onto the sponge surface by these hydrogen atoms.

$$[Ni(NH_3)_4]^{2+}(aq) + 2H(ads) + 2OH^-(aq) \longrightarrow Ni(s) + 4NH_3(aq) + 2H_2O(aq) \quad (2.4)$$

Some of the adsorbed hydrogen atoms combine with the visible release of hydrogen gas.

$$2H(ads) \longrightarrow H_2(g)\uparrow \quad (2.5)$$

Also, phosphorous is released and forms a nickel-phosphorous alloy [120].

$$[H_2PO_2]^-(aq) + H(ads) \longrightarrow P(s) + H_2O + OH^-(aq) \quad (2.6)$$

According to observations, evidence of hydrogen evolution indicated that nickel deposition was taking place and the higher the rate of hydrogen evolution, the higher was the rate of nickel deposition.

There is no established simple way to maintain the composition of this solution during the electroless plating process. Nickel (II), hydroxide and hypohosphite become depleted with time.

It was found that at pH > 9 NH_4Cl was sufficient to keep Ni^{2+} soluble and stable in the solution. According to this finding, a new and simplified composition of the solution was developed for nickel electroless plating. The advantages of this solution are increased stability and ease of maintenance. The composition of this simplified solution is given below.

Condition	Value
$NiSO_4.6H_2O$	20 g/L
H_3PO_2 (conc.)	25 mL/L
NH_4OH	sufficient to maintain pH > 9
pH	9.0 – 9.5
Temperature	40 – 45°C
Immersion time	8 – 15 min.

Here, NH_4OH acts as both a complexing agent and a pH buffering agent. As nickel and the reducing agent become exhausted during electroless plating, $NiSO_4.6H_2O$ and H_3PO_2 should be added to the bath as required. Addition of $NiSO_4.6H_2O$, usually as a concentrated $NiSO_4$ solution together with H_3PO_2 typically makes the solution green due to the lowering of the pH below 8. In some cases, a green precipitate of $Ni(OH)_2$ formed. Addition of excess NH_4OH to give pH > 9 results in dissolution and the development of a blue solution as $[Ni(NH_3)_4]^{2+}$ forms as required for electroless plating. This discernible change in colour facilitates maintenance of the solution.

A further modification was made in response to the progressive accumulation of SO_4^{2-} in these electroless plating solutions. An alternative salt to $NiSO_4$ was prepared. Here, $NiSO_4$ solution was added to a NaOH solution with stirring, giving rise to precipitation of $Ni(OH)_2$, which was separated from the solution by filtration. The wet $Ni(OH)_2$ precipitate was then added gradually to a H_3PO_2 solution with stirring until no more $Ni(OH)_2$ could be dissolved to give rise to a $Ni_3(PO_2)_2$ solution.

$$3\ Ni(OH)_2(s) + 2\ H_3PO_2(aq) \longrightarrow Ni_3(PO_2)_2(aq) + 3\ H_2O(aq) \quad (2.7)$$

This modified solution for electroless nickel plating is given below:

Condition	Value
$Ni_3(PO_2)_2$ saturated solution	20 mL/L
NH_4OH	sufficient to maintain pH > 9
pH	8.5 – 9.5
Temperature	40 – 45°C
Immersion time	8 – 15 min.

The $Ni_3(PO_2)_2$ solution is green in colour. When added to sufficient NH_4OH solution to give pH > 9, it turns blue without precipitation and it is immediately available for electroless plating. As a consequence, solutions for electroless plating of nickel were modified with this convenient solution together with NH_4OH. Following electroless plating, the nickel coated sponge was washed with water.

2.3 Electroplating

The uniform deposition of a thin nickel layer throughout the sponge by electroless plating made the sponge conductive and capable of undergoing conventional electroplating. This process provides an opportunity to coat the sponge with a thick uniform nickel layer. The composition of the electroplating solution and conditions are given below [120].

It was found that a low pH assists the formation of a uniform nickel deposit throughout the sponge. After electroplating, the sponge must be rinsed with water and dried, prior to burning in a H_2 flame.

Condition	Value
$NiSO_4.6H_2O$	250 – 300 g/L
$NiCl_2$	30 – 50 g/L
H_3BO_3 (conc.)	35 – 40 g/L
pH	1 – 3
Temperature	40 – 50 °C
plating current	50 – 80 mA/cm^{2*}
plating time	30 – 40 min

* geometric projected area.

2.4 Treatment in H_2 flames

The polyurethane sponge substrate is flammable. The bulk of this material may be initially removed by burning the electroplated sponge in air. This produced a 'raw sponge nickel' contaminated with incomplete polyurethane combustion products and inorganic phosphorous from the electroless plating. This raw sponge nickel was hard and brittle, presumably due to the nickel coating consisting of individual metal crystals rather than a single continuous mass of nickel, and required treatment in a H_2 flame. The rationale for burning in a H_2 flame includes

i) Removal of the remaining organic material, inorganic phosphorous and other contaminants;

ii) Reduction of hardness and brittleness;

iii) Relief of mechanical stresses; and

iv) Reduction of nickel oxide layers formed during polyurethane combustion in air.

After treatment in a H_2 flame, the sponge nickel became flexible and white. However, its surface remained partially oxidized. In order to obtain a bright silver luster the sponge nickel was further reduced in a furnace at 700°C for 30 min and cooled to ambient temperature while purging with 'forming' gas (5% H_2 in N_2).

2.5 Modification of the catalyzing

If the sponge can adsorb palladium chloride on its surface, which is then reduced and precipitated on the sponge surface, the catalyzing process will become simple and easy to carry out without spoiling the expensive palladium chloride solution by introducing stannous chloride in it. Also, there will be more catalyst or palladium particles precipitated on the sponge surface, enhancing the nickel electroless plating process. Such treatment is different from traditional two-step catalyzing in consequence and therefore has different characteristics. Their differences are show below.

Traditional two-step treatment (Section 2.2.3)	Proposed modified treatment
Procedure: 1. Soak sponge sheet with stannous chloride 2. Wash with water 3. Soak in palladium chloride solution 4. Rinse with water	Procedure: 1. Soak sponge sheet in palladium solution 2. Dry 3. Soak with reducting agent solution 4. Wash with water
Advantage: 1. Mature practical technology	Advantage: 1. Prevents spoiling of costly palladium solution 2. Less washing and less disposal 3. The amount of catalyst on the surface can be controlled as required 4. Low maintenance
Disadvantage 1. Spoils costly palladium chloride solution 2. More disposal 3. Higher maintenance	Disadvantage 1. Not mature 2. Needs effort to develop.

4. The amount of catalyst can not be controlled	

Such treatment has been mentioned previously [120], but no practical details were provided and it is believed impractical. The modification procedure was designed on the basic materials used in the traditional two-step method shown below:

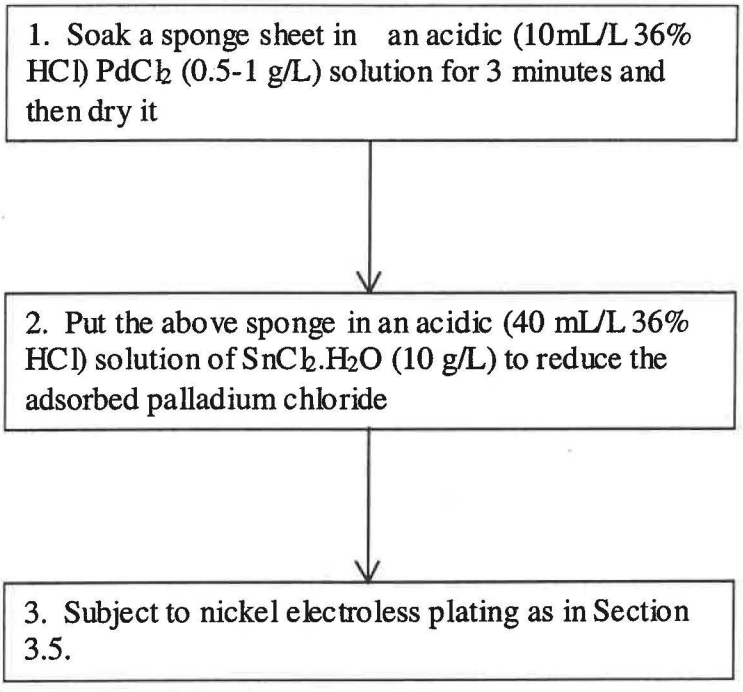

A small piece of sponge sheet was soaked in the palladium chloride solution thoroughly and then dried completely. It was believed that the sponge surface was covered with sufficient palladium chloride. The amount of palladium chloride on the sponge surface is related to the concentration of palladium chloride in solution and therefore can be controlled through the concentration.

Given the reduction and oxidation potentials [121]:

$$Sn^{4+}(aq) + 2e \longrightarrow Sn^{2+}(aq) \quad E^o = 0.15\ V \tag{2.8}$$

$$Pd^{2+}(aq) + 2e \longrightarrow Pd(s) \qquad E^o = 0.83\ V \tag{2.9}$$

Palladium chloride adsorbed on the sponge surface was expected to be reduced in the presence of stannous chloride as found in the preparation of the colloidal palladium solution (Section 3.2.3). However, it was found that such treatment does not result in a sponge catalytic for electroless Ni plating, which suggested that metallic palladium particles were not formed in this process.

Stannous chloride can reduce palladium chloride in aqueous solution as in the preparation of colloidal palladium solution. Also, stannous chloride, when absorbed on a sponge surface, can reduce palladium chloride and precipitate metallic palladium on the sponge surface. Conversely, stannous chloride in solution appears not to be able to reduce palladium chloride previously adsorbed on the sponge surface. Elucidating this difference in mechanisms is essential to further modifications.

The solution to this problem arose from recognition of the solubility of $PdCl_2$. Adsorption of palladium (II) onto the foam followed by immersion in stannous chloride merely resulted in leaching of $PdCl_2$ into the bulk solution. If adsorption of palladium (II) onto the template material was to be successful, then development of an immobilization technique prior to reduction was required. Based on this consideration a new reducing system in alkaline conditions was employed – that of alkaline formalin. This high pH (pH > 10) aqueous solution of formaldehyde is widely used in electroless copper deposition [120]. The high pH ensures immobilization of palladium (II) via formation of a $Pd(OH)_2$ precipitate on the polyurethane sponge

$$PdCl_2\,(aq) + 2OH^-\,(aq) \longrightarrow Pd(OH)_2\,(s) + 2Cl^-\,(aq) \tag{2.10}$$

Consequently, a palladium (II) reducing solution was optimised consisting of 40% (v/v) formalin and NaOH (50 g/L) in water. Catalysing now involved soaking the template in an aqueous $PdCl_2$ solution (0.3 g/L) for 30 sec followed by drying in a stream of warm air. The palladium (II) coated sponge was then placed in the alkaline formalin solution at 50°C

for 3 min. Over this time the light brown absorbed $PdCl_2$ (that appeared immediately on immersion) was converted to a light gray layer of palladium metal. Hydrogen gas evolution was also observed due to

$$Pd(OH)_2(s) + 2HCHO(aq) \longrightarrow Pd(s) + 2HCOO^-(aq) + 2H_2O(aq) \quad (2.11)$$

followed by

$$HCHO(aq) + 2OH^-(aq) \longrightarrow 0.5H_2(g) + HCOO^-(aq) + H_2O(aq) \quad (2.12)$$

This modified catalysing procedure has low maintenance and can be readily controlled. Figure 2.3 shows the sponge nickel prepared by this method.

As an aside to the development of sponge nickel current collectors, this simplified nickel deposition technique has also been used for other purposes in the Massey University electrochemistry laboratories. A prime example is use in combination with ink-jet printing of $PdCl_2$ solutions to produce conducting nickel pathways on plastic overhead transparencies.

2.6 Cu electroless plating to replace Ni deposit

The palladium chloride used in the conventional catalyzing procedure for nickel electroless plating is relatively expensive and attention must be paid to recovery. Further, any Pd^0 exposed to electrolyte in the nickel zinc cells will promote hydrogen evolution.

The purpose of electroless plating of nickel is to make the sponge conductive prior to electrodepositon of nickel. Consequently, it is possible that copper electroless plating may well be used to replace the nickel electroless deposition. Here, silver is the catalyst for copper electroless plating and has a cost 1% of that for palladium.

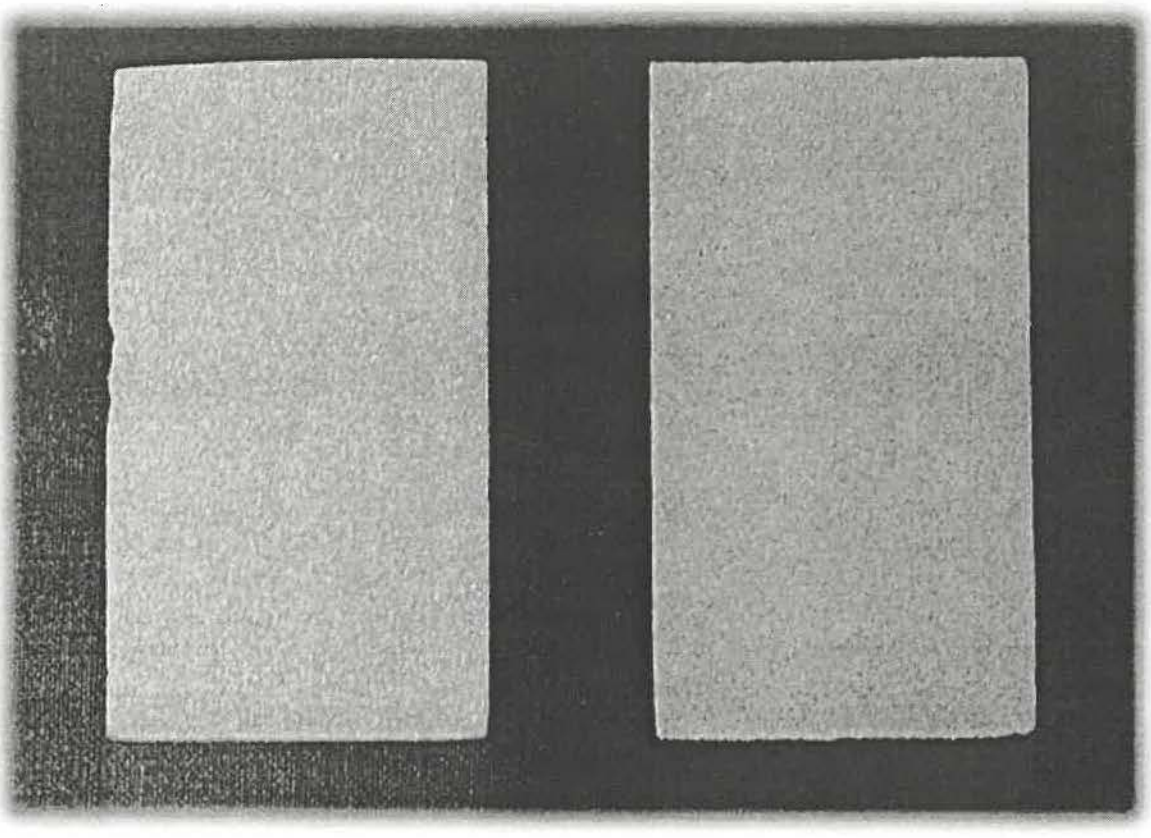

Fig. 2.3 Photograph of the prepared sponge nickel.

The technology used in copper electoless plating for plastics was adopted here [120]. Similar to the two-step catalyzing procedure in nickel electroless plating (Section 2.2.3), silver is normally deposited in a two-step procedure in copper electroless plating.

The polymer sponge was immersed in an acidic (40 g/L 36% HCl) stannous chloride solution (10 g/L $SnCl_2.H_2O$) at 20-25°C for 3 minutes. After immersion, it was rinsed gently but thoroughly to remove excess stannous chloride from the polymer surface. Then, it was immersed in aqueous ammonium silver nitrate solution consisting of $AgNO_3$ (2-5 g/L) and 25% NH_4OH (20-25 g/L) at 18-30°C for 1-5 minutes to provide adsorbed silver via

$$Sn^{2+}_{abs} + 2[Ag(NH_3)_3]^+ + 2OH^-(aq) \longrightarrow Sn(OH)_4(s) + 2Ag_{ads} + 6NH_3(aq) \qquad (2.13)$$

After rinsing thoroughly with water to remove loose silver particles, the sponge was placed directly into the copper electroless plating bath. The experimental condition for the electroless copper plating is given below:

Condition	Value
$CuSO_4.5H_2O$	10 g/L
$K.NaC_4O_6.4H_2O$	25 g/L
NaOH	15 g/L
Formlin(36-40%)	5-8 mL/L
Temperature	15-35°C
time	15-30 min.

Copper is deposited onto the catalyzed surface of the sponge. The reactions related to copper deposition are given below [120].

$$HCHO(aq) + 2OH^-(aq) \longrightarrow H(abs) + HCOO^-(aq) + H_2O(aq) \qquad (2.14)$$

$$Cu^{2+}(complexed) + H(ads) + OH^{-}(aq) \longrightarrow Cu(s) + H_2O(aq) \quad (2.15)$$

$$2H(ads) \longrightarrow H_2(g) \quad (2.16)$$

The primary problem with this alternative approach is similar to that found in nickel electroless plating procedure for the efficiency of washing. If too little washing takes place, excess silver deposition will occur; if too much washing is employed, a uniform coating of silver will not eventuate. Consequently, an alternative approach to immobilizing silver on the sponge substrate was developed.

A piece of cleaned and dry sponge was soaked in an aqueous silver nitrate solution (6 g/L $AgNO_3$) for 3 minutes at room temperature and then dried thoroughly with warm air. It was established that after exposure to sunlight for 12-24 hours, a silver lusting coating was formed on the sponge surface. This occurs due to the photo-induced oxidation of the sponge constituents coupled with silver (I) reduction. The catalyzing utility and immobilizing of this layer was readily demonstrated by immersion of the sponge in the copper electroless plating bath. A uniform copper deposit was formed only in 5 minutes approximately three times more rapidly than in the previous case.

Condition	Value
$AgNO_3$	6g/L
NH_4OH	30ml/L
Sodium dodecylsulphate	1-3g/L
time	10-20min.

The use of ammonium silver nitrate solution in place of silver nitrate solution enables long term storage of silver (I) solution. Use of sodium dodecylsulphate as a surfactant ensured that the sponge was wetted thoroughly.

Silver nitrate is more readily reduced than palladium chloride. Consequently, the silver nitrate adsorbed by the sponge was readily reduced with the same alkaline formalin solution.

A piece of white nylon separator was immersed in the ammonium silver nitrate solution, dried completely with warm air and then was immersed in the alkaline formalin solution identical to that used for reduction of palladium chloride. It was found that the white nylon separator became black immediately on entering the solution even at room temperature. This indicates that a large amount of silver catalyzing centers was formed, ready for copper electroless plating. It was shown that uniform copper was formed only in a few minutes when the nylon separator was placed in the copper electroless plating bath. The sponge was tested in the same way. It was found that copper was successfully deposited on the sponge, which was then subjected to nickel electroplating and a uniform nickel coating was obtained throughout the sponge.

Unlike the stable nickel deposit, copper deposit on the sponge was found to oxidize readily upon exposure to air.

2.7 Conclusions

Sponge nickel was successfully prepared using polyurethane sponge as the template for nickel electroless plating and nickel electroplating. Nickel electroless plating was employed to make the polymeric sponge conductive while nickel electroplating provided further nickel coating onto the sponge template.

Conventional electroless plating procedures were unsuitable for the polymeric sponge due to its softness and high porosity. Modifications were made to the catalyzing process, which becomes simple, stable and reliable, and superior to the conventional processes. The modified catalysing process is not only suitable for the sponge but also for other materials such as paper, polymer overheads and ceramics. No attention is required in the modified

catalyzing process to the recovery of palladium chloride due to high efficiency of palladium utility.

The solution of electroless plating was modified and optimized, which is more stable with low maintenance.

Copper electroless plating together with the modified catalyzing process is an alternative to nickel electroless plating, but the copper deposit was sensitive to oxidation in the air.

Nickel electroless plating with its modified catalyzing process, optimized plating solution and stable nickel deposit makes it superior to the copper electroless plating for use in preparation of sponge nickel.

Chapter Three Preliminary work on the nickel zinc cell

3.1 Introduction

In order to begin with a attempt to solve the problems with nickel zinc cells, it was necessary to develop test procedures with the simplest nickel zinc cells before any improvement or modification to these cells, particularly with respect to the zinc active mass. It was anticipated that the dominant problems with nickel zinc cells such as shape change and dendrite growth would be encountered early in this preliminary work. The results would provide a practical benchmark against which later improvements could be compared. A further benefit would be to gain experience in designing and assembling cells and the selection of cell components and test equipment. Instead of merely copying others work, the modification to the cells must be based on the findings and understanding through the preliminary work on the zinc electrode shape change and zinc dendrite growth.

3.2 Preliminary Test Cell

The size of the cells in preliminary work was determined by the size of commercially available sponge nickel (approximately AA sized) that was to be used as the current collector for the nickel electrodes.

Several different materials such as copper foil, graphite cloth, brass mesh and even sponge nickel had been attempted for use as the zinc electrode current collector during the course of this work.

Copper foil was too soft and needed significant effort to cut slots in it. Furthermore, it proved to be uneasy to paste the slotted thin copper foil with zinc oxide mass.

Graphite cloth, which is very stable and has a high overpotential for hydrogen evolution, was a good candidate material for use as the zinc electrode current collector. It had high specific area superior to copper foil for pasting, but it was found to be difficult to electrically connect this graphite cloth to a nickel tag or ribbon for use as a terminal.

Sponge nickel was the best for pasting and connecting to a nickel terminal, but the low overpotential for hydrogen evolution inhibited the reduction of zinc active mass. Furthermore, the zinc metal dissolved in the alkaline electrolyte with hydrogen evolution on this nickel surface.

Brass mesh (40 × 40) could be used in several layers by spot welding, to yield a high specific area. The overpotential of hydrogen evolution on brass mesh was sufficiently high that zinc oxide hosted in the brass mesh could be readily reduced without hydrogen evolution. Consequently, it was found that brass mesh was the best material to make the zinc electrode current collectors.

According to past experience in electroplating, when an object is electroplated in the plating bath, metal dendrites always grow at the edges where the local current density is much higher than the average. This suggests that high current densities may enhance the formation and growth of zinc dendrites during charge in the Ni-Zn cells. To retain low current density at the zinc electrode, the cell structure with one nickel electrode sandwiched between two zinc electrodes would be employed in these preliminary cells. In order to avoid any mechanical damage to the electrodes in cell construction which could occur during rolling the sandwiched electrodes, planar plate nickel and zinc electrodes would be used instead of the 'jelly roll' configuration. The planar electrode assembly would be held in vertical orientation in a Perspex prismatic cell case. The nominal charge capacity was 1 Ah, higher than AA sized nickel cadmium cells with capacities ranging from 0.35 to 0.60 Ah.

3.2.1 Zinc Electrodes

Brass mesh of 40 × 40 mesh size (40 wires per inch) was used as purchased from Mico Metals Ltd., Palmerston North to prepare the zinc electrode current collector as shown in Fig. 3.1. Three layers of this brass mesh were welded together by spot welding to create a high surface area current collector with sufficient internal interstitial spaces to host the

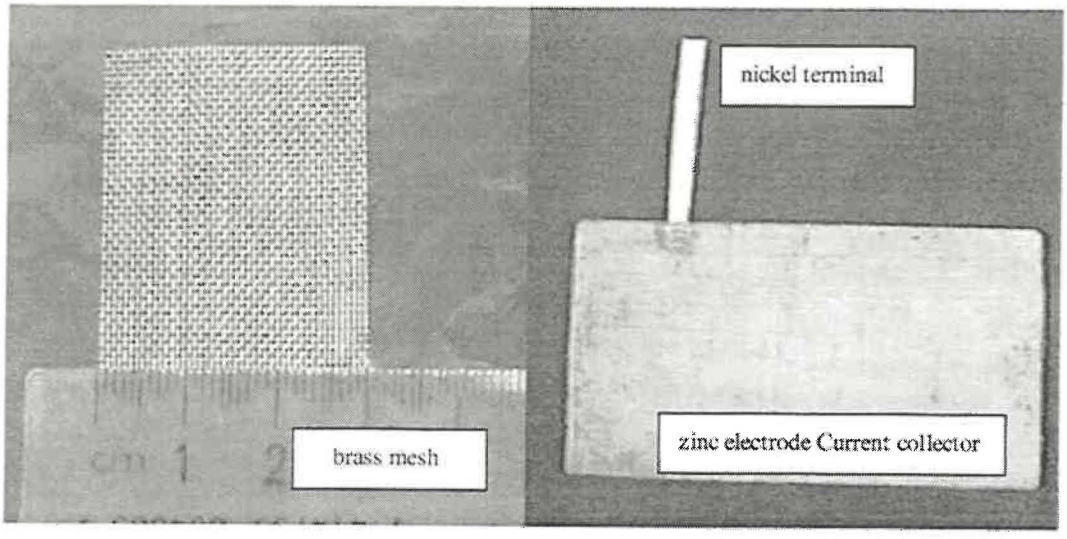

Fig. 3.1 The brass mesh (40 × 40), current collector and nickel terminal for the zinc electrodes.

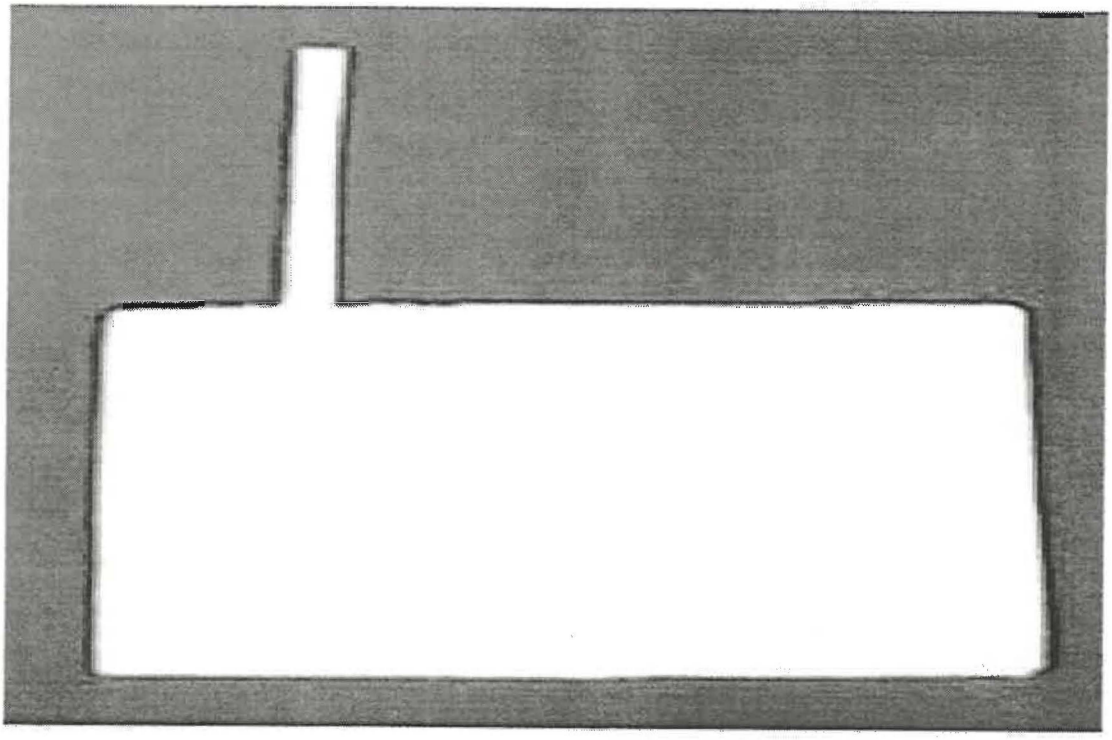

Fig. 3.2 A complete zinc electrode formed by pasting zinc oxide onto the three-layered brass mesh current collector.

zinc active mass. The size of the zinc electrode current collector was 88 mm (width) × 59 mm (height) × 2 mm (thickness).

Nickel foil (width 4 mm, thickness 0.2 mm) which is very stable in alkaline electrolyte, was used as the terminal by spot welding onto the brass mesh current collector, 20 mm away from the vertical edge of the brass mesh assembly as shown in Fig. 3.1. The welding site and the lower 5 mm of the nickel tag was coated with epoxy glue to prevent hydrogen evolution at the nickel surface since the overpotential for hydrogen evolution is significantly lower on this metal than on either zinc or brass. The epoxy coating also provided the welding site protection from corrosion.

The zinc active mass consisted of zinc oxide together with carboxymethylcellulose (CMC) as a structural binder [26] at a ratio of 0.1 mole ZnO : 0.01g CMC. CMC (0.03g) was dissolved in 2 mL water at room temperature in a beaker. Then, 0.3 mole of zinc oxide was added into this CMC solution and mixed thoroughly with addition of further water to form a paste. About 0.25 mole of zinc oxide was pasted onto the two zinc current collectors using a spatula. The pasted current collector was pressed with a bench top vice to squeeze excess water out of the active mass.

This process resulted in the finished zinc electrode with damp zinc oxide firmly pasted on, and in, the brass mesh assembly. These damp electrodes were used immediately without further drying. If drying took place, the firmly pasted zinc oxide became cracked and prone to sledding from the current collector. A pasted zinc electrode is shown in Fig. 3.2.

In contrast to the commercial non-woven nylon separators used in nickel cadmium batteries that have been tested in nickel zinc cells by others [122], woven nylon cloth, which was purchased from Arthur Toye Fabrics Ltd., Palmerston North, was employed in these preliminary test cells. This separator material was selected primarily because of its selectable thickness and density, ease of handling and the immediate availability from retail fabric outlets. The pasted and pressed zinc electrode without drying was enclosed tightly with two layers of woven nylon cloth heat-sealed at the edges.

3.2.2 Nickel electrodes

Sponge nickel purchased from JJJ Battery Company Ltd., Jiangmen, Guangdong, P.R. China was used as the current collector for the nickel electrode. The size of the sponge nickel was 85 mm (width) × 56 mm (height) × 2.5 mm (thickness), and was slightly smaller than the zinc electrodes. Nickel foil (width 4 mm, thickness 0.2 mm) was welded onto the sponge nickel 20 mm from the vertical edge of the nickel sponge to provide the terminal as shown in Fig. 3.3. Unlike the nickel terminal on the zinc electrode, there was no need to shroud this site with epoxy glue.

About 0.2 mole of nickel (II) hydroxide and 6g of graphite were granulated together with water 20-30 mL at room temperature. Then, 0.02 mole of cobalt sulfate was thoroughly dissolved in the mixture followed by addition of 10 mL KOH solution containing 0.06 mole of KOH with stirring. Cobalt hydroxide was homogeneously mixed with the granulated nickel hydroxide and graphite mixture. The final precipitated mixture separated from the water formed the required paste, which was then applied to the sponge nickel using a spatula. The pasted sponge nickel was carefully pressed in a bench top vice to squeeze excess water out of the paste to form the required nickel electrodes. The pasted nickel electrode was dried in the oven at 120°C for 5 hours. As with the zinc electrode, the dried nickel electrode was enclosed with two layers of woven nylon cloth, heat sealed at the edges.

3.2.3 Reference electrode

The cell voltage and the potentials of both nickel and zinc electrodes were required to be monitored to assess the state of the cell and electrodes during cycling. According to these variations of potential, it can be determined which electrode is the capacity limiting electrode during discharge – the electrode that alters potential the most under load at the end of discharge is likely to have the limiting capacity. Small declines in the cell potential or voltage during charge may also indicate the formation of electrically shorting dendrites.

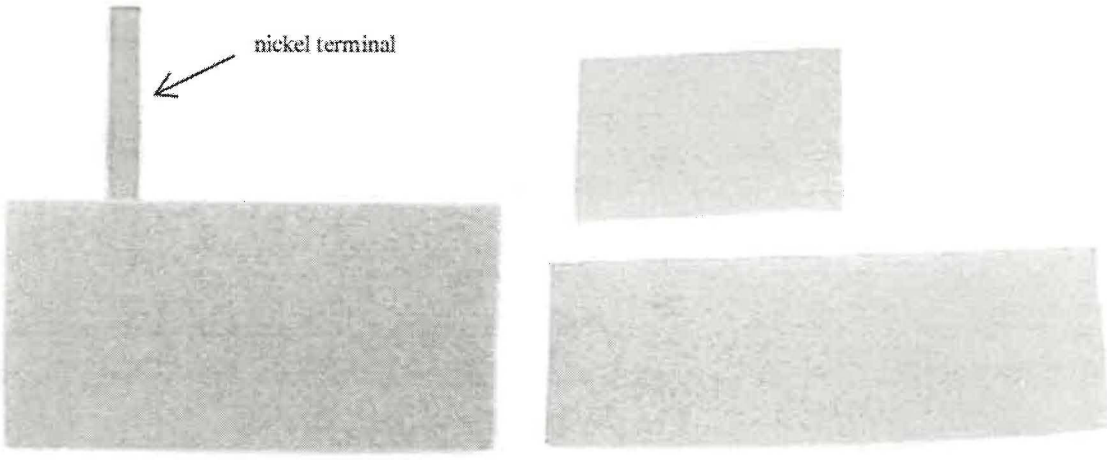

Fig. 3.3 The sponge nickel and nickel terminal for the nickel electrode.

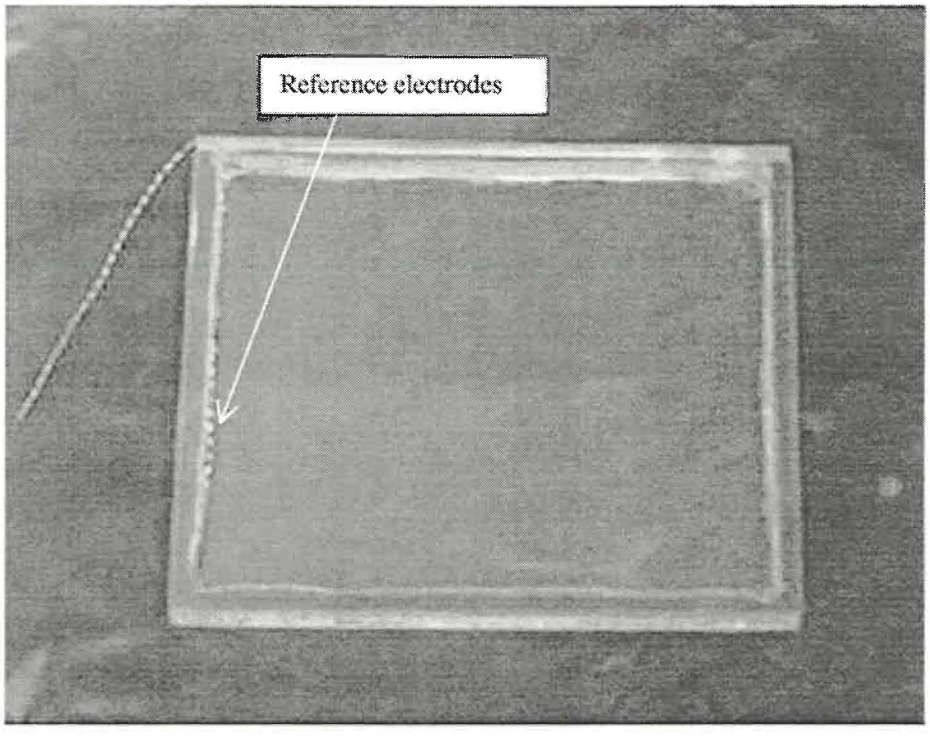

Fig. 3.4 The cell case with reference electrode (stainless wire).

Hg/HgO electrodes are usually used as the reference electrodes in the testing of alkaline batteries and have also been used in the investigation of the nickel-zinc system [72, 103]. The construction of small or micro Hg/HgO reference electrodes that could be placed in, or incorporated into, the cells was considered an unnecessary challenge for the project. In addition to micro Hg/HgO reference electrodes, the conventional Hg/HgO electrode can also be located in a separate reference compartment that is filled with the same alkaline electrolyte as that for the cell with connection to the cell via a capillary tube [90]. The construction and maintenance of such a setup were considered too unwieldy for practical use during the anticipated prolonged testing periods. Consequently, an alternative approach was adopted based on simplicity and fitness for the intended purpose.

Stainless steel is very stable in water and in alkaline electrolytes because of passive film formation. Stainless steel (an alloy of iron, nickel and chromium) and its passive films (a mixture of iron, nickel and chromium oxides) were considered as a candidate for development of a simple and robust pseudo reference electrode. Consequently, a thin stainless steel wire from 10 × 10 stainless steel mesh was employed as the reference electrode with one end fixed at the cell case bottom corner so that this wire was in contact with the electrolyte without touching the electrodes, as shown in Fig. 3.4. The ease of construction permitted inclusion of this type of reference electrode in all test cells. In this preliminary work, the possibility and performance of such proposed reference electrode was established and in 30% (w/w) KOH saturated with respect to zincate this electrode was found to have potential of –0.272 V against the Ag/AgCl electrode.

3.2.4 Cell case and assembly

Transparent Perspex was used as the structural material for cell case manufacture. This transparency enabled direct observation of events in the cell during cycling. Perspex is stable in strongly alkaline solutions and not subject to embrittlement or opacity. Cell structural components were cut directly from commercially available sheets. 2 mm thick Perspex sheet was used to make the wall of the cell case and 10 mm thick sheet to make the

frame. The case was glued with an adhesive formed by dissolving finely-divided Perspex shavings in chloroform (*ca.* 10-20 g/100mL) to form a viscous liquid. After applying this glue, the cell components were held under pressure in a bench top vice and heated to *ca.* 50°C for 24 hours. Figure 3.4 shows the cell case incorporating the stainless steel wire as the reference electrode.

The nylon enclosed nickel electrode was held between two nylon enclosed zinc electrodes and then placed in the cell case and glued. A small hole was made at the top of the cell for injection of electrolyte and venting of gas.

3.3 Charge/Discharge Cycling Equipment

The computer controlled cycling system consisted of two independent power supplies and an analog/digital convertor and switching interface connected to a computer. Figure 3.5 shows a photograph and a schematic diagram of this cycling equipment. On the basis of the expected charging and discharging conditions for nickel-zinc cell cycling, Dr Simon Hall designed both the software and the hardware for the cycling equipment. A detailed description of the components and computer software for the cycle equipment is given in Appendix 1.

The analog/digital interface board (K-2805, Dick Smith Ltd., Palmerston North) was programmed using a software core developed by Dr Simon Brown (formerly Institute of Fundamental Science). This test equipment was constructed by the Electronics Workshop in the Institute of Fundamental Sciences at Massey University. The analog/digital converter was an 8-bit device capable of encoding potentials over the range 0-5 V at a 20 mV resolution. Of the two power supplies (Dick Smith Ltd.) shown in Fig. 3.6, which could be set at either constant current (0-5 A) or constant voltage (0-30 V) output, one was for charge and the other for discharge. In all experiments constant current conditions were used. The currents for charge and discharge were set as required prior to cycling and monitored using digital multimeters. It was established that these power supplies exhibited negligible drift in the set current over many weeks of continuous operation.

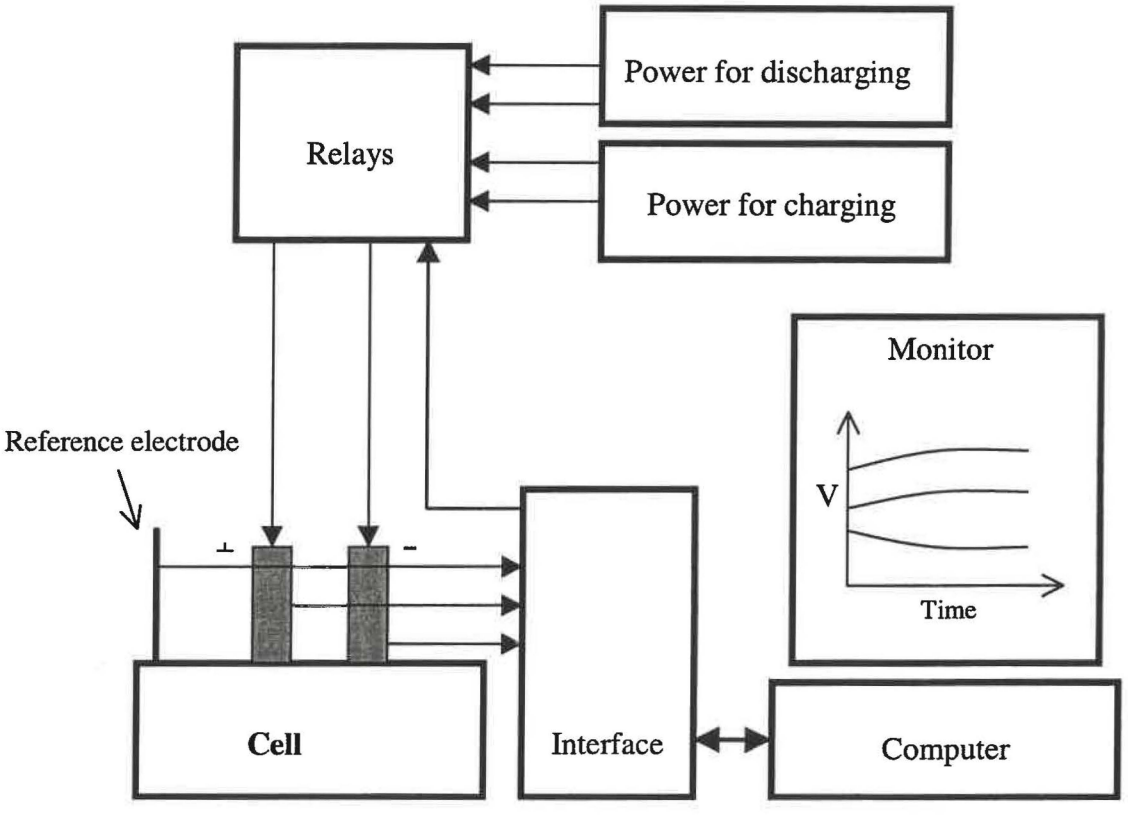

Fig. 3.5 Photograph and schematic diagram of the computer aided charge/discharge cycling system.

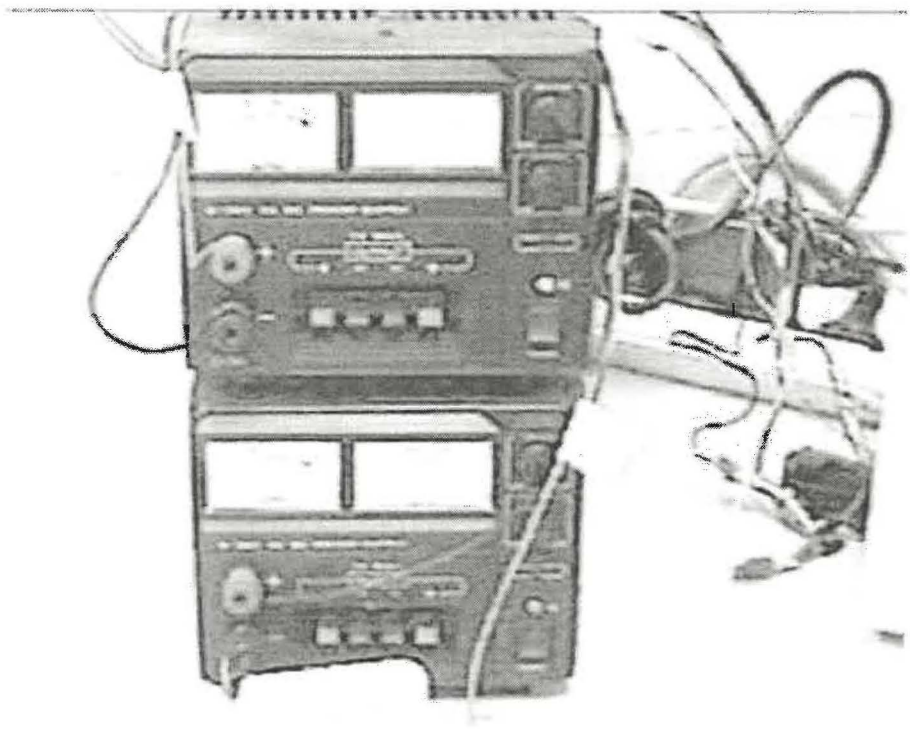

Fig. 3.6 Two power supplies for charge and discharge. These power supplies could either be set at constant current (0-5 A) or constant voltage (0-30V).

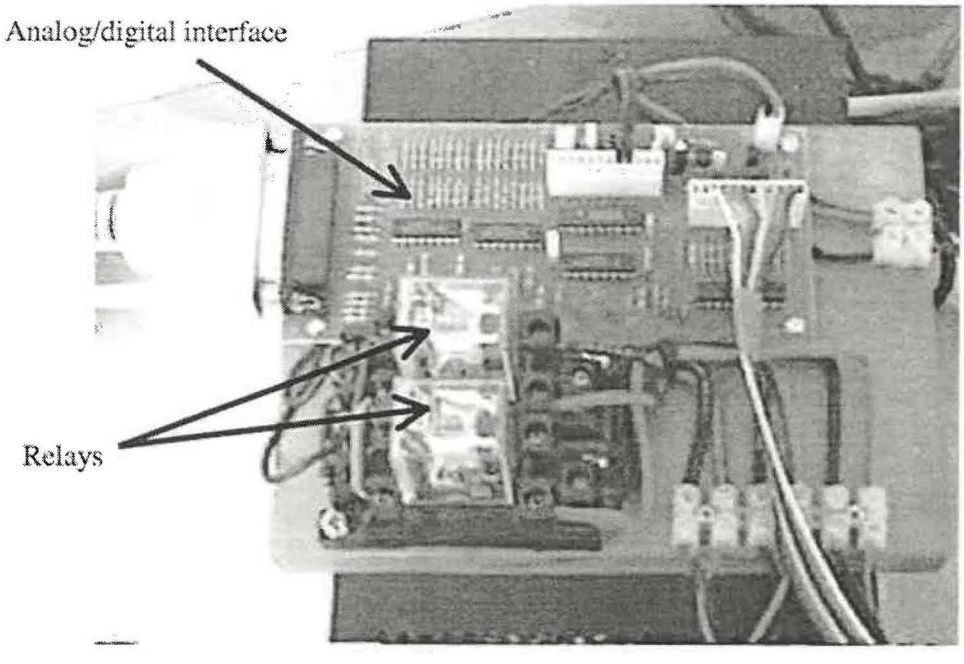

Fig. 3.7 The power relays and analog/digital interface.

Through the analog/digital interface, the computer could read and record the cell voltage and the potentials of the nickel and zinc electrodes. This computer could give signals to switch the relays (double pole, double throw as shown in Fig. 3.7) upon achieving the set time, cell voltage or the electrode potential that had been input in the computer programs. Through the relays attached with the interface, the computer could set the power supplies to charging, discharging or open circuit for the cell as required for a particular cycle regime.

The cell voltage, E_{cell}, and nickel and zinc electrode potentials, E_{Ni} and E_{Zn} respectively, were plotted as a function of time on the monitor screen during cycling so that the trends in cell behaviors became immediately apparent. In addition to this plot, the cell voltage and the electrode potentials, time elapsed, cycle number, charging and discharging current, location in the regimen, cutting voltage, depth of discharge and the intervals for data reading were continuously displayed on the screen. Upon completing a charge/discharge cycle, all of the data recorded was saved as a unique file on the hard disk and then copied to the floppy disk permitting analysis of this data at a second computer without interruption of the cycling process.

The discharge process could be controlled either by time (discharge capacity) or by the cell voltage. Open circuit conditions were usually imposed after charge and discharge for examination of the cell voltage and electrode potentials after charge and discharge. Figure 3.8 shows a photograph of the screen display.

3.4 Cell Formation & Cycling

The cell (Cell #3.1) was filled with the 30% (w/w) KOH electrolyte and the electrodes were soaked for 10 hours. After soaking, the cell was subjected to two identical formation cycles under the following regime:

i) Charging at 160 mA for 10 hours (charging capacity was 1.6 Ah);

ii) 5 minutes at open circuit;

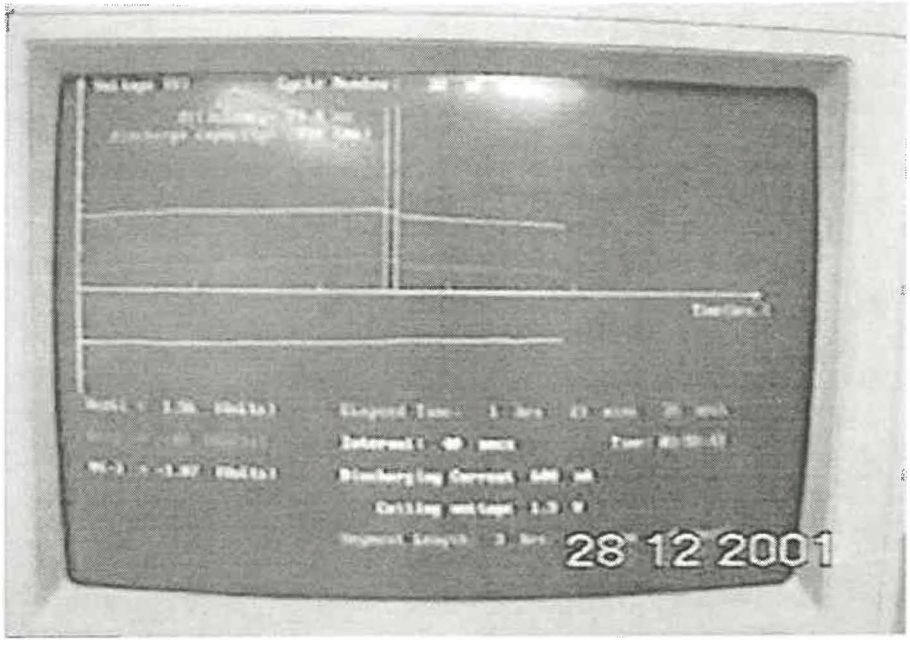

Fig. 3.8 Photograph of the screen displaying during charge/discharge cycling.

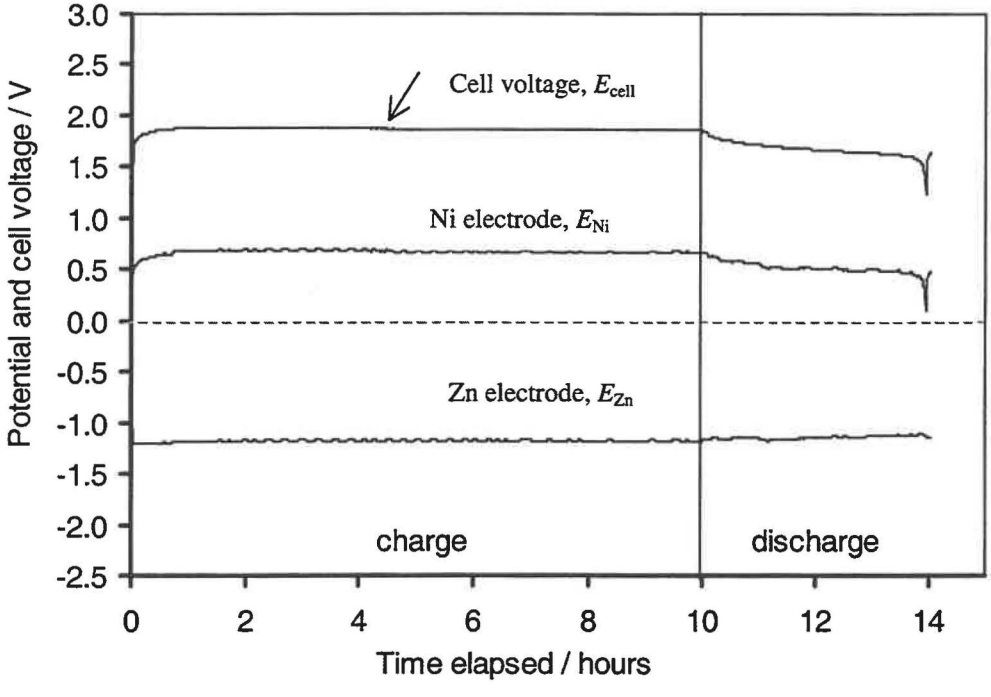

Fig. 3.9 The first formation cycle for Cell #3.1.

iii) Discharging at 160 mA until the cell voltage dropped below 1.3 V (discharge cutting voltage); followed by

iv) 5 minutes at open circuit prior to the next cycle.

The cell, electrode potentials and the time elapsed were recorded, displayed and stored every 40 seconds. Figure 3.9 shows the cell voltage and electrode potentials as a function of time during the first formation cycle. After 4 hours of charging there was a small drop in cell voltage, E_{cell}. In general, the cell voltage should progressively increase with time during charging. This small drop in potential (indicated by an arrow in Fig. 3.9) was likely caused by the development of an internal electrical short due to the growth of conducting zinc metal dendrites from the zinc electrode through the separator to the nickel electrode.

The variation of the potentials of both nickel and zinc electrodes with respect to the stainless steel reference electrode were successfully recorded during the first formation cycle. There were, however, simultaneous fluctuations in both nickel and zinc electrode potentials in the same direction which are ascribable to instability of the pseudo reference electrode. This was likely due to the surface state of the stainless steel wire incompletely approaching the equilibrium potential.

At the end of discharge, the typical rapid decline in cell voltage can be correlated with the change in potential for the nickel electrode, indicating that this was the capacity limiting electrode.

Figure 3.10 shows the potential profile for the second formation cycle of Cell #3.1. In comparison with the first formation cycle in Fig. 3.9, the reference electrode became more stable in this second formation cycle with smaller and less frequent fluctuations in potentials for both nickel and zinc electrodes. The zinc electrode potential remained relatively unchanged from the beginning to the end of charge demonstrating good charge acceptance and incomplete exhaustion of the ZnO active mass as expected given the large theoretical capacity (13.4 Ah). The nickel electrode potential increased at the beginning of

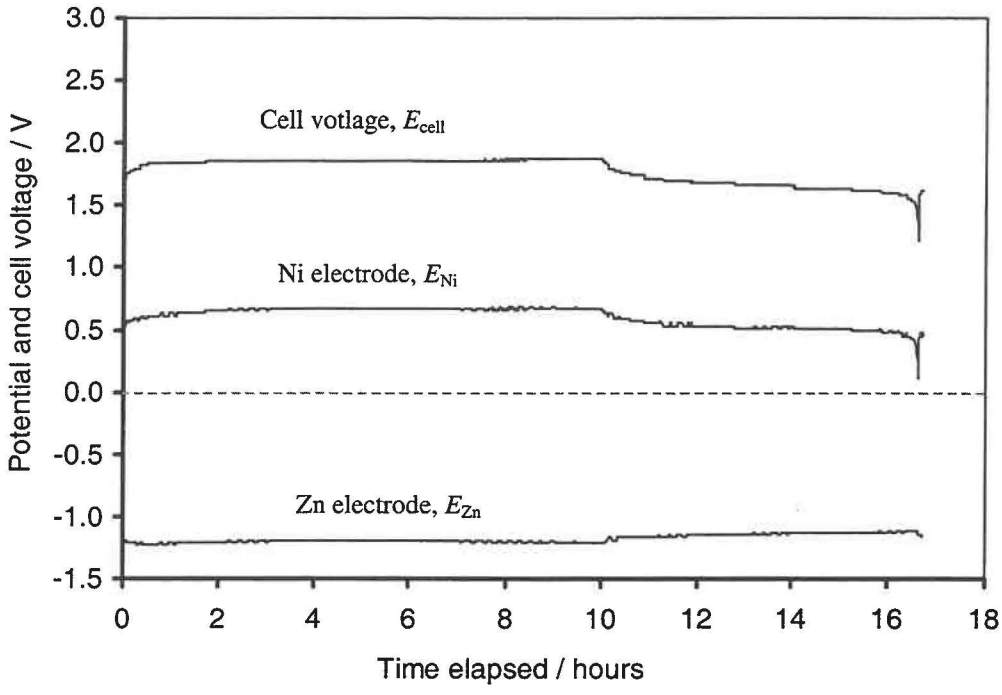

Fig. 3.10 The second formation cycle for Cell #3.1.

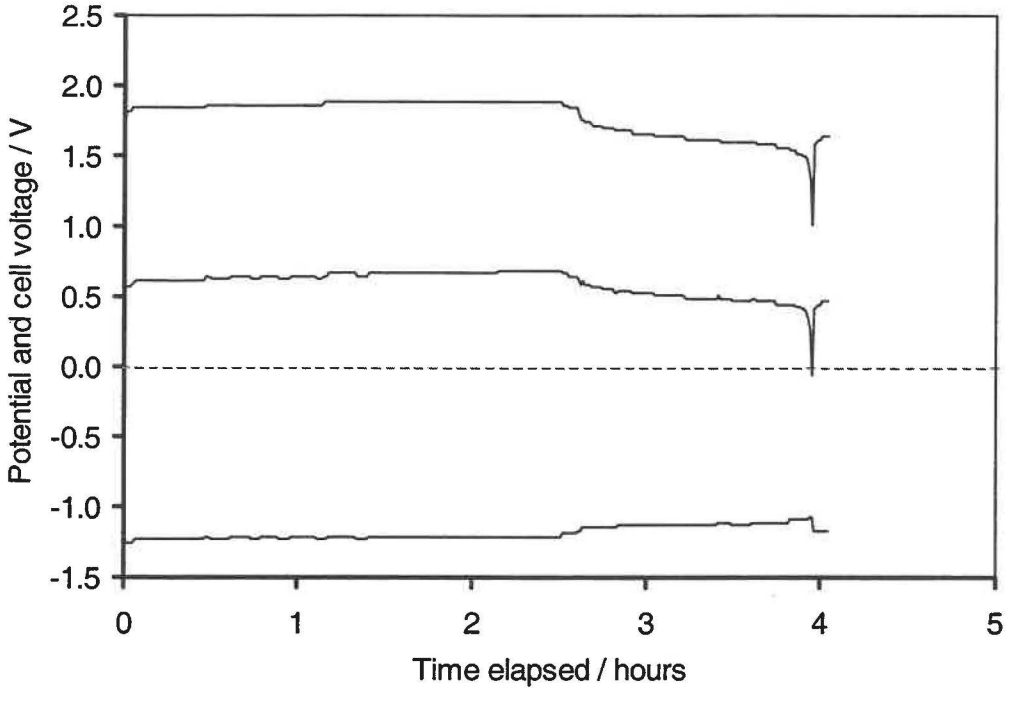

Fig. 3.11 The first regular charge/discharge cycle for Cell #3.1.

charge and consequently contributed to the cell potential increase.

The slight decline in the cell voltage during charge did not appear in the second formation cycle, suggesting that the dendrites formed during the first formation cycle may well have dissolved during the discharge process.

The discharge/charge efficiency provides a measure of the recyclability of the secondary battery. The efficiency for this constant current charge – constant current discharge is defined by

$$\% \text{ efficiency} = \frac{\text{discharge current} \times \text{discharge time}}{\text{charge current} \times \text{charge time}} \times 100\% \qquad (3.1)$$

The discharge/charge efficiency increased from 38.7% in the first formation cycle to 65.1% in the second formation cycle consistent with an increasing network of conductive pathways through the active mass of both the nickel and zinc electrodes.

By the end of discharge, the zinc electrode potential remained quite stable while the nickel electrode potential dropped rapidly, resulted in the cell voltage declining to the cutting voltage of 1.3 V. The nickel electrode was, therefore, the capacity limiting electrode. In the second formation cycle, the nickel electrode was fully discharged while the zinc electrode was partially discharged according to the zinc electrode potential by the end of discharge.

After two formation cycles, the cell was subjected to regular 1 Ah cycles with the regime given below:

i) Charging at 400 mA for 2.5 hours;

ii) 5 minutes at open circuit;

iii) Discharging at 600 mA until the cell voltage dropped to 1.3 V; followed by

iv) 5 minutes at open circuit prior to the next cycle.

The cell and electrode potentials were recorded, displayed and stored every 40 seconds. Figure 3.11 shows the potential profile for the first regular cycle. By comparison with the second formation cycle in Fig. 3.10, even fewer electrode potential fluctuations prevailed in this first regular cycle, indicating that the reference electrode had nearly approached an equilibrium. The zinc electrode potential remained unchanged during charge with only the nickel electrode contributing to the cell voltage increase. The unchanged zinc electrode potential suggested that it had been incompletely discharged in the formation cycles. The nickel electrode remained the capacity limiting electrode in this first regular cycle.

Figure 3.12 shows the efficiency as a function of cycle number for Cell #3.1. After the third cycle the cell operated at better than 92% for 30 cycles following which there was a rapid decline in performance so that after the 47^{th} cycle there was effectively no charge storage capacity in this cell.

The potential profile for the 32^{nd} cycle is shown in Fig. 3.13 where an efficiency of 90.4% was attained. It can be seen that the cell voltage dropped in the last 10 minutes of charging as indicated by an arrow, which is consistent with internal shorting caused by zinc dendrites. The formation of these dendrites led to the rapid failure of the cell. The nickel electrode was more sensitive to the dendrites with its potential dropped, resulting in the cell voltage dropped. In contrast to the nickel electrode, the zinc electrode potential did not respond to the dendrites due to its higher capacity and better charge acceptance in the previous cycles. This is confirmed indirectly during the discharge where the nickel electrode was the capacity limiting electrode for this cycle.

Figure 3.14 shows the potential profile for the 49^{th} cycle where the cell failed completely. The internal shortage was so significant that the cell was unable to accept any charge during the charging process as evidenced by the low cell potential. In earlier cycles, the end

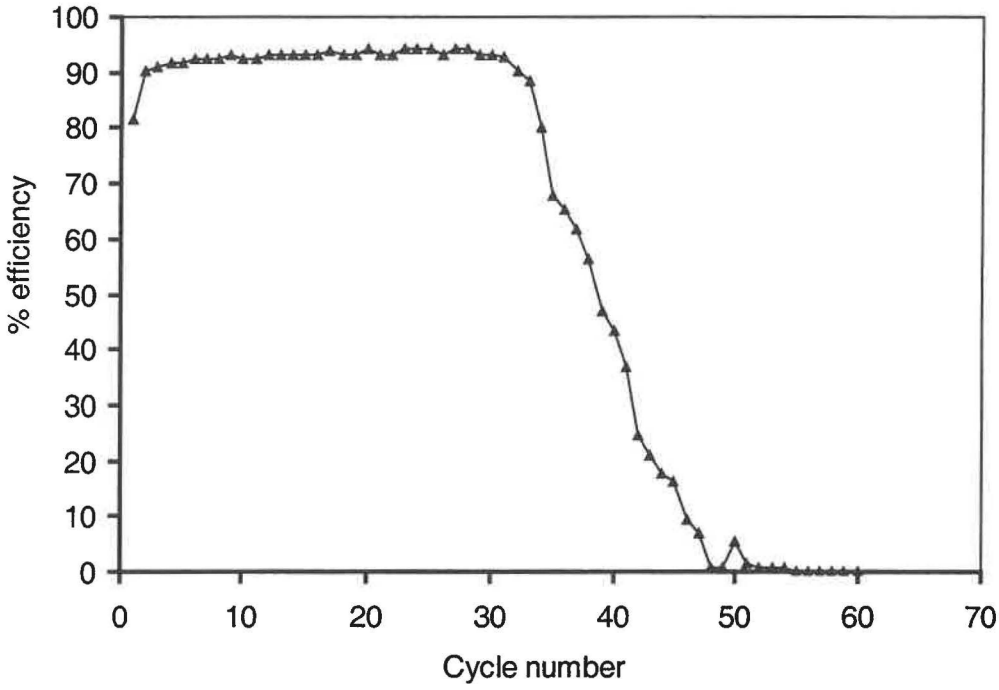

Fig. 3.12 Variation of discharge/charge efficiency as a function of the cycle number for Cell #3.1.

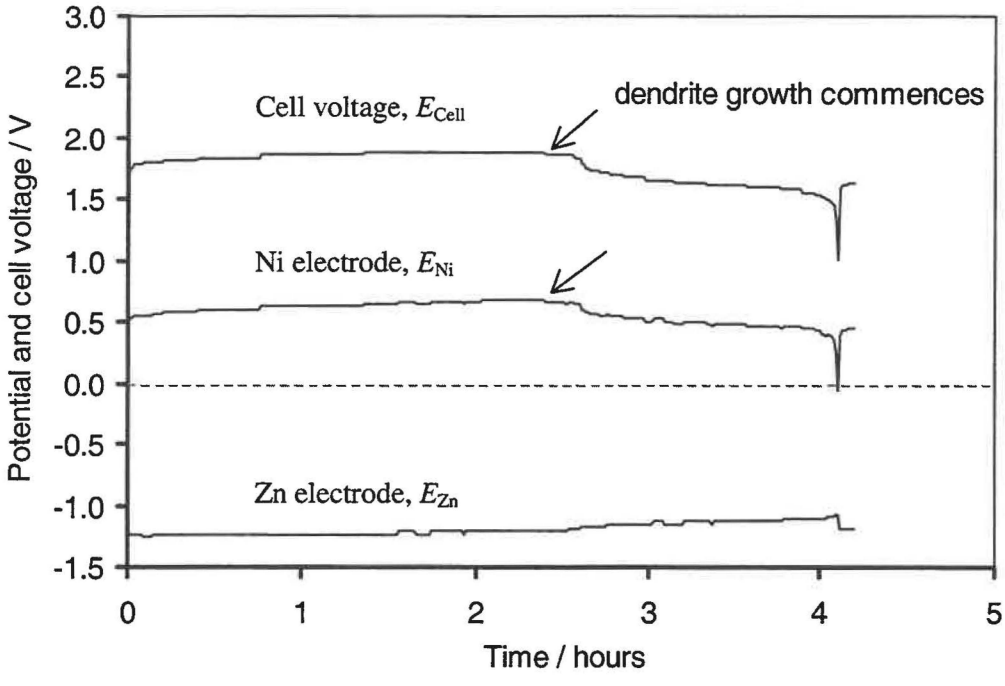

Fig. 3.13 Cycle 32 where small delines in E_{cell} at the end of charge are consitent with dendrite growth for Cell #3.1.

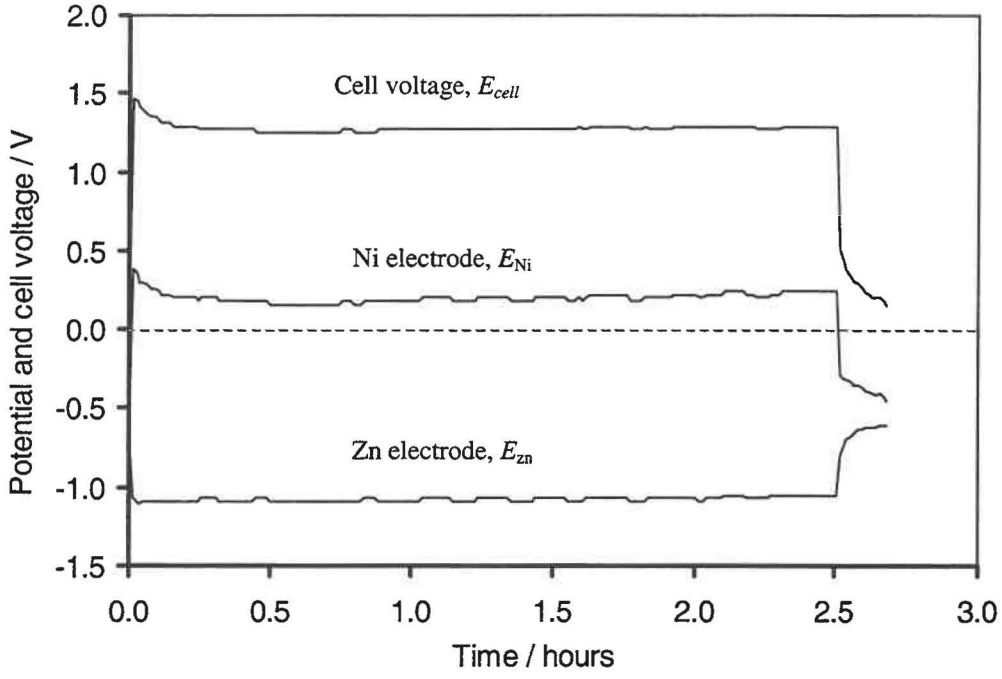

Fig. 3.14 Cycle 49 for Cell #3.1where no discharge capability was evident.

of charge cell voltage was typically 1.89 V with the initial cell voltage in excess of 1.7 V in the first 34 cycles. In contrast, during this last cycle the cell voltage commenced at 1.5 V but then rapidly fell to 1.25 V due to pronounced electrical shorting between the two electrodes. Consequently, the discharge/charge efficiency was effectively zero in this cycle.

The testing of Cell #3.1 demonstrated that the cycling system was reliable and met the needs of the nickel zinc cell cycling. Six sets of the same cycling system were constructed, so that more cells could be cycled simultaneously.

When the cell failed, solid white zinc active mass was observed to have diffused and filled the woven nylon separators that enclosed the zinc electrodes. Some of the white active mass had also redistributed throughout the electrode assembly so that opaque deposits of ZnO or $Zn(OH)_2$ were located at the bottom of the cell. The clear electrolyte became cloudy when the electrolyte was moved with turning the cell as shown in Fig. 3.15. In order to examine what had happened inside the cell, Cell #3.1 was disassembled.

It was found that zinc active mass had diffused into and through the separators with some white zinc active material covering the surface of the nickel electrode. The zinc active mass became a loose mass and no longer adhered to the brass mesh as it had been during application.

The cell failed because of the internal shortage caused by zinc dendrites. However, it was not possible to ascertain whether the dendrites were from deposition of zincate from the electrolyte or from the direct reduction of the zinc oxide and zinc hydroxide that had diffused and remained in the separators. It was possible that dendrites were from either the reduction of both zincate in the electrolyte or the reduction of solid zinc active mass, a mixture of zinc oxide and zinc hydroxide that had diffused into the separators. In order to understand the differences in reduction between zincate, zinc oxide and zinc hydroxide, it is necessary to investigate the reduction behaviours of zincate, solid zinc oxide and zinc hydroxide, which is correlated with the zinc dendrite initiation and growth.

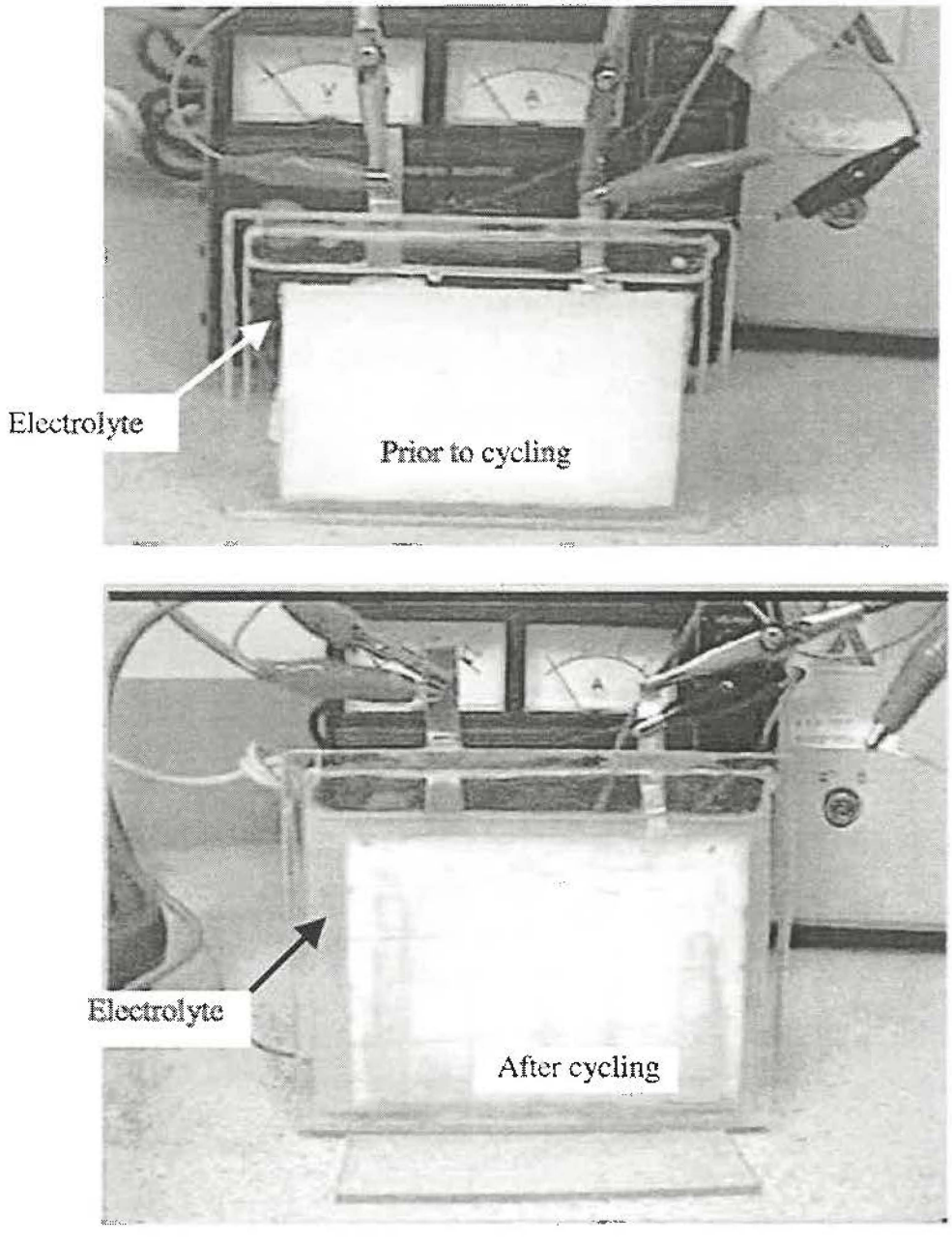

Fig. 3.15 Redistribution of zinc active mass through Cell #3.1.

The zinc active mass resembled the paste when zinc oxide was mixed with water before pasting onto the brass mesh. It seems that the zinc active mass, which should be a mixture of zinc oxide and zinc hydroxide during and after cycling, could not remain bound. The solubility of the zinc active mass in alkaline electrolytes may account for the weakened binding in the zinc active mass during and after cycling. The alkaline electrolyte, which can dissolve ZnO and $Zn(OH)_2$, has greater accessability to the boundaries between zinc active mass particles so that the preferential dissolution here may result in weakening the binding between these particles, causing dispersion of zinc active mass in the electrolyte. This assumption was confirmed with a simple test.

Zinc active mass identical to that used in Cell #3.1 was pasted onto single layer of brass mesh and was pressed with a bench top vice to squeeze excess water out. The pasted brass mesh was placed in 30% KOH solution in a beaker. After several minutes, all of the zinc active mass was shed from the brass mesh and sank at the bottom of the beaker without distinct dissolution in the electrolyte. Apparently, the binding between zinc active mass particles is destroyed by the infiltrating alkaline electrolyte.

3.5 Conclusions

The computer controlled cycling equipment including the hardware and software had been tested, and shown to be stable and reliable and met all the needs as designed. The cell voltage and the potentials of nickel electrode and zinc electrode, which are associated with state of the cell and the electrodes, were displayed on the screen *in situ* while the cell being cycled. The data in each cycle was recorded with the computer in the hard disk and floppy disk for further investigation.

The reference electrode comprising a stainless wire has been successfully tested as the simplest but reliable reference electrode that can be readily built in the Ni-Zn cell cases for monitoring the nickel and zinc electrode potentials. In the future work, each of the cells would have such a robust reference electrode.

The Ni-Zn cell failed because of zinc dendrites. It was not possible to identify whether the dendrites were from the reduction of zincate in the electrolyte or from the reduction of solid zinc hydroxide that had diffused in the separators. The differences in reduction behaviors between aqueous zincate, solid zinc oxide and zinc hydroxide required investigation. These results will be reported in Chapter 4.

The phenomenon of zinc electrode shape change was evident with gross diffusion of the white solid zinc active mass. After cycling, the initial solid zinc active mass adhered in the brass mesh became a loose mass, some of which diffused and filled the separators and even diffused into the electrolyte. The accessability of the alkaline electrolyte to the zinc electrode, which partially dissolves the zinc active mass, particularly at the boundaries of zinc particles, was the main cause for the gross diffusion. The binding between zinc particles was significantly weakened with dissolving. The accessability of the alkaline electrolyte to the zinc electrode must be restricted as to retard the gross diffusion of zinc active mass, which is associated with the zinc electrode shape change and the zinc dendrites initiation and growth. The work on restricting the accessibility of the alkaline electrolyte leading to nickel zinc cells with much prolonged cycle life will be reported in Chapter 5 and Chapter 6.

Chapter Four Electrolyte modification

4.1 Introduction

It has been proposed that it is the high solubility of zincate in alkaline solution and the propensity for the formation of zincate super-saturated electrolyte solutions during discharge that are strongly associated with shape change and dendrite growth [70]. Most of the previous investigations have focused on addition of $Ca(OH)_2$ in the zinc electrode to decrease the solubility of zinc active mass through the formation of insoluble calcium zincate [32-35, 38, 67, 72-74, 75-77, 78-86]. Some others have also explored the use of lower KOH concentration electrolytes to avoid appreciable zincate solubility [34, 95-102]. Use of these electrolytes, however, results in higher internal resistance and inferior nickel electrode performance.

In contrast to ZnO or $Zn(OH)_2$ in the zinc electrode, $Cd(OH)_2$ (the active mass of the cadmium electrode in Ni-Cd cells) is insoluble even in highly alkaline electrolyte. This could be the main reason for why the Ni-Cd cells are free from the problems with the electrode shape change and dendrite growth and may account for the differences in cycle performance between the Ni-Zn and Ni-Cd cells.

Since the charge acceptance of zinc active materials approaches almost 100% [23], no attention has been paid to the reduction characteristics of these zinc active materials, such as ZnO and $Zn(OH)_2$, in Ni-Zn cells during charge. The zinc active materials Zn(s), ZnO(s), $Zn(OH)_2$(s) and $Zn(OH)_4^{2-}$(aq) coexist at the zinc electrode. During charging, they are reduced simultaneously at the zinc electrode, but there must be a competition in reduction rates between ZnO(s), $Zn(OH)_2$(s) and $Zn(OH)_4^{2-}$(aq). Consequently, additives which promote the reduction of ZnO(s) and $Zn(OH)_2$(s) and/or decrease the rate of $Zn(OH)_4^{2-}$(aq) reduction could potentially be employed to inhibit or even prevent dendrite growth and shape change. The charging reactions for these species are

$$Zn(OH)_2(s) + 2e^- \longrightarrow Zn(s) + 2OH^-(aq) \qquad E^\circ = -1.249\ V \qquad (4.1)$$

$$Zn(OH)_4^{2-}(aq) + 2e^- \longrightarrow Zn(s) + 4OH^-(aq) \qquad E^\circ = -1.199\ V \qquad (4.2)$$

$$ZnO(s) + H_2O(aq) + 2e^- \longrightarrow Zn(s) + 2OH^-(aq) \qquad E^\circ = -1.260\ V \qquad (4.3)$$

According to these standard reduction potentials [121], $Zn(OH)_4^{2-}(aq)$ may be reduced more readily than ZnO(s) and $Zn(OH)_2(s)$ during charge.

During charge or after charge, the electrolyte becomes unsaturated with respect to zincate due to this possible preferential reduction of zincate. This promotes the dissolution of Zn(s), ZnO(s) and $Zn(OH)_2(s)$ in the electrolyte via the following reactions.

$$Zn(s) + 2H_2O(aq) \longrightarrow Zn(OH)_2(s) + H_2(g) \qquad (4.4)$$

$$ZnO(s) + H_2O(aq) \longrightarrow Zn(OH)_2(s) \qquad (4.5)$$

$$Zn(OH)_2(s) + 2OH^-(aq) \rightleftharpoons Zn(OH)_4^{2-}(aq) \qquad (4.6)$$

These dissolution processes are one means by which shape change takes place – those solid phases dissolve as zincate and then become re-deposited during zincate reduction elsewhere on the zinc electrode plates during charging. Some of the zincate reduced may also contribute to the formation and propagation of zinc dendrites. Provided that the electrochemical reduction of $Zn(OH)_4^{2-}(aq)$ is inhibited or prevented by some means, the zinc dendrite growth, the extent of Zn(s), ZnO(s) and $Zn(OH)_2(s)$ dissolution from the zinc electrode and hence shape change will also be diminished as a consequence.

In an attempt to search for the additives to retard the reduction of zincate without inhibiting the reduction of ZnO and zinc discharge products, the electrochemical behaviours of $Zn(OH)_4^{2-}(aq)$, ZnO(s) and other discharge products like $Zn(OH)_2$ were investigated and will be described in this chapter.

4.2 Solubility of zinc materials

The dissolution of ZnO in alkaline electrolyte is not only a thermodynamic process but also a kinetic process. Solubility of zincate is usually quoted in terms of the equivalent mass of ZnO. In a previous investigation [71], the electrolyte of 8.6 M KOH saturated with zincate was prepared from reagent grade 80 wt % KOH hydrated and ZnO with distilled deionized water. The concentration of zincate of this resulting solution was 5 wt % of ZnO. As mentioned in a review [16], the equilibrium solubility of ZnO increases from 6 g/L in 10 wt % KOH to 53 g/L in 30 wt % KOH solution. According to another description[70], the electrolyte super-saturated with zincate was only "100 ml of 31 wt % KOH with several grams of solid ZnO in it". This saturation was established visually – the electrolyte was deemed saturated with respect to zincate when no further ZnO dissolved in the electrolyte [70].

The solubility of ZnO(s) reported here was determined in a similar manner under the specified conditions. There was no attempt to establish the true thermodynamic solubility at equilibrium. It may be that supersaturated solutions were formed on occasion but, if so, these remained in the soluble state for many months as would be required in a practical nickel-zinc battery. The zinc content of each solution was determined using Atomic Absorption Spectroscopy (AAS).

First, the effect of temperature on apparent solubility of ZnO was established. Excess solid ZnO powder was stirred in 30 wt % of KOH solution in 200 mL covered plastic beakers for 24 hours at the stated temperature, filtered, and then analysed by AAS. At 27°C the solubility of ZnO was found to be 47.0 g/L whilst at 97°C it was 37.6 g/L.

It was found that metallic Zn powder could react in both the above filtered electrolytes, as evidenced by the evolution of hydrogen via the reaction

$$Zn\,(s) + 2H_2O(l) \longrightarrow Zn(OH)_2(s) + H_2\,(g) \qquad (4.7)$$

followed by

$$Zn(OH)_2(s) + 2OH^-\,(aq) \rightleftharpoons Zn(OH)_4^{2-}(aq) \qquad (4.8)$$

The absence of white solid $Zn(OH)_2$ passivating the zinc powder suggested that both the 27°C and 97°C incubated electrolytes were not actually or completely saturated with respect to zincate or $Zn(OH)_2(s)$. Excess zinc powder with some sponge Ni as a catalyst for the Zn dissolution via hydrogen evolution at nickel surface was added into each of the two filtered electrolytes described above. These were stirred at the original incubation temperatures for 24 hours by which time in each case white $Zn(OH)_2(s)$ was observed on the surface of the zinc powder with the cessation of hydrogen evolution. Analysis by AAS showed that using this method, the solubility at 97°C had increased from 37.6 to 54.7 g/L and at 27°C from 47.0 to 60.0 g/L with respect to ZnO.

In order to increase the initial solubility or concentration of zincate in the electrolyte used for Ni-Zn cells, addition of excess ZnO is not sufficient – excess zinc powder and metallic nickel as a catalyst should be added to the electrolyte until white $Zn(OH)_2(s)$ is formed. This saturation of zincate will not only prevent dissolution of the discharge product $Zn(OH)_2(s)$ via reaction (4.8), but also prevent the self-discharge of the charged zinc electrode via reaction (4.7).

4.3 Reduction of $Zn(OH)_4^{2-}$, ZnO and the electrode discharge products

It would seem that the high solubility of zincate in the strongly alkaline electrolyte is associated with zinc electrode shape change and dendrite growth. Dendrites are believed to arise from reduction of $Zn(OH)_4^{2-}(aq)$ onto one face of the zinc metal crystals during charge so that long needles of conducting material form.

Electrolyte saturated with zincate at the end of discharge will become unsaturated during charge due to the removal of $Zn(OH)_4^{2-}(aq)$ from the electrolyte by reduction. Also during or after charge, Zn, ZnO(s) and $Zn(OH)_2(s)$ located at the zinc electrode will partially dissolve in the zincate-unsaturated electrolyte. The electrochemical reduction of ZnO(s) and $Zn(OH)_2(s)$ will also influence the reduction of $Zn(OH)_4^{2-}(aq)$. The overall rate of $Zn(OH)_4^{2-}(aq)$ reduction will be the result of competition in reduction between ZnO(s), $Zn(OH)_2(s)$ and $Zn(OH)_4^{2-}(aq)$ together with the rates of Zn, ZnO(s) and $Zn(OH)_2(s)$ conversion to $Zn(OH)_4^{2-}(aq)$. These processes rely not only on the thermodynamics but also on the heterogeneous kinetic processes. The standard

reduction potentials can only be used to describe their difference in reduction possibilities, rather than their reduction rates.

It is beyond the scope of this project to establish electrode kinetics for each of these reactions. Instead, the goal is to establish phenomenologically the means by which shape change and dendrite growth on practical nickel-zinc cells may be eliminated.

Linear Sweeping Voltammetry (LSV) was employed to provide a means for studying the reduction behaviour of $Zn(OH)_4^{2-}(aq)$, ZnO(s) and zinc discharge products. This technique, whilst in no way mimicking the potential-time profile arising in practical cells, provides a rapid means for establishing the potential region in which each electrode process takes place.

4.3.1 Reduction of $Zn(OH)_4^{2-}(aq)$

The working electrode was a cast zinc (Lot No.740510, Peking Chemical Works, P.R.China) cylinder 8 mm in diameter shrouded with a PVC holder so that only the end face of the cylinder was exposed to the electrolyte. The reference electrode was an Ag/AgCl filled with 3 mol/L NaCl (Bioanalytical Systems Inc., Indiana, USA) with an extra bridge to give a potential of +197 mV vs SHE. The counter electrode was a platinum wire (area 1 cm^2). A schematic diagram for the test cell is shown in Fig. 4.1. The electrochemical experiments were controlled by a BAS 100B/W digital potentiostat (Bioanalytical Systems Inc., Indiana, USA). LSV experiments were conducted with a static working electrode facing upwards in a quiescent electrolyte at 20°C.

A saturated zincate solution (60.0 g/L of ZnO) in 30% KOH was prepared using the method described in Section 4.2. Figure 4.2 shows the reduction characteristics of $Zn(OH)_4^{2-}(aq)$ during linear sweep voltammetry. The single sweep commenced at -1510 mV vs Ag/AgCl where reduction of zincate commenced and then was swept to -2010 mV vs Ag/AgCl.

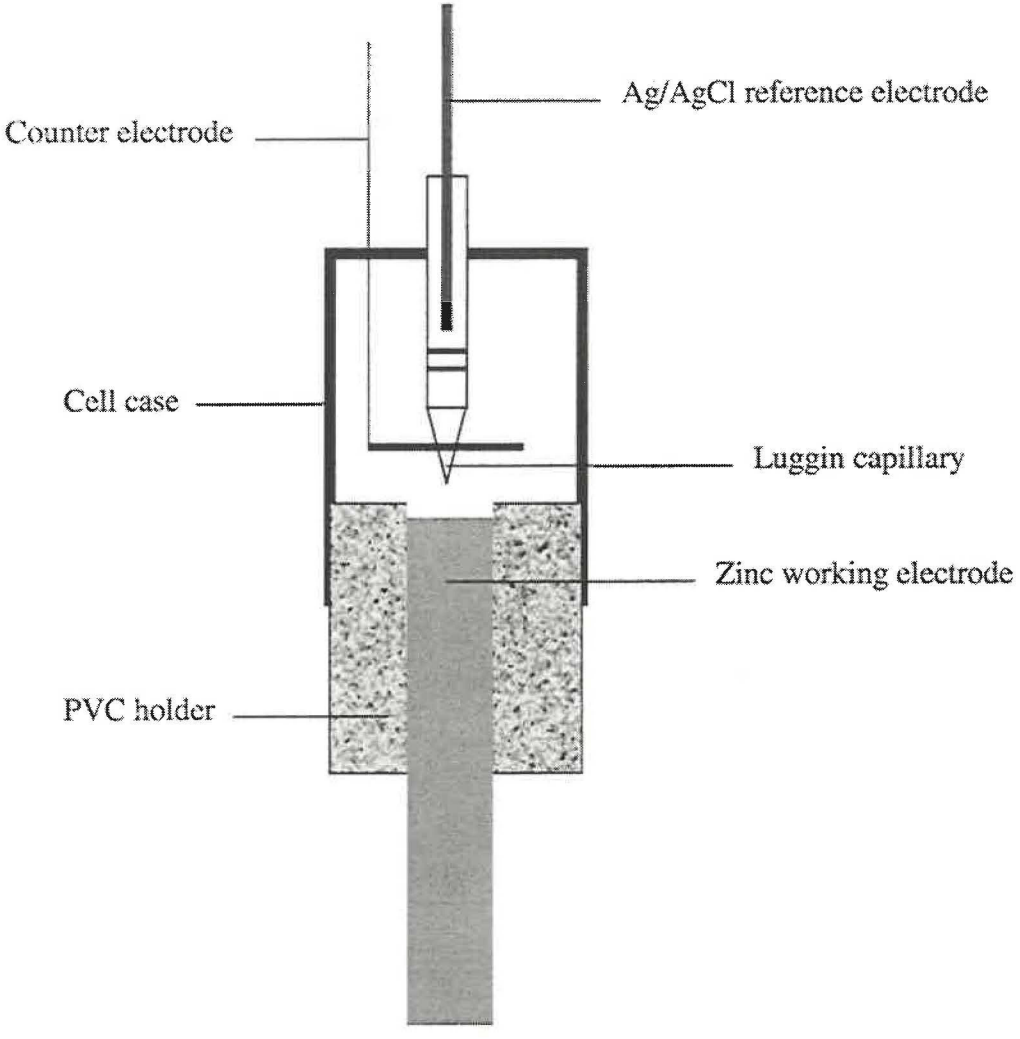

Fig. 4.1 Schematic diagram of the testing cell for investigating the reduction of zincate, ZnO and zinc discharge products.

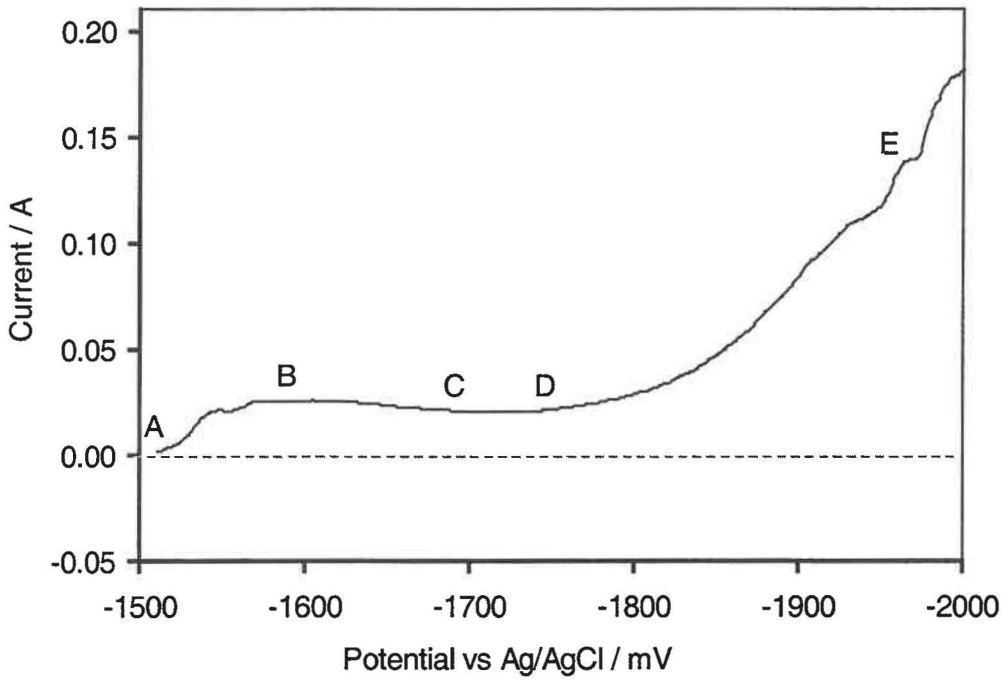

Fig. 4.2 Cathodic polarization of a zinc metal electrode in 7 M KOH saturated with respect to zincate (60 g/L of ZnO).

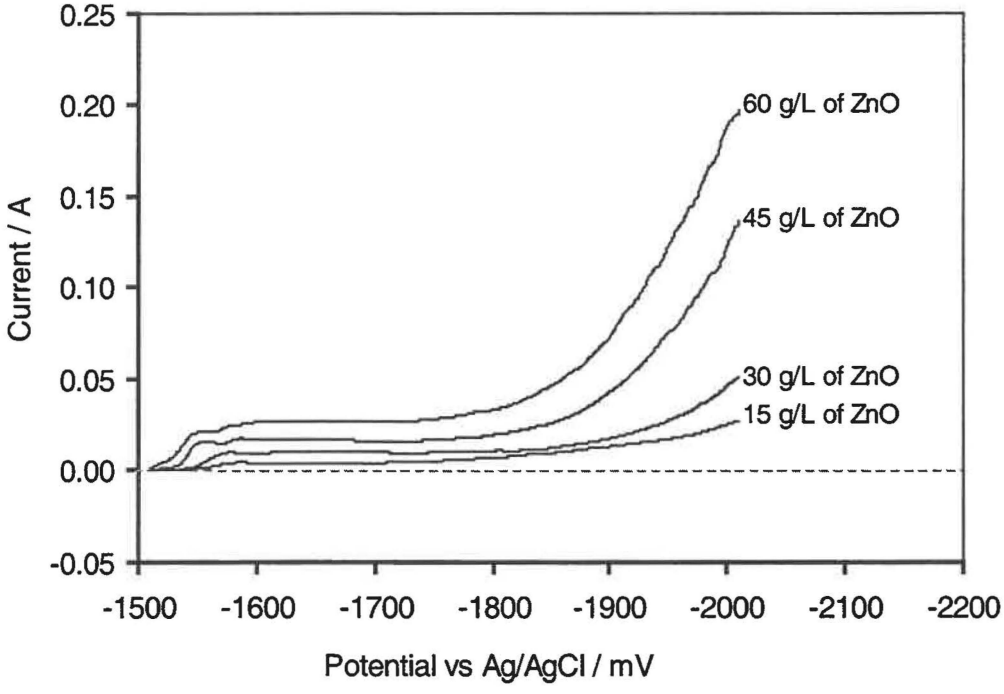

Fig. 4.3 Effect of zincate concentration on the cathodic polarization of a zinc metal electrode in 7 M KOH.

The cathodic polarization curve may be considered as consisting of four parts with start and end points labelled on the plot.

First the segment from A to B is where the reduction rate of the $Zn(OH)_4^{2-}(aq)$ increased with more negative potentials indicating charge-transport control. There is some evidence for nucleation and growth phenomena in this region with peaks at –1545 and –1570 mV vs Ag/AgCl. The study of this nucleation and growth behaviour falls outside the scope of this project and will not be discussed in any further detail. From B to C, the rate of $Zn(OH)_4^{2-}(aq)$ reduction decreased slightly due to exhaustion of $Zn(OH)_4^{2-}(aq)$ ions in the near vicinity of the electrode. In segment C to D, the current remained stable with no H_2 evolution evident, which suggested that the reduction rate of $Zn(OH)_4^{2-}(aq)$ may be controlled by the diffusion rate of $Zn(OH)_4^{2-}(aq)$ from the bulk of the electrolyte to the working electrode surface. At point D, H_2 began to evolve with visible gas bubbles departing the electrode. From D to E, H_2 evolution occurred together with the reduction of $Zn(OH)_4^{2-}(aq)$, the former increasing exponentially with more negative potentials.

In a quiescent solution the reduction of zincate would be expected to be maintained at the diffusion limiting rate observed in segment C to D. However, the forced convection afforded by H_2 bubble movement promoted the replenishment of $Zn(OH)_4^{2-}(aq)$ to the electrode surface so that the reduction rate for zincate depended in part on the rate of H_2 evolution.

If segment C to D represents a diffusion-controlled process, then this region should exhibit concentration dependence. According to Fick's first law of diffusion [121], the flux of $Zn(OH)_4^{2-}(aq)$, J, is proportional to the concentration gradient of $Zn(OH)_4^{2-}(aq)$, dc/dx, at the electrode surface.

$$J = -D \cdot dc/dx \qquad (4.9)$$

If it is assumed that in this region the concentration of zincate at the electrode surface is zero, then dc/dx should be directly proportional to the bulk concentration. The effect of concentration of $Zn(OH)_4^{2-}(aq)$ on the reduction rate of $Zn(OH)_4^{2-}(aq)$ in LSV was

investigated to test this hypothesis.

Figure 4.3 shows the reduction characteristics of $Zn(OH)_4^{2-}(aq)$ for a range of zincate concentrations during linear sweep cathodic polarization. The reduction rate of $Zn(OH)_4^{2-}(aq)$ controlled by diffusion increased with the concentration of $Zn(OH)_4^{2-}(aq)$. Figure 4.4 shows the effect of $Zn(OH)_4^{2-}(aq)$ concentration on the reduction rate of $Zn(OH)_4^{2-}(aq)$ controlled by diffusion at –1700 mV (selected as a midway point for segment C to D). The reduction rate of $Zn(OH)_4^{2-}(aq)$ was linear with zincate concentration, in accordance with the Fick's first law of diffusion, although this trend did not pass through the origin as might have been expected. In region D to E where H_2 evolution occurred simultaneously with reduction of $Zn(OH)_4^{2-}(aq)$, the total current is far from linear with $Zn(OH)_4^{2-}(aq)$ concentration due to the forced convection by hydrogen evolution.

It can be seen in Fig. 4.3 that the point at which reduction commenced was not altered by zincate concentration. The likely nucleation and growth peaks do alter, moving to more cathodic potentials with lower zincate concentrations.

Upon consideration of Fick's First Law, the flux of zincate to the electrode can be decreased not only by decreasing the zincate concentration, but also by increasing the diffusion coefficient. The diffusion coefficient is determined by the hydrodynamic radius for the diffusing species according to the Stokes-Einstein relationship

$$D = \frac{kT}{6\pi\eta a} \tag{4.10}$$

where k is the Boltzmann constant, T the temperature (K), η, the absolute viscosity (N s m^{-2}) and α is the radius (m), a fixed, although temperature dependent parameter, for a given species. If the composition of the diffusing species were to be altered, by for example forming a strong ion-pair between zincate and a large cationic species, then D could be decreased. The more convenient method for decreasing the diffusion coefficient is to increase the viscosity of the electrolyte.

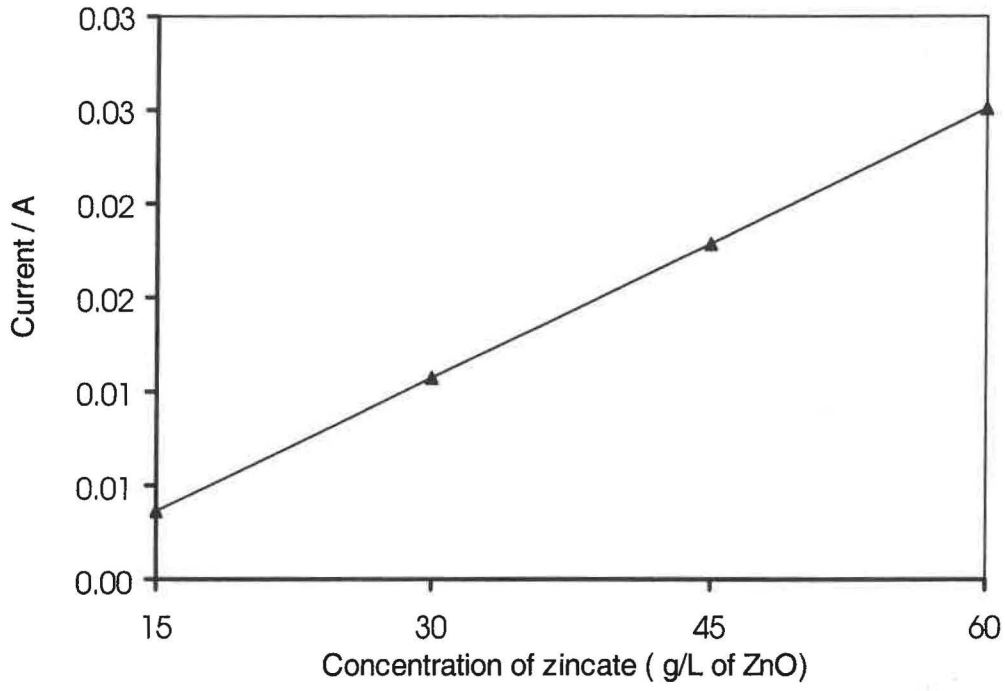

Fig. 4.4 Effect of zincate concentration on the diffusion controlled reduction rate of zincate at a zinc metal electrode in 7 M KOH at –1700mV vs Ag/AgCl during the LSV experiment shown in Fig. 4.2.

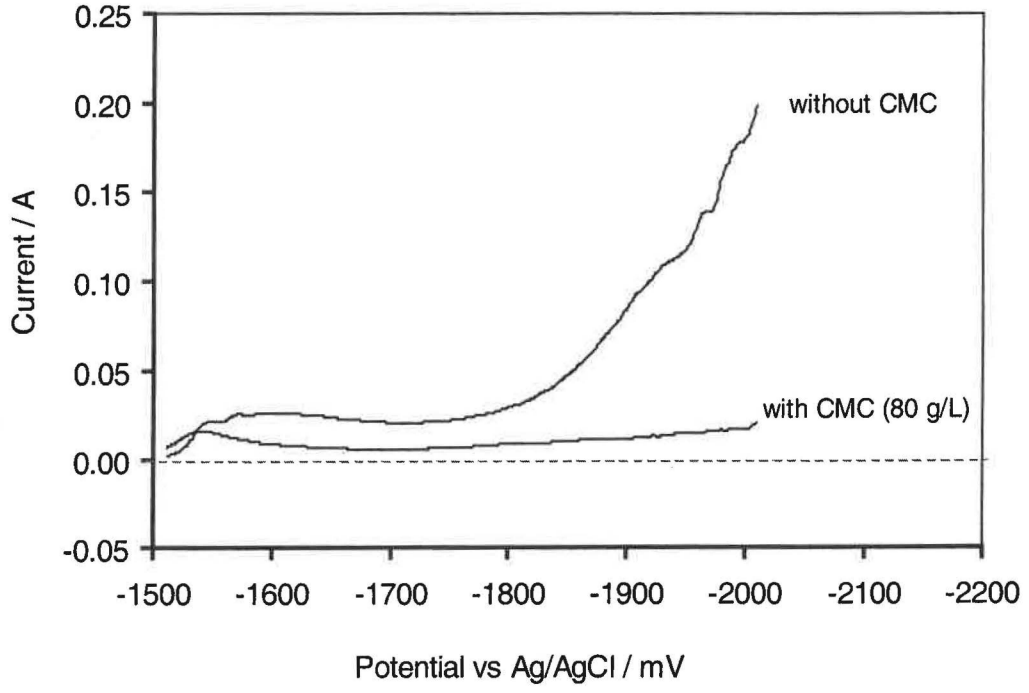

Fig. 4.5 Effect of CMC on the cathodic polarization of a zinc metal electrode in 7 M KOH saturated with respect to zincate (60 g/L of ZnO).

The sodium salts of carboxymethylcellulose (CMC) are gel additives often used for primary alkaline manganese batteries to immobilize the electrolyte for prevention of leakage [1]. Addition of CMC to the electrolyte may also act to decrease the diffusion coefficient *D* of $Zn(OH)_4^{2-}$ and therefore reduce the flux of $Zn(OH)_4^{2-}$(aq) and its reduction rate during cathodic polarization in this case.

Figure 4.5 shows voltammograms in the presence and absence of CMC (80 g/L) in 60.0 g/L ZnO saturated 30% KOH. The addition of CMC produces a voltammogram similar to the original LSV but lower in magnitude. In segment A to B, the reduction rate of the $Zn(OH)_4^{2-}$(aq) was decreased in the presence of CMC and the nucleation and growth peaks were shifted to less cathodic potentials. The first reduction also commenced at less cathodic potentials.

In segments B to C where a depletion in zincate develops in the vicinity of the electrode, this decline is more pronounced in the presence of CMC. This is consistent with the impaired ability of the diffusing species to move through a more viscous electrolyte.

As in the absence of CMC, from C to D, the current remained stable, although at a much lower value than that with the electrolyte free from CMC. This again suggests that the reduction rate of $Zn(OH)_4^{2-}$(aq) was controlled by the lower diffusion rate of $Zn(OH)_4^{2-}$(aq) from the electrolyte to the working electrode surface. At D, H_2 began to evolve but at a lower rate than in the less viscous electrolyte.

The H_2 evolution induced forced convection region from D to E is far less pronounced in the presence of CMC consistent with the increased viscosity. This more viscous system inhibited not only the movement of zincate but also markedly hindered the movement of H_2 vertically through the electrolyte.

Figure 4.6 shows the effect of varying the CMC concentration on the reduction of zincate.

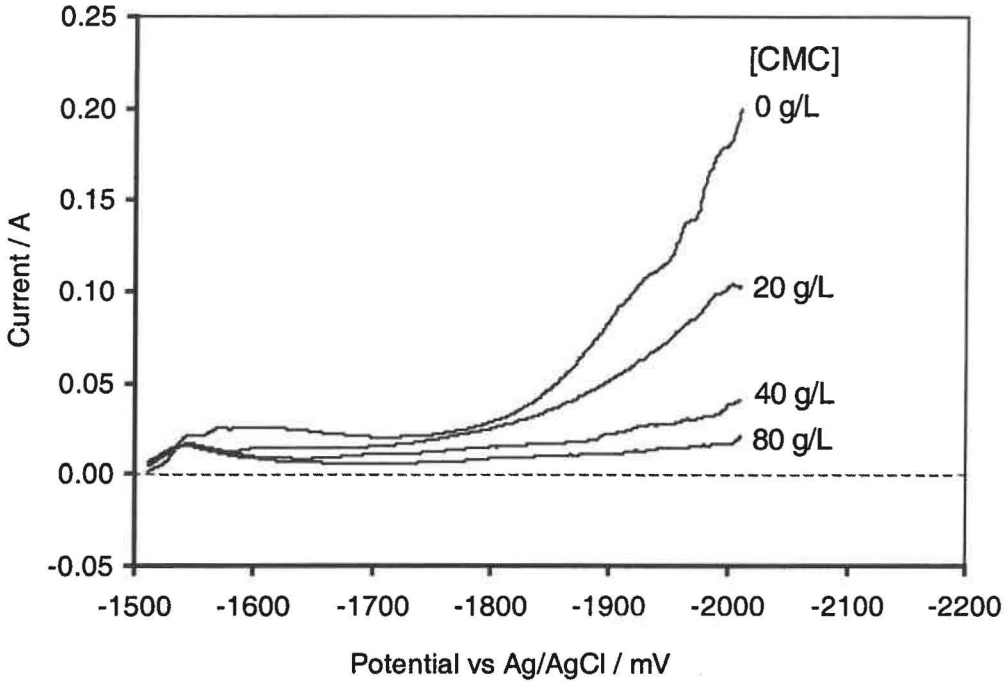

Fig. 4.6 Effect of CMC concentration on the cathodic polarization of a zinc metal electrode in 7 M KOH saturated with respect to zincate (60 g/L of ZnO).

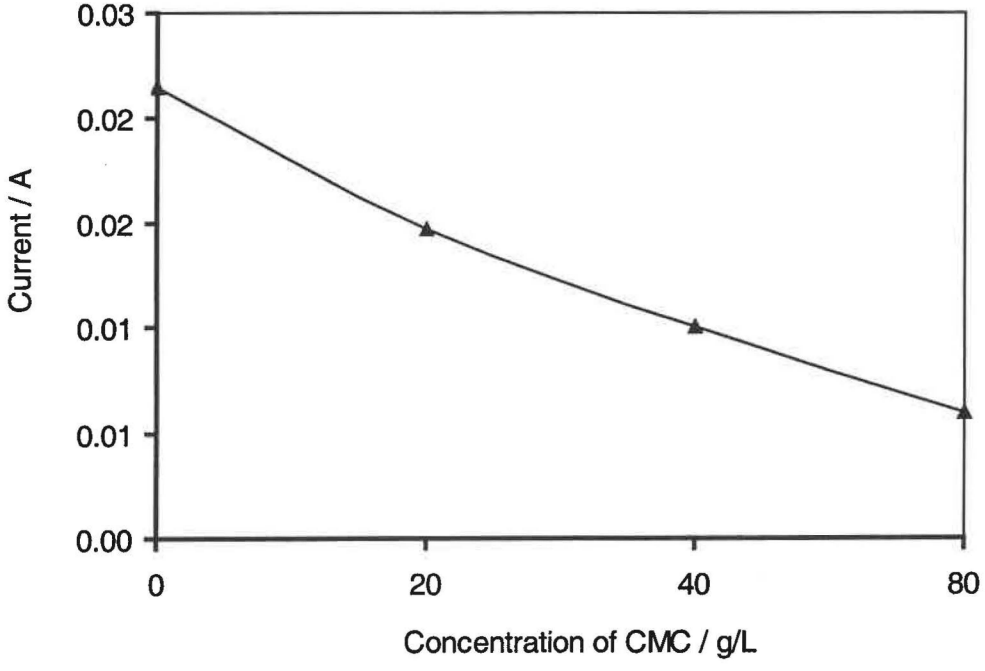

Fig. 4.7 Effect of CMC concentration on the diffusion controlled reduction rate of zincate at a zinc metal electrode in 7 M KOH saturated with respect to zincate (60 g/L of ZnO).

First, there is little effect on segment A to B. In contrast, the diffusion controlled reduction of $Zn(OH)_4^{2-}(aq)$ was substantially decreased with increasing CMC concentrations. The overall rate of reduction in region D to E markedly decreased which may suggest that the H_2 evolution was also suppressed in the presence of CMC to a greater extent than expected by diffusion or convection.

Figure 4.7 shows the effect of CMC concentration on the rate of $Zn(OH)_4^{2-}(aq)$ reduction at –1720 mV in the diffusion-controlled segment C to D. There was an exponential decrease in rate of $Zn(OH)_4^{2-}(aq)$ with increasing CMC concentration so that at 80 g/L CMC the rate was only 25% of that in the absence of CMC. According to this result, addition of gel additives may inhibit the dendrite growth and the zinc electrode shape change simply by decreasing the rate of diffusion. This may account for the increase in performance with the addition of polyethylene oxide in the electrolyte on the nickel-zinc cell cycle life [109].

As a more subtle approach than either decreasing zincate concentration or increasing the viscosity of the electrolyte, one might also explore the use of additives to alter the overpotential for zincate reduction. Such additives may adhere strongly to the electrode surface so that the overpotential for the electrode reaction increases. Based upon electrostatic considerations, positively charged additives would be the most favoured under these reducing conditions. One such group of compounds, which have been used in Zn-Br batteries, are the quaternary ammonium salts [106]. As used in Zn-Br cells, addition of tetrabutylammonium bromide in the electrolyte, a $ZnBr_2$ solution, the zinc dendrite growth will be greatly inhibited. The strongly absorbed positively charge tetrabutylammonium ions on zinc surface may account for the retarded zinc dendrite growth.

Figure 4.8 shows the effect of the addition of tetrabutylammonium hydroxide (TBAH) on the reduction rate of $Zn(OH)_4^{2-}(aq)$. Here, the 30% KOH saturated with 60.0 g/L of ZnO electrolyte was saturated with TBAH, which has an estimated solubility of ca. < 2 g/L. In the presence of TBAH there is a marked decrease in zincate reduction. The first important observation is that the first onset of reduction is shifted cathodically from

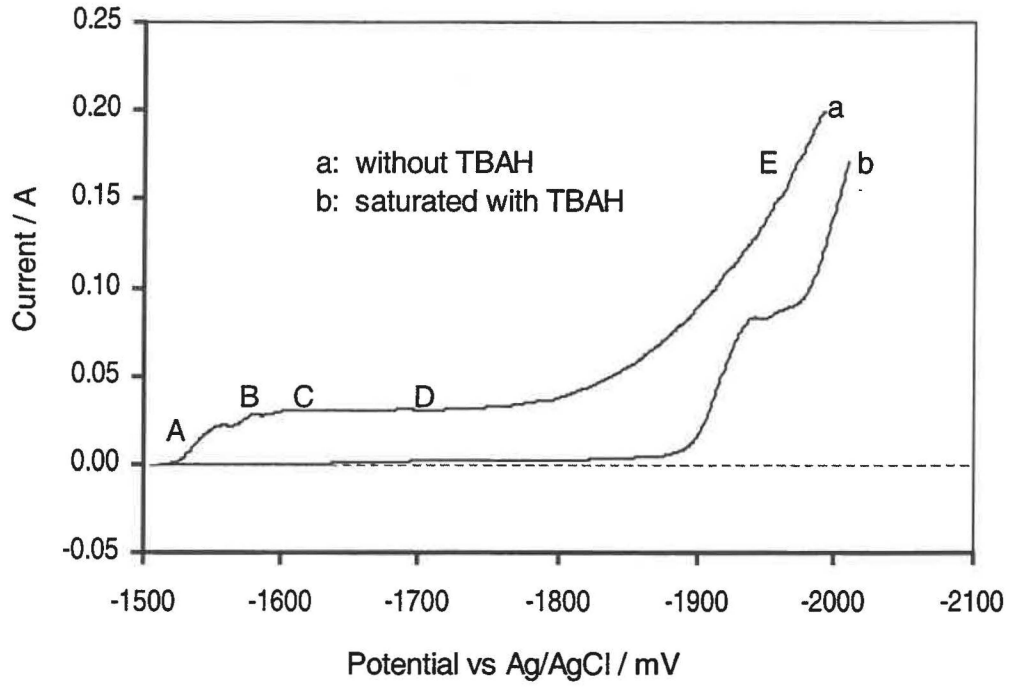

Fig. 4.8 Effect of tetrabutylammonium hydroxide (TBAH) on the cathodic polarization of a zinc metal electrode in 7 M KOH saturated with respect to zincate (60 g/L of ZnO).

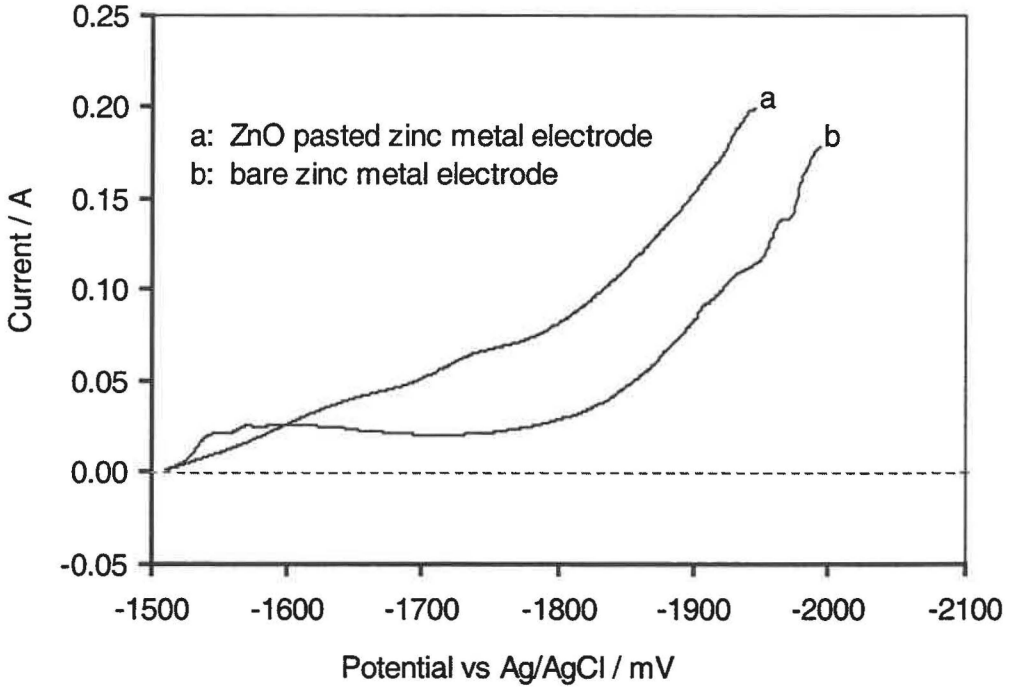

Fig. 4.9 Cathodic polarization of a ZnO(s)-pasted zinc metal electrode in 7 M KOH saturated with zincate (60 g/L of ZnO).

–1510 mV to –1630 mV vs Ag/AgCl in the presence of TBAH indicating that the overpotential for reduction has significantly increased. Secondly, once reduction commences, TBAH prevents the rapid rise in current as found in segment A to B in Fig. 4.2. Instead, the current only develops to a low potential-invariant value by segment C to D, about 6% of that in Fig. 4.2. It is proposed that the tetrabutylammonium ions absorb strongly onto the zinc working electrode surface and act as a hydrophobic barrier for zincate participation in the reduction process. Furthermore, the use of the TBAH saturated electrolyte has also provided an increase in overpotential for H_2 evolution from *ca.* –1750 mV to –1870 mV vs Ag/AgCl. Once H_2 evolution commenced some zincate reduction did take place as evidenced by new layers of zinc metal depositing on the electrode. This, however, takes place at potentials some 350 mV more negative than that observed in Fig. 4.2.

In comparison with the use of CMC additive or employment of electrolyte with low zincate concentrations, TBAH is a much more effective additive to inhibit the reduction of $Zn(OH)_4^{2-}(aq)$. Provided this quaternary ammonium species does not block reduction of all zinc (II) species it could be used as an additive in the electrolyte to prevent dendrite growth and the zinc electrode shape change.

During zinc electrode charging (in unmodified electrolytes), $Zn(OH)_4^{2-}(aq)$, ZnO(s) and $Zn(OH)_2(s)$ may be reduced or deposited simultaneously, albeit at differing rates. Having established that the reduction of zincate may be blocked and that a practical saturation of the electrolyte with zincate has been established, then provided ZnO (s) and $Zn(OH)_2$ (s) remain capable of undergoing reduction, there is prospect for formation of a dendrite and shape change free system.

4.3.2 Reduction of ZnO(s)

ZnO(s) is the predominantly used material for the preparation of pasted zinc electrodes. The differences between the reduction of ZnO(s) and $Zn(OH)_4^{2-}(aq)$ were investigated using LSV. It is impossible to investigate the reduction of ZnO(s) in strong alkaline solutions in the absence of zincate since this soluble species will spontaneously form due to reaction (4.8). However, the combined reduction of ZnO(s) and zincate can be

studied in the presence of a fixed $Zn(OH)_4^{2-}(aq)$ concentration as afforded by the new saturated solution.

In order to study the reduction of ZnO(s) onto zinc metal electrodes in the presence of $Zn(OH)_4^{2-}(aq)$, the working electrode was deposited with a 2 mm thick layer of ZnO(s) by manually packing the solid material onto a PVC sleeved electrode as shown in Fig. 4.1 followed by centrifugation at 3500 rpm for 8 min. The electrolyte was 7 mol/L KOH saturated with at 60.0 g/L ZnO as established in Section 4.2.

Figure 4.9 shows the LSV of the ZnO-packed electrode in comparison with the zincate-only system shown in Fig. 4.2. Unlike the zincate-only reduction, the ZnO-packed electrode does not show the distinct regions A to D. No nucleation and growth events are discernible and no diffusion-limiting current forms. Instead, there is an almost exponential increase in current throughout the potential range indicating that the reduction is predominantly controlled by charge-transfer. In contrast to the zincate-only system (H_2 evolution commenced at potentials more negative than –1780 mV vs Ag/AgCl (Fig. 4.2). It is impossible to distinguish between zinc (II) reduction and H_2 evolution in this voltammogram (Fig. 4.9). At a potential of –1590 mV vs Ag/AgCl nearly 200 mV less cathodic than –1780 mV vs Ag/AgCl the rate of zinc (II) reduction at the ZnO-packed electrode exceeds that of the zincate-only system. That a diffusion-limiting case does not develop at the ZnO-packed electrode is due to the immediate availability of the reactant on the surface of the electrode. Such zinc oxide reduction is thought to lead to the development of a porous metallic zinc rather than lead to the formation of dendrites [16] and is favoured for practical zinc electrodes.

The issue now remained that, whilst the desirable ZnO(s) reduction is more rapid than zincate reduction in saturated solutions, what would the effect of TBAH on zinc oxide reduction be? Figure 4.10 shows the effects of combining zincate saturation (60.0 g/L ZnO) and TBAH saturation on ZnO-packed electrodes. Here, the potential for the first onset of reduction has moved cathodically from –1510 mV to –1610 mV vs Ag/AgCl in the presence of TBAH. In contrast to zincate reduction in the zincate-only case, once ZnO (s) reduction commences it increases rapidly with more cathodic potentials so that by –1820 mV vs Ag/AgCl the same rate of reduction in the absence of TBAH is achieved.

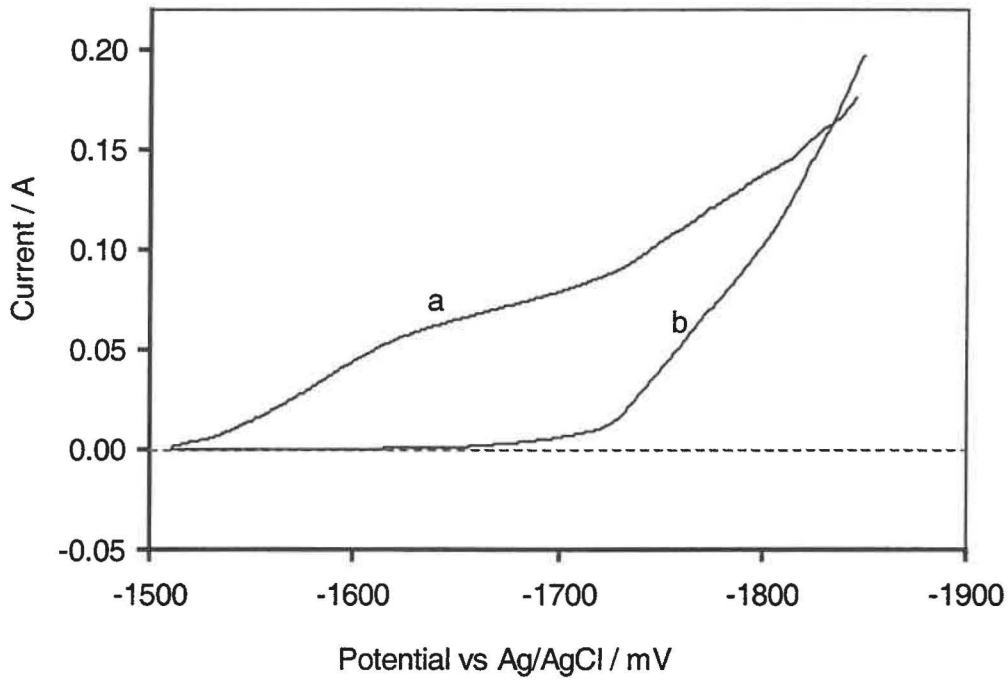

Fig. 4.10 Effect of tetrabutylammonium hydroxide (TBAH) on the cathodic polarization of a ZnO(s)-pasted zinc metal electrode in 7 M KOH saturated with respect to zincate (60 g/L of ZnO). Curve **a:** without TBAH; Curve **b:** saturated with TBAH.

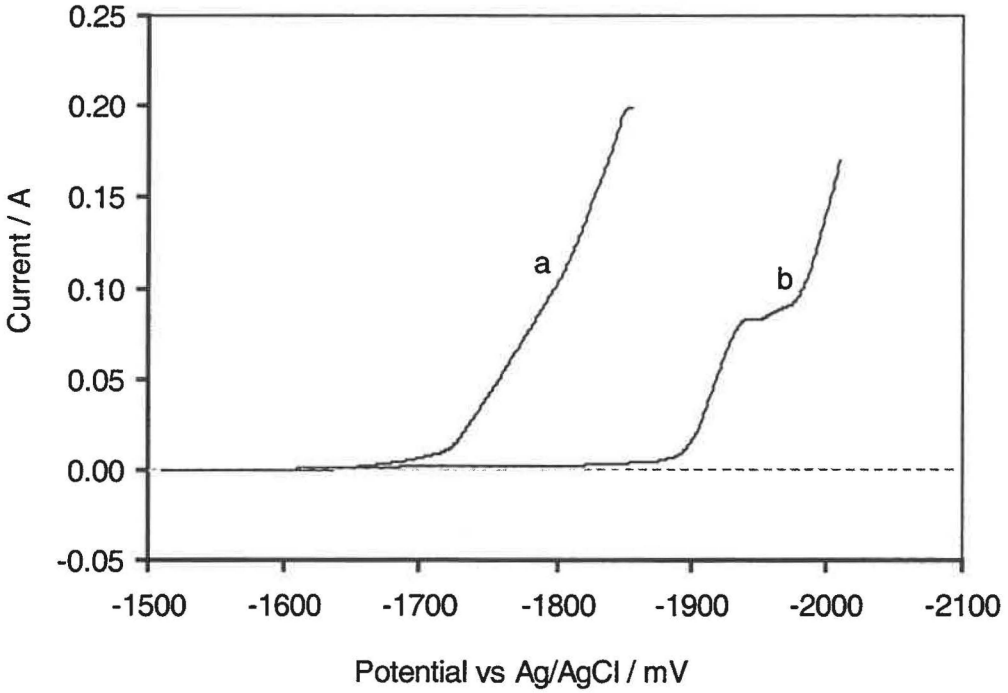

Fig. 4.11 Comparison between the effect of electrolyte saturation with tetrabutylammonium hydroxide (TBAH) and zincate (60 g/L of ZnO) on ZnO(s)-pasted (curve **a**) and bare zinc metal electrodes (curve **b**).

Consequently, although the overpotential for zinc oxide reduction is increased by saturation with TBAH, reduction is not prevented unlike the case for zincate where reduction is effectively blocked except at the most extreme cathodic limits where H_2 evolution disrupts the adsorbed TBAH layer. The difference between zinc oxide and zincate in reduction in the presence of TBAH is distinctly shown in Fig. 4.11.

4.3.3 Reduction of the zinc discharge products

Whilst ZnO-packed electrodes may adequately simulate the charging of a newly pasted electrode during a formation cycle, it does not provide a good measure of the charging of a many-cycled battery electrode. In such electrodes the discharge products consist of a mixture of $Zn(OH)_2(s)$ and ZnO(s) with composition and crystallinity dependent on temperature, elapsed time since formation, depth of discharge and depth within the porous battery plate. Having established that ZnO(s) may be reduced in the presence of the zincate-inhibiting TBAH, it remains to establish whether the zinc electrode discharge products will reduce in the presence of this compound.

It is beyond the scope of this project to explore the precise composition of these zinc (II) discharge species. It is sufficient for the development of a practical rechargeable zinc electrode to show that that whatever solid zinc (II) species formed on the electrode during discharge are capable on being reduced in the presence of TBAH together with zincate-saturated electrolytes to prevent dendrite growth and shape change.

In order to study the reduction characteristics of zinc discharge product, the initial potential for LSV was moved to a more positive value so that the zinc working electrode was initially simulating the discharge process in a nickel-zinc cell. During this oxidation the surface became covered with a layer of white discharge products. As the potential of the working electrode became more negative and passed though –1510 mV vs Ag/AgCl the zinc discharge product was reduced as evidenced by the loss of the white layer and the formation of a new zinc metal layer.

Figure 4.12 shows the voltammograms for this process in a zincate saturated (60.0 g/L ZnO) in the absence of TBAH.

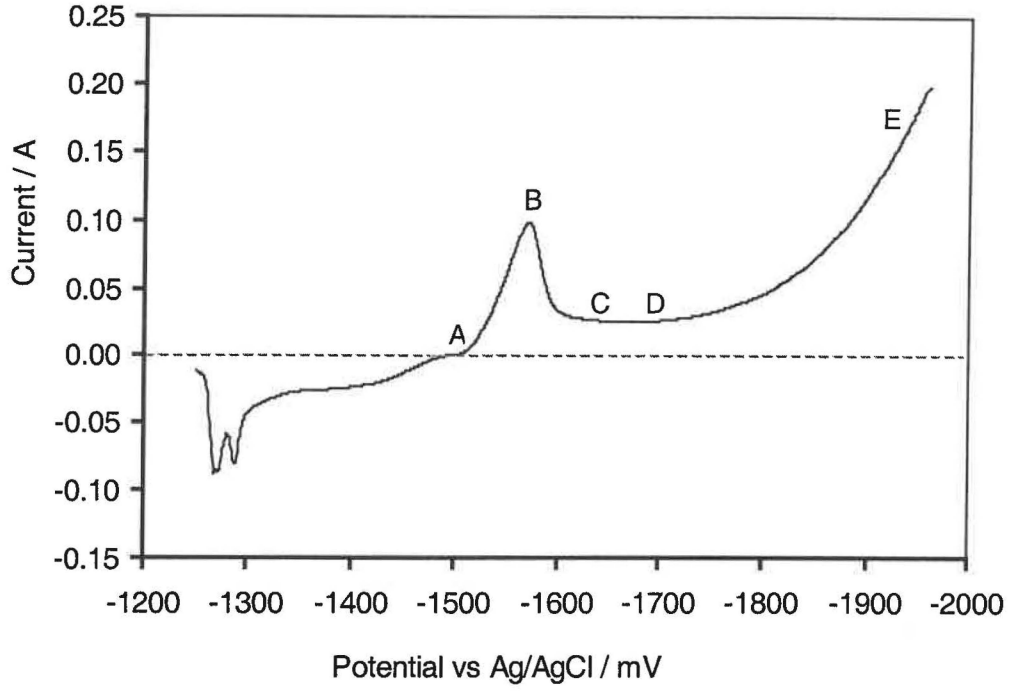

Fig. 4.12 Cathodic linear sweep polarization commencing from an oxidizing potential for a zinc metal electrode in 7 M KOH saturated with respect to zincate (60 g/L of ZnO).

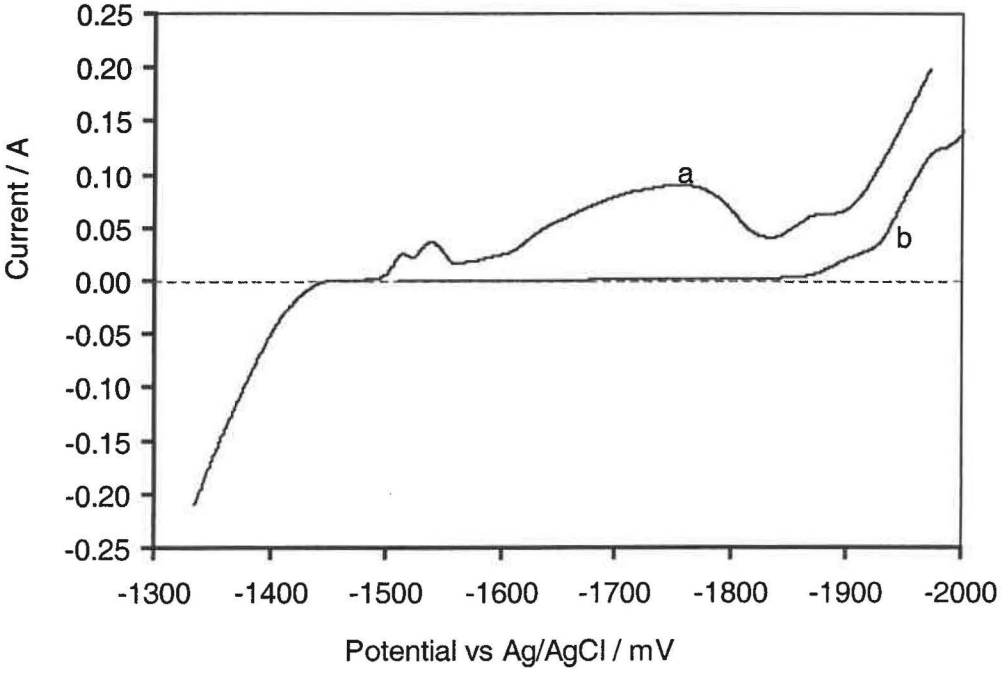

Fig. 4.13 Comparison of the effect of tetrabutylammonium hydroxide (TBAH) on reduction of zincate (curve **b**) and the zinc discharge product (curve **a**) in 7 M KOH saturated with respect to zincate (60 g/L of ZnO). Curve **a**: cathodic linear sweep polarization commenced at –1250 mV vs Ag/AgCl (as discharge condition). Curve **b**: cathodic linear sweep polarization commenced at –1510 mV vs Ag/AgCl.

Prior to point A, the surface of the zinc working electrode was oxidized and covered with a layer of zinc discharge product. At point A, the oxidation ceased as the potential reached the resting potential. In contrast to reduction of a zincate-only system (Fig. 4.2) there is a pronounced reduction peak during segment A to B. This is proposed to be the rapid reduction of newly formed solid discharge products residing on the electrode surface together with the zincate from the electrolyte. It should be noted that this reduction process is more facile than the reduction of solid ZnO on the ZnO-packed electrode (Fig. 4.9). Once these zinc discharge products become exhausted the reduction decreased from segment B to C as the process became confined to that of zincate reduction and a diffusion-limiting current from segment C to D identical to that found for the zincate-only system was established. H_2 evolution took place, in segment D to E, at a greater rate on this previously discharged electrode compared to the zincate-only case presumably as a consequence of a higher surface that was a porous network of metallic zinc forming on this electrode.

Figure 4.13 shows the effect of TBAH on the combined reduction of zincate and the zinc discharge product. In contrast to the reduction of both zincate and ZnO(s), where there were large increases in the overpotential for first reduction in the presence of TBAH, there is no such overpotential for the zinc discharge product and reduction commences at –1510 mV vs Ag/AgCl as in Fig. 4.2. The large peak in Fig. 4.12 in segment A to C, due to the reduction of newly formed discharge products, is much diminished by TBAH and more closely resembles segment A to C in Fig. 4.2 for the zincate-only system. The reduction of the discharge products appears to be shifted to more cathodic potentials by TBAH so that a broad peak from –1600 mV to –1840 mV vs Ag/AgCl develops before H_2 evolution commences.

These results for both ZnO-packed (Fig. 4.11) and previously discharged zinc electrodes (Fig. 4.13) in the presence of TBAH were strongly encouraging for the development of zinc electrodes free of shape change and dendrite growth.

4.4 Comparison of a range of quaternary ammonium compounds

Having established that the quaternary ammonium salt TBAH showed efficacy in

blocking zincate reduction whilst still permitting zinc discharge product and ZnO(s) reduction, it was considered appropriate to investigate whether any other quaternary ammonium hydroxides could also achieve this result to a greater or lesser extent.

Figure 4.14 shows the effects of two other tetraalkylammonium hydroxides on the reduction behaviour of zincate. Both tetramethylammonium hydroxide (TMAH) and tertraethylammonium hydroxide (TEAH) have appreciably higher solubilities in 30% KOH. It was found that at low concentration both tetraalkylammonium hydroxides had little effect on zincate reduction. Only when the concentration was increased significantly did zincate-inhibition take place. In Fig. 4.14 where the inferior and incomplete inhibition of zincate reduction required 80 g/L of each of these compounds in comparison with complete inhibition by TBAH at *ca.* < 2 g/L (Fig. 4.7). TMAH did not alter the potential for the onset of reduction whilst TEAH increased the overpotential by some 70 mV. Both TMAH and TEAH gave rise to diffusion-limiting regions with currents ca. 50% of that for zincate-only solutions. This may indicate that these two tetraalkylammonium hydroxides act only as ion-pairing agents with zincate rather than forming a barrier film on the electrode surface. N,N,N,N',N',N'-diethyltetramethylethylenediammonium hydroxide was synthesised† to determine whether there was any advantage in employing a multiple cationically charged species. Figure 4.15 shows the voltammograms for a saturated solution (10 g/L) of N,N,N,N',N',N'-diethyltetramethylethylenediammonium hydroxide in zincate saturated electrolyte. Here the ethylenediamine based compound shows almost identical behaviour to that of TBAH at a similar molar concentration. Given that no distinct advantages were found for this more complicated quaternary ammonium compound, all future work employed the use of 30% KOH saturated with TBAH and saturated with $Zn(OH)_2$.

† Ethylenediamine reacted with excess methyl bromide at about 60°C for 48 hours. Excess KOH solution was added into the mixture and stirred. The insoluble final product (top layer) was separated from the KOH solution.

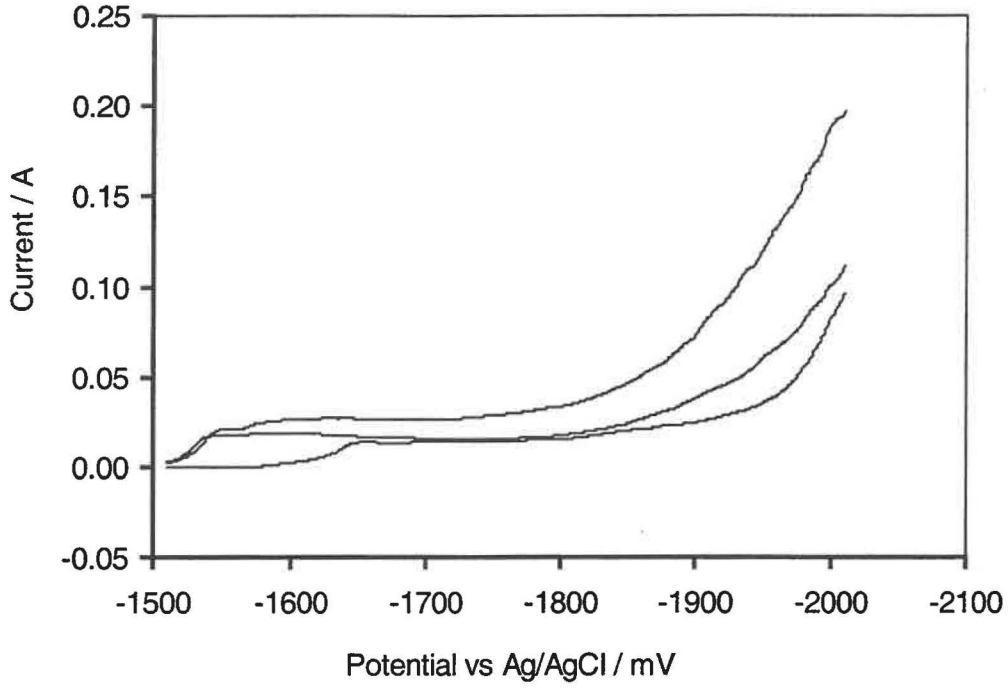

Fig. 4.14 Effect of tetramethylammonium and tetraethylammonium hydroxides on the cathodic polarization of a zinc metal electrode in 7 M KOH saturated with respect to zincate (60 g/L of ZnO). Curve **a** is from Fig. 4.1 for comparison.

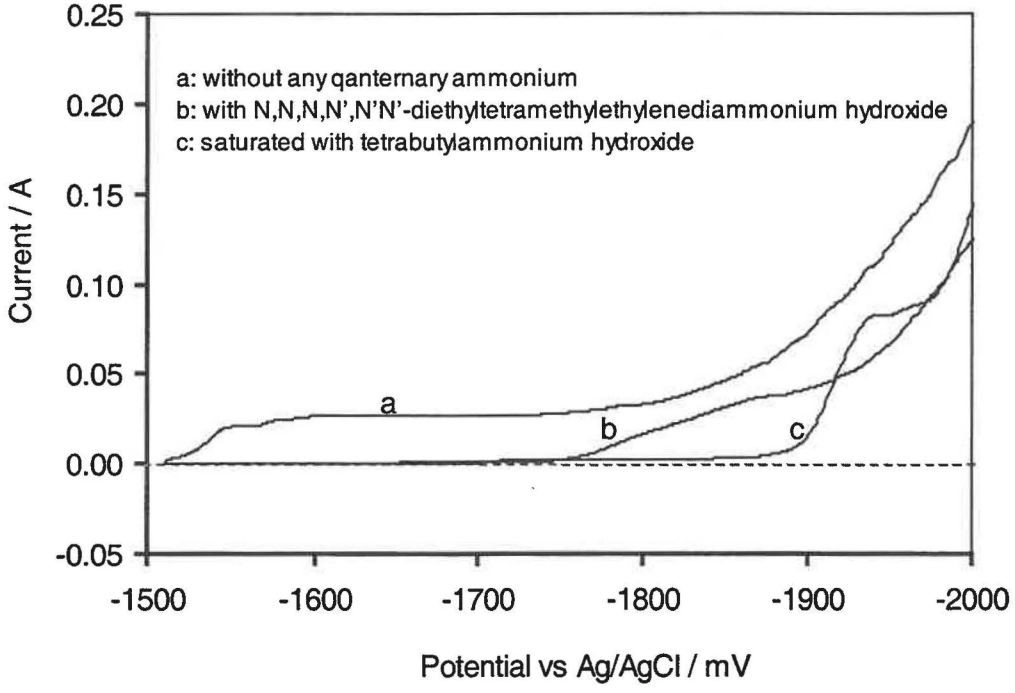

Fig. 4.15 Effect of N,N,N,N,N,N-diethyltetramethyllienediammonium hydroxide (10 g/L) on the cathodic polarization of a zinc metal electrode in 7 M KOH saturated with respect to zincate (60 g/L of ZnO). Curve **a** is from Fig. 4.1 and curve **c** is from Fig. 4.7 for comparison.

4.5 Conclusions

The formation of zincate by the dissolution of zinc active mass and its subsequent reduction is associated with the failures of the Ni-Zn cells. These failures arise from the zinc electrode shape change and zinc dendrite growth. The reduction of zincate, zinc oxide and zinc discharge products has been investigated with an attempt to establish a practical method for inhibiting the reduction of zincate.

The reduction of zincate is a diffusion controlled process. Increasing the electrolyte viscosity by addition CMC in the electrolyte could significantly decreased the reduction rate of zincate.

In contrast to zincate, the reduction of solid ZnO and zinc discharge products is not controlled by diffusion.

It was found that quaternary ammonium salts with low solubility in 30 wt % KOH electrolyte could efficiently prevent the reduction of zincate during charge or cathodic polarization without inhibiting the reduction of either solid zinc oxide or solid zinc discharge products. The modified electrolyte saturated with TBAH and zincate, which is expected to be effective in retarding zinc electrode shape change and zinc dendrites, was used as the electrolyte in the experimental nickel zinc cells as described in Chapters 5, 6 and 7.

Chapter Five Cell Structure Modification

5.1 Introduction

The cycle-life performance of the Ni-Zn system is affected by a number of parameters. These include the composition and disposition of the active masses, the electrolyte, the cell structure and the cycling regime. In this chapter the role of the cell structure is explored and optimised.

The first criterion to be established with respect to cell structure is the number of nickel and zinc electrodes in the test cell. According to the results presented in Chapter 4 concerning the reduction of zincate and zinc discharge products, more negative overpotentials and/or higher current densities at the zinc electrode during the charging process promote the reduction of zincate that is the resource for zinc dendrite growth. For a given charging current, a cell with one nickel electrode placed between two zinc electrodes is likely to exhibit less dendrite growth compared to a cell with one zinc electrode placed between two nickel electrodes. Similarly, the larger the area (the geometric or projected area will be quoted rather than the true active surface area of the porous electrode) of the zinc electrodes, the lower the current density and less likelihood of dendrite growth. Consequently, test cells were constructed with one planar nickel electrode sandwiched between two planar zinc electrodes.

Cairns *et al.* [70] used a single zinc electrode (7.0cm × 6.2 cm) held between two nickel electrodes in their experimental nickel zinc cells. It seemed that they failed to account for the effect of zinc electrode current density on the performance of the cells. Here, cells having identical size zinc and nickel planar electrodes in a vertical assembly were initially constructed in order to gain practical understanding of the effects of relative size and disposition on the cell performance.

The work reported here in this and the following chapters was conducted in parallel. Consequently, whilst Chapter 6 reports the modification of the zinc active mass, the

optimized composition was used in cells reported in this chapter. The electrolyte was not optimized but saturated with respect to ZnO and TBAH.

5.2 Cell #5.1: Identical sized nickel and zinc electrodes

The planar zinc and nickel electrodes had a projected area of 8.8 cm × 5.8 cm in Cell #5.1. The nickel electrodes were identical in composition and preparation to those described in Section 3.4. About 0.12 mole of nickel active mass (nickel hydroxide) was pasted onto the sponge nickel current collector. The theoretical capacity of the nickel electrode was *ca.* 3.2 Ah.

Three layers of 40 × 40 brass mesh spot welded together on average every 1 cm (both on the edge and across the middle of the mesh) were used as the zinc current collector. Nickel ribbon was spot welded onto one corner of the brass mesh to provide an electrical terminal as in Fig. 3.1.

The zinc active mass was identical in preparation and composition to the optimized mixture described in Chapter 6 and consisted of 8.0 g of zinc stearate, 3.0 g of graphite and 0.2 mol of $Zn(OH)_2$. The electrolyte was 30% w/w KOH saturated with $Zn(OH)_2$ and TBAH. The addition of zinc stearate into the zinc active mass was to make the zinc active mass hydrophobic, eliminating the access of the electrolyte into the zinc active mass. This is explored in depth in the following chapter. About 0.13 mole of the zinc active mass (with respect to zinc) was pasted onto the two zinc electrodes. The theoretical capacity of the two zinc electrodes was *ca.* 7 Ah.

Each of the nickel and zinc electrodes was individually wrapped with a single layer of woven nylon cloth. A single layer of thicker woven nylon cloth (Arthur Toye Ltd., Palmerston North.) was placed either side of the wrapped nickel nickel electrode before placing between the two wrapped zinc electrodes. This thicker woven nylon cloth acted as a separator material. Several layers of 60 × 60 nylon mesh (Arthur Toye Ltd., Palmerston North) mesh were placed on one outer face of electrode assembly to ensure

an even pressure across the electrode assembly when gluing the perspex case under pressure. A stainless steel pseudo reference electrode was included in the cell case as described in Section 3.5. The cell case had external dimensions of 11 cm (width) × 8.6 cm (height) × 1.0 cm (thickness) and was constructed from Perspex sheet as described in Section 3.6.

5.2.1 Cycle-life performance of Cell #5.1

The cell was flooded with *ca.* 22 mL electrolyte (saturated with ZnO and TBAH, Section 4.3) so that the top of the electrode assembly was just immersed. The electrodes were soaked for at least one hour, with gentle agitation to remove entrapped air bubbles prior to any passage of current through the cell. The cell was subjected to two identical formation cycles with the following regime:

i) Charge at 150 mA for 9 hours (1.35 Ah);

ii) 5 minutes at open circuit;

iii) Discharge at 150 mA until the cell voltage dropped below 1.3 V (cutting voltage); followed by

iv) 5 minutes at open circuit.

Figure 5.1 shows the potential-time profile for Cell #5.1 during this formation stage. The discharge/charge efficiency was 45% (0.61 Ah discharge) for the first cycle and increased to 60% (0.81 Ah discharge) for the second cycle. The positive or nickel electrode was the capacity-limiting electrode as evidenced by the more rapid change in dE_{Ni}/dt than $|dE_{Zn}|/dt$ at the end of each of the discharge steps. In addition, the nickel electrode potential decline was responsible for the cell voltage dropped to 1.3V at the end of discharge as shown in Fig. 5.1.

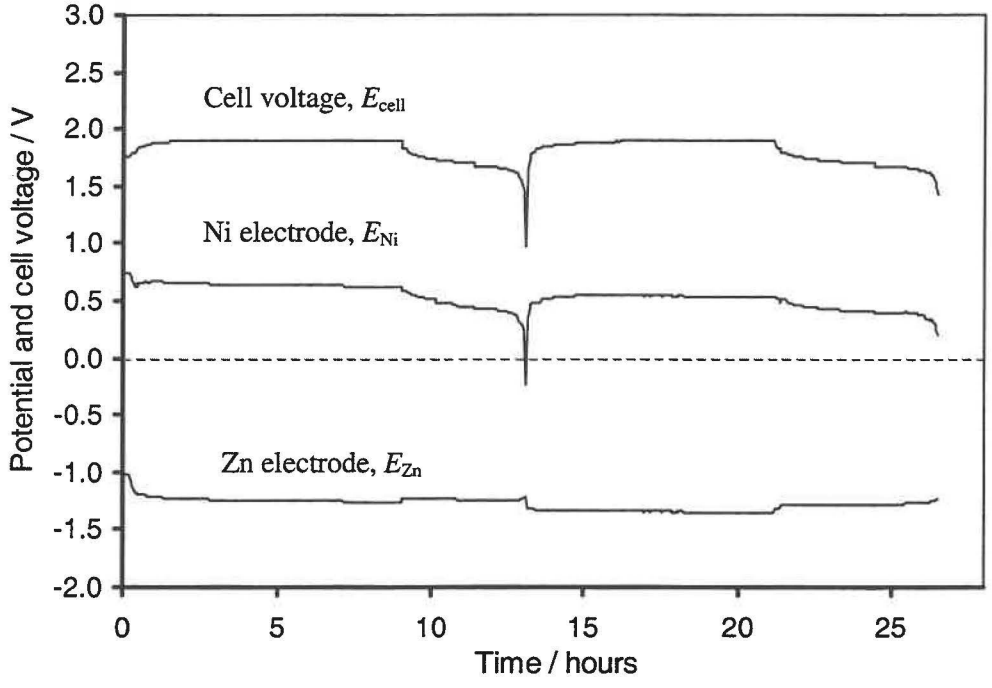

Fig. 5.1 Cell voltage and electrode potential variation in two formation cycles for Cell #5.1.

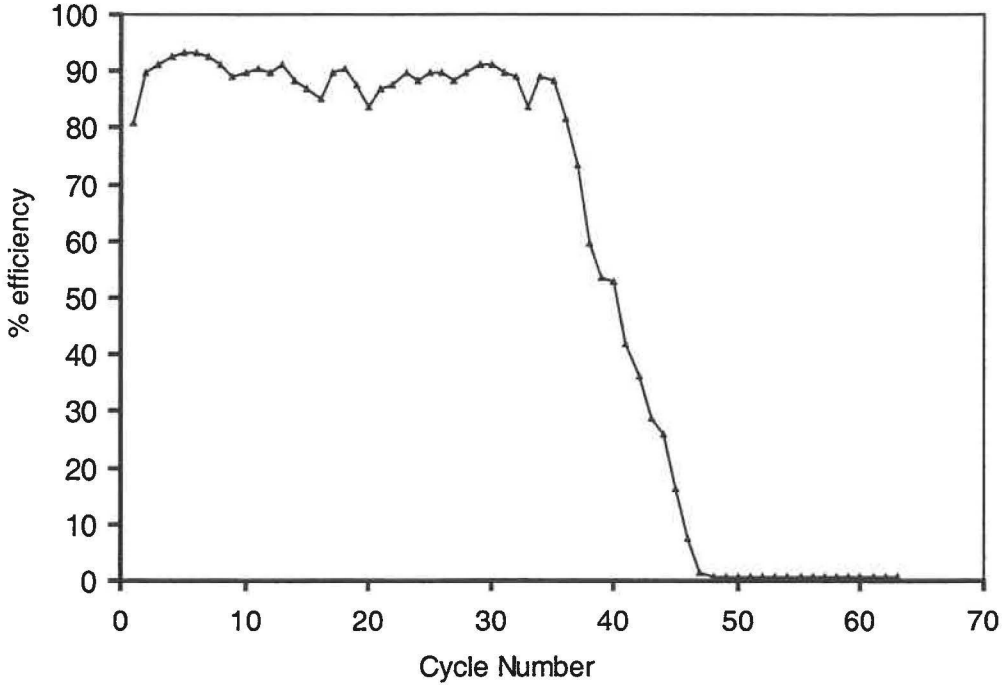

Fig. 5.2 Discharge/charge efficiency as a function of cycle number for Cell #5.1.

After completion of the two formation cycles the cell was subjected to regular charge/discharge cycles. The regular cycle regimen is given below:

i) Charge at 400 mA for 2.5 hours;

ii) 5 minutes at open circuit;

iii) Discharging at 450 mA until the cell potential dropped below 1.3 V (cutting voltage); and

iv) A further 5 minutes at open circuit before commencing the next cycle.

Figure 5.2 displays the discharge/charge efficiency against cycle number for the cycling of Cell #5.1. The efficiency increased from 80% to 94% over the first 5 cycles. This increase in performance is assumed to relate to the progressive electrochemical utilization of the active mass in each of the nickel and zinc electrodes. The cell remained nickel-limiting during these 5 cycles. After attaining 94% efficiency the cell then exhibited an irregular decline to 90% efficiency at 30 cycles and fell below the benchmark criteria of 80% after 36 cycles. Catastrophic decline occurred after this, so that at 45 cycles only 16% efficiency was achieved and after 47 cycles the capacity fell to effectively zero. Charge/discharge cycling was terminated at 63 cycles after no recovery of discharge capacity was evident for 15 cycles. This rapid decline in performance is thought to result from electrical shorting through the nylon mesh separator between the zinc and nickel electrodes caused by zinc dendrite growth. One parameter, which provides supportive evidence for this assumption, is the cell voltage just at the end of each charging period while with charging current passing the cell, $E_{cell,eoc}$. According to [1]:

$$E_{cell,\,eoc} = E_{oc} + \eta_{Ni} + \eta_{Zn} + IR = E_{Ni,\,eq} - E_{Zn,\,eq} + \eta_{Ni} + \eta_{Zn} + IR \qquad (5.1)$$

where

E_{oc} is the open circuit voltage of the cell, dependant on the depth of charge;

$E_{Ni,\,eq}$ is the nickel electrode potential at equilibrium, dependant on the depth of charge;

$E_{Zn,\,eq}$ is the zinc electrode potential at equilibrium, dependant on the depth of charge;

η_{Ni} is the overvoltage or overpotential of the nickel electrode during charge with the current I;

η_{Zn} is the overvoltage or overpotential of the zinc electrode during charge with the current I;

I is the charging current passing the cell; and

R is the internal resistance of the cell.

Whilst $E_{cell,eoc}$ does not necessarily provide an adequate measure of the state of charge capacity for a cell, its value reflects the depth of charge and internal resistance that are affected by the dendrites formed during charge. Any deviation below the normal end of charge cell voltage may indicate that a spontaneous discharge process is taking place under 'open circuit' conditions. This discharge is enabled by direct electrical connection through the separators by conducting zinc dendrites. In the case that the nickel and zinc electrodes are connected or partially connected with such conducting zinc dendrites formed during charge, the charge acceptance of the cell will be reduced, resulting in lower depth of charge upon completion of charge with lower $E_{cell,eoc}$. Due to the partial electrical connection by zinc dendrites, the internal resistance decreases to some degree, leading to a lower cell voltage during charge contributed by lower IR in equation (5.1).

Figure 5.3 shows the cell voltage and the nickel and zinc electrode potentials at the end of charge against the cycle number for Cell #5.1. The end of charge cell voltage increases only slightly over the first 34 cycles (1.84 to 1.88 V). Following this, $E_{cell,eoc}$ falls markedly as does the discharge/charge efficiency in Fig. 5.2. This progressive decline in $E_{cell,eoc}$ after 34 cycles could reasonably be due to a progressive increase in the number

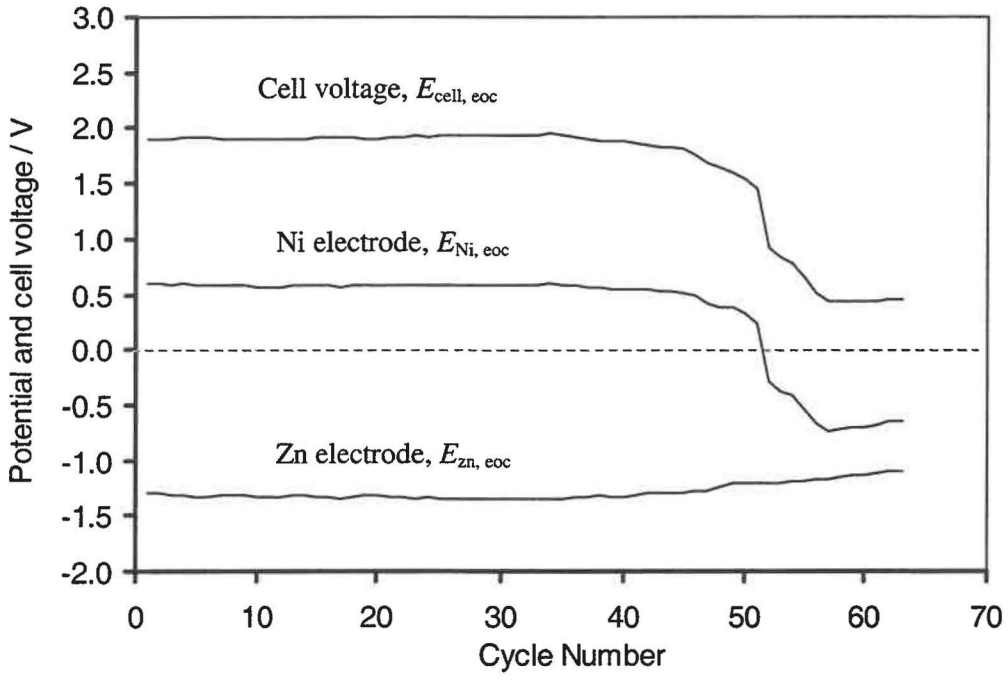

Fig. 5.3 Variation of cell voltage and electrode potentials at the end of charge as a function of the cycle number for Cell #5.1.

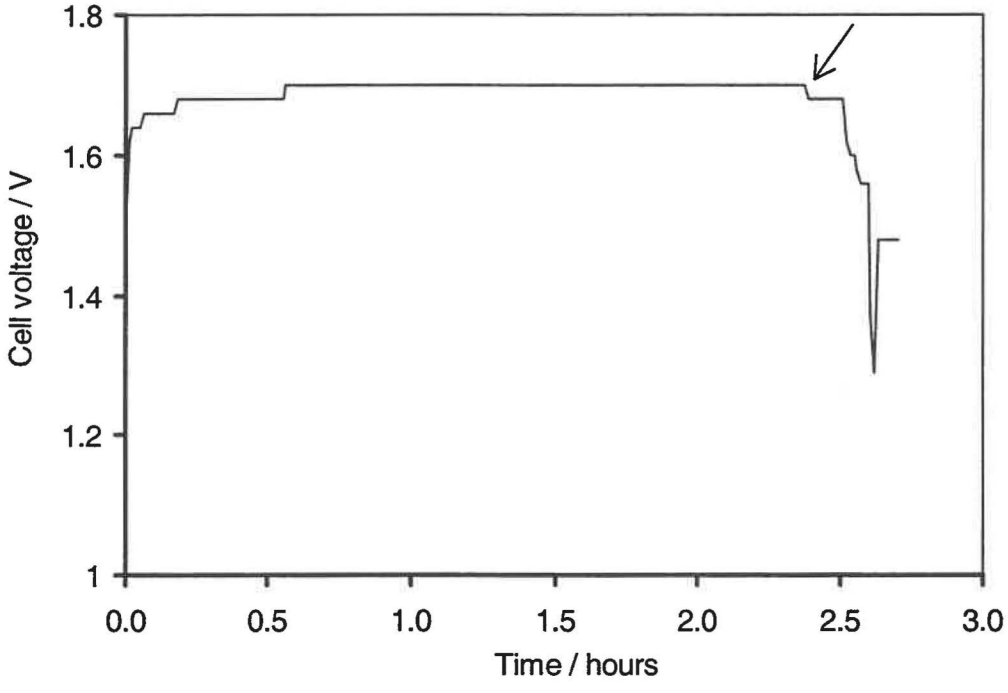

Fig. 5.4 Variation of cell voltage during cycle 47 for Cell #5.1 with evidence for dendrite growth as indicated by the arrow.

of dendrites bridging between the zinc and nickel electrodes. Similar electrode kinetics and discharge capacities prevail at each electrode since the potentials of the zinc and nickel electrodes contribute to a similar extent to the decline in $E_{cell,eoc}$ shown in Fig. 5.3. Clearly, the deleterious effects of the assumed dendrite growth are far more pronounced on the nickel electrode. This susceptibility of the nickel electrode may have arisen from the lower capacity of this electrode compared to the two zinc electrodes. During the dendrite-induced discharge of the cell under charging conditions the nickel electrode may already be partially discharged. In contrast the extra capacity of the zinc electrodes permits retention of its potential.

Further evidence suggestive of dendrite formation is obtained by monitoring E_{cell} during the charging process for later cycles of Cell #5.1. Figure 5.4 shows the charge and discharge profile for cycle 47. Compared to earlier cycles the cell never attains a cell potential greater than 1.7 V. This suggests that dendrites are likely to be present throughout the entire charging process. The drop in potential in the last 10 minutes of the charging stage may well be due to the onset of further dendrites bridging the separator. This would act to increase the rate of self-discharge and account for the drop in potential.

5.2.2 Structural analysis of Cell #5.1

The charge/discharge profiles described above only provide a strong indication that dendrite growth was causing the decline in performance. Confirmation was required before further modifications could be made to the cell structure. Consequently, Cell #5.1 was cut open and disassembled after a further charging period after cycle 63. Visual examination revealed the following features on the zinc electrodes:

i) The active mass was no longer present on the current collector to a width of 0.5 – 1.0 cm at the edges of the plates. This was particularly evident along the bottom edges of the electrode.

ii) Zinc dendrites were observed on the brass mesh immediately adjacent to this active mass-depleted region. More dendrites grew along the bottom edges of the electrode.

iii) The remainder of the zinc electrodes remained unchanged suggesting that the redistribution of zinc active mass had been prevented for the most part in the presence of saturated TBAH in the electrolyte and zinc stearate in the zinc active mass.

A schematic diagram of these findings is shown in Fig. 5.5.

It is postulated here that there is a correlation between the edge removal of the zinc active mass and the accessibility of the electrolyte. During discharge the oxidation of the zinc active mass is favoured at the edges due to

$$Zn(s) + 2OH^-(aq) \longrightarrow Zn(OH)_2(s) + 2e^- \qquad (5.2)$$

Some of the discharge product then dissolves to form zincate

$$Zn(OH)_2(s) + 2OH^-(aq) \longrightarrow Zn(OH)_4^{2-}(aq) \qquad (5.3)$$

The electrolyte in Cell #5.1 was saturated with TBAH. In Chapter 4 this was shown to prevent the bulk reduction of zincate from the electrolyte and during subsequent charging, the reduction of zincate to reform the active mass was partially suppressed. Consequently, there is a progressive removal of active mass from the edges and net movement of zinc into the electrolyte phase.

With the removal of the active mass from the brass current collector the growth of dendrites becomes more favourable. The spontaneous formation of the zinc nuclei on the brass mesh adjacent to the remaining active mass during charging in high concentrations

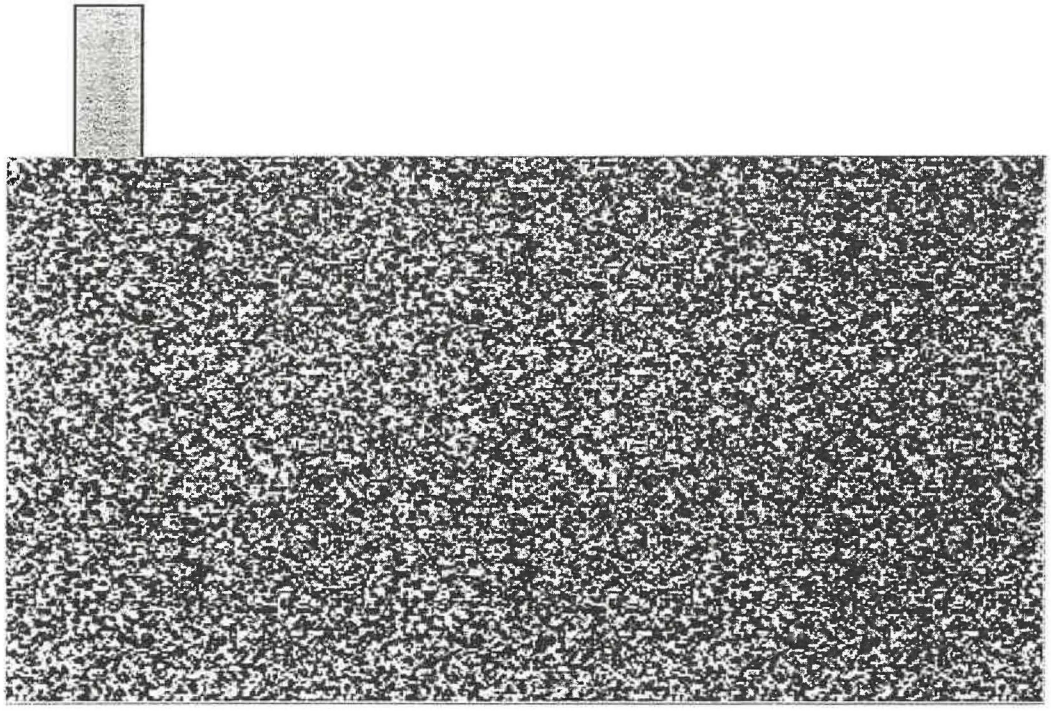

Before cycling

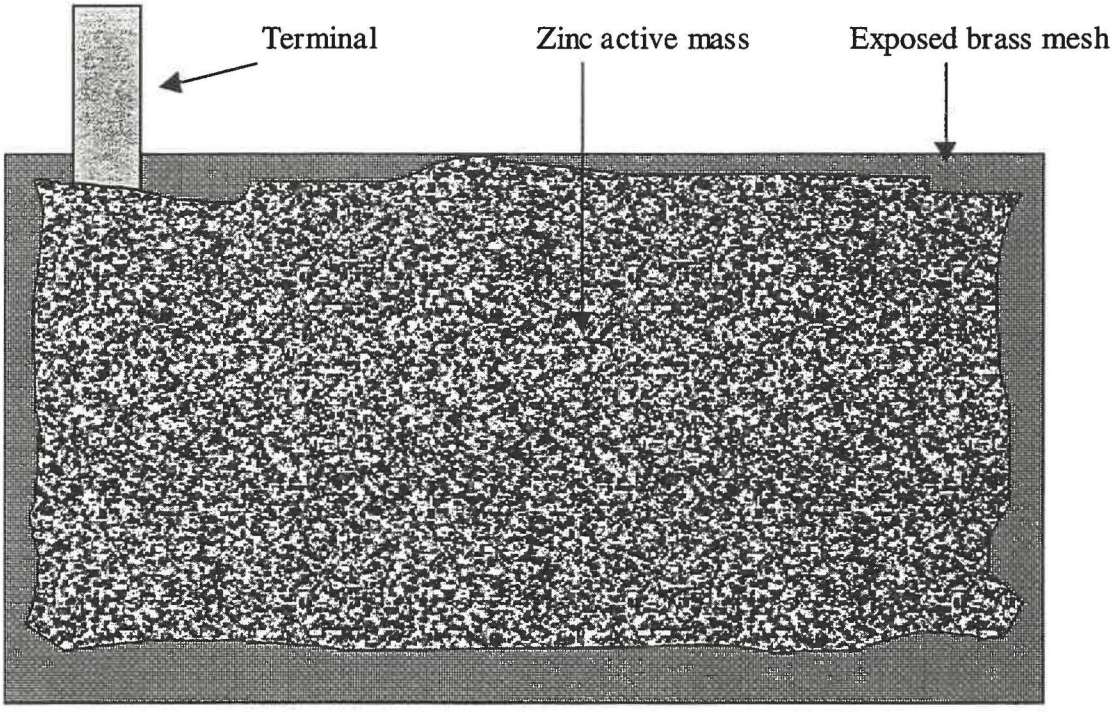

After cycling

Fig. 5.5 A schematic diagram of the dissolution of zinc active mass from the zinc electrode edges after cycling for Cell #5.1.

of zincate would lead to the production of dendrites preferentially growing at their tips. This process is evidently not favoured in the center of the zinc electrode where there is limited accessibility of the electrolyte. The net rate of dendrite oxidation during discharge appears to be less than the net rate of formation during charging so that an accumulation of dendrites occurs.

A further factor that favours the formation of dendrites is the progressive increase in local current density at the edges of the remaining zinc active mass. As active mass is depleted the total charging current remains constant so that the effective current density at these edges increases. This combination of increasing charging current density and accessability to high zincate concentrations act to promote dendrite growth.

The addition of TBAH to the electrolyte and zinc stearate into the zinc active mass successfully prevent bulk relocation of the zinc active mass, but in regions where there is free access of the electrolyte to the active mass dissolution to give zincate occurs, current densities increase and dendrites form. This is particularly the case at the lower edge of the electrodes where stratification of the electrolyte ensures high concentrations of zincate.

Consequently, further modifications of the cell structure were required to restrict access of electrolyte to all of the zinc active mass and to prevent regions of high current density forming. These modifications are embodied in Cell #5.2.

5.3 Cell #5.2

5.3.1 Introduction

Any efforts to keep the electrolyte from entering the edges between the nickel and zinc electrodes were thought to assist with prevention of dendrite growth. If the nickel and zinc electrodes could be held in firm contact at their edges, the ability of electrolyte to enter the electrodes at the edges would be decreased. This might be achieved through the use of additional pressure across the face of the electrodes. It was found, however, that

the inevitably lower loadings of nickel and zinc active mass at the electrode edges prevented this being a practical solution. Instead, it was found that if the electrode assembly described in Section 5.2 was bound together by winding with Nylon thread (PG Spin Line, 6lb) together with some additional pressure across the electrode face then good electrode-electrode contact was ensured at the edges.

A further modification to form Cell #5.2 was the disposition of the electrolyte in the cell. The continued use of flooded cells as in Cell #5.1 in view of the predicted role of electrolyte accessibility was thought to be detrimental. A new cell structure was designed that provided a reservoir for the electrolyte that was not in direct contact with the electrode assembly. This new structure shown in schematic form in Fig. 5.6 met the needs to avoid high accessibility of electrolyte to zinc electrode edges and also prevented loss of electrolyte from the active mass. Here, the electrolyte is stored at the bottom of the cell and does not directly wet even the lower edge of the wrapped and wound electrode assembly.

Cell #5.2 was identical in active mass composition and otherwise identical in construction to Cell #5.1. A reassessment of the quantity of active mass suggested that increasing the formation charge could increase the overall capacity of the cell. Consequently, the two formation cycles were conducted with the regimen given below:

i) Charge at 150 mA for 15 hours (2.25 Ah);

ii) 5 minutes at open circuit;

iii) Discharge at 150 mA until the cell potential dropped below 1.3 V; followed by

iv) 5 minutes at open circuit.

These formation cycles are shown in Fig. 5.7. As for Cell #5.1 the discharge capacity increased from 40.0% to 63.9% over the two formation cycles.

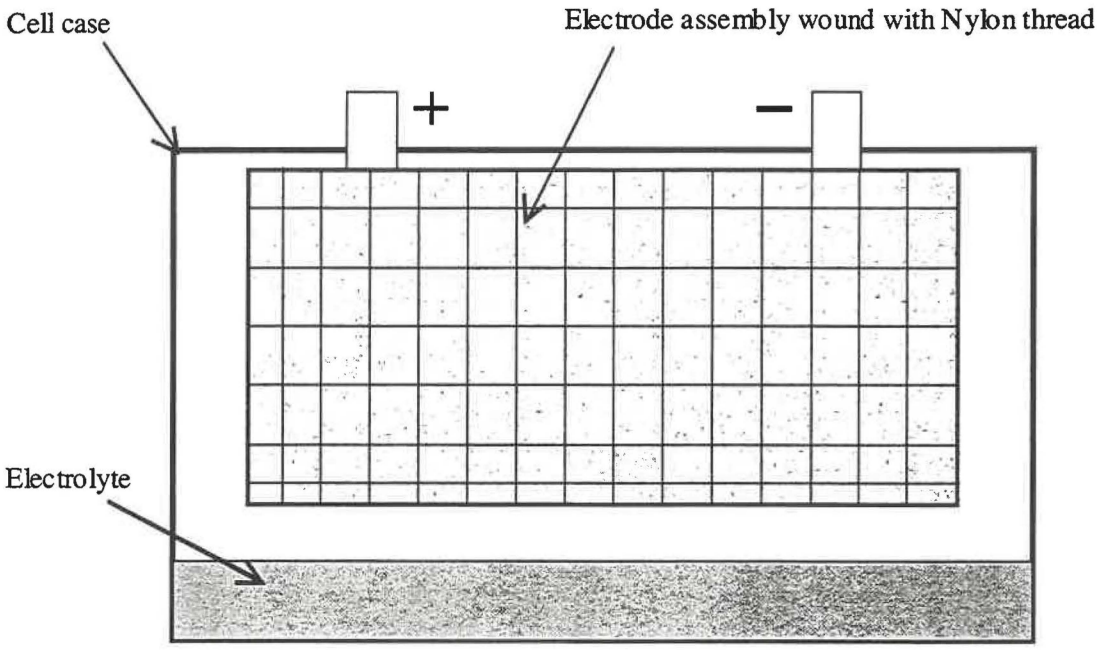

Fig. 5.6 Modified cell structure for Cell #5.2.

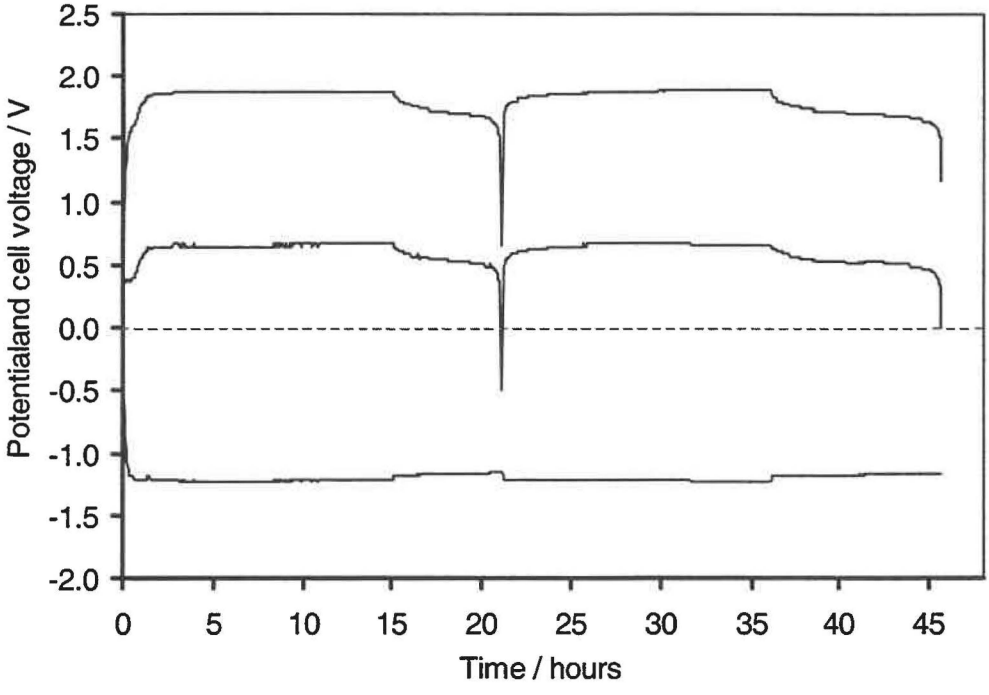

Fig. 5.7 Variation of cell voltage and electrode potentials in two formation cycles for Cell #5.2.

5.3.2 Cycle-life Performance

The regular charge/discharge cycling regimen is given below:

i) Charge at 500 mA for 2 hours (1 Ah);

ii) 5 minutes at open circuit;

iii) Discharge at 450 mA until the cell voltage dropped below 1.3 V; followed by

iv) 5 minutes at open circuit prior to the next cycle.

The discharge/charge efficiency is shown as a function cycle number in Fig. 5.8. The efficiency remained at better than 90% for 226 cycles and dropped below 80% on cycle 227. This compares extremely favourably with the 36 charge/discharge cycles at better than 80% efficiency attainable by Cell #5.1. The modifications to the cell structure clearly provided beneficial results. In a similar manner to Cell #5.1, Cell #5.2 exhibited a rapid decline in performance. Cell #5.2 failed completely only 5 cycles after dropping below 80% efficiency.

The end of charge cell voltage, $E_{cell,eoc}$, was again used to examine the mode of failure. This is shown in Fig. 5.9 as a function of cycle number. A number of points are evident when this is compared with the data for Cell #5.1 (Fig. 5.3). First, Cell #5.2 maintains a higher $E_{cell,eoc}$ at all cycles than Cell #5.1. Secondly, $E_{cell,eoc}$ steadily increases over the first 60 cycles from 1.80 V to 2.15 V, Cell #5.1 only exhibits a small increase in $E_{cell,eoc}$. Thirdly, having attained an $E_{cell,eoc}$ of 2.15 V this is then maintained for over 150 cycles. Finally, when Cell #5.2 fails beyond 227 cycles there is no accompanying catastrophic drop in $E_{cell,eoc}$, which is in direct contrast to Cell #5.1.

According to the nickel and zinc electrode potential shown in Fig. 5.9, unlike Cell #5.1 the relative changes in the end of charge potential for zinc and nickel electrodes are similar and are consistent with the absence of dendrites.

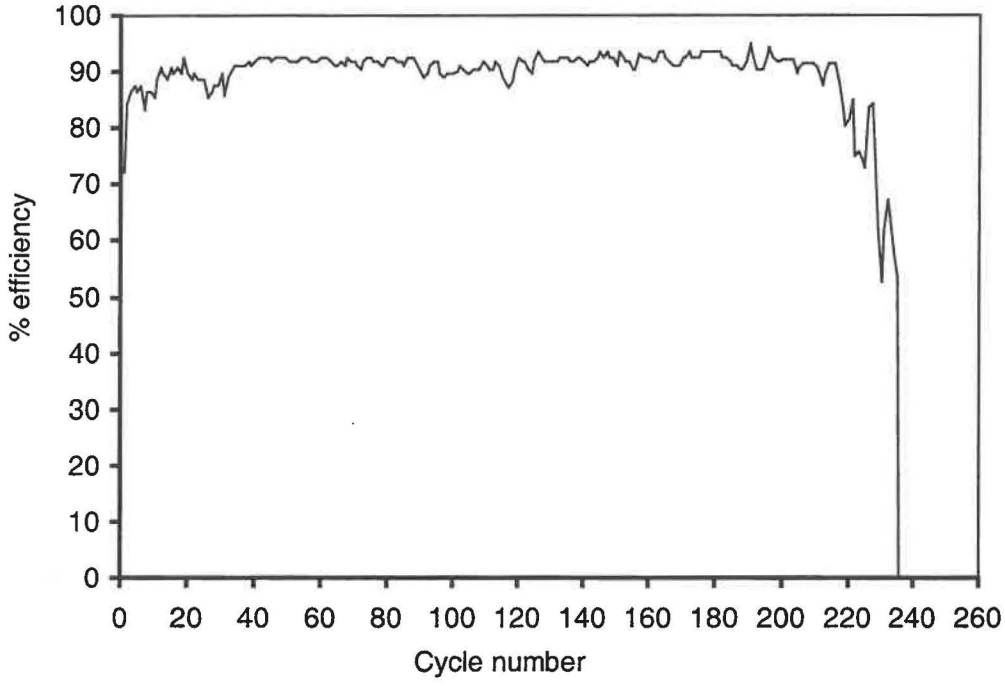

Fig. 5.8 Discharge/charge efficiency variation as a function of cycle number for Cell #5.2.

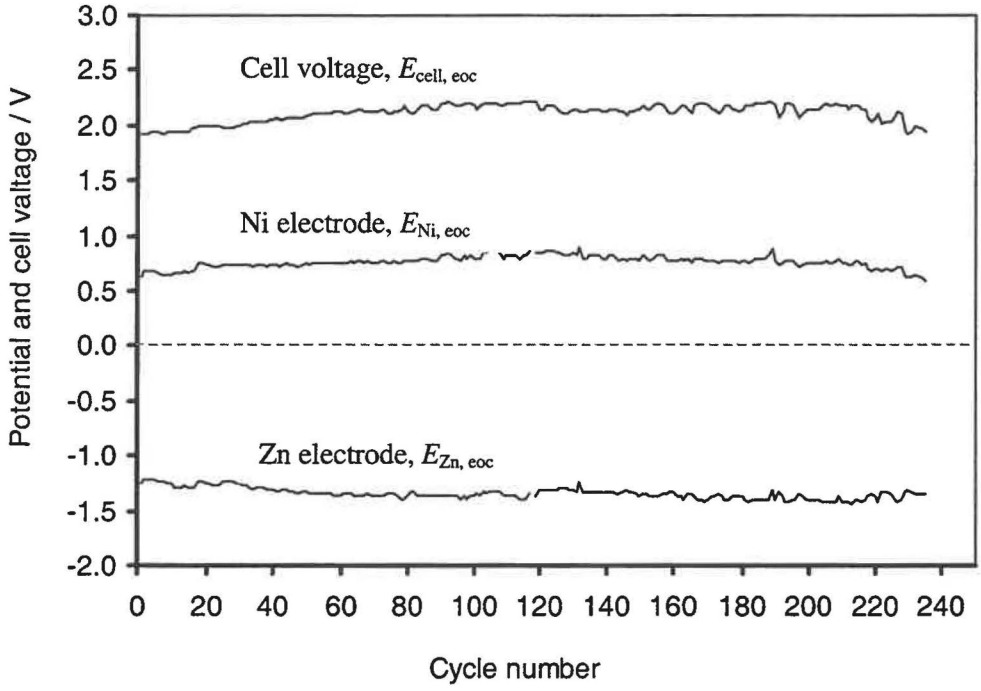

Fig. 5.9 Variation of cell voltage and electrode potentials at end of charge as a function of cycle number for Cell #5.2.

There is also no evidence for dendrite formation during charging of the later cycles for Cell #5.2. Figure 5.10 shows the charge/discharge potential profile for cycle 238 immediately prior to complete failure of Cell #5.2. In comparison to the similar profile for Cell #5.1 (Fig. 5.4), E_{cell} is higher at all points during the charge process and there is no marked decline in E_{cell} before end of charge. There is, however, a small but progressive decline in E_{cell} during charge with cycling. Whilst gross dendrite growth appears to have been inhibited in Cell #5.2, this progressive decline in E_{cell} may be consistent with the formation of 'semi-shorting' dendrites. These semi-shorting dendrites forming pathways between the zinc and nickel electrodes but with appreciable electrical resistance. Consequently, self-discharge takes place but at lower rates so that E_{cell} remains at a relatively high value without a drop during charge.

Even though this cell failed due to the formation of dendrites, albeit semi-shorting in nature, the cycle-life performance was significantly extended over that for Cell #5.1. This strongly supports the hypothesis made earlier that restricting the accessability of the electrolyte to the active mass is beneficial.

5.3.3 Electrolyte Movement

Visual inspection of Cell #5.2 during cycling revealed a significant factor with respect to electrolyte disposition. During each charging process electrolyte was ejected from the electrode assembly and collected in the reservoir at the bottom of the cell. This increase in the electrolyte volume can be accounted for by the charge reactions at the zinc electrode:

$$Zn(OH)_2 \cdot nH_2O(s) + 2e^- \longrightarrow Zn(s) + 2OH^-(aq) + nH_2O(aq) \qquad (5.4)$$

and at the nickel electrode:

$$Ni(OH)_2(s) + OH^-(aq) \longrightarrow NiOOH(s) + H_2O(aq) + e^- \qquad (5.5)$$

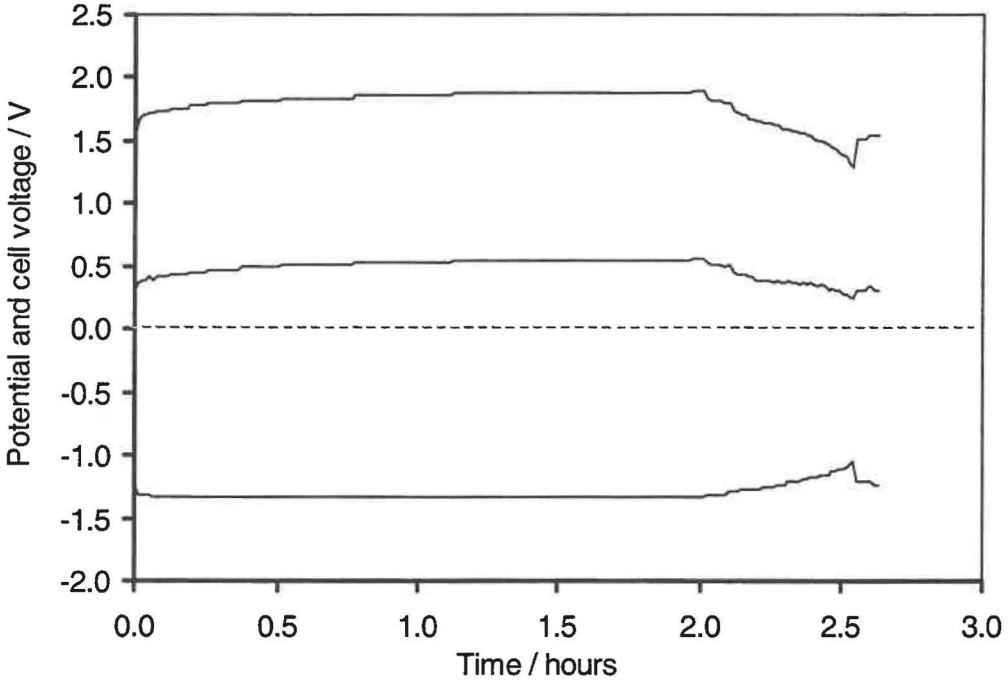

Fig. 5.10 Variation of cell voltage and electrode potentials during cycle 238 for Cell #5.2.

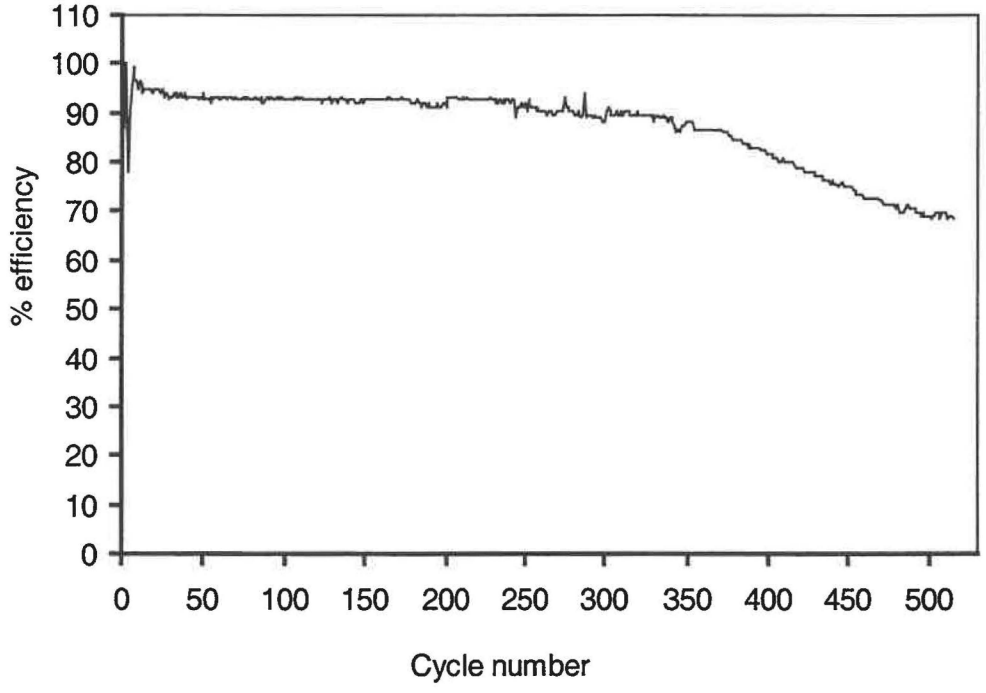

Fig. 5.11 Discharge/charge efficiency variation as a function of cycle number for Cell #5.3.

For every 2 electrons transferred, 2 molecules of H_2O are produced at the nickel electrode and a further n molecules of H_2O are produced at the zinc electrode from the hydrated $Zn(OH)_2$. It should be noted that there is not net consumption or production of OH^- so that overall there is a net dilution of the alkaline electrolyte.

It is inevitable that both hydrogen and oxygen gas are also produced. At the zinc electrode this is caused by overcharge

$$2H_2O(aq) + 2e^- \longrightarrow H_2(g) + 2OH^-(aq) \qquad (5.6)$$

and by corrosion of metallic zinc

$$Zn(s) + H_2O(aq) \longrightarrow Zn(OH)_2(s) + H_2(g) \qquad (5.7)$$

At the nickel electrode oxygen is also generated by overcharge

$$2OH^-(aq) \longrightarrow 1/2\ O_2(g) + H_2O(aq) + 2e^- \qquad (5.8)$$

and by decomposition of NiO_2

$$NiO_2(s) + 2OH^-(aq) \longrightarrow Ni(OH)_2(s) + O_2(g) + 2e^- \qquad (5.9)$$

This gaseous oxygen and hydrogen will displace the electrolyte in the porous active mass and the separator material.

The relative quantity of electrolyte residing in the separator and woven nylon cloth wrapping was minimised by winding the electrode assembly tightly with nylon thread. Consequently, as electrolyte is ejected from the active mass and collected in the reservoir, there are decreased quantities of dissolved zincate at the zinc electrode and hence dendrite growth is diminished.

The electrolyte stored at the bottom of the cell remained clear with no solid suspended zinc oxides. This demonstrated that the use of hydrophobic zinc stearate in the zinc active mass and a thoroughly $Zn(OH)_2$ saturated electrolyte prevents redistribution of zinc through the cell.

The above describes the ejection of electrolyte during charging. A mechanism must exist for relocation of the electrolyte from the reservoir into the active mass so that discharge may take place:

$$NiOOH(s) + e^- + H_2O(aq) \longrightarrow Ni(OH)_2(s) + OH^-(aq) \quad (5.10)$$

$$Zn(s) + 2OH^-(aq) + nH_2O(aq) \longrightarrow Zn(OH)_2.nH_2O(s) + 2e^- \quad (5.11)$$

During discharge much of the oxygen and hydrogen remaining in electrical contact with the active mass at each electrode will be consumed resulting in production of H_2O and acting to draw electrolyte back into the porous active mass.

5.3.4 Mechanism for Electrolyte Movement

It is important to identify the means by which electrolyte ejected from the active mass during charging and collected in the reservoir can make its way against gravity into the electrode assembly during discharge. Transfer through the gas phase is a possibility but it is likely to be at an insufficient rate and would be confined to the water component alone – KOH is unable to transfer as a vapour. No mechanism exists for formation of an electrolyte aerosol in the reservoir so this route is also not possible.

Careful inspection of the electrolyte in the cell revealed the likely mechanism. The Perspex used to make the cell was hydrophobic and could not be wetted with water alone. However, in contact with alkaline electrolyte it became relatively hydrophilic. The electrolyte was observed to have a low contact angle with the vertical face of the Perspex case that was well-wetted by the electrolyte. The wetting of the Perspex wall extended up

to the point against which the nylon mesh-electrode assembly was held tightly. It is proposed that the mesh provided a network of pores through which the electrolyte could rise due to capillary attraction. In this way electrolyte could penetrate the active mass horizontally throughout the height of the electrode assembly. It is also presumed that the nylon mesh provided an additional, but small, reservoir for the electrolyte.

This restricted access of the electrolyte to the active mass in combination with saturation of the electrolyte with TBAH and zincate decreased the propensity for dendrite formation and growth. That dendrite formation was observed at the lower edge of the electrode assembly can be accounted for by this lower location having more electrolyte in close proximity during charging. As electrolyte is ejected from the active mass, this material moves down the Perspex wall to the reservoir. Before dropping down to the reservoir the ejected electrolyte must pass the lower edge of the electrode assembly. The Nylon cloth acts as a small reservoir particularly at the edges so that the passing electrolyte is temporarily collected at the lower edge of the electrode assembly. The temporary collection of electrolyte with the formation of a drip edge at the bottom of the electrodes dictates that the lower edge at various points in the cycle process will have greater than desirable access to the electrolyte. Consequently, the most prevalent site for dendrite growth in Cell #5.2 is at the lower edge as observed.

Modifications to Cell #5.2 were then considered in the light of these findings – the need for an electrolyte reservoir, restricted access to this electrolyte, the role of capillary action and the need to avoid a drip edge.

5.4 Cell #5.3: a wrapped and bagged cell

Cell #5.3 consisted of two 9.2 cm × 6.4 cm zinc electrodes and a single 8.7 cm × 5.9 cm nickel electrode. Slightly larger zinc electrodes were thought appropriate to avoid higher local current density along the zinc electrode edges. It was assembled identically to Cell #5.2 with the following modification. After winding the electrode assembly with nylon thread, a shrink warp plastic bag sealed by a soldering iron, but open at the upper

edge, encapsulated the electrode assembly tightly. A hair drier was used to heat the encapsulated electrode assembly to make the plastic bag shrink.

This bagging process restricted the total electrolyte volume with which the electrode active mass was in contact and removed the potential for electrolyte collection at the lower edges. Electrolyte both enters and is ejected through the opening at the top edge. Capillary action enables the movement of electrolyte to the top of the bag via the Perspex walls. Nylon mesh was spread outside the plastic bag to apply additional even pressure onto the electrode assembly and acted as a pathway for vertical electrolyte movement.

5.4.1 Charge/Discharge process

After two formation cycles, the cell was subjected to regular cycles with the regimen given below:

i) Charge at 400 mA for 2.5 hours;

ii) 5 minutes at open circuit;

iii) Discharge at 600 mA until cell voltage dropped below 1.3V; followed by

iv) 5 minute at open circuit prior to the next cycle.

During charge electrolyte was observed to depart the electrode assembly at the bag opening as predicted and collected outside of the plastic bag without direct contact with the electrode assembly. One consequence of bagging the electrodes was that these now revert to the flooded situation as in Cell #5.1 and earlier cells. Here, electrolyte only departs the electrode environment when the bag is filled completely by electrolyte. It is significant, however, that unlike Cell #5.1, this flooding is by a relatively small volume of electrolyte with a limited quantity of zincate. Furthermore, this restricted-volume flooding approach ensures an even distribution throughout the height of the electrode

assembly. This is in contrast to Cell #5.2 where a gravity-induced electrolyte gradient is likely to develop over the electrode height.

The restricted-volume electrolyte may also diminish the net rate of dendrite production. Whilst saturation of the electrolyte by TBAH does diminish the rate of dendrite formation zincate by

$$Zn(OH)_4^{2-}(aq) + 2e^- \longrightarrow Zn(s) + 4OH^-(aq) \qquad (5.12)$$

During charge and even after charge the close containment of the hydroxide ions released from the reduction of zincate and zinc hydroxide within the porous active mass and separator system dictates that the rate of zinc oxidation is increased due to the increased OH^- concentration

$$Zn(s) + 2H_2O + 2OH^-(aq) \longrightarrow Zn(OH)_4^{2-}(aq) + H_2(g) \qquad (5.13)$$

This self-discharge process occurs more rapidly at the high surface area, newly formed zinc dendrites so that the net rate of dendrite formation is decreased. In the unconstrained Cell #5.1 and Cell #5.2 this local increase in $[OH^-]$ is not as pronounced due to the higher accessibility of the bulk electrolyte.

Just as it is proposed that the high surface area and newly-formed zinc dendrites are likely to be the most susceptible to chemical oxidation, it is also proposed that any dendrites remaining at the end of the charging phase will be amongst the first metallic zinc oxidized during discharge.

5.4.2 Charge/Discharge Cycling

Figure 5.11 shows the discharge/charge efficiency as a function of cycle number. After some fluctuation during the first 10 cycles the efficiency remained relatively constant at 94% for the first 250 cycles. Two distinct periods of relatively linear declines in

efficiency were then observed. The first from 94% at 250 cycles to 87% at 360 cycles and the second from 87% at 360 cycles to 70% at 480 cycles, passing through the 80% benchmark at 407 cycles. Cycling was terminated at 515 cycles (68%).

Overall, Cell #5.3 demonstrated a two-fold improvement in cycle-life performance over that for Cell #5.2 (Fig. 5.8).

If the decline in Cell #5.3 cycle-life performance was due to dendrite formation, be it either shorting or semi-shorting, then there should be an accompanying decline in the end of charge cell, $E_{\text{cell, eoc}}$. Figure 5.12, however, demonstrates that this parameter remains relatively unchanged at 1.97 V until 450 cycles for Cell #5.3. Even after this, the decline was only to 1.8 V and remained at this level until cycling was terminated at 515 cycles.

Inspection of the cell voltage and electrode potentials during charging for a selection of cycle numbers revealed no evidence for dendrite growth leading to either shorting or semi-shorting until 369 cycles. By 369 cycles, while the end of charge cell voltage remained at 1.97V and no semi-shorting commenced, the cell discharge/charge efficiency had declined to 86.75% at cycle 368. In order to identify the cause for the efficiency decline prior to the commencement of semi-shorting, the variation of the cell voltage and electrode potentials in cycle 160 and 368 is compared in Fig. 5.13. The end of charge cell voltage in both cycles was 1.97 V. There is no difference in charge phase between cycle 160 and 368. However, at the end of discharge dE_{cell}/dt in cycle 368 is higher than that in cycle 160. It is difficult to identify the difference in the nickel electrode performance between cycle 160 and 368. Unlike Cell #5.1 and Cell #5.2, this constrained-volume cell exhibits zinc-limiting features. At the end of discharge, the greatest contribution to dE_{cell}/dt is $|dE_{\text{Zn}}|/dt$ as shown in Fig. 5.13. This strongly indicates that the zinc electrode has undergone a decrease in active surface area, either through loss of active mass, sintering of the porous structure, or by passivation, contributing to discharge/charge efficiency decline in 368 cycles before semi-shorting commencement.

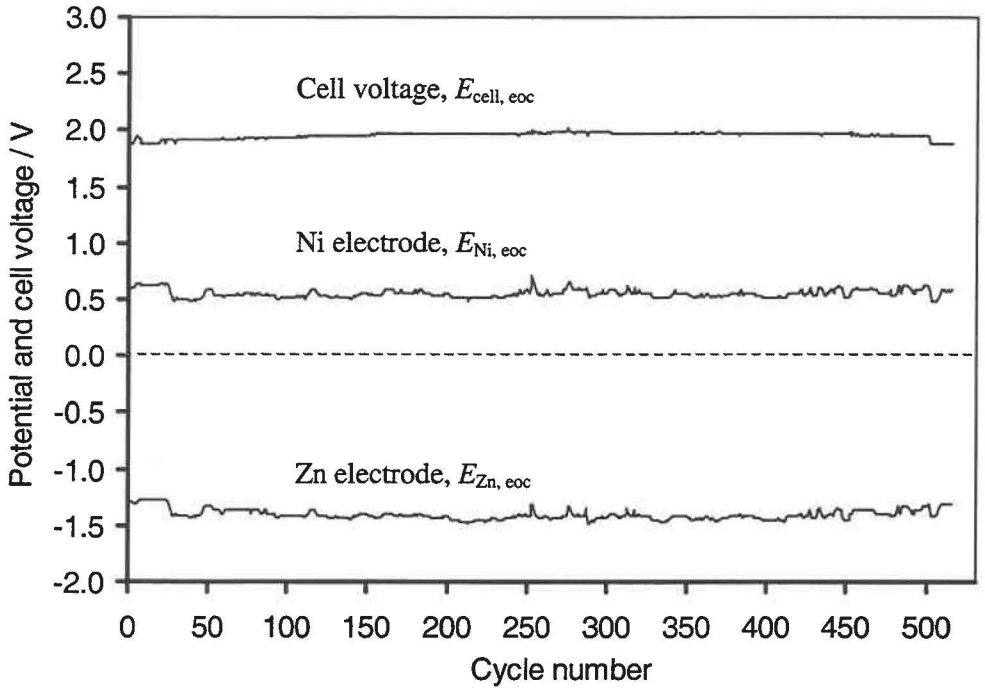

Fig. 5.12 Variation of the electrode potential and cell voltage at end of charge as a function of cycle number for Cell #5.3.

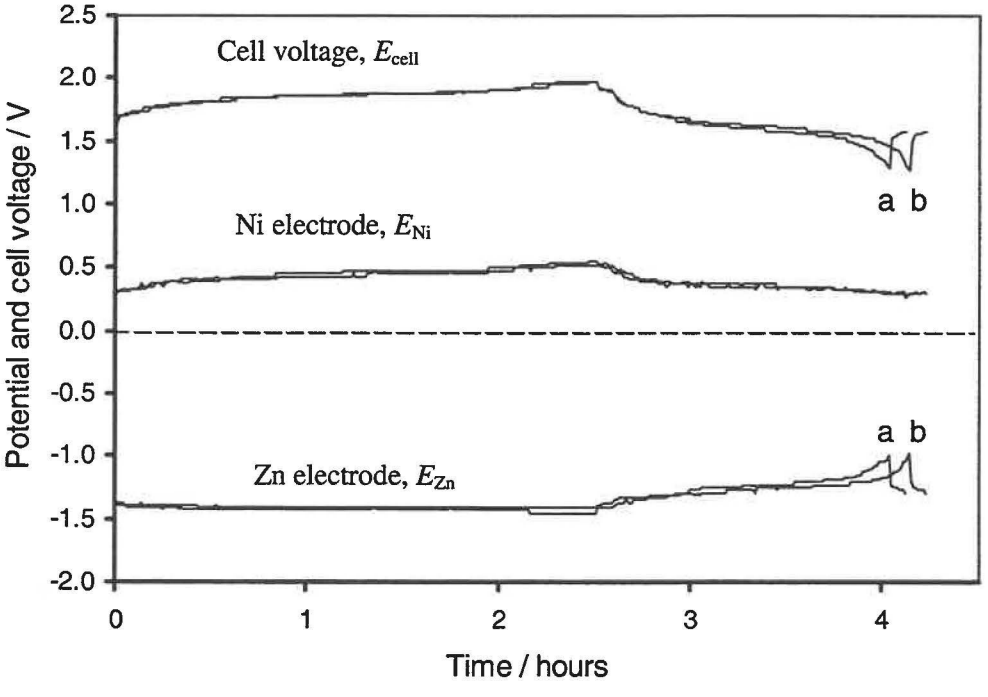

Fig. 5.13 Comparison of cycle 160 and 368 for Cell #5.3. Curve **a**: cycle 368; Curve **b**: cycle 160.

Loss of active mass is unlikely as this was not evident in earlier cells and the bagged structure prevents gross movement of the active mass away from the current collector. The loss of active surface area, be it due to passivation or sintering, increases the current density over the remaining operable regions of the zinc electrode and promotes the growth of dendrites. This in turn initiates internal shorting and rapid cell failure.

Semi-shorting caused by dendrites is observed beyond 369 cycles. Figure 5.14 shows the charge/discharge profile for cycle 369, the first cycle where semi-shorting caused by dendrites is observed immediately prior to the end of charge. In following cycles dendrites were observed to form at progressively earlier times.

The correlation between dendrite appearance due to the increase in local current density and cell failure is reinforced in Fig. 5.15. Here, the cell discharge/charge efficiency is shown as a function of % of charge capacity at which dendrites are first observed as a dip in E_{cell} for cycles 380 to 500. A progressive decline in discharge efficiency is found with earlier onset of dendrite growth.

As a consequence, the improving early inhibition of dendrite growth through development of a restricted-volume cell in combination with saturation of the electrolyte by TBAH has revealed the next performance-limiting parameter for the nickel-zinc system. This new limiting feature is either passivation or sintering of the zinc active mass. This problem will be addressed in the following chapter.

5.5 Conclusions

The accessability of electrolyte to the electrode assembly was associated with dissolution of the zinc active mass, causing gross diffusion of zinc active mass. Traditional cell structures like those for ordinary nickel cadmium cells with ready accession of electrolyte to the electrode assembly were not suitable for use in nickel zinc cells.

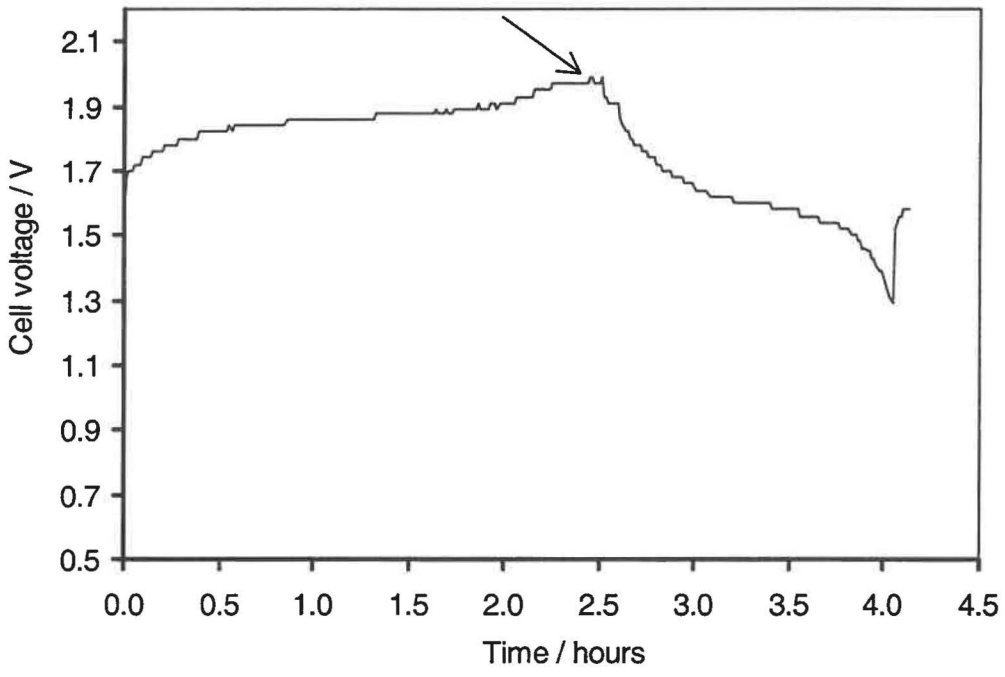

Fig. 5.14 Cycle 369 with evidence of dendrite growth (Cell #5.3) as indicated by the arrow.

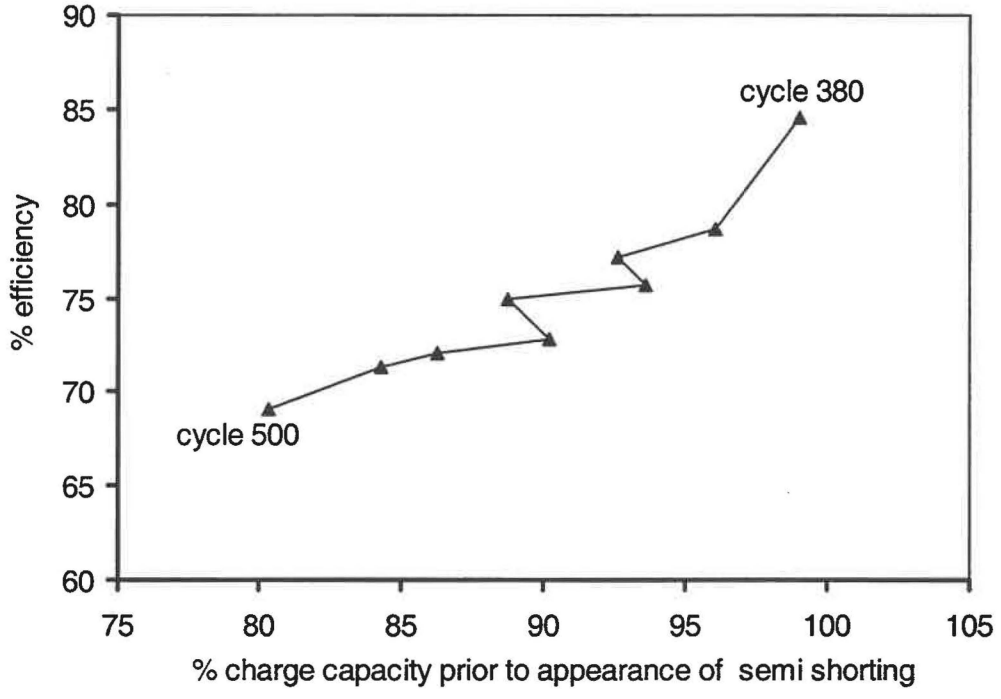

Fig. 5.15 Discharge/charge efficiency as a function of the depth of charge prior to semi-shorting from 380 to 500 cycles for Cell#5.3.

The first modification to the cell structure was made through winding the electrode assembly with Nylon thread and applying pressure on the face of the electrode assembly. The electrolyte accessing the interface between nickel and zinc electrode was believed to be restricted. It was found the cell failed with semi-shorting caused by dendrite growth. More dendrites were formed at the edges of the electrode where the electrolyte could be accessed more readily.

The second modification was made to avoid the electrode assembly being flooded. The bulk electrolyte was stored at the cell bottom as a reservoir without touching the electrode assembly. The cell cycle life was much prolonged. By comparison with the flooded cell, the accessability of the electrolyte to the electrode assembly was much restricted, leading to improved cycle life. The cell also failed with semi-shorting from zinc dendrites that formed along the lower edges of the zinc electrodes where more of electrolyte was gathered. The findings indicated that the distribution of the electrolyte needed further improvement.

The third modification was made to improve the distribution and access restriction of electrolyte to the electrode assembly. The electrode assembly was wound with Nylon thread and bagged with a plastic bag that was open at the top edge and then shrunk with hot air. The electrode assembly was tightly bagged with minimal space where the electrolyte could reside. In the cell case, the bulk electrolyte was separated from the electrode assembly by the plastic bag. The discharge/charge efficiency of this cell was over 70% for 500 cycles. It was thought that the cell structure was successfully optimized, and was used in the cells for zinc active mass modification.

Chapter Six Modification of the Zinc Active Mass

6.1 Introduction

Zinc oxide is commercially available as a high purity bulk material and this may suggest that zinc oxide could be the preferred source of zinc active mass in nickel-zinc cells. As indicated in Chapters 4 and 5, the zinc active mass may also consist of other ingredients as required. As described in Chapter 3, zinc oxide is not stable in the highly alkaline electrolyte and will undergo conversion to zinc hydroxide and zincate during charge/discharge cycling or by direct hydrolysis.

Hydrolysis:

$$ZnO(s) + H_2O(aq) \longrightarrow Zn(OH)_2(s) \qquad (6.1)$$

$$Zn(OH)_2(s) + 2OH^-(aq) \longrightarrow Zn(OH)_4^{2-}(aq) \qquad (6.2)$$

Charging:

$$ZnO(s) + H_2O(aq) + 2e^- \longrightarrow Zn(s) + 2OH^-(aq) \qquad (6.3)$$

Discharging:

$$Zn(s) + 2OH^-(aq) \longrightarrow Zn(OH)_2(s) \qquad (6.4)$$

The hydrolysis of zinc oxide and zinc hydroxide must result in a change in the disposition of the active mass. In Chapter 3 it was shown that dissolution of zinc oxide in the alkaline electrolyte, which may change the interface of the zinc active mass particles, permitted the rapid relocation of solid zinc oxide and zinc hydroxide materials throughout the cell via a gross diffusion process. Therefore, the zinc oxide active mass should be the subject of investigation for either modification, or complete alteration, to obtain the chemically and physically stable active mass required to attain the goals of long cycle life.

The first means for achieving this goal is the use of zinc hydroxide rather than zinc oxide as an active mass material. Given that the zinc oxide will convert to zinc hydroxide in the alkaline electrolyte, then the physical changes associated with this

process can be eliminated through pasting this inevitable product. There were two potential sources for this zinc hydroxide – either direct from chemical suppliers as a granulated powder, or indirectly by preparation in the laboratory. Whilst there is a handling advantage in using the zinc hydroxide granulated powder (weighing, transferring from vessel to vessel) there is a distinct disadvantage in achieving thorough mixing of other ingredients to form a homogenous paste. Such mixing may be more readily achieved through the co-precipitation of zinc hydroxide from aqueous zinc (II) solutions in the presence of the other soluble and insoluble ingredients. As a consequence, this approach was employed here.

6.2 Design and preparation of the zinc active mass

In order to impede or prevent the gross diffusion of zinc active mass throughout the cells and hence prolong the cycle life, the zinc active mass required modification to make it more hydrophobic. As established in the previous chapter, test cells exhibited marked improvement in cycle life with restricted access of the electrolyte to the electrode assembly and zinc active mass. Polytetrafluoroethylene (PTFE) has been used as a 'binder' in zinc active masses by a number of investigators [66, 69, 86-88, 91]. The PTFE used by these workers in nickel-zinc cells are small solid particles ranging 1-5 μm dispersed in water with the aid of the surfactant Triton-10 [69, 86, 87]. It remains a question as to how PFTE can effectively 'bind' zinc oxide particles at the typically low levels of 2-4% (w/w) in the final paste. Given the findings in Chapter 5 on the benefits of restricting accessibility of the electrolyte to the electrode assembly and to the active mass, it is likely that the role of PTFE is to simply increase the hydrophobicity, rather than 'binding' *per se* the zinc oxide/zinc hydroxide particles together.

An alternative route to that of PTFE to produce a hydrophobic zinc active mass is reported in this chapter. The zinc and calcium stearic acid salts zinc stearate and calcium stearate have been used as highly hydrophobic materials in many applications ranging from coatings for plastic casting, dye surfaces to hydrophobic abrasive surfaces in sand paper. In contrast to aqueous PTFE dispersions that are toxic to organs such as liver, bone marrow, pancreas, kidneys and male reproductive that are stated in the PTFE product specification (Aldrich Chemical Company, Inc.), zinc stearate and calcium stearate have low toxicity, are relatively inexpensive and may be prepared *in situ*.

Through making the zinc active mass hydrophobic by homogeneous dispersal of zinc or calcium stearate in the zinc active mass, the accessibility of the alkaline electrolyte to the zinc active mass, particularly to the boundaries of the zinc active mass particles, may be significantly restricted. The initial modified zinc active mass consisted of a mixture of zinc hydroxide, zinc or calcium stearate and graphite powder. The latter was added to increase the electrical conductivity of the active mass, particularly in the discharged state, or during the early stages of the formation cycles.

Solid zinc hydroxide was prepared *in situ* by mixing an aqueous solution of zinc sulfate and sodium hydroxide. Zinc sulfate was used rather than zinc chloride since corrosion, particularly of the nickel electrode current collector and its terminal, would occur in the presence of chloride. This corrosion was confirmed by using zinc chloride where cell cycle failure was observed within 5 cycles due to severe corrosion at the nickel electrode. In contrast there was no evidence for sulfate-induced corrosion of any of the nickel-zinc battery components.

The proportions of zinc (II), stearate salts and graphite are identified for each cell in this chapter. The method for preparing the active mass was for the most part identical in each case (variations stated for each cell) as detailed in the following section.

6.2.1 Preparation of zinc hydroxide-graphite suspension

Zinc sulfate was dissolved in water and heated to 50-60°C. Aqueous sodium hydroxide was prepared as a separate solution. Graphite was dispersed in the sodium hydroxide solution, since a higher degree of dispersal was achieved in this solution compared to that in the zinc sulfate solution. The sodium hydroxide dispersed with graphite solution was added slowly with stirring into the zinc sulfate solution. Then a grey suspension of a zinc hydroxide graphite mixture, was formed. Graphite provided nuclei for zinc hydroxide precipitation and therefore the graphite was initially mixed with the suspended zinc hydroxide. The pH was adjusted to pH 8-9.

6.2.2 Dispersion with calcium or zinc stearate

A potassium stearate solution at 50-60°C prepared from a stoichiometric mixture of stearic acid and potassium hydroxide was added slowly with stirring into the zinc hydroxide-graphite suspension at 50-60°C. The pH of this mixture was adjusted to 8-9. The mixture was stirred for 5-10 minutes to ensure thorough mixing of potassium stearate with the zinc hydroxide graphite particles.

Depending on whether a calcium stearate or zinc stearate material was required either a calcium nitrate or zinc sulfate solution was added slowly with stirring into the mixture. While the calcium nitrate or zinc sulfate solution was added into the suspension, insoluble calcium stearate or zinc stearate was precipitated on surfaces of the existing zinc hydroxide-graphite particles that acted as the nuclei for the precipitation. As a result, the insoluble hydrophobic calcium stearate or zinc stearate was highly dispersed among the zinc hydroxide-graphite particles, making them hydrophobic by precipitation on the surface of the particles.

As zinc sulfate solution or calcium nitrate solution was added, the relatively stable suspension was broken due to the formation of hydrophobic zinc active mass and turned into a grey precipitate. This final precipitated mixture was heated to 70°C and stirred for a further 10 minutes. Upon cessation of stirring the active mass mixture settled on the bottom of the beaker as a grey precipitate. After cooling to room temperature, this active mass was filtered and washed with water. In the latter stages of this research project it was established that this washing step was not necessary. In contrast, on the one occasion where calcium chloride was used in place of calcium nitrate (charge/discharge cycling results not reported here), even after rigorous washing water, the entrained chloride in the active mass caused pronounced corrosion to the nickel electrode current collector and its terminal.

Unlike previous active mass preparations in this project, the active mass was not compounded as a dry material that requires wetting with water or electrolyte to form a material suitable for pasting on the current collector. In this new preparation, the active mass was maintained in a wet state and immediately available for pasting. Furthermore, if this new active mass were dried, then it was found to be highly hydrophobic. Such

dry powders could not be wetted with water and they floated on the surface as a consequence. However, given sufficient time the dry active mass could be gradually wetted in the alkaline electrolyte (30% KOH).

If the wet active mass was pressed to squeeze out the water without prior drying, a hard hydrophobic sheet was formed. This greatly assisted with the overall electrode preparation process. Immediately after pasting, good contact of the active mass with the current collector was achieved by pressing the electrode in a bench top vice.

Stearate was included in the zinc electrode to make the active mass hydrophobic. The extent of electrolyte accessibility had already been shown to play an important role in cycle life performance as described in Chapter 5. This had primarily been achieved by modification of the structural components of the nickel-zinc cell. Clearly, the relative amount of stearate in the zinc active mass was expected to play an important role in determining the performance of the cells. A number of cells with varying amounts of stearate are reported in the following sections.

6.3 Cells #6.1 & #6.2: 38.3% (w/w) zinc stearate

The zinc active mass used to paste the zinc electrodes for Cell #6.1 was prepared as described in the previous section with 0.1 mol zinc hydroxide, 8 g zinc stearate and 3 g graphite. This constituted a zinc active mass with 38.3% (w/w) of zinc stearate. Cell #6.1 was assembled otherwise identically to that for the wrapped and bagged Cell #5.3 reported in Chapter 5. The electrolyte was 30% (w/w) KOH saturated with zinc oxide (60 g/L) and tetrabutylamonium hydroxide, the latter for inhibition of zincate reduction as established in Chapter 4.

The cell was subjected to two formation cycles. The formation cycle regime is given below:

i) Charging at 160mA for 10 hours;

ii) 5 minutes at open circuit;

iii) Discharging at 160mA until the cell voltage dropped to 1.3V; and

iv) 5 minutes at open circuit prior to the next cycle.

After two formation cycles, the cell was then subjected to regular cycles under the regimen given below:

i) Charging at 400mA for 2.5 hours;

ii) 5 minutes at open circuit;

iii) Discharging at 500mA until the cell voltage dropped to 1.3V;

iv) 5 minutes at open circuit prior to the next cycle; followed by

v) 40 seconds intervals for reading, saving and displaying the date.

Figures 6.1 and 6.2 show the discharge/charge efficiency and end of charge cell voltage, $E_{cell,eoc}$ as a function of cycle number for Cell #6.1 respectively. The efficiency declined to 69.1% in only 13 cycles with an accompanying decline in $E_{cell,eoc}$ indicative that pronounced dendrite formation had commenced at a far earlier point than expected. This formation of dendrites is confirmed in Fig. 6.3 by a decline in E_{cell} at the end of charge for the cycle 12.

A duplicate cell to Cell #6.1 was constructed to determine whether this rapid failure was due to the active mass modifications. Cell #6.2 was subjected to the same formation and regular cycles as Cell #6.1. This cell also failed far earlier than anticipated, maintaining better than 80% capacity for only 45 cycles as shown in Fig. 6.4.

After these failures, the cells were disassembled for examination after a further charging period (with no following discharge, to leave the electrodes in the charged state). There was no visible change compared to Cell #4.1 in the zinc active mass pasted onto the current collector except for several dendrites that had punctured the separators. It was

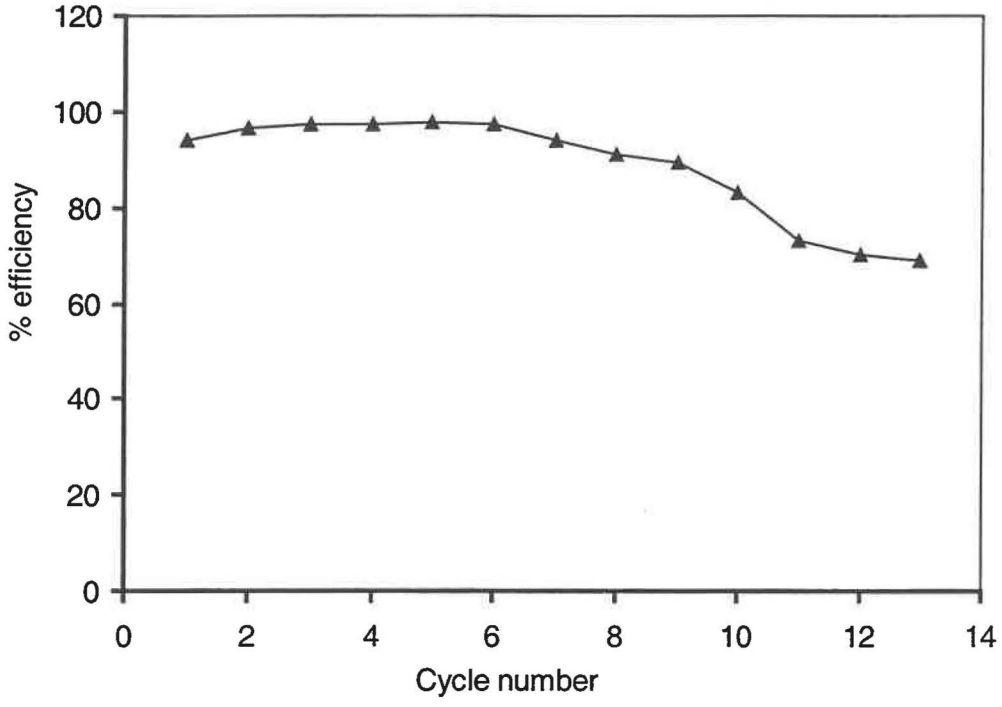

Fig. 6.1 Discharge/charge efficiency as a function of cycle number for Cell #6.1.

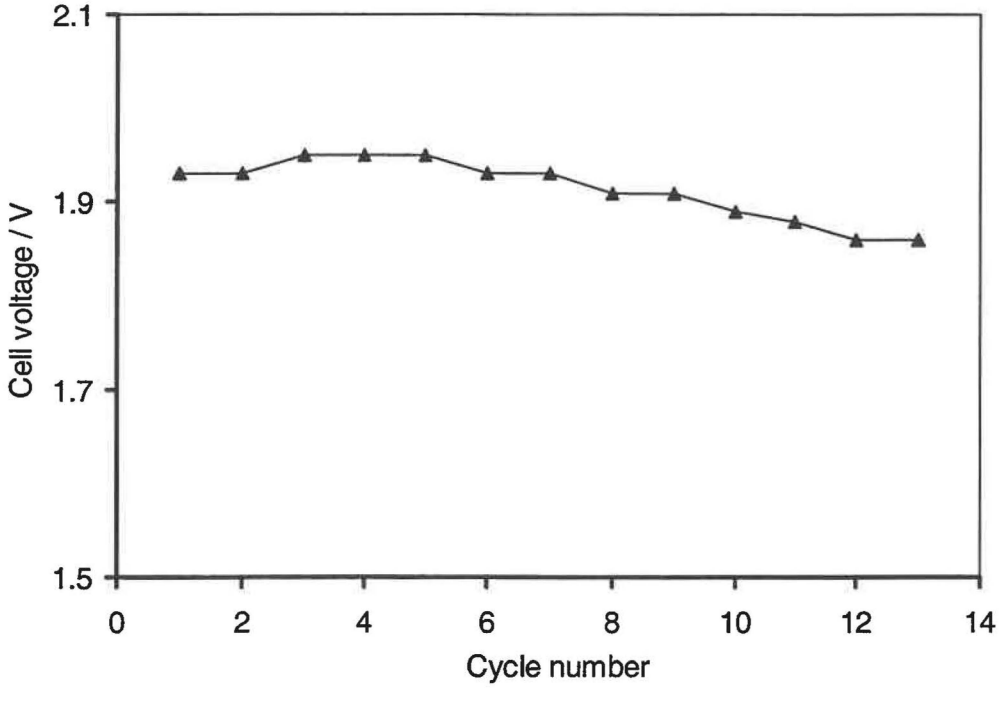

Fig. 6.2 End of charge cell voltage as a function of cycle number for Cell #6.1.

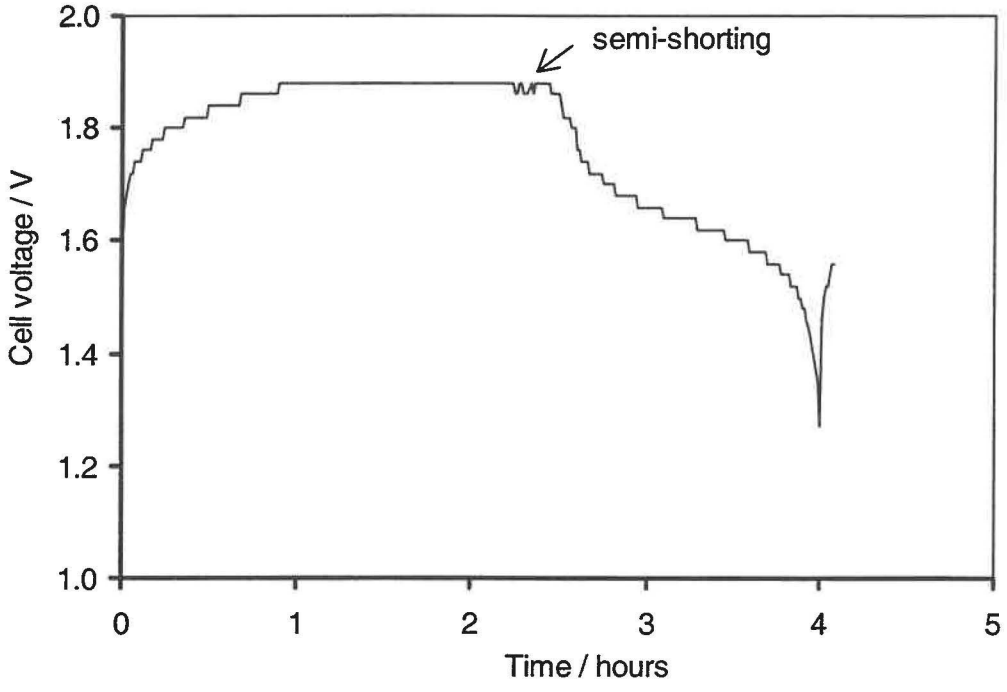

Fig. 6.3 Cell voltage variation in cycle 12 for Cell #6.1 with evidence of dendrite growth as indicated by the arrow.

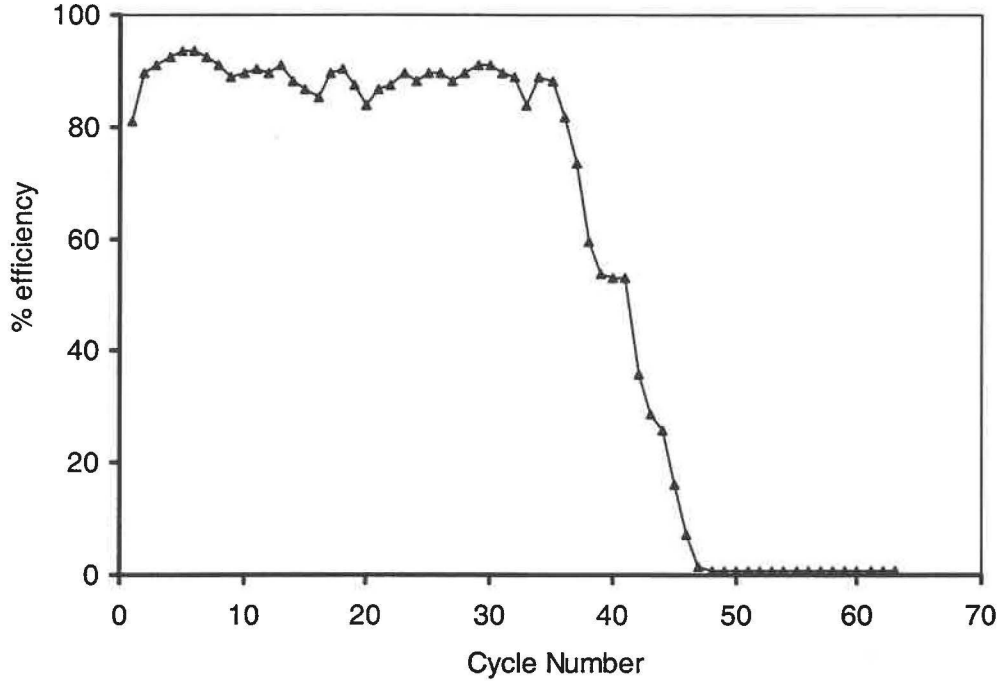

Fig. 6.4 Discharge/charge efficiency as a function of cycle number for Cell #6.2.

found, however, that only a thin layer of active mass in good contact with the brass mesh current collector was activated in the formation and subsequent cycling. The remaining active mass remained unchanged from the original paste with no visual evidence of having taken part in the previous charge-discharge cycles.

It was deduced that the zinc stearate content was too high with its precipitate covering the zinc hydroxide-graphite particles and consequently too little electrolyte was accessible to the electrode. The zinc stearate precipitate covering the zinc hydroxide-graphite particles, therefore, insulated the active particles as well. Only a small quantity of this hydrophobic mass immediately in contact with the brass mesh participated in the charge-discharge process. However, given the absence of the network of metallic zinc in the active mass, this participation was at a high local current density, which promoted the formation of zinc dendrites even though the electrolyte had been saturated with tetrabutylammonium hydroxide. If this interpretation was correct, then reducing the amount of the zinc stearate in the zinc active mass should prove beneficial to the activity.

6.4 Cell #6.3: 18.9% (w/w) zinc stearate

The zinc active mass used to paste the zinc electrodes for Cell #6.3 was prepared as described in Section 6.2 with 0.1 mol zinc hydroxide, 3 g zinc stearate and 3 g graphite. This constituted a zinc active mass with about 18.9% (w/w) zinc stearate, approximately one half of that for Cells #6.1 and #6.2. Cell #6.3 was constructed otherwise identically to that Cells #6.1 and #6.2. This cell was subjected to identical formation and regular cycling as for Cells #6.1 and #6.2.

Figure 6.5 shows the variation of the discharge/charge efficiency versus cycle number for Cell #6.3. In comparison with either Cells #6.1 or #6.2, this test cell with only 18.9% zinc stearate exhibited far superior cycle life performance and survived for more than 800 charge/discharge cycles.

A number of new features are evident in this and many other subsequent high cycle life test cells. The first is that with increased longevity of the test cells the likelihood of failure of the battery cycling equipment increased. At approximately 4 hours duration

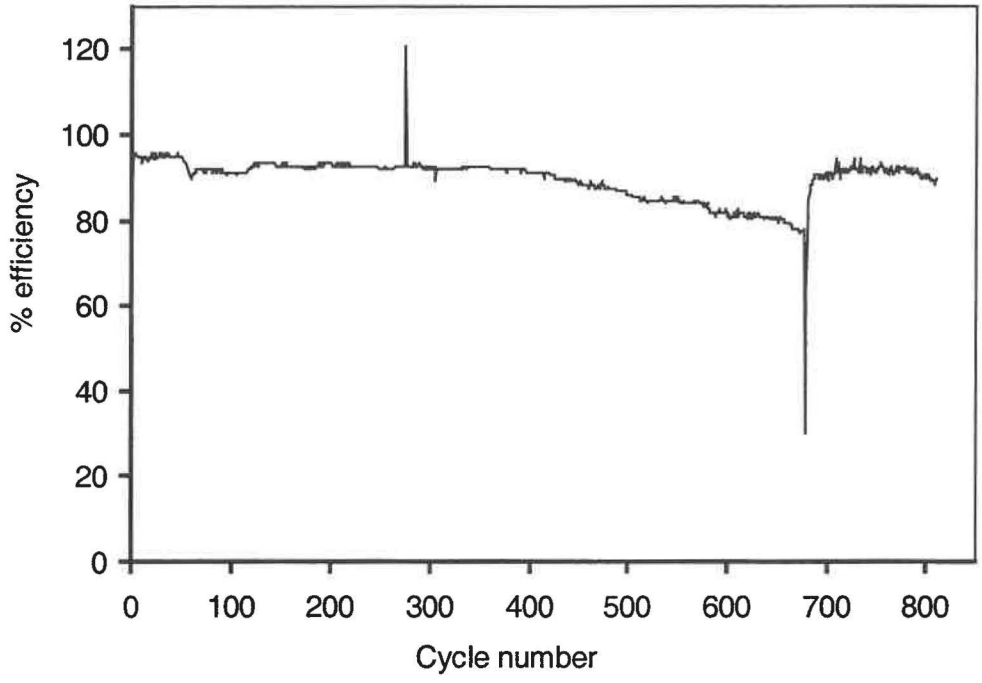

Fig. 6.5 Discharge/charge efficiency as a function of cycle number with much prolonged cycle life for Cell #6.3.

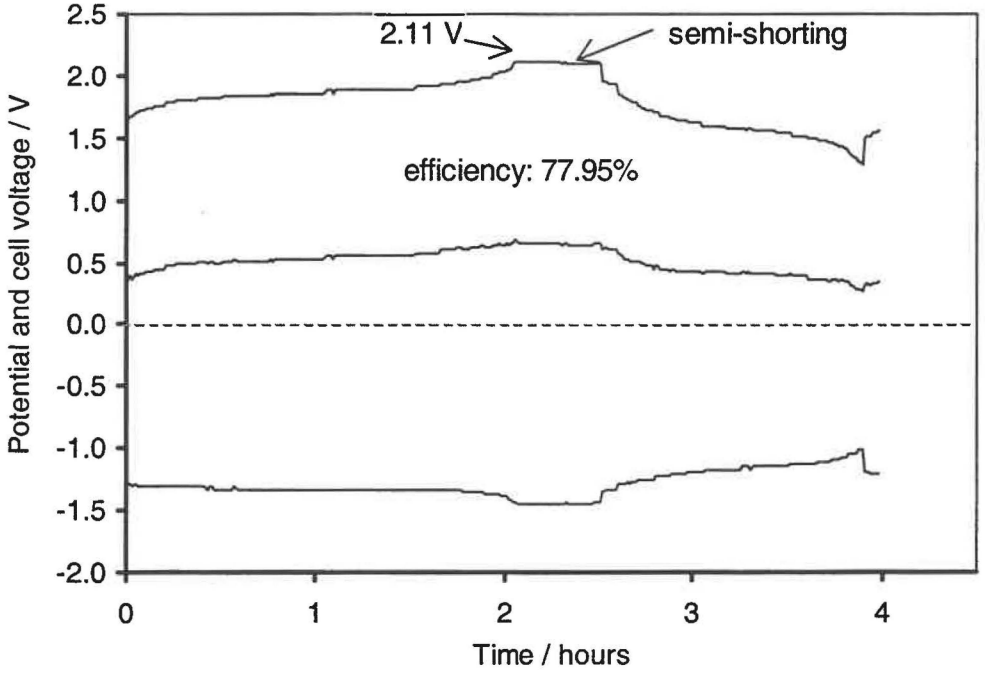

Fig. 6.6 Variation of electrode potential and cell voltage in cycle 667 with evidence of semi-shorting for Cell #6.3 as indicated by the arrow.

for every charge/discharge cycle, the 800 cycles shown in Fig. 6.5 represents in excess of 120 days of continuous testing. These equipment failures were found to be caused by power cuts, power fluctuations leading to erroneous computer activity, or undiagnosable errors in the ADC/DAC equipment causing the switching relays to fail to change state at the end of a segment in the charge/discharge cycle. Power failures were relatively rare and were readily dealt with by manually recommencing the charge/discharge cycle. Power fluctuations were more damaging since they left test cells in a continuous charge or continuous discharge state. These were fortunately rare since they usually terminated an experiment. The relay switching error was the most frequent problem with failure to switch from charging to discharging conditions being the most frequently encountered. One such example of relay switching failure is evident in Fig. 6.5 as a marked increase in the capacity for cycle 276. This was due to the switching relays failing to switch from open circuit at the end of charging to discharge conditions for cycle 275. Consequently, the discharge for cycle 276 is for two complete charging cycles, with no intervening discharge (the cell remained at open circuit during normal discharge). This accounts for the greater than 100% capacity. Despite being an untoward event, this failure demonstrated the robustness of the cell to overcharge conditions. The rapid return of efficiency to pre-relay failure levels demonstrated that no long-term damage to the cell had taken place. Under such conditions one might have expected the growth of dendrites to arise from overcharge. That this did not take place on this, and other, overcharge occasions was taken as a positive result.

The second new feature evident in Fig. 6.5 is that the cell was capable of recovery when dendrite growth caused semi-internal shortage during charge. Over the first 400 cycles the capacity for Cell #6.3 only declined from 94% to 91%. Following this, there was a period of more rapid decline to 78.0% for cycle 677 (falling below 80% benchmark capacity at cycle 620). The rapid decline in efficiency was associated with the dendrites that caused semi-shorting.

Cycle 677 was a critical cycle. After this cycle the cell was deliberately externally shorted for 24 hours and then subjected to the regular cycles again. Figure 6.6 shows the electrode potential and cell voltage E_{cell} during charging and discharging for cycle 667. There is some evidence for formation of semi-shorting dendrites with a slight decline in E_{cell} at the end of the charging process. Because of the new cell structure developed in

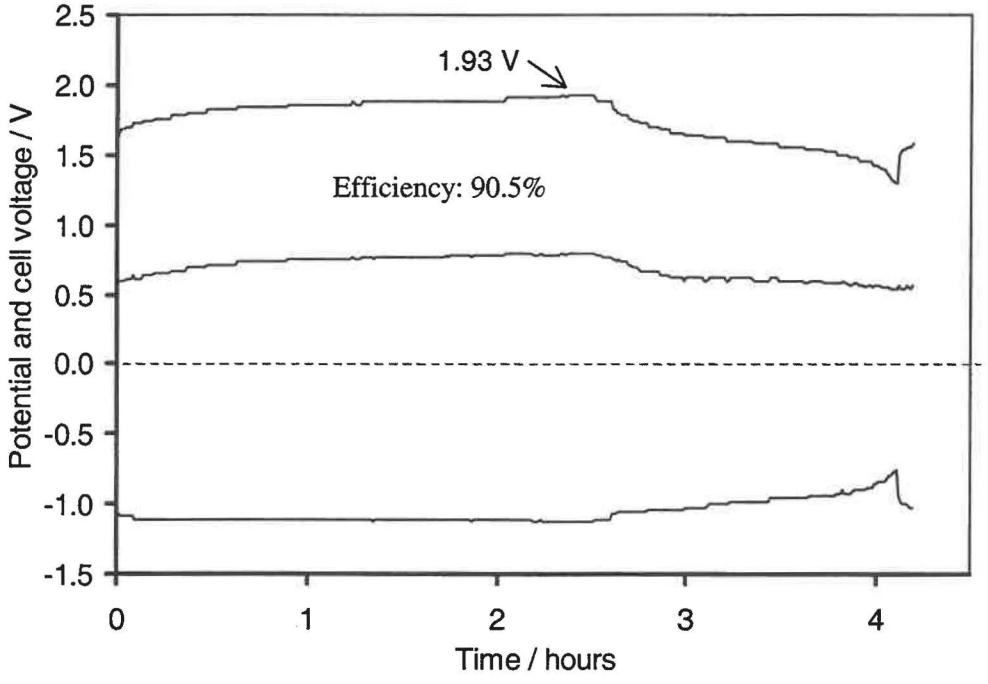

Fig. 6.7 Electrode potential and cell voltage variation for cycle 687 of Cell #6.3 with no semi-shorting appearance.

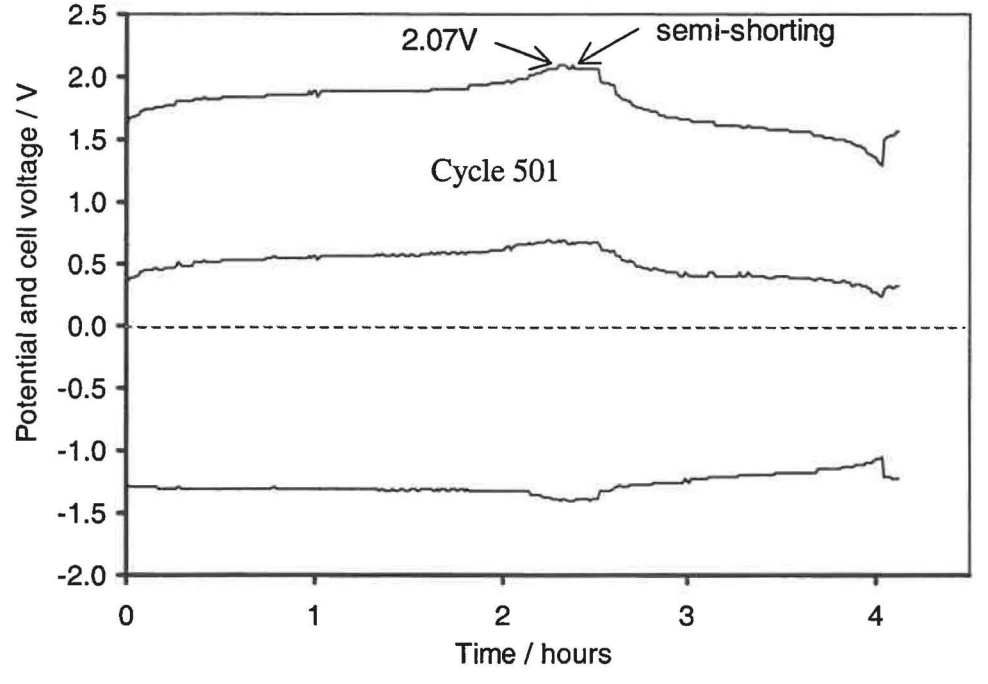

Fig. 6.8 The first cycle (cycle 501) with appearance of semi-shorting for Cell #6.3.

Chapter 5, the cell was believed capable of recovery if the declined efficiency was associated with dendrite growth. One means to remove semi-shorting dendrites is to subject the test cell to a prolonged discharge period until the cell is completely exhausted. This is in stark contrast to the programmed cessation of discharge when E_{cell} falls below 1.3 V. To test whether or not the predicted semi-shorting dendrites could be removed by this process, Cell #6.3 was subjected to deliberate external shorting for 24 hours after the discharge segment for cycle 677. After this exhaustive discharge normal cycling was immediately resumed. On the first cycle after this treatment only 30% efficiency was attained, however, within the following 5 cycles the efficiency had increased beyond that for cycle 677. This sharp increase in efficiency demonstrated that the deliberate external shorting did afford a recovery of discharge capacity and the removal of semi-shorting dendrites. Figure 6.7 shows the 10^{th} cycle (cycle 687) after the deliberate external shorting. It can be seen that no semi-shorting appeared while the cell voltage approached 1.95V at the end of charge in this cycle and the efficiency increased to 90.5%.

If the dendrites were responsible for the declined efficiency, then the efficiency should commence decline with the onset of semi-shorting. Data analysis searching for the first cycle with semi-shorting appearance revealed that semi-shorting initially appeared during cycle 501. Figure 6.8 shows the electrode potential and cell voltage for this first onset of semi-shorting. Given that the semi-shorting might be the only cause for efficiency decline, then the efficiency should have been stable for the first 501 cycles. Figure 6.5 indicates that by cycle 500 the efficiency had declined, which indicates that there must be some other causes responsible for the decline in efficiency.

Figure 6.9 shows the last cycle (cycle 500) before semi-shorting appeared. The most important feature for cycle 500 is that the cell voltage approached the plateau value of 2.07 V during charge. It was noted that when the cell voltage approached this plateau, a significant rate of hydrogen evolution was observed. This plateau cell voltage is significantly higher than those found at end of charge earlier in the cycle life of Cell #6.3. For example, figure 6.10 shows the potential profile for cycle 100 where the cell voltage did not rise above 1.97 V during charge.

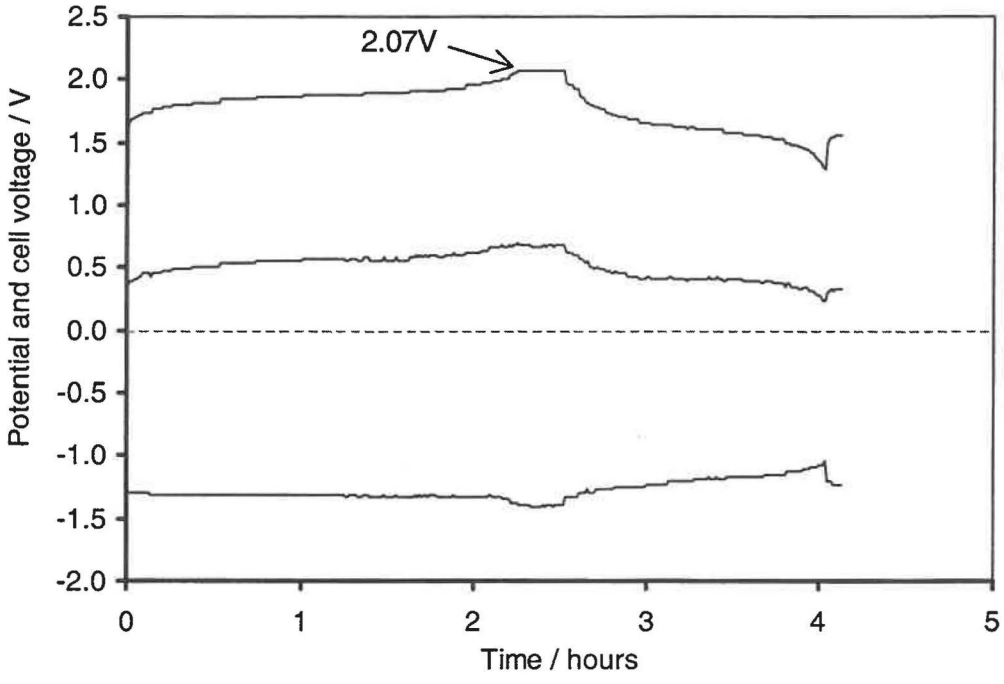

Fig. 6.9 Last cycle before appearance of semi-shorting (cycle 500) for Cell #6.3.

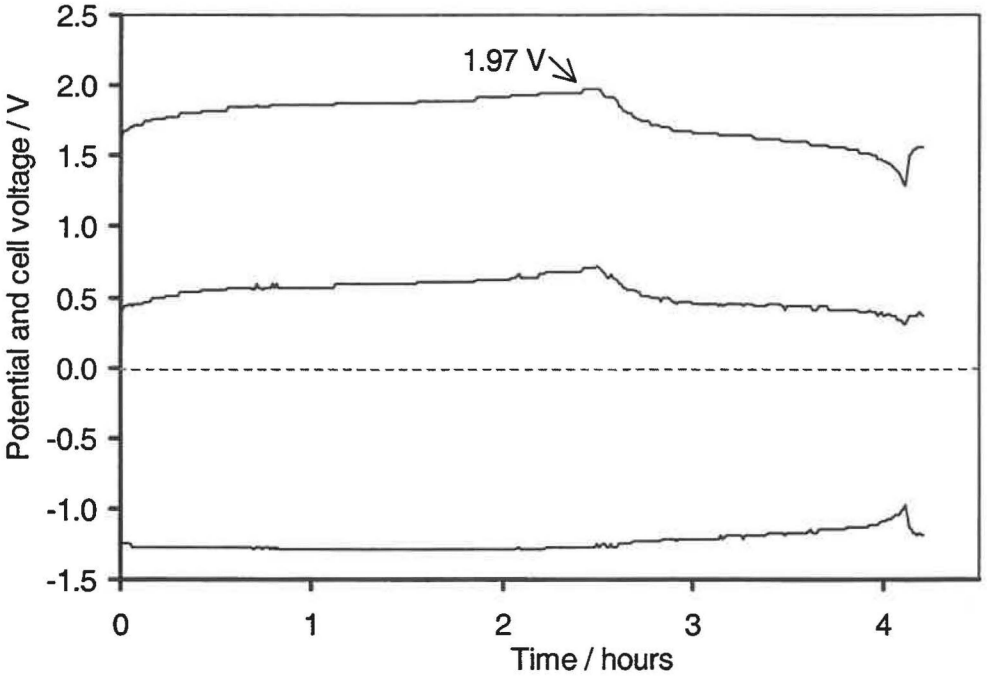

Fig. 6.10 Variation of electrode potential and cell voltage in cycle 100 for Cell #6.3.

Figure 6.11 is a combined plot of Figs.s 6.9 and 6.10 to facilitate comparison of cycles 100 and 500 for Cell #6.3. A number of comparisons may be made.

Charging:

i) The end of charge cell voltage in cycle 500 was higher than that in cycle 100 (2.07 V vs 1.97 V);

ii) The nickel electrode potential at the end of charge in cycle 500 was, however, slightly lower than that for cycle 100. As a consequence, the nickel electrode had no contribution to the higher end of charge cell voltage in cycle 500; and

iii) The zinc electrode potential at the end of charge in cycle 500 was much higher than that in cycle 100.

Consequently, only the zinc electrode did contribute to the cell voltage approaching the plateau value 2.07V in cycle 500. According to this, the gas evolved when the cell voltage attained the plateau value should be hydrogen from the overcharged zinc electrode rather than the oxygen from the nickel electrode.

Discharging:

i) There is no significant difference in the decline in potential of the zinc electrode between cycle 100 and cycle 500 towards the end of discharge. However, the nickel electrode potential declined more rapidly in cycle 500 than in cycle 100, contributing to the decline in efficiency;

ii) In comparison with cycle 100, the lower nickel electrode potential at the end of charge during cycle 500 indicates that the charge acceptance was inferior, leading to a faster decline in potential near the end of discharge; and

iii) The consequent overcharge of the zinc electrode in subsequent cycles causing hydrogen evolution must be associated with the efficiency decline.

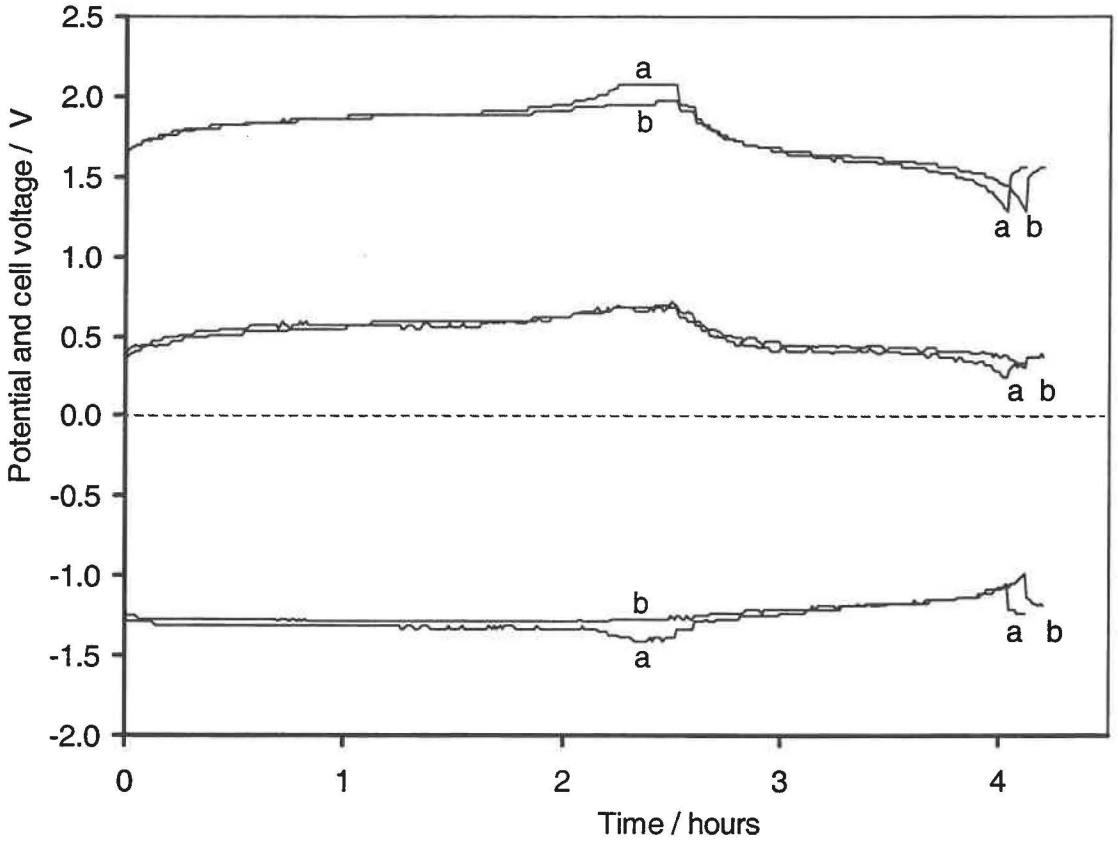

Fig. 6.11 Difference between cycle 100 (curve **b**) and cycle 500 (curve **a**) in potential and cell voltage for Cell #6.3.

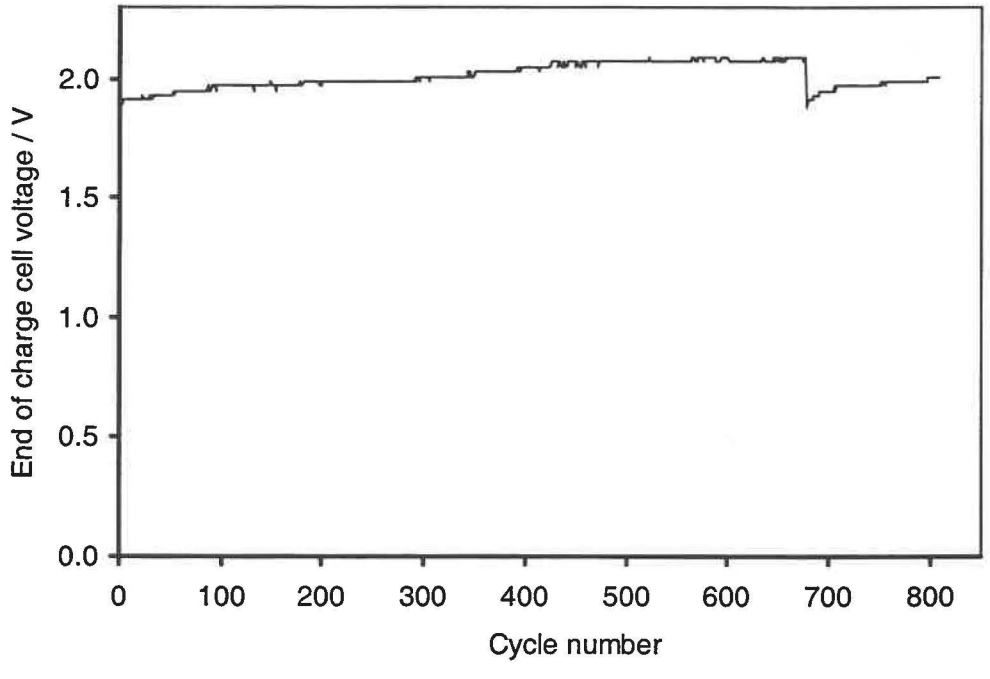

Fig. 6.12 End of charge cell voltage as a function of cycle number for Cell #6.3.

Diffusion of this hydrogen to the nickel electrode resulted in a self-discharge process.

$$H_2(g) + 2NiOOH(s) \longrightarrow 2Ni(OH)_2(s) \qquad (6.5)$$

This further contributed to a progressive decline in efficiency. The greater the discharge imbalance between the nickel and zinc electrodes leads to progressively greater hydrogen discharge at the nickel electrode.

Given that the overcharged zinc electrodes causing hydrogen evolution is responsible for the efficiency declined through reducing the charge acceptance of nickel electrode, then eliminating hydrogen evolution at the zinc electrodes would result in nickel electrode improvement and recovery of the cell.

Deliberate external shorting after cycle 677 provided extra zinc hydroxide at the zinc electrode and removal of overcharge together with elimination of hydrogen evolution at the zinc electrode. This led to a progressive increase in % efficiency for 150 cycles until the imbalance between the nickel and zinc electrode capacities appeared once more.

Figure 6.12 shows the variation of the end of charge cell voltage as a function of cycle number. Just as there are two stages in cell efficiency there are two discernible stages in $E_{cell,eoc}$. For the first 400 cycles, where efficiency is maintained between 94% and 91%, $E_{cell,eoc}$ exhibits a steady increase from 1.9 V to 2.1 V. Following this increase, $E_{cell,eoc}$ remains relatively constant until cycle 677 whilst the cell efficiency commences a period of more rapid decline. This decline in efficiency is not inconsistent with the anticipated increase in hydrogen evolution and the formation and proliferation of dendrites. After deliberate external shorting the correlation between increasing $E_{cell,eoc}$ and high efficiency does appear to follow until cycle 790. However, beyond this cycle, efficiency commences a more rapid decline before $E_{cell,eoc}$ increased to 2 V. Consequently, the decline in efficiency for the post-external shorting case can not be only attributed to hydrogen evolution. Indeed, the low value for $E_{cell,eoc}$ may be better accounted for by the formation of further semi-shorting dendrites.

By cycle 689 the efficiency had increased to 90.5%, a level that was last obtained on cycle 450. The efficiency remained stable over 91% until cycle 790, but then

commenced a rapid decline. Cycling was terminated after cycle 809 at 90% efficiency due to the need to use the test equipment for further modified cells.

6.5 Cells #6.4 & #6.5: 18.9% (w/w) calcium stearate

Cell #6.4 was similar in construction to Cell #6.3 with a number of modifications relating to the zinc active mass and electrode current collector. These modifications were made in the hope that the high cycle life exhibited by Cell #6.3 could be improved. The modifications included:

i) Replacement of zinc stearate with calcium stearate;

ii) Addition of solid potassium hydroxide into the wet zinc active mass at the ratio of 0.3 g to every 0.1 mol $Zn(OH)_2$; and

iii) Modification of the interface between the brass mesh and the zinc active mass by coating the brass current collector with zinc metal prior to pasting with the active mass. The zinc coating was obtained by electroplating at 5 A for 2 minutes for each of the two current collectors.

The zinc active mass used to paste the zinc electrodes for Cell #6.4 was prepared as described in Section 6.2 with 0.1 mol zinc hydroxide, 3 g calcium stearate and 3 g graphite. This constituted a zinc active mass with 18.9% (w/w) of calcium stearate, approximately one half of that for Cells #6.1 and #6.2.

Calcium stearate was used in place of zinc stearate to avoid the possibility that zinc stearate was participating in the electrode reactions. The balance between hydrophobicity and accessibility of the electrolyte to the active mass is likely to be highly balanced. Deliberate addition of solid potassium hydroxide by grinding with the zinc hydroxide-graphite-calcium stearate active mass provided a reservoir of potassium hydroxide immediately available within the active mass during the formation process. The formation process was also predicted to be assisted by the electroplated zinc on the brass mesh. The nucleation and growth of zinc metal onto pre-existing zinc is more likely to be a facile process than growth onto brass.

Cell #6.4 was subjected to two formation cycles identical to those for Cells #6.1, #6.2 and #6.3 prior to regular cycling. The regular cycles were modified from those for these earlier cells with the regime given below:

i) Charging at 500mA for 2 hours;

ii) 5 minutes at open circuit;

iii) Discharging at 600 mA until the cell potential dropped to 1.3 V; followed by

iv) 5 minutes at open circuit prior to the next cycle.

As a result of the higher rates of charge and discharge 10% more cycles could be achieved within a given time compared to those for Cells #6.1, #6.2 and #6.3.

Figure 6.13 shows the cell efficiency as a function of cycle number. This cell suffered five periods of overcharge (labelled 1-5) during the 200 days of continuous cycling due to relay switching errors. Two deliberate external shortages were also made to the cell to arrest declines in efficiency (labelled A and B).

In a similar manner to Cell #6.3, Cell #6.4 exhibited two distinct regions of efficiency prior to deliberate external shorting. Ignoring the first 20 cycles, Cell #6.4 showed a high, and even slightly increasing discharge capacity from 92% to 94% over the first 560 cycles. Following this, there was a steady decline to 84.9% by cycle 720. During these first 720 cycles there were 4 periods of overcharging of the cell due to equipment failure. As in the case for the single such event for Cell #6.3 no long lasting effects were discernible.

Figure 6.14 shows E_{cell} during the charge and discharge process for cycle 160 immediately after overcharging on cycle 159. There is no evidence for dendrite growth during the prolonged periods at the E_{cell} plateau of 1.95 V. The only artifact of this overcharge in this case is the negative drift in E_{pos} and E_{neg} due to the oxygen evolution shifting the potential of the reference electrode.

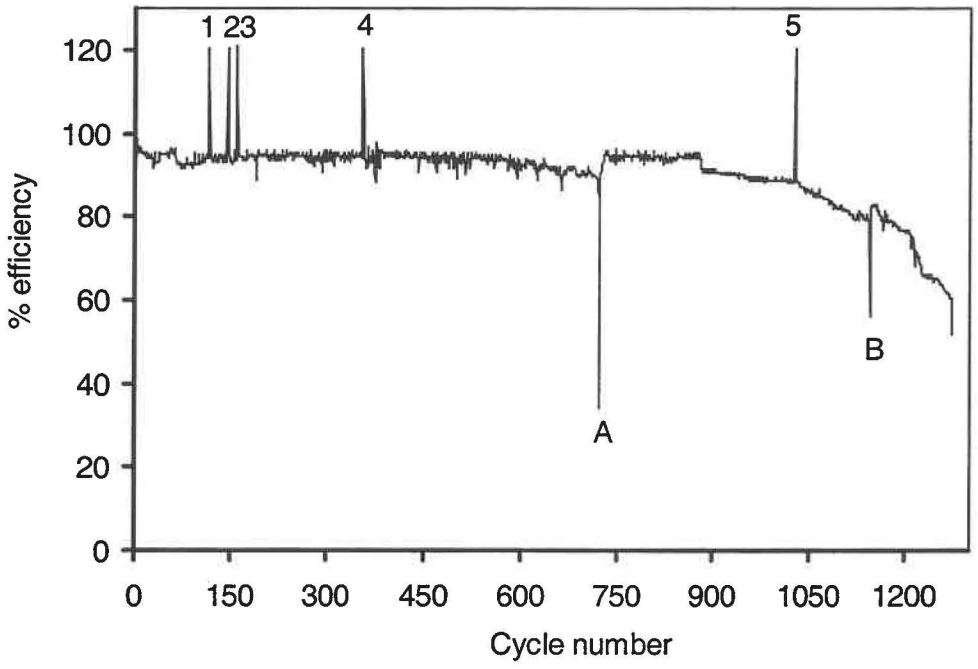

Fig. 6.13 Discharge/charge efficiency as a function of cycle number for Cell #6.4 (periods of relay failure are labelled 1-5 and deliberate 24 hour shortages are labelled A and B).

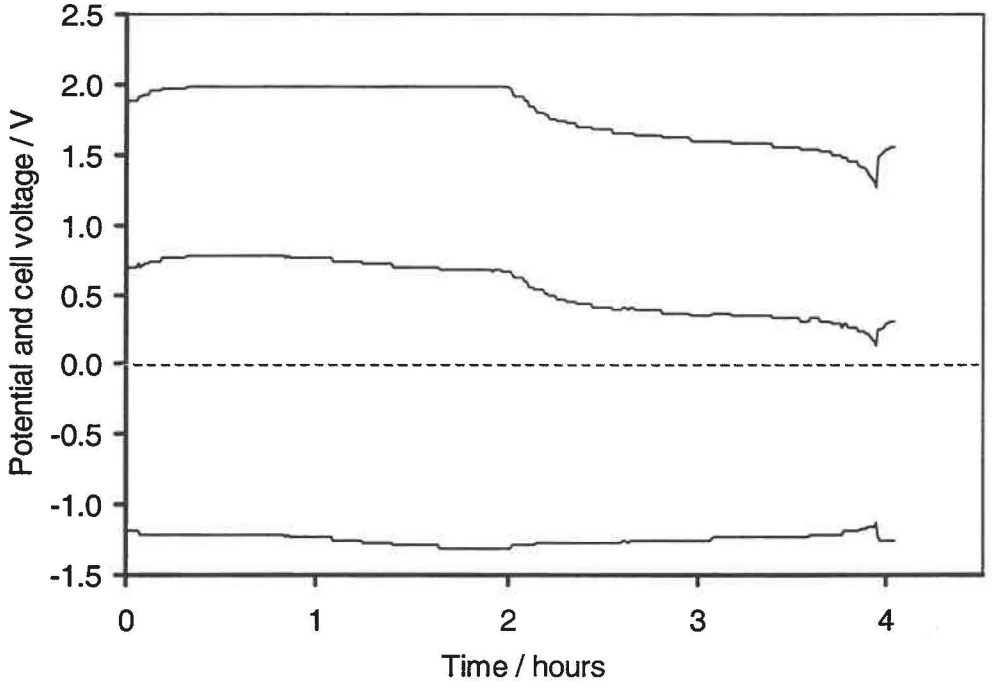

Fig. 6.14 Variation of electrode potential and cell voltage during cycle 160 for Cell #6.4.

It would seem that hydrogen evolution did not take place suggesting that the capacity of the zinc electrodes was higher than that of the nickel electrode and oxygen was partly re-reduced at zinc electrodes, reducing the chance for the zinc electrodes to be overcharged.

Cycle 720 with its efficiency reduced to 84.9% was also a critical cycle, after which the cell was deliberately shorted for 24 hours. By comparison with Cell #6.3, which was deliberately shorted after cycle 677 (when efficiency declined to 78.0% and semi-shorting had appeared by cycle 500), Cell #6.4 did not undergo semi-shorting in 720 cycles even after suffering four periods of overcharge due to equipment failure.

Semi-shorting or dendrite growth was not responsible for the efficiency decline by 720 cycles. In order to investigate the causes for this decline in efficiency, the potential profile for cycle 100 is compared with that for cycle 720 as shown in Fig. 6.15. In contrast to cycle 100 during the charging process, it is clear that the cell was overcharged in cycle 720 but there is no evidence for semi-shorting. The potentials of both nickel and zinc electrodes approached at the plateaus, leading the cell voltage increased to the plateau value. Four periods of overcharge due to equipment failures during the first 720 cycles contributed to the overcharge of the cell.

According to the potential variation during discharge, both nickel and zinc electrodes contributed to the cell voltage decline in cycle 720 in contrast to cycle 100 with the zinc electrode potential dropped more rapidly at end of discharge. The zinc electrode potential 5 minutes after charge in cycle 720 was higher than that in cycle 100, but it declined more rapidly during discharge, suggesting that passivation of the zinc electrode had developed gradually during the previous 720 cycles.

As in the case for Cell #6.3, there was a pronounced recovery of discharge capacity after deliberate external shorting of Cell #6.4 with capacity returning to 94% (pre-650th cycle levels) within a few cycles. This capacity was maintained until 880 cycles after which there was an abrupt drop to 90% and then a progressive decline to 87% by cycle 1029 where an overcharge event (the fifth overcharge) occurred and caused semi-shorting as shown in Fig. 6.16. Before this fifth overcharge, no semi-shorting had been evident.

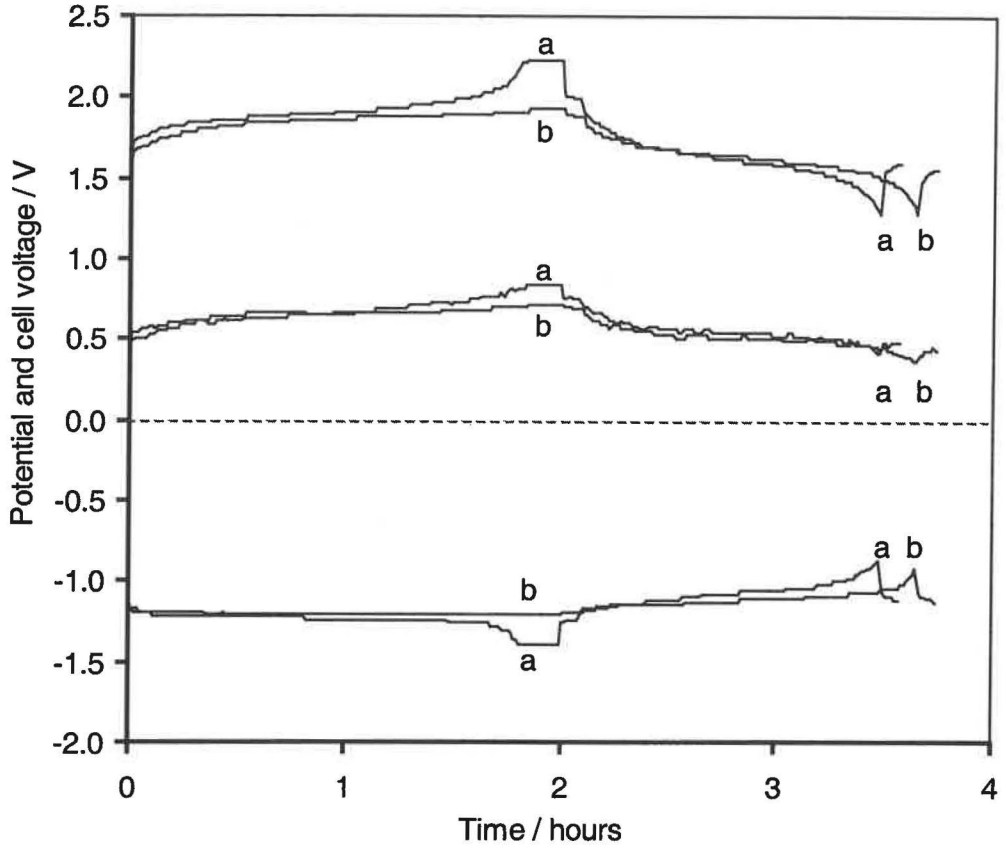

Fig. 6.15 Differences between cycle 100 (curve **b**) and cycle 720 (curve **a**) in potential and cell voltage for Cell #6.4.

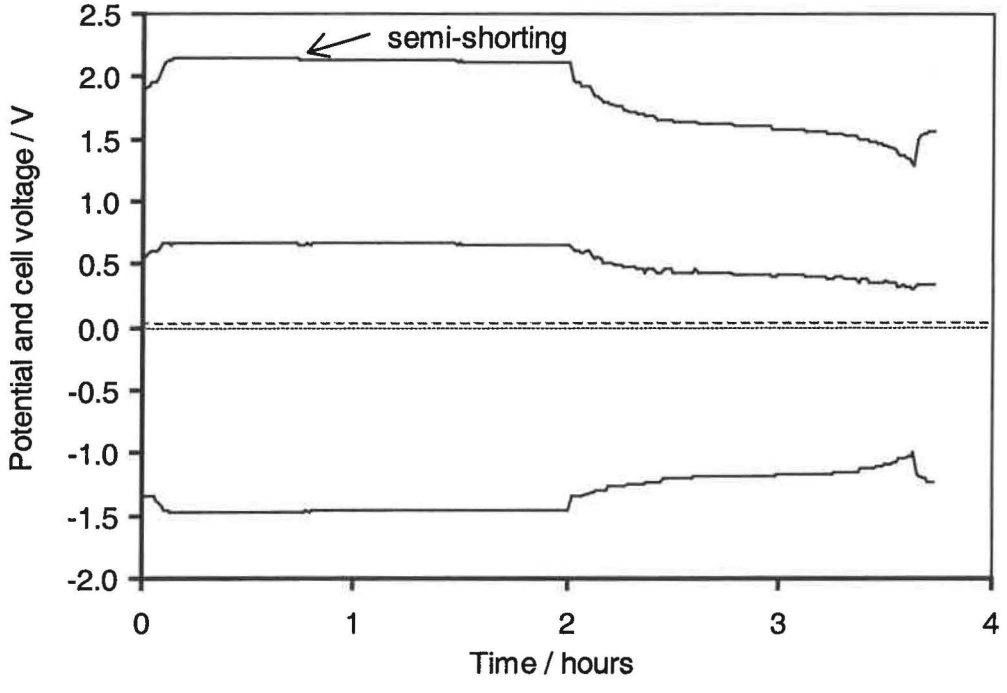

Fig. 6.16 Overcharge during cycle 1029 causing semi-shorting for Cell #6.4 as indicated by the arrow.

Figure 6.17 shows the potential profile for cycle 738 and cycle 1027 with no semi-shorting on cycle 1027. By comparison with cycle 738 where the efficiency increased to 93.6% after deliberate external shorting, the causes for the efficiency decline in cycle 1027 with efficiency 88.2% became distinct. The zinc electrode became overcharged by the end of charge in cycle 1027, leading to a decline in charge acceptance of the nickel electrode due to hydrogen evolution as described in the case for the Cell #6.3. The passivation of the zinc electrode gradually developed by cycle 1027, resulting in the zinc electrode potential declining more rapidly during discharge.

Overcharge in cycle 1029 caused semi-shorting, leading to a more rapid efficiency decline to 75% by cycle 1140. A deliberate 24 hour external short was again applied to halt this decline, but the efficiency did not increase to a significant extent and an even more rapid decline took place in the ensuing cycles. Cycling was terminated at 1280 cycles after recovery was not attained.

Visual inspection of the cell during cycling revealed that considerable swelling had taken place and zinc active mass, particularly metallic zinc, was accumulated at the center of the electrode. Metallic zinc at this location could not be completely oxidized at the end of discharge. This is a typical phenomenon of shape change, associated with the development of passivation in the zinc electrode. This swelling was progressive and non-reversible, and did not apparently alter between charged and discharged states of the battery. This could indicate that the swelling is related to the zinc active mass and may also relate to the postulated development of passivation of the zinc electrode.

Modifications to the electrolyte had considerably lowered the rate of zinc active mass redistribution and have certainly prevented the gross redistribution due to zincate solubility so that in excess of 1100 charge/discharge cycles are now obtainable. The efforts to date in modifying cell structures, electrolyte composition and active mass composition, have not prevented this phenomenon but have prolonged the cell cycle life significantly.

A duplicate cell to Cell #6.4 was constructed (Cell #6.5). It was subjected to identical formation and regular cycling. Figures 6.18 and 6.19 show the discharge/charge efficiency and end of charge cell voltage as a function of cycle number respectively.

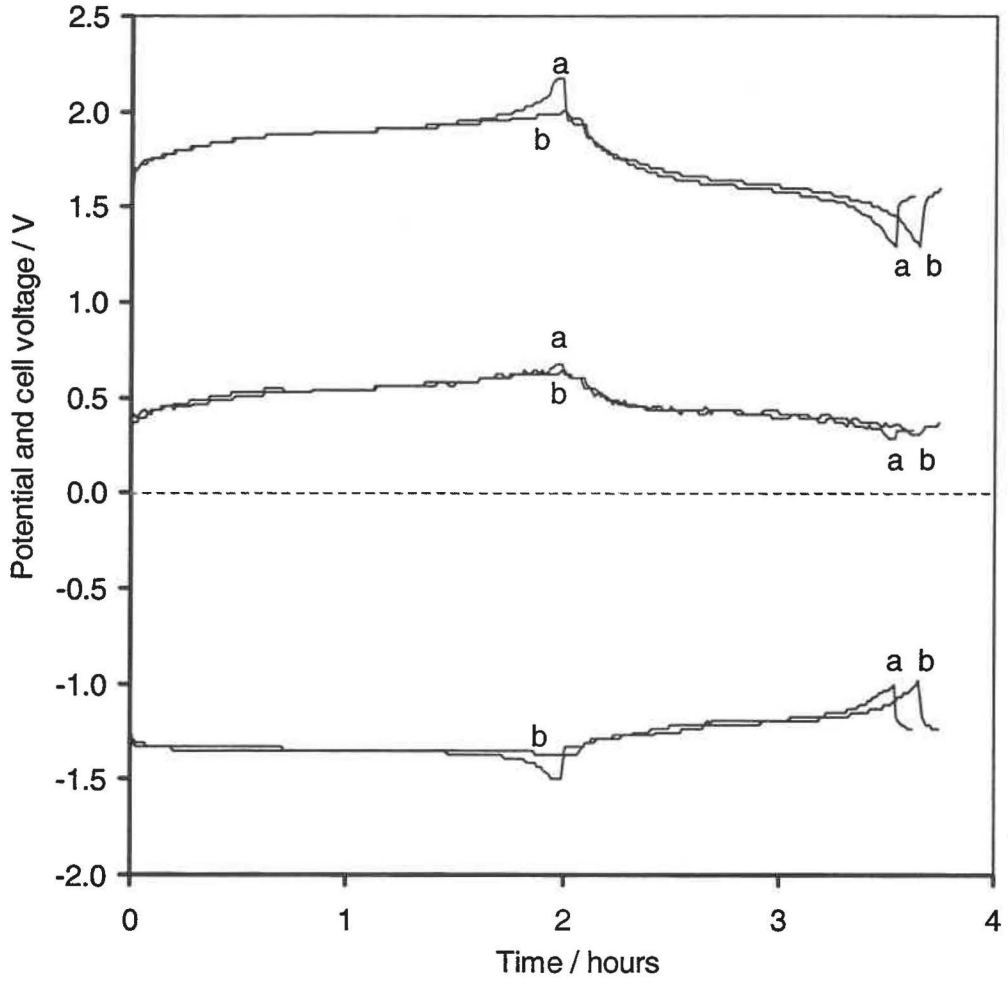

Fig. 6.17 Differences between cycle 738 (curve **b**) and cycle 1027 (curve **a**) in electrode potential and cell voltage for Cell #6.4.

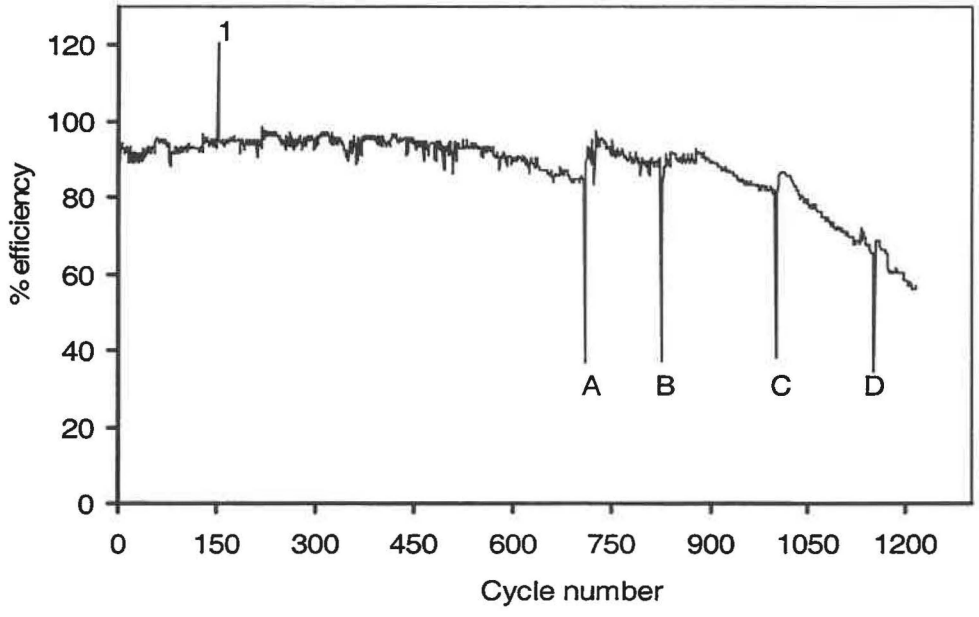

Fig. 6.18 Discharge/charge efficiency as a function of cycle numbers for Cell #6.5 (relay failure is labelled 1 and deliberate shortages are labelled A-D).

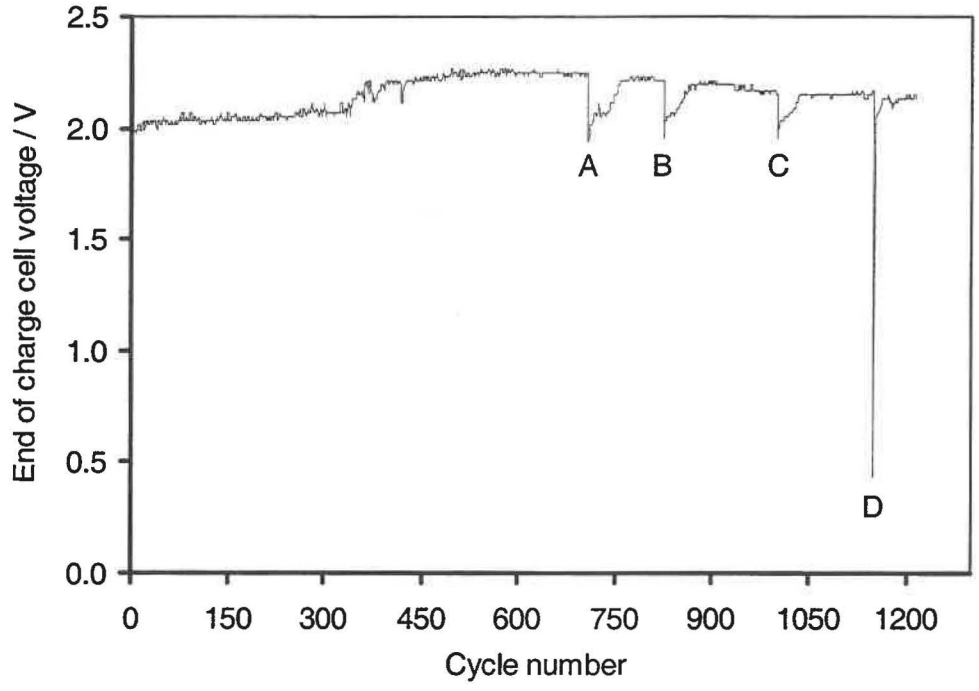

Fig. 6.19 End of charge cell voltage as a function of cycle number for Cell #6.5 (deliberate shortages are labelled A-D).

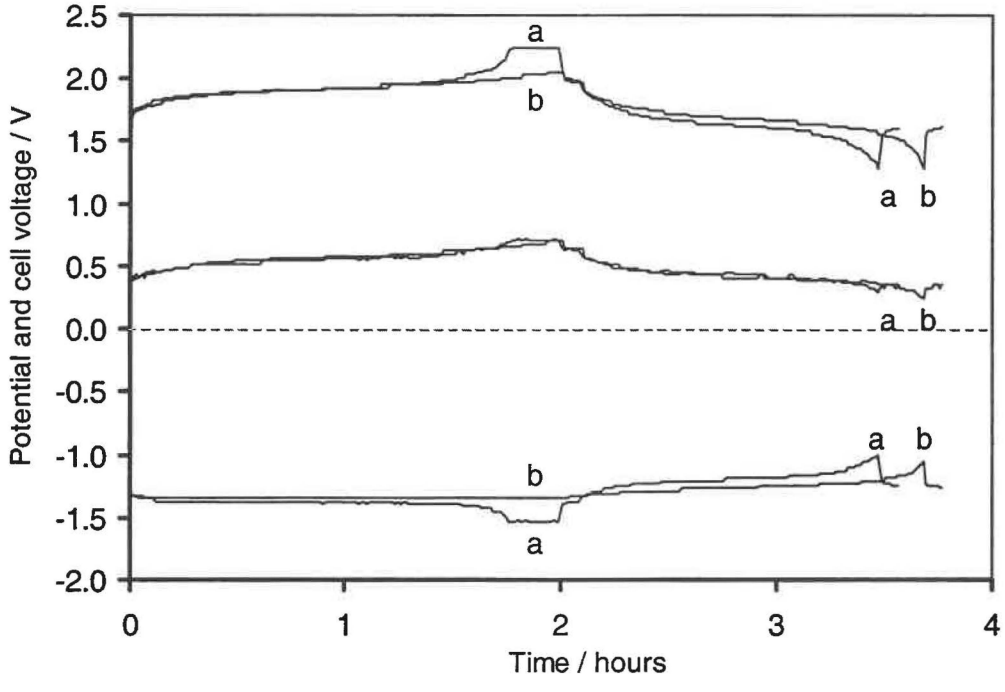

Fig. 6.20 Differences between cycle 140 (curve **b**) and cycle 706 (curve **a**) in electrode potential and cell voltage for Cell #6.5.

These results are similar in nature to those for Cell #6.4. However, one overcharge event took place and one deliberate external shorting was applied after 707 cycles. Just as in the case for Cell #6.4 there is an association between the steady rise in $E_{cell,eoc}$ and high efficiency. The marked step in $E_{cell,eoc}$ takes place at only 340 cycles compared to 560 cycles in Cell #6.4. This may have arisen from the high values for $E_{cell,eoc}$ at low cycle numbers. Cell #6.4 commenced regular cycling with an $E_{cell,eoc}$ of 1.9 V. In contrast, Cell #6.5 commenced cycling with an $E_{cell,eoc}$ of 2.0 V.

By comparison of cycle 140 and cycle 706 for Cell #6.5 in Fig. 6.20, the cause for the efficiency decline becomes apparent. These events are similar to those for Cell #6.4. Cycle 140, with an efficiency of 95.0%, was one cycle before the overcharge event took place while cycle 706, with an efficiency having reduced to 84.5%, was one cycle before the first deliberate external shorting for Cell #6.5. Here, the zinc electrode was overcharged on cycle 706 during the charge phase. The passivation of the zinc electrode had developed to a considerable extend as indicated by the zinc electrode potential decline during discharge.

Semi-shorting, however, also contributed to the efficiency decline. Semi-shorting was apparent in some cycles, such as on cycle 702 and cycle 703, but not evident during other cycles, such as 704th, 705th and 706th cycles.

Examination of E_{cell} during charge/discharge cycling suggested that progressive passivation and subsequent overcharging of the zinc electrodes was occurring to a greater extent in this cell than in Cell #6.4.

External shorting after cycle 707 was able to halt the overcharge and passivation temporarily, but could not prevent the overcharge and the passivation from further development. Internal shorting through dendrite formation eventually resulted from the overcharge. Swelling of this cell was also observed.

6.6 Cell #6.6: 5.8% (w/w) calcium stearate

Cell #6.6 was identical to Cells #6.4 and #6.5 with the exception that the calcium stearate was reduced to 0.8 g for every 0.1 mol of zinc hydroxide to give a 5.8% (w/w)

calcium stearate in the active mass. The cell was subjected to formation and regular cycles identical to those for Cells #6.4 and #6.5.

Figure 6.21 shows the two formation cycles. There was a decline in E_{cell} during the second formation charge consistent with dendrite growth, which did not continue when the cell was subjected to regular cycles. The plot of charge/discharge efficiency as a function of cycle number is shown in Fig. 6.22. Here, efficiencies greater than 90% were maintained for only 100 cycles, after which there was a steady decline in performance. Examination of E_{cell} during charge /discharge cycling did not reveal any further evidence for dendrite formation to account for this decline.

In contrast to cycle 50, the last cycle (cycle 241) shown in Fig. 6.23 clearly indicated that pronounced passivation was responsible for the decline in performance. Here, overcharging of the cell arose from the developing passivation of the zinc electrode.

Given the poor initial performance of this cell, efforts were not made to attempt recovery by deliberate shorting and cycling was terminated at cycle 241. It would appear that lower calcium stearate concentration in the zinc active mass could not effectively halt the development of the zinc electrode passivation or the zinc electrode shape change.

6.7 Conclusions

Zinc oxide, if used as the zinc active mass, will eventually convert into zinc hydroxide either by hydrolysis in the alkaline electrolyte, or by charge/discharge cycling. Such chemical change may, consequently, result in physical change of the zinc active mass. To avoid such physical and chemical changes, zinc hydroxide rather than zinc oxide was used as the active mass. Solubility was the main reason for its gross diffusion in the electrode. Introducing highly hydrophobic zinc stearate or calcium stearate converted the zinc hydroxide into a hydrophobic mass by precipitating zinc stearate or calcium stearate onto the surface of the zinc hydroxide particles. This hydrophobicility gave rise to an active mass much less susceptible to physical changes.

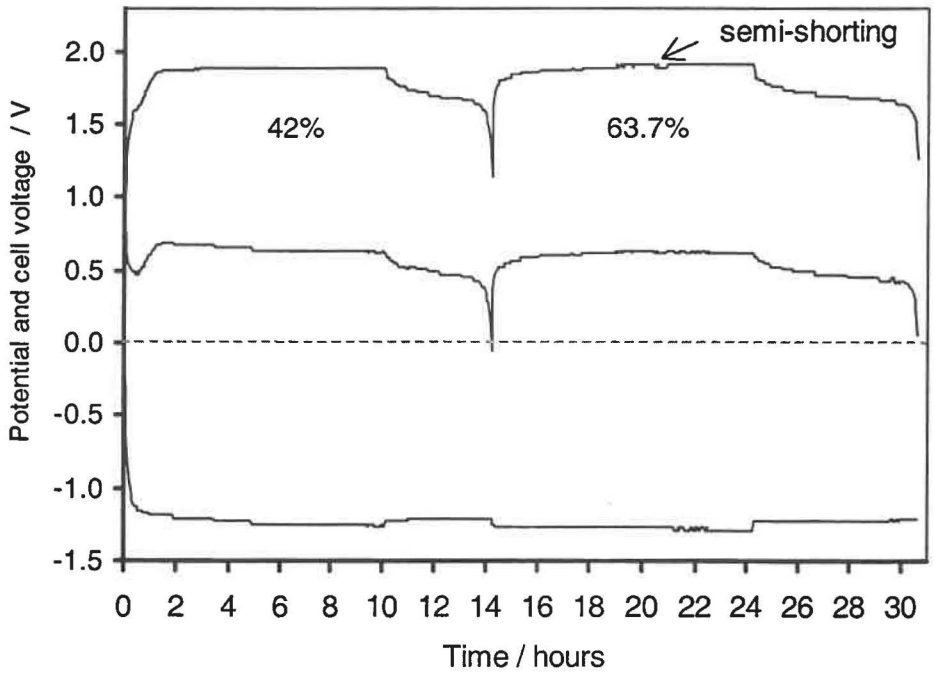

Fig. 6.21 Two formation cycles for Cell #6.6 (evidence for dendrite growth is indicated by the arrow).

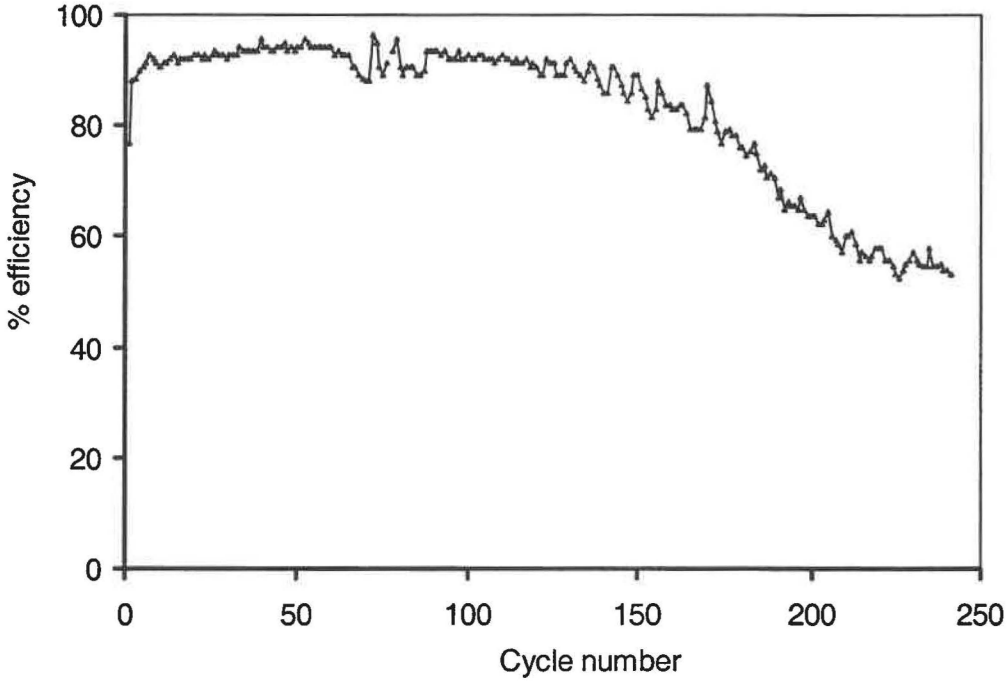

Fig. 6.22 Discharge/charge efficiency as a function of cycle number for Cell #6.6.

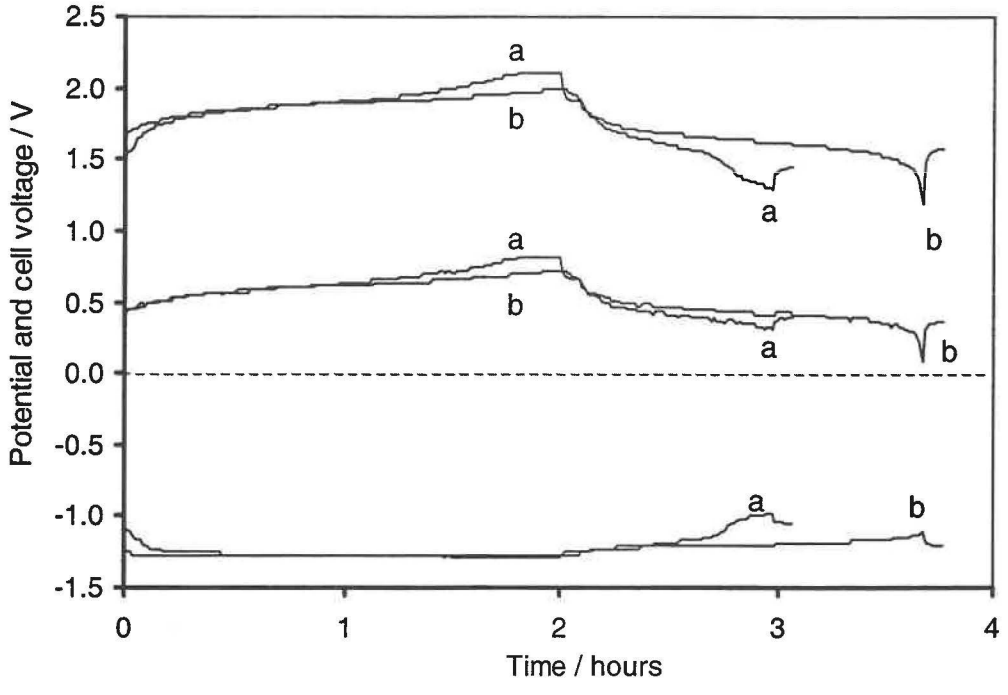

Fig. 6.23 Differences between cycle 50 (curve **b**) and 241 (curve **a**) in electrode potential and cell voltage for Cell #6.6.

The cells with the modified zinc active mass were tested to evaluate the modification. It was found that the amount of content of stearate had a significant effect on the cell cycle life.

A high content of zinc stearate, 38.3% (w/w), significantly reduced the electrochemical activity of the zinc active mass and therefore greatly increased local current density during charge. This promoted the formation and growth of zinc dendrites, ultimately leading to cell failure.

A lower content of zinc stearate, 5.8% (w/w), was insufficient to eliminate the zinc electrode shape change associated with the diffusion of zinc active mass.

Success was established with an intermediate zinc stearate content, 20% (w/w). The cycle life was prolonged in excess of 1100 cycles (Cells #6.4 and 6.5). In addition, electroplating zinc on the brass mesh current collector and mixing potassium hydroxide directly into the zinc active mass also positively prolonged the cycle life performance.

Chapter Seven Scale Up of Test Cells

7.1 Introduction

The previous chapters describe the successes in incorporating the alterations to the electrolyte, cell structure and active mass into 1 Ah test cells that far exceed the performance of nickel-zinc test cells reported by other workers in the field [18, 25-27]. As far as can be ascertained, Cells #6.4 and #6.5 exhibit the most prolonged cycle life performance of any other nickel zinc battery described in the open literature.

These successes, however, are confined to one-off laboratory test cells. It is appropriate to consider the practicalities of incorporating these findings into cells that approach those finding practical utility. Before discussing these considerations, it is useful to summarize those issues requiring further work. These include: prevention of active mass swelling; gas recombination; use of sealed cells with over pressure venting; and optimization of the specific capacity, both with respect to weight (Ah/kg) and volume (Ah/L). These issues fall beyond the scope of the present project, which was confined to developing high cycle life zinc electrodes.

Despite these issues that are effectively insurmountable within this project, there was merit in pursuing a short part to the overall project to identify the likely practical usage of the new zinc electrode.

There is a mismatch between the planar plate geometry and 1 Ah capacity of the test cells with respect to practical application. This geometry and capacity are entirely suitable for laboratory-based experiments since they offer ease of assembly and construction of electrodes. This is not the case for practical rechargeable batteries.

One ampere-hour cells are usually D-sized cylindrical batteries constructed using a 'jelly-roll' approach. Here the positive and negative electrodes consist of narrow strips with similar shaped separators that are spiral wound to form a cylindrical assembly.

Planar plate rechargeable batteries are predominantly used in relatively large (i.e. > 1 L in volume) storage batteries with 10 Ah per cell an effective lower limit. Many of these planar plate cells are usually present as a series of cells housed within a single 'monoblock' as in the 12 V lead-acid battery system. The exceptions to the generalizations above are those planar plate 1 Ah cells used in portable battery operated power tools and video cameras.

Development of a practical cell from the test cells described in previous chapters requires making a choice between scaling up from 1 Ah to at least 10 Ah, if planar plate construction is retained, or to transfer the active mass and electrolyte accessibility findings to the jelly-roll format. The jelly-roll approach is the least desirable for two main reasons:

i) There is a significant engineering task in ensuring uniform pasting onto curved current collectors with ever decreasing tightness of spiral towards the center of the cell. This is commercially achieved by sophisticated computer-controlled pasting equipment – a resource not available to this project where pasting was perfomed by hand. Failure to address these pasting requirements results in either cracking of the active mass (with direct exposure of the current collector to the electrolyte) on the outer face of the spiral, or increased thickness on the inner face.

ii) Whilst 1 Ah D-sized rechargeable cells exist, the ever-increasing trend of miniaturization of electronic goods (with concomitant decrease in power consumption) dictates that the majority of rechargeable batteries for consumer use are AA-size. These typically range in capacity from 400 mAh to 650 mAh. As a result, adoption of the jelly-roll approach would also require consideration of miniaturization. Here, the as yet unresolved challenges of specific capacity (particularly in terms of volume), swelling, gas recombination and venting would be critical. Also, in the laboratory setting it is far easier to scale up than to miniaturise.

Consequently, pursuing the jelly-roll path was considered too large a task to consider at the end of the present project and was rejected. Instead, a small body of work towards increasing the size and number of electrodes in cells with larger capacity was undertaken.

7.2 Cells #7.1 & #7.2: 5-plate cells

The highly successful Cells #6.4 and #6.5 were '3-plate' cells consisting of one nickel and two zinc electrodes. The first attempt at increasing the capacity by increasing the size and the number of electrodes involved the development of 5-plate cells, comprising 3 zinc electrodes interleaved by 2 nickel electrodes. The size of the zinc electrodes, larger than that of those in the previous cells, was 8.3 cm × 8.3 cm while the nickel electrodes were 7.8 cm × 7.8 cm. These zinc electrodes were similar to those employed in Evercel's 10Ah nickel zinc cells. The construction, electrolyte and active mass composition were otherwise identical to those for Cells #6.4 and #6.5.

Two layers of woven nylon cloth were used to wrap each zinc and nickel electrode. The two wrapped nickel electrodes were interleaved between the three zinc electrodes. This assembly of electrodes was tightly wound with nylon thread and enclosed in a shrink-wrap plastic bag open along the top edge. The electrodes were soaked with electrolyte (30% KOH saturated with TBAH and with respect to zincate) for 12 hours with occasional gentle agitation to displace air bubbles. The cell was then subjected to two formation cycles with the regimen given below:

i) Charging at 300 mA for 10 hours;

ii) 5 minutes at open circuit;

iii) Discharging at 300mA until the cell voltage dropped to 1.3 V; and

iv) 5 minutes at open circuit.

The cell voltage and electrode potentials during the first formation cycle are shown as a function of time in Fig. 7.1. The efficiency in this first formation cycle was 48.0%. During this first formation cycle the zinc electrode potential remained unchanged throughout the discharge, indicating that the nickel electrodes were capacity limiting. Figure 7.2 shows the cell voltage and electrode potentials during the second formation cycle. Here, as experience

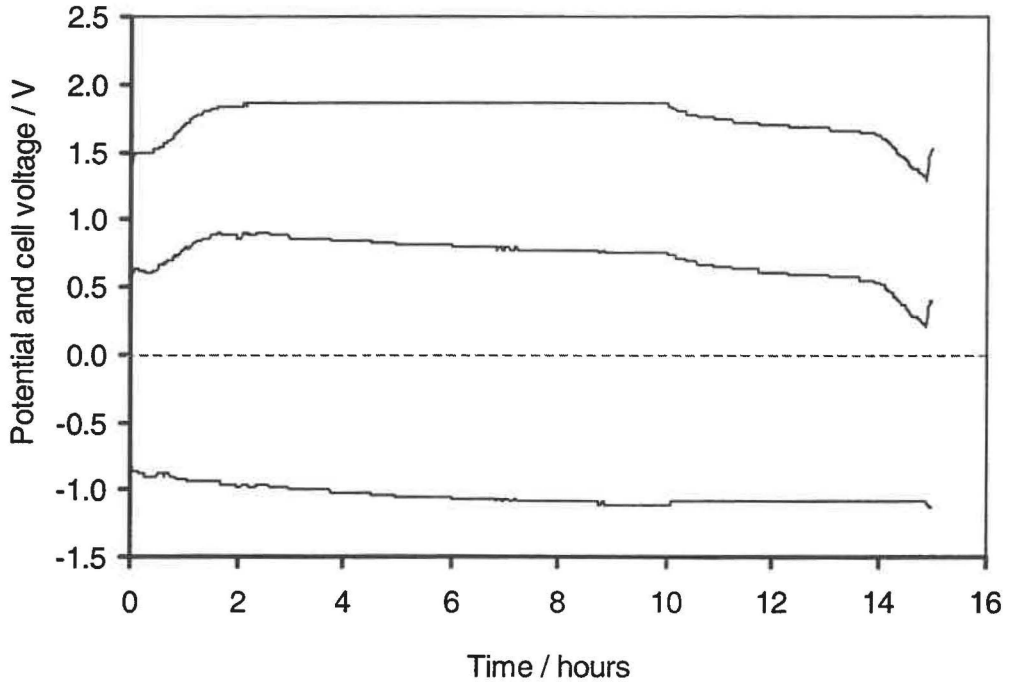

Fig. 7.1 First formation cycle for Cell #7.1.

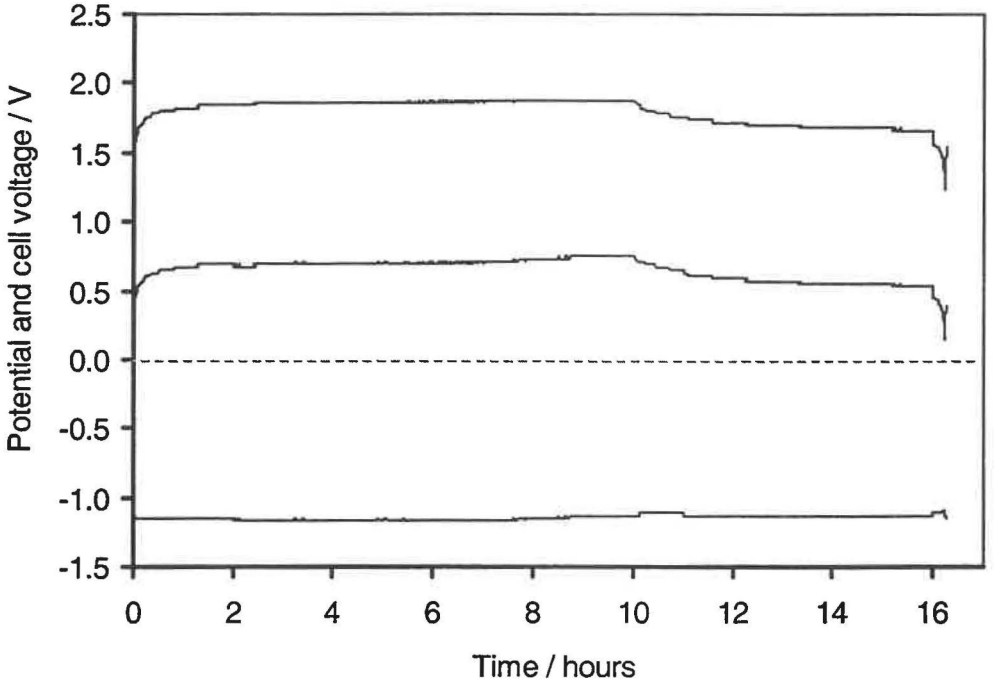

Fig. 7.2 Second formation cycle for Cell #7.1.

with previous 3-plate cells had shown, there was not an unexpected increase in efficiency to 61.4% for this second cycle and the cell remained limited by the nickel electrodes.

After the two formation cycles, the cell was subjected to regular cycles with the regimen given below:

i) Charging at 1200 mA for 2.5 hours;

ii) 5 minutes at open circuit;

iii) Discharging at 1500mA until the cell voltage dropped to 1.3 V; followed by

iv) 5 minutes at open circuit prior to the next cycle.

The cell discharge/charge efficiency is shown as a function of cycle number in Fig. 7.3. It can be seen that the efficiency declined from 97.9% in the cycle 5 to 69.1% in cycle 13. Cycling was terminated after this poor performance. This rapid decline in capacity can be accounted for by examination of the cell potential during the 12^{th} charge/discharge cycle as shown in Fig. 7.4. This reveals evidence during charge for internal shorting during charge caused by dendrite growth.

As noticed in previous 1Ah cells, charge and discharge reactions were observed to take place at the back sides of the two zinc electrodes facing the case walls. This was evident from the zinc active mass changing in colour during charge or discharge. Disassembly of the cell after a further charge beyond cycle 13 resulted in a previously unobserved phenomenon in the 3-plate cells. Dendrites were found at the central zinc electrode located between the two nickel electrodes. This indicated that the charging current density at this central zinc electrode was much higher than at the side zinc electrodes.

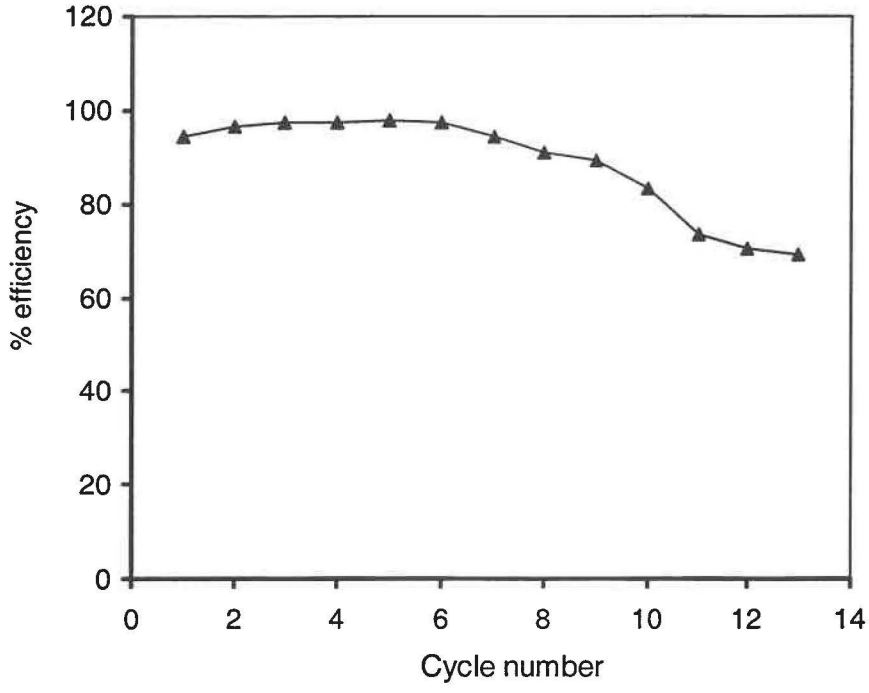

Fig. 7.3 Discharge/charge efficiency against cycle number for Cell #7.1.

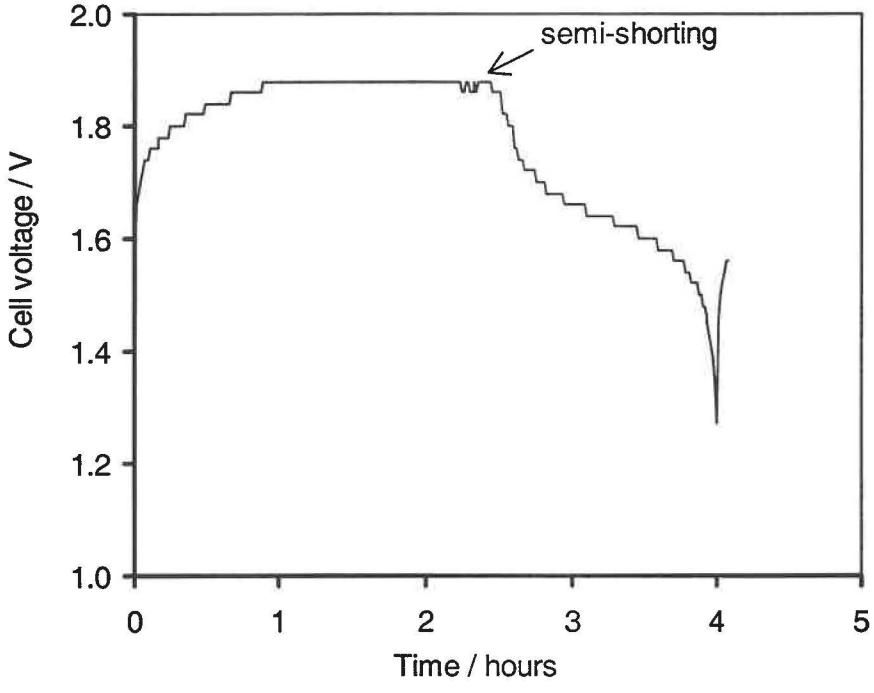

Fig. 7.4 Variation of cell voltage in cycle 12 for Cell #7.1 with evidence for semi-shorting as indicated by the arrow.

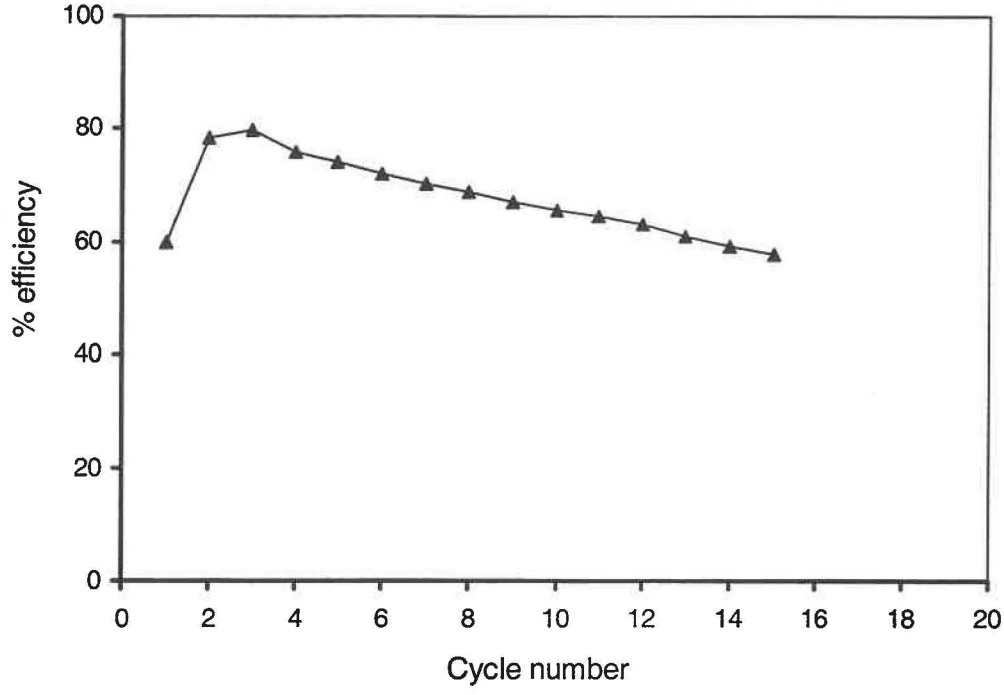

Fig. 7.5 Discharge/charge efficiency against cycle number for Cell #7.2.

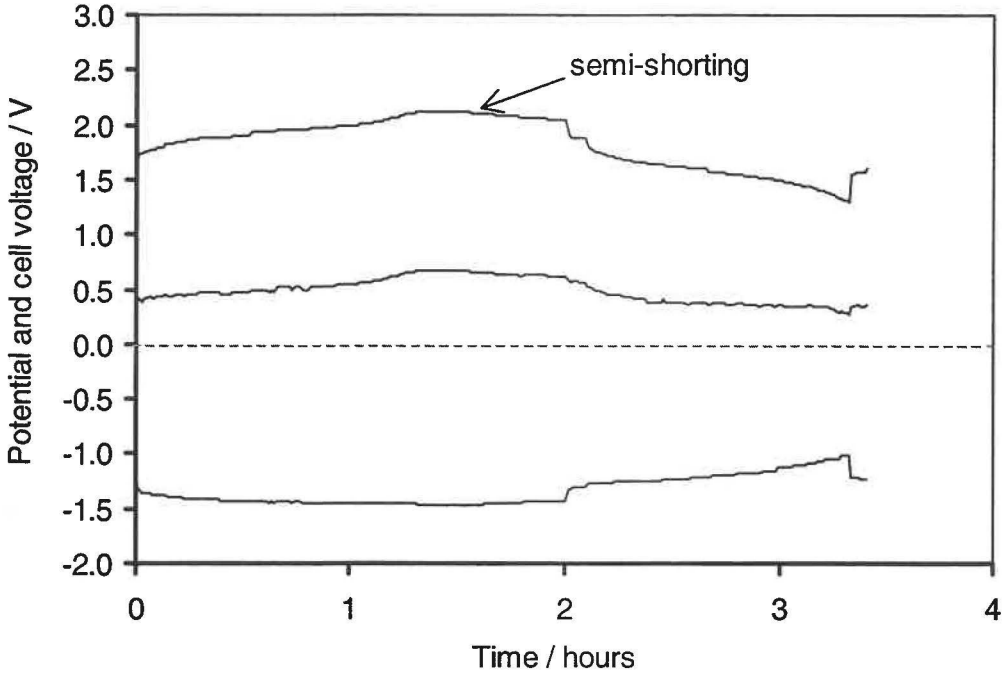

Fig. 7.6 Variation of electrode potentials and cell voltage in cycle 13 for Cell #7.2 with evidence for semi-shorting as indicated by the arrow.

A duplicate of Cell #7.1 was prepared, formed and cycled (Cell #7.2). The regular cycle regime was altered slightly from that for Cell #7.1 in charging phase: charging was at 1500 mA for 2 hours. Figure 7.5 shows the discharge/charge efficiency as a function of cycle number for Cell #7.2. In an identical manner to Cell #7.1, this duplicate showed a marked decline in efficiency at early cycle numbers from 79.3% in cycle 3 to 57.9% by cycle 15. Again, this early cell failure could be traced to premature dendrite formation as shown in the potential time profile in Fig. 7.6 for cycle 13 where internal shorting appeared during charge caused by dendrite growth.

The failure of these two 5-plate cells was not entirely unexpected. Success with small cells does not ensure that this success will be transferred in a simple way to larger cells. Conversely, larger cells will be only successful if preceding small cells operate satisfactorily.

Figure 7.7 shows a schematic representation for the arrangement of the nickel and zinc electrodes in the 5-plate cells. For the two nickel electrodes, there is no difference in position, therefore, there should be no difference in charge and discharge behavior. In contrast, the three zinc electrodes are not all identical. The two outer zinc electrodes are the same, but the central zinc electrode is quite different from these. Each outer zinc electrode has only one side facing a nickel electrode but its two sides, participate in the charge/discharge reactions with only half of a nickel electrode. This is also the case in all previous test 1Ah cells. In contrast, each side of the central zinc electrode is facing a nickel electrode and participates in the charge/discharge reactions with half of a nickel electrode. Consequently, the current density of this central electrode may well be significantly higher than that for the outer zinc electrodes during charge and discharge. In hindsight, it should not have been surprising that, if dendrite growth were to occur, it should have first appeared at the central zinc electrode in Cells #7.1 and #7.2.

Several means were considered for decreasing the current density imbalance between the inner and outer zinc electrodes. The first was to not have an inner zinc electrode (as in the previous 3-plate cells). The second was to increase the number of bifacial inner zinc plates.

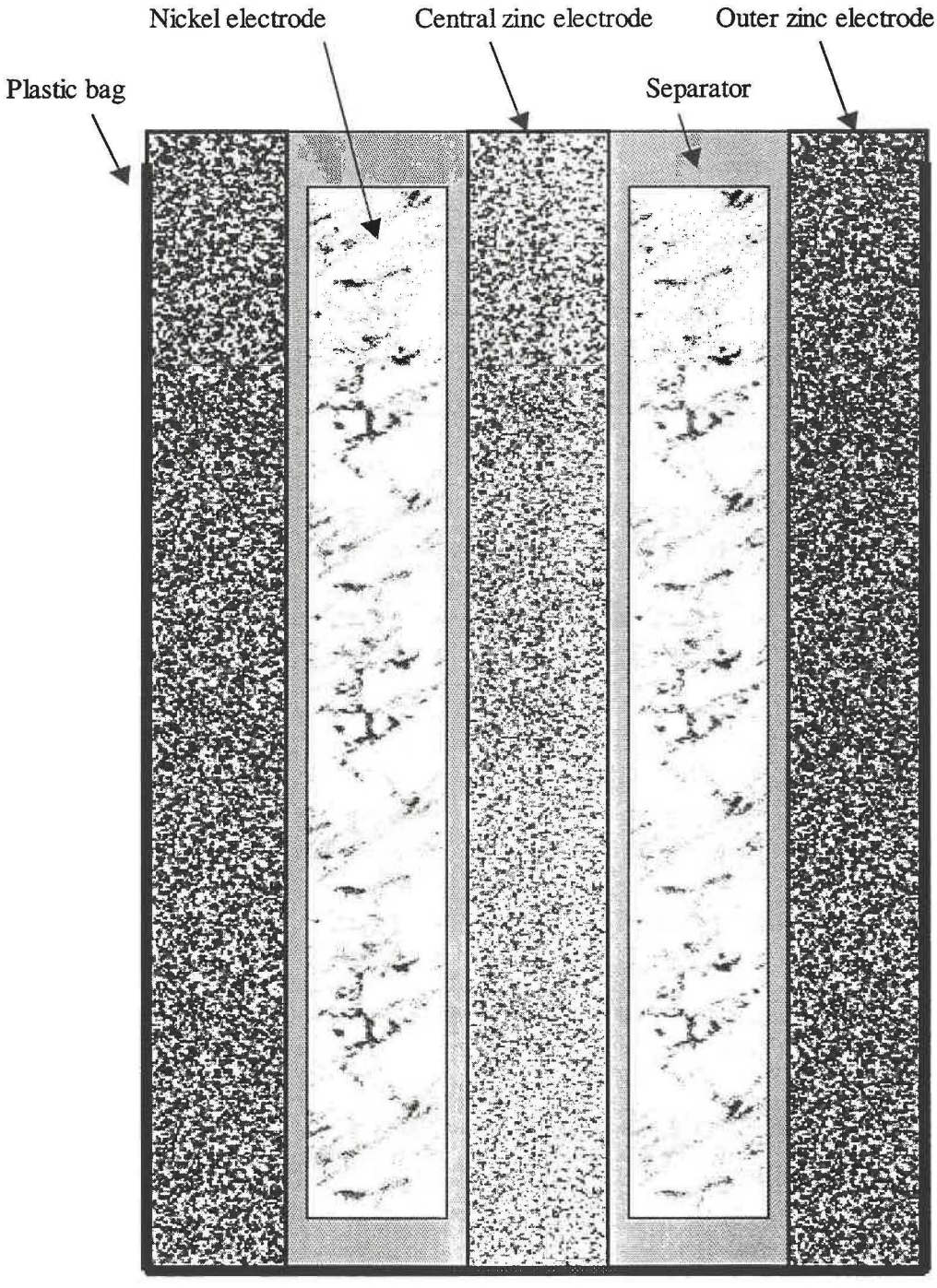

Fig. 7.7 Arrangement of the electrodes in the scaled cells (Cells #7.1 and #7.2).

Here, the ratio of outer to inner zinc plates decreases markedly with increase in the total number of plates from 2:1 for 5-plate, to 2:2 for 7-plate, and 2:4 for 9-plate cells. The third option is to remove outer zinc plates completely by employing outer nickel electrodes. For example, such a 3-plate cell would comprise one zinc sandwiched between 2 nickel electrodes.

Given the equipment limitations, time, and material resources remaining for this project, the second option of assembling multiple plate cells was not practical. With this option, not only would multiple electrodes of near-identical active mass loadings require construction, but also new cell casings, terminal resistance matching and large scale electrolyte management regime would require consideration. Furthermore, the swelling noted in Cells #6.3 and #6.4 would be expected to multiply linearly with the number of plates. If this were not dealt with then cell rupturing would not be unlikely. Consequently, the construction of multiple plate nickel-zinc cells fell outside the intended goals of the project. If this were to be the focus, then a comprehensive multi-disciplinary engineering project would be required with a clear commercial endpoint in mind.

The third option for removal of the outer zinc electrodes is also not appropriate for this study. If such a 3-plate system were constructed consisting of two nickel and one zinc electrodes then this would have lower capacity than the preceding cells in this study. This runs counter to the stated goal in this chapter to develop higher capacity planar plate cells.

As a consequence of these considerations and given the time constraints for the project, the first option was adopted – the return to use of 3-plate (2 zinc and 1 nickel electrode) cells. The approach to increase the capacity of 3-plate cells is described in the following section.

7.3 Cell #7.3: 2 × 3-plate in parallel

Figure 7.8 shows a schematic representation of the modified arrangement of the electrodes for the parallel 3-plate Cell #7.3. Each 3-plate assembly consisting of 2 zinc electrodes and a single nickel electrode in identical format to those for Cells #6.4 and #6.5 except for its

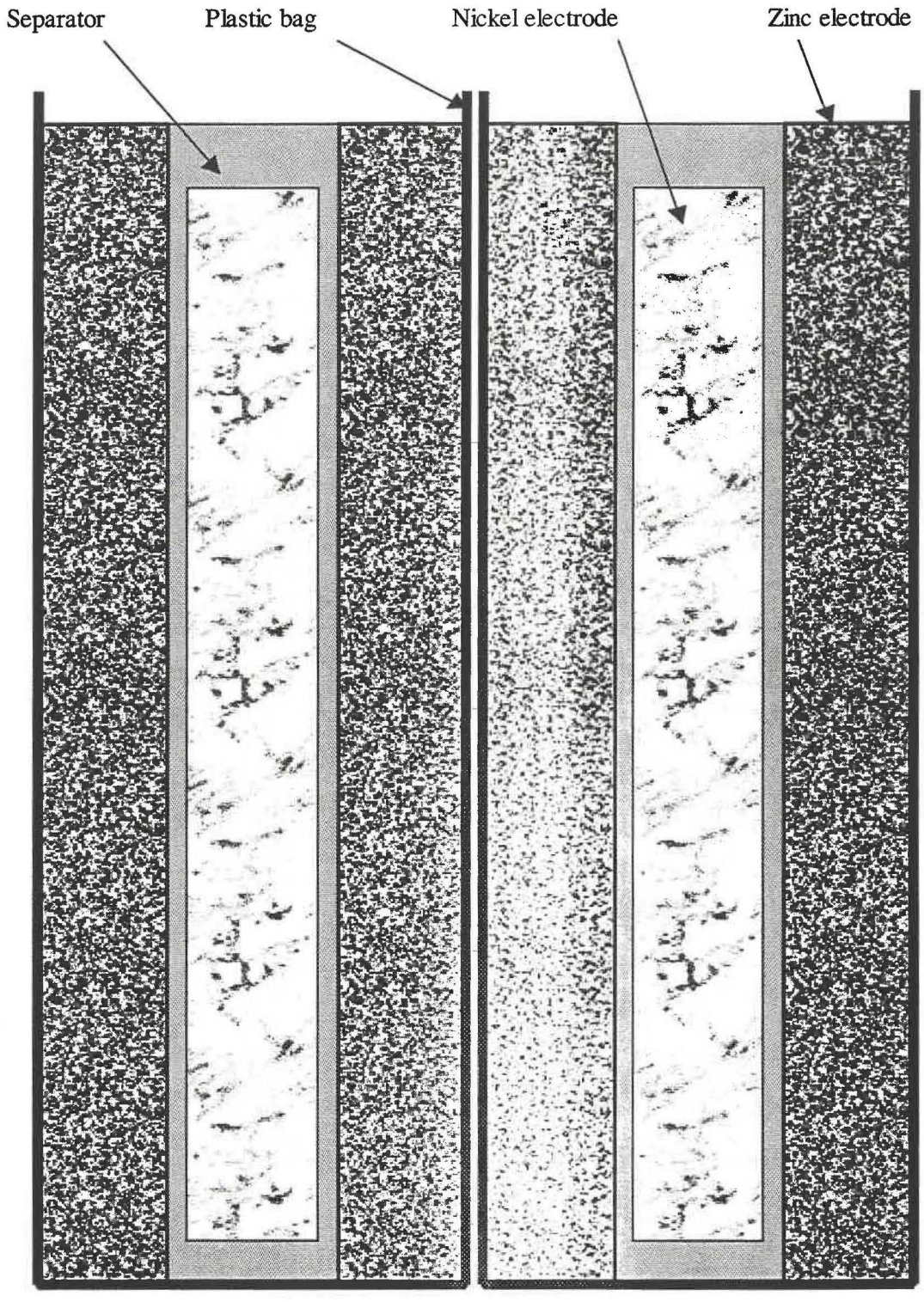

Fig. 7.8 Modified arrangement of the electrodes in the scaled cells (Cells #7.3, #7.4 and #7.5).

larger size was wound with nylon thread and bagged in shrink-wrap plastic bag. Two such units were placed side by side and connected in parallel with spot-welded nickel tags.

All of the zinc electrodes were in the same relative position and consequently there was no difference between the zinc electrodes in charge and mass exchange with the nickel electrodes. Each unit takes the advantages of the previous cells with one nickel electrode placed between two zinc electrodes. There is no electrolyte flow between the two 3-plate units but there is a charge exchange between the two units.

The two units may have unequal charge acceptance, but the unit with higher charge acceptance will take more charge during charge. During discharge, the unit with more charge will release more charge by the end of discharge. Therefore, two such units are able to adjust to keep balance in charged and discharged states. Such balance is necessary to keep each unit under appropriate charge/discharge condition in cycling.

Cell #7.3 was subjected to two formation cycles with the regimen given below:

i) Charging at 380 mA for 8 hours;

ii) 5 minutes at open circuit;

iii) Discharging at 380 mA until the cell voltage dropped to 1.3 V; followed by

iv) 5 minutes at open circuit.

Regular cycling was carried out with the regimen identical to that for Cell #7.2. Figure 7.9 shows the discharge/charge efficiency as a function of cycle number for Cell #7.3. It can be seen that its performance was much improved in comparison with the two 5-plate Cells #7.1 and #7.2 and at early cycles performed similarly to Cells #6.4 and #6.5. However, the efficiency declined rapidly after the cycle 50.

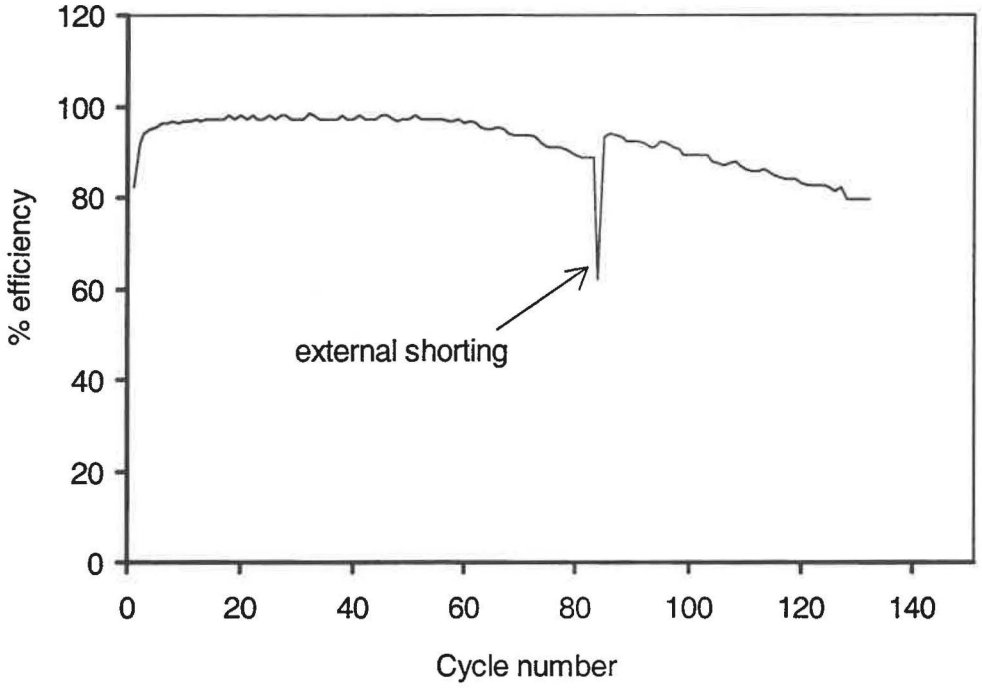

Fig. 7.9 Discharge/charge efficiency against cycle number for Cell #7.3.

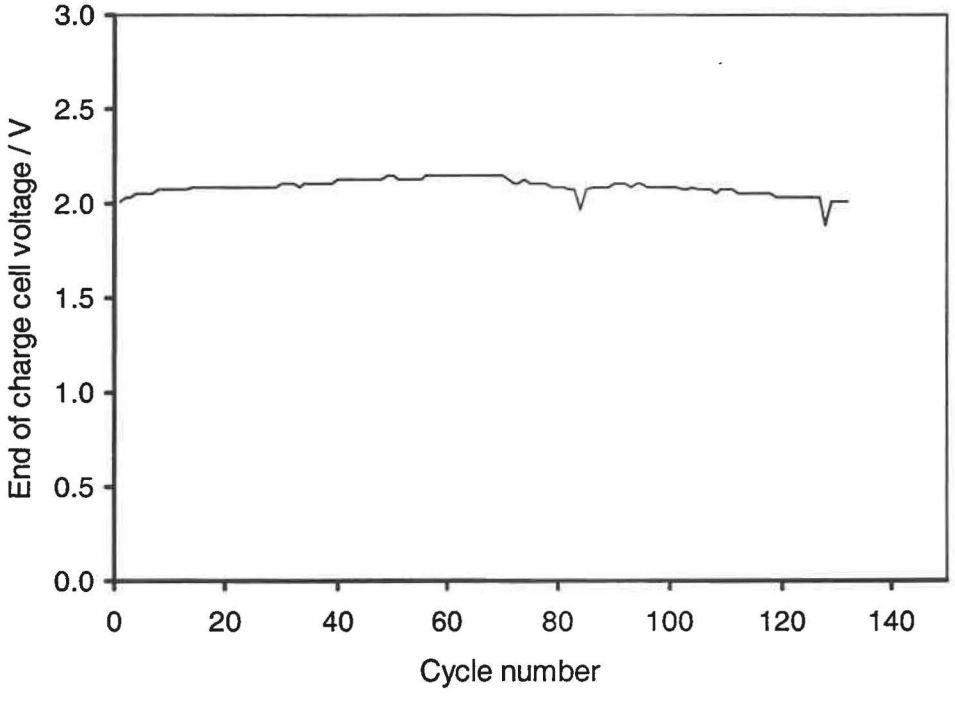

Fig. 7.10 End of charge cell voltage against cycle number for Cell #7.3.

Figure 7.10 shows the end of charge cell voltage as a function of cycle number. The end of charge cell voltage declined beyond 72 cycles. Data analysis revealed that the end of charge cell voltage commenced to decline in cycle 72 where the cell voltage declined from 2.15 V to 2.13 V just 80 seconds before the end of charge, indicating semi-shorting associated with dendrite growth.

Figure 7.11 shows the potential and cell voltage varied in the cycle 72 with semi-shorting appearance. Within 72 cycles the declined discharge/charge efficiency was due to cell overcharging. As seen in Fig. 7.11, the cell had suffered from overcharge prior to the semi-shorting appearance. After cycle 83 where efficiency dropped to 88.7%, the cell was deliberately externally shorted for complete discharge. After the external shortage, the efficiency increased in the subsequent cycles.

Figure 7.12 shows the cycle 86 where efficiency increased to 94.2%. The end of charge cell voltage dropped to 2.07 V from 2.11 V before external shortage. The increased efficiency and decline in cell voltage after external shortage confirmed that the cell had been overcharged.

Figure 7.13 shows the cycle 96 that had a declined efficiency of 91.8% and appearance of overcharge with the cell voltage remaining high at 2.09 V near the end of charge. Ignoring the overcharge, the cell was continuously cycled until the efficiency declined below 80% in cycle 132. Continuous overcharge resulted in internal shortage. Figure 7.14 shows the last cycle (cycle 132) that displayed evidence of semi-shorting.

A duplicate cell to Cell #7.3 was constructed (Cell #7.4). Cell #7.4 was subjected to regular cycling with the same regime after two formation cycles. Figure 7.15 shows the discharge/charge efficiency against cycle number. The cell efficiency gradually declined in a similar manner to Cell #7.3. Overcharge of the cell was associated with the declining efficiency. This cell underwent three periods of deliberate external shorting labelled A, B, C in Fig. 7.15.

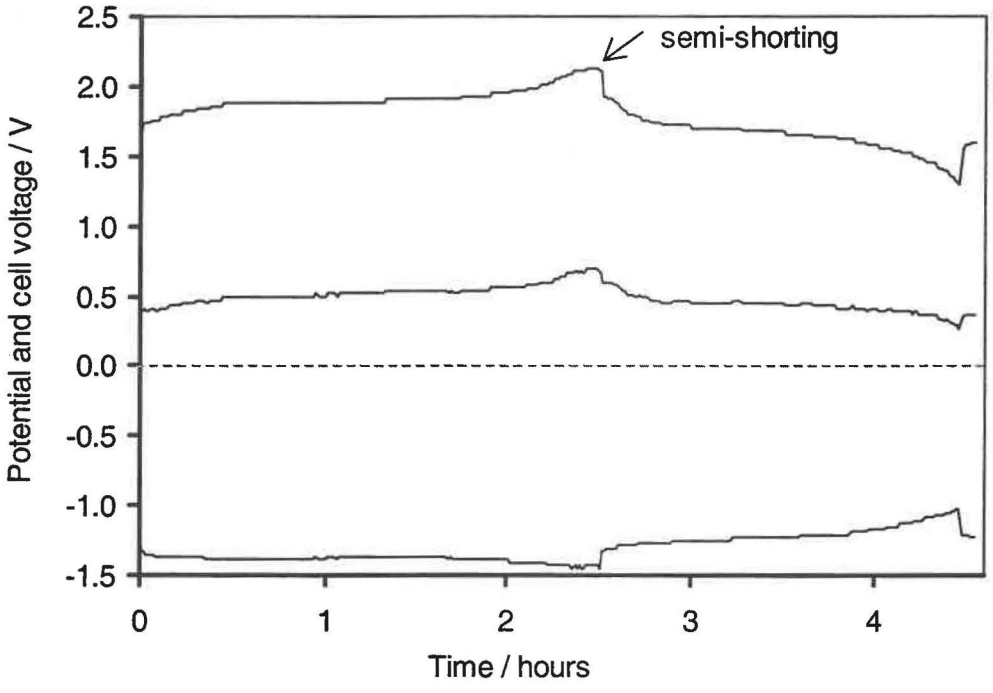

Fig. 7.11 Potential and cell voltage variation in cycle 72 for Cell #7.3 (commencement of semi-shorting is indicated by the arrow).

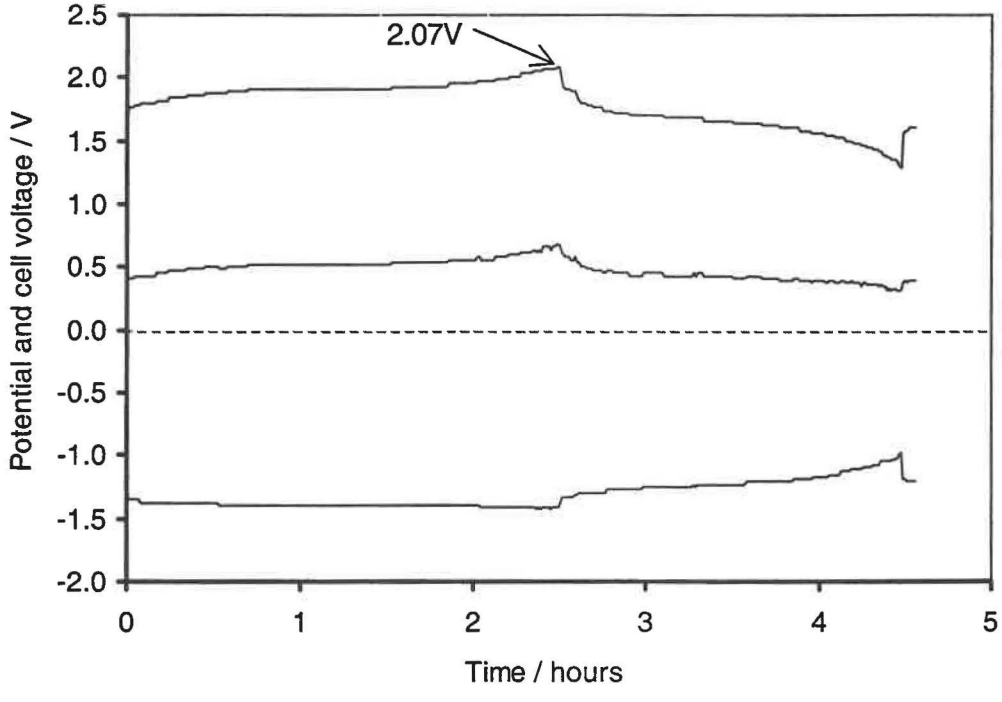

Fig. 7.12 Cycle 82 with reduced end of charge cell voltage after external shortage for Cell #7.3.

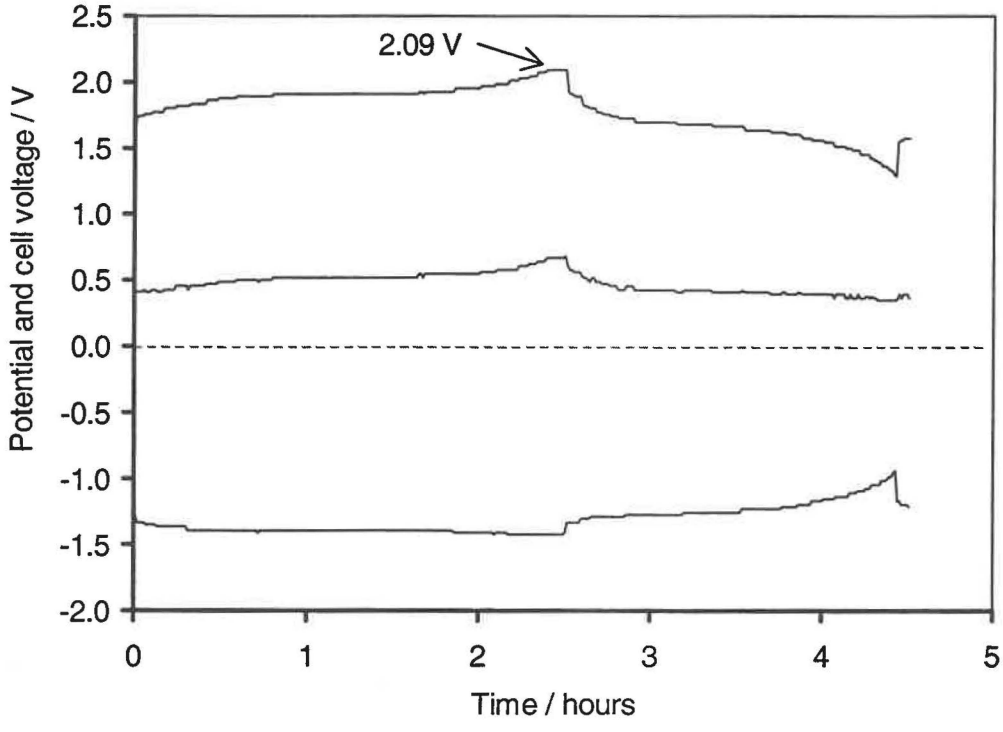

Fig. 7.13 Cycle 96 for Cell #7.3 with evidence of overcharge as indicated by the arrow.

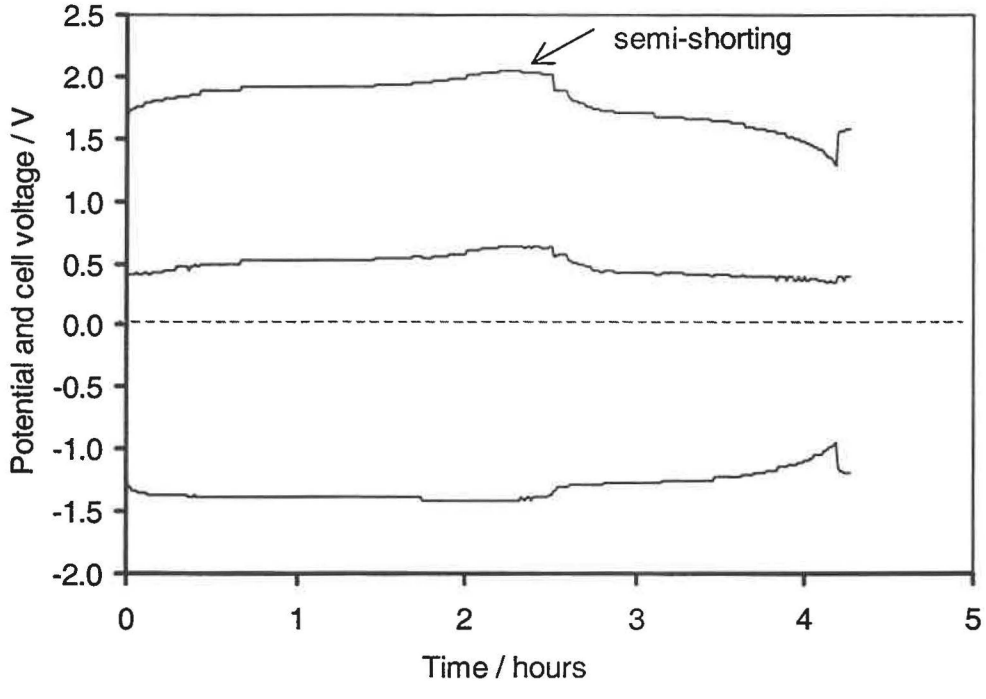

Fig. 7.14 Cycle 132 for Cell #7.3 with evidence for semi-shorting as indicated by the arrow.

This cell was cycled at a deliberately high rate to decrease the cycle duration. The cutting voltage of 1.3V was perceived to be too high under such a high discharge current of 1500 mA. It was considered important to increase the depth of discharge so as to avoid overcharge of the nickel and zinc electrodes. There were two options for increasing the depth of discharge:

i) Reduce the discharge current;

ii) Reduce the cutting voltage.

At a given discharge cutting voltage, the discharge capacity of a cell under a given charge capacity is a function of the discharge current. Reducing the discharge current results in the increased discharge capacity or depth of discharge. Reducing the discharge current was an option to increase the depth of discharge, but it would proportionally prolong the time for discharge.

At a given discharge current, the discharge capacity, or depth of discharge, under a given charge capacity is a function of the discharge cutting voltage. Reducing the cutting voltage leads to an increased discharge capacity or depth of discharge but only slightly prolongs the discharging time. This was considered as more convenient and superior to the option of reducing the discharging current.

Beyond external shorting at C it was decided to reduce the cutting voltage from 1.3 V to 0.8 V without changing the charging and discharging currents. Reduction of the cutting voltage to 0.8 V increases the depth of discharge that preserves more zinc hydroxide for the followed charging, hence reduces the possibility for the zinc electrodes to become overcharged. After reducing the cutting voltage beyond cycle 232, the efficiency increased to 96.9% in cycle 240. With this increase in efficiency, a significantly lower rate of decline in efficiency was observed as a consequence of reducing the cutting voltage.

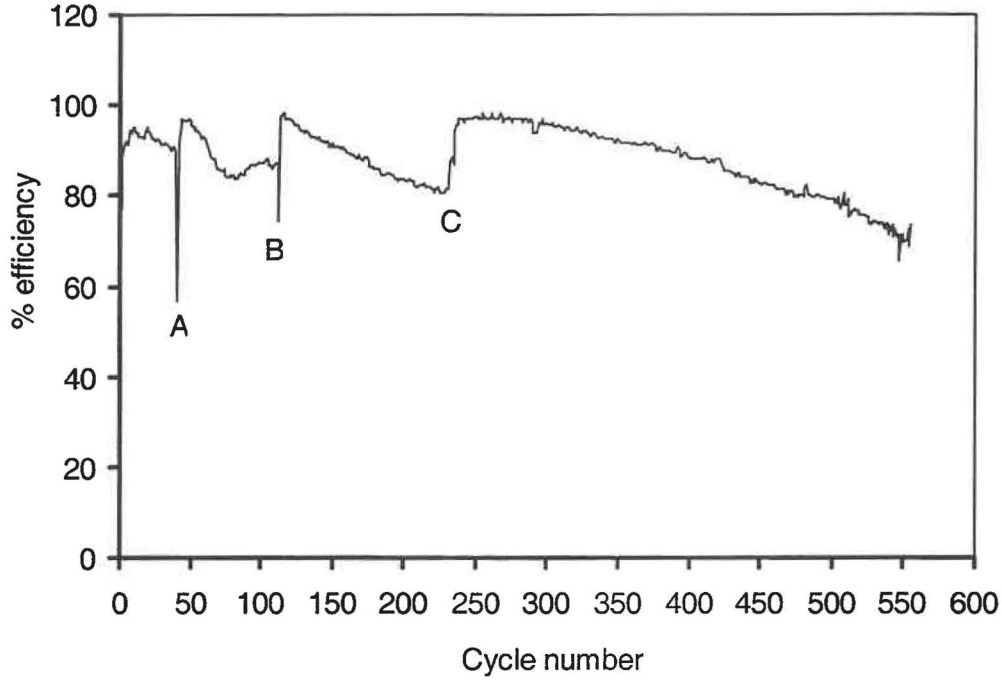

Fig. 7.15 Discharge/charge efficiency against cycle number for Cell #7.4.

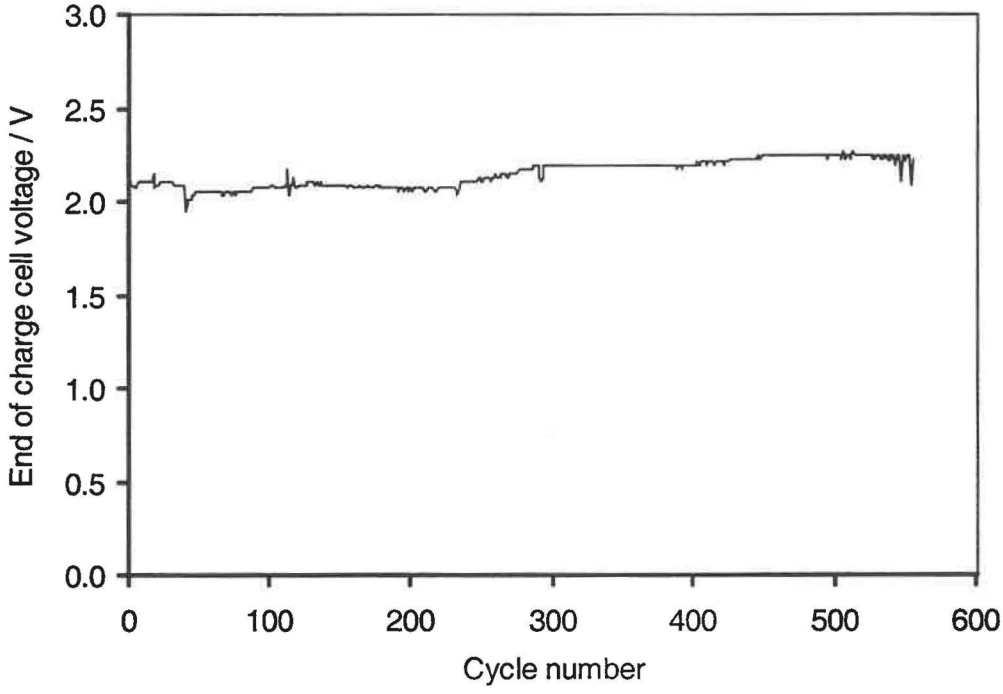

Fig. 7.16 End of charge cell voltage against cycle number for Cell #7.4.

When the discharge/charge efficiency had recovered, it was decided that no more electrolyte would be added to the cell. Cycling was terminated when the discharge/charge efficiency declined to 68.8% in cycle 554. The failure was caused by a combination of lack of electrolyte together with shape change that resulted in the swelling of electrode assembly. Semi-shorting was not the cause for the efficiency decline. Figure 7.16 shows the end of charge cell voltage profile where the cell voltage remained quite high at 2.25V until the cell failed due to electrolyte exhaustion.

Figure 7.17 shows the potential profile for cycle 520. During charge, the zinc electrodes were overcharged first with hydrogen evolution. This hydrogen evolution resulted in the electrode potentials of both nickel and zinc electrodes moving towards more positive potentials by altering the potential of the stainless steel pseudo reference electrode. Later, the nickel electrodes were overcharged with resulting oxygen evolution. Oxygen evolution resulted in the electrode potentials of both nickel and zinc electrodes moving towards more negative potentials due to the reference electrode potential altering. The potential of the zinc electrode declined rapidly during discharge as shown in Fig. 7.17. When the electrolyte became inadequate in the cell, the passivation of the zinc electrodes became dominant with respect to contribution to the cell voltage decline during the discharge phase.

Shape change is quite distinct in this larger, long-cycled cell shown in Fig. 7.18. White zinc active mass accumulated at the center of the zinc electrodes. The zinc mass accumulation at the center could only be partly oxidized during discharge and this was associated with the restricted diffusion of electrolyte to the center. The optimized cell structure and zinc active mass restricted access of the electrolyte to the electrode assembly and the zinc active mass. It is significantly more difficult in this larger cell for the electrolyte to diffuse to the center of the zinc electrodes than to the edges of the zinc electrodes. The center of the zinc electrodes remained in an electrolyte-starved state during discharge. The situation deteriorated further with cessation of electrolyte addition into the cell in the later cycles. The metallic zinc at the center had higher propensity to passivate during discharge in an electrolyte-starved state. The metallic zinc at the edges was preferentially oxidized and partly dissolved in the electrolyte during discharge.

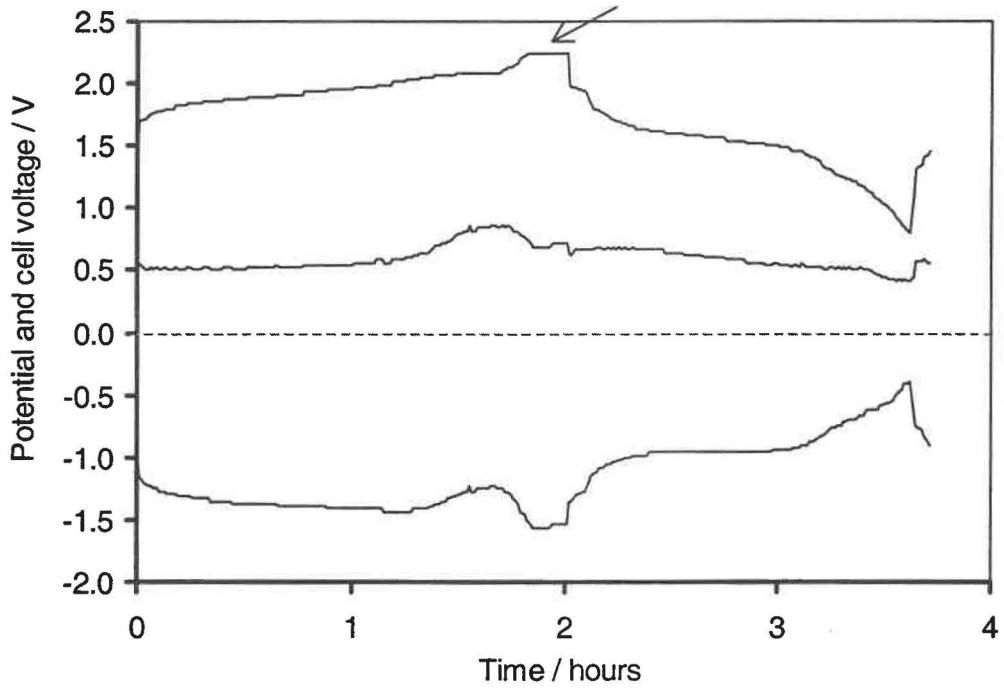

Fig. 7.17 Cycle 520 for Cell #7.4 with evidence of overcharge as indicated by the arrow.

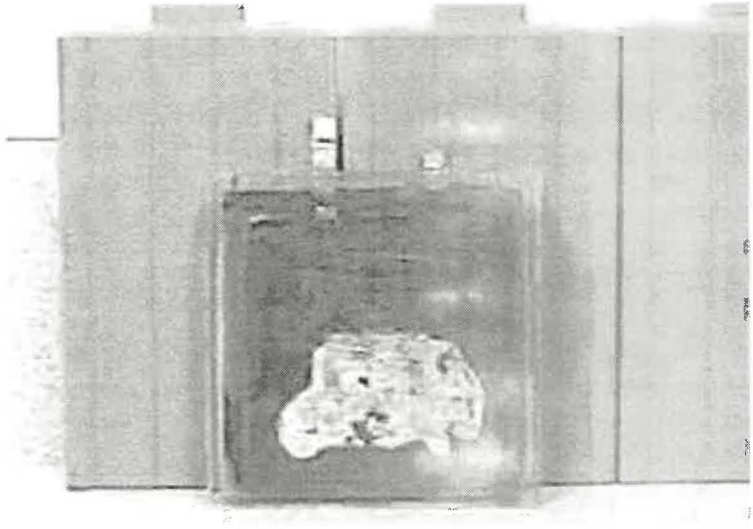

Fig. 7.18 Photograph of Cell #7.4 after cycling. Zinc is observed to accumulate at the center of the electrodes.

Because of these differences in passivation, the metallic zinc in the electrode center was unable to be totally oxidized. In the subsequent charge phases, zincate from the electrolyte, some of which may have come from the dissolved zinc at the edges, had a higher potential to deposit at the center because of the high conductivity resulting from the accumulated metallic zinc. Also, the redeposition of zincate from the electrolyte should have lower overpotential on a metallic zinc surface.

As the electrolyte become exhausted and the zinc electrodes became continuously overcharged, internal shorting caused by zinc dendrites finally occurred as shown in Fig. 7.19 with evidence for semi-shorting in cycle 547.

A duplicate cell to Cell #7.3 was constructed (Cell #7.5). After two formation cycles, the cell was subjected to regular cycling with the same regime except for the discharge cutting voltage. This was set at 0.8 V rather than 1.3 V. As it was anticipated that the cell would perform in a superior fashion to Cell #7.4, no additional electrolyte was added into the cell during cycling.

Figure 7.20 shows the efficiency as a function of cycle number for Cell #7.5. Because of acceleration in hardware problems with time, the cell underwent nineteen overcharge events due to relay switching errors. Each period of overcharge occurred after the former discharge had been terminated by the relays. No action was taken to remedy the relay switching problems due to an overriding need to determine the susceptibility of this cell to overcharge.

Figure 7.21 shows the end of charge cell voltage, $E_{cell,eoc}$, as a function of cycle number. The cell voltage commenced a gradual decline from the cycle 323 as a result of dendrite growth. It was observed that this cell voltage decline correlated with the progressive exhaustion of electrolyte and dendrite growth. The electrolyte level was down to the bottom of the electrode assembly when cycling was terminated.

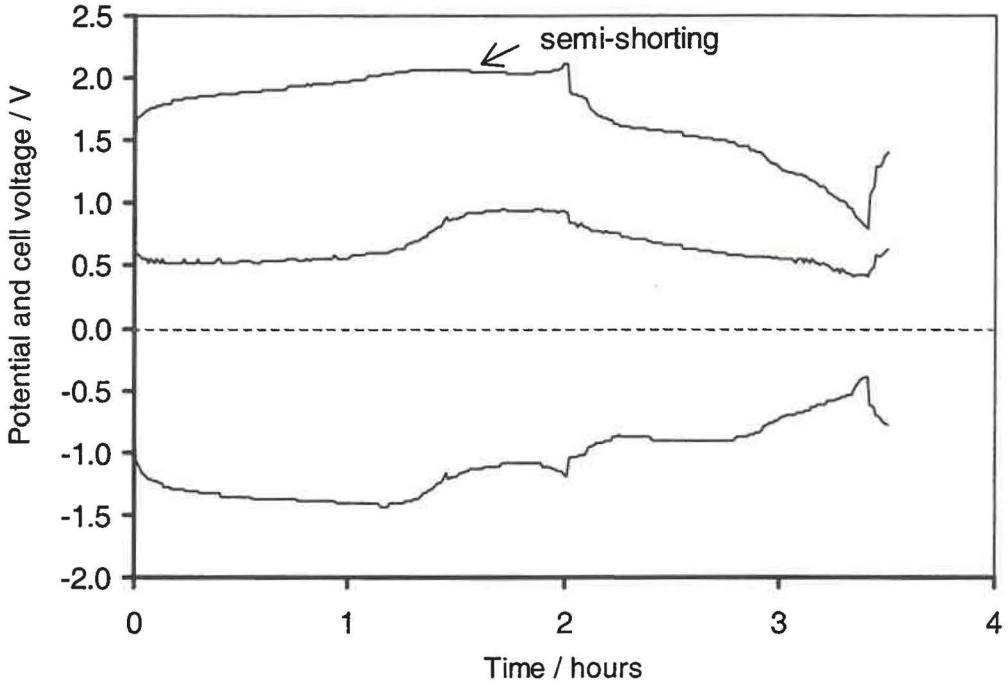

Fig. 7.19 Cycle 547 for Cell #7.4 with evidence for semi-shorting as indicated by the arrow.

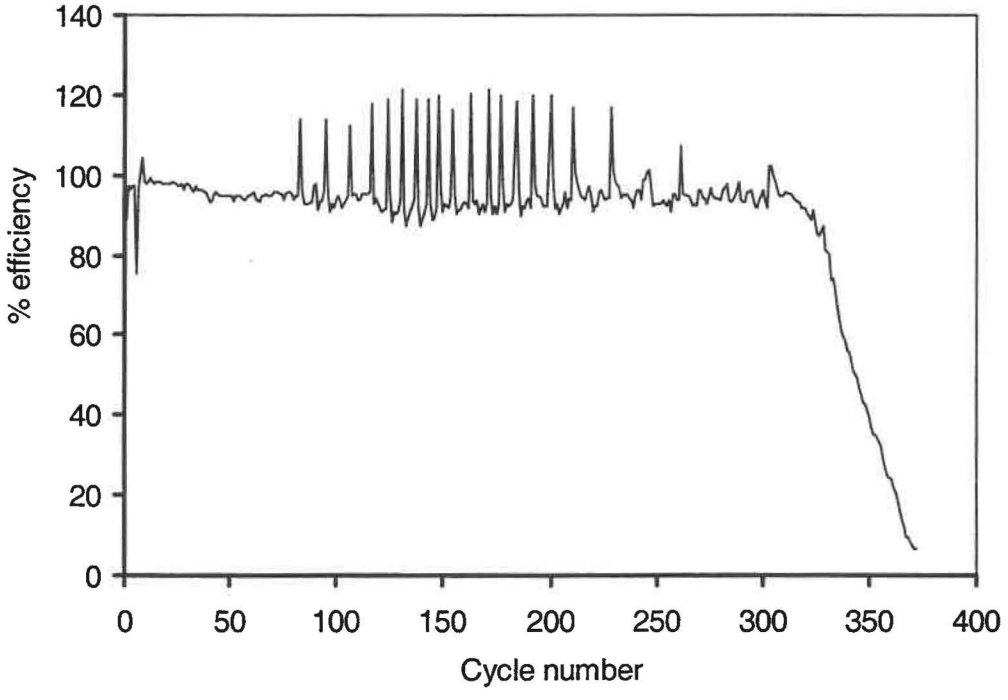

Fig. 7.20 Discharge/charge efficiency against cycle number for Cell #7.5 with nineteen overcharge events.

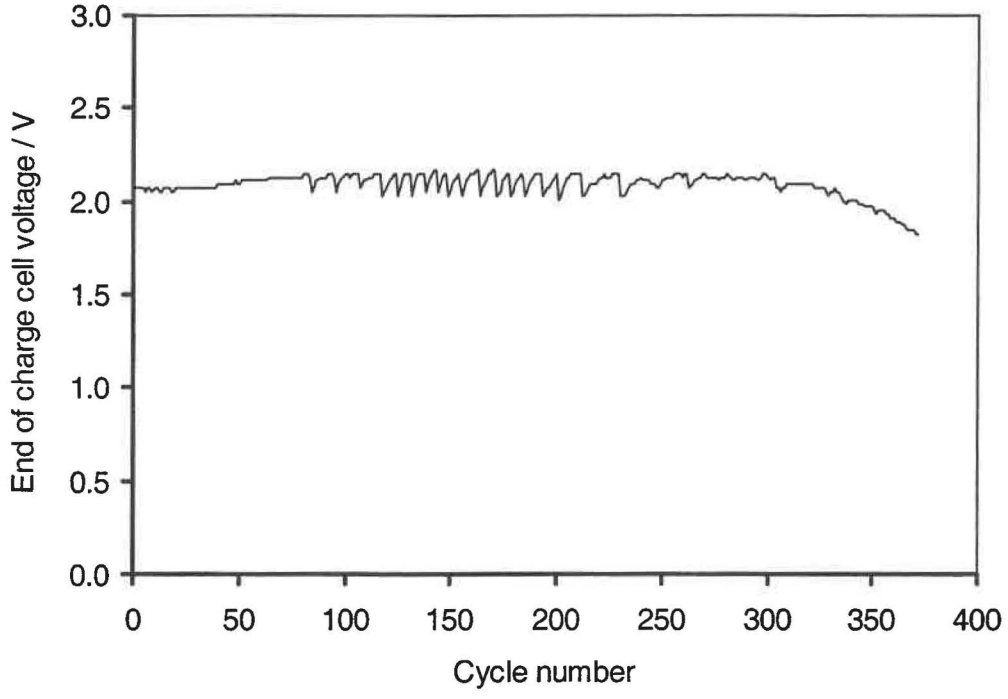

Fig. 7.21 End of charge cell voltage against cycle number for Cell #7.5.

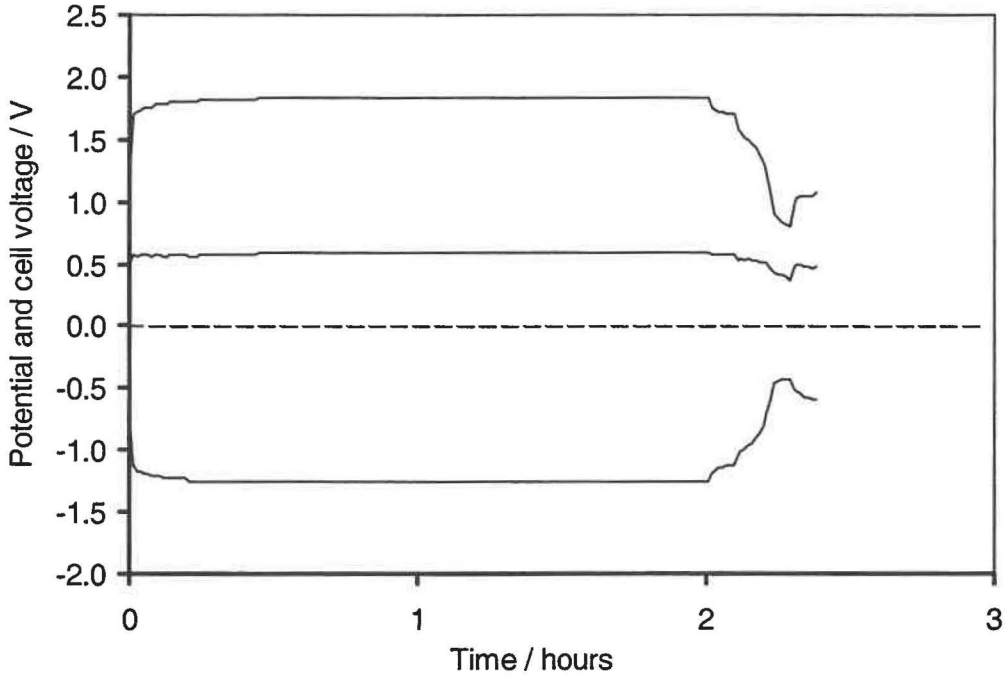

Fig. 7.22 Cycle 368 for Cell #7.5 with low cell voltage during charge.

Figure 7.22 shows the potential profile for cycle 368. There was no drop in cell voltage during the charge phase but the end of charge cell voltage remained low at 1.84 V. Nevertheless, more than 300 cycles were attained with discharge/charge efficiency greater than 90% sufficient to demonstrate the significant progress in this scaled up cell. Although cycling terminated with exhaustion of the electrolyte it is likely that replenishment, or use of gas recombination devices within the cell would have extended the life of this cell considerably.

7.4 Conclusions

Cells were successfully scaled up from 1 Ah to 3 Ah by incorporating modifications to the cell structure and reduction of the discharge cutting voltage. It was anticipated that further scale up could be achieved.

The successful-scaled cell consisted of two units connected in parallel. Each was identical to, and took the advantages of, the earlier cells (Cell #6.4 and #6.5) except for their larger size. There was charge exchange between the units but without mass exchange. The passivation of the zinc electrode proved to increase because of these larger sized electrodes. Increasing the depth of discharge by reducing the discharge cutting voltage significantly prolonged the cycle life. Shape change associated with the inadequate electrolyte diffusion to the electrode center was the dominant cause of cell failure. In order to prolong the cycle life, gas recombination should be introduced to the scaled cells and electrolyte diffusion in the electrodes should be improved in future work.

Chapter Eight Conclusions

8.1 Introduction

The cycle life of nickel zinc cells is affected by many parameters, none of which can be ignored in an attempt to solve the problems with nickel zinc cells and hence to prolong the cycle life. Each of the parameters, including the current collector, electrolyte, cell structure and zinc active mass, has been accounted for and investigated in detail. The results lead to experimental nickel zinc cells succeeding with cycle life in excess of 1200 cycles at high rates of charge/discharge. This is superior to any other nickel zinc cells reported in the literature. The technology developed in the study has potential for commercialization. A summary of the work that has been performed now follows.

8.2 Preparation of sponge nickel

Sponge nickel or foam nickel is an important material used as the current collector for nickel electrodes. The specific advantages of sponge nickel makes it a potential replacement for the sintered nickel used in manufacturing Ni-Cd, Ni-MH and Ni-Zn cells. As the methods of preparing sponge nickel appear to have remained as trade-secrets, preparation of sponge nickel proved to be an important aim of this study.

With polymer sponge as the template, sponge nickel was successfully prepared in the laboratory consisting of the processes given below:

i) Electroless plating of an organic polymer sponge sheet with nickel;

ii) Electroplating the nickel-coated sponge sheet with additional nickel;

iii) Treating the electroplated sponge in a hydrogen flame.

The traditional method of nickel electroless plating was tested but could not readily coat the template with a uniform nickel coating. Modifications were made on the traditional method of nickel electroless plating.

Catalyzing was the most important process to form metallic palladium particles on the surface of the template (sponge). A simple but reliable and stable process was established as given below:

i) Soak the template in a $PdCl_2$ solution (> 0.3 g/L) and then dry it;

ii) Soak the dried template in alkaline formalin solution consisting of 40ml/L of formalin (40% w/w) and 50g/L of NaOH at > 50°C for 5 minutes;

iii) Wash the template ready for electroless plating.

Through the above treatment, the surface of the template was covered evenly with catalytic metal palladium particles.

The solution of electroless plating was also modified and became straightforward with low maintenance. The method and conditions are given below:

Condition	Value
Saturated $Ni_3(PO_2)_2$ solution	20 g/L
NH_4OH	sufficient to maintain pH
pH	8.5 – 9.5
Temperature	40 – 45 °C
Immersion time	8 – 15 min

The saturated $Ni_3(PO_2)_2$ solution was obtained by dissolving wet $Ni(OH)_2$ in H_3PO_2 solutions, where wet $Ni(OH)_2$ was prepared by mixing $NiSO_4$ solution with NaOH solution stoichemetrically.

8.3 Preliminary work

The electrode potential of nickel and zinc electrodes indicates the state of the nickel and zinc electrodes in a nickel zinc cell during charge or discharge, which is related to the performance of this cell. Through the preliminary work on the simple nickel zinc cell it was shown that stainless steel wire could be used as a simple and stable pseudo reference electrode. With the aid of these reference electrodes, it was possible to identify which of the electrodes were the capacity limiting electrodes.

The computer aided cycling equipment designed by Dr Simon Hall was tested and proved to meet all of the needs as required. The cell voltage, nickel and zinc electrode potentials were read and saved in the computer and displayed as plots against the time elapsed on the monitor, showing the states of the cell and the nickel and zinc electrodes during charge and discharge. Through the plot of cell voltage against the time elapsed displayed on the monitor, semi shorting could be detected in situ as it appeared causing the cell voltage slightly dropped.

The cell with the simplest zinc active mass consisting of zinc oxide and CMC failed with semi shorting caused by zinc dendrites in 45 cycles shown in Fig. 3.12.

Gross zinc active mass diffusion was the most significant phenomenon. It was found through opening the failed cell that the zinc active mass was no longer a solid mass adhered to the brass mesh. Some of the zinc active mass had diffused into the separators and even to the nickel electrode.

It was impossible to identify whether the dendrites were from the reduction of zincate in the electrode or from the reduction of solid zinc active mass in the separators. This indicated

that the reduction of zincate, zinc oxide and zinc hydroxide should come under intensive investigation. It was apparent that the ready access of the electrolyte to the zinc electrode was involved in the dissolution of the zinc active mass associated with the gross diffusion. It was considered that the access of the electrolyte to the electrode assembly should be restricted to prevent the gross diffusion.

8.4 Electrolyte modification

The dissolution of zinc active mass in alkaline electrolyte was associated with the zinc electrode shape change. The use of lower concentration of KOH electrolyte could reduce the dissolution of zinc active mass, but the performance of the nickel electrode would be sacrificed. The alternative to reduce the dissolution of zinc active mass was to saturate the electrolyte with respect to zincate.

It was found that the traditional method was unable to saturate the electrolyte by dissolving zinc oxide until no more can be dissolved. Metallic zinc powder could still be dissolved in the alkaline electrolyte saturated with zinc oxide by traditional methods. It was discovered that the electrolyte could be saturated with respect to zincate by dissolving additional zinc oxide and metallic zinc powder at room temperature in the presence of sponge nickel as a catalyst to dissolve zinc powder. The concentration of zincate (60 g/L of ZnO) in such obtained electrolyte was higher that reported elsewhere and no further zinc could be dissolved in this electrolyte as evidenced by the formation of white zinc hydroxide precipitate.

The dissolution of zinc active mass could be impeded by saturating the electrolyte with respect to zincate. However, introducing more zincate into the electrolyte promoted the reduction of zincate, which is associated with the zinc electrode shape change. It was revealed through linear sweep cathodic polarization that the reduction of zincate was a diffusion controlled process in accordance with Fick's first law.

In consideration of Fick's first law, anything that can change the diffusion coefficient may also affect the reduction of zincate, such as the addition of CMC to the electrolyte.

It was found that the reduction of solid zinc oxide and zinc hydroxide was not a diffusion controlled process, which was different from the reduction of zincate.

According to their differences in reduction and Fick's first law, it was found that quaternary ammonium hydroxides dissolved in the electrolyte could efficiently inhibit the reduction of zincate without significant effect on the reduction of solid zinc oxide and zinc hydroxide. Among the quaternary ammonium hydroxides, tetrabutylammonium hydroxide saturated in the electrolyte was found to be the best in retarding the reduction of zincate.

The electrolyte of 30% w/w KOH saturated with respect to zincate and with tetrabutylammonium hydroxide was chosen as the electrolyte for use in all future nickel zinc cells.

8.5 Modification of cell structure

The accession of electrolyte to the electrode assembly was associated with dissolution of the zinc active mass and the zinc dendrite growth. Ordinary cell structures like those used in Ni-Cd cells with ready accession of electrolyte to the electrode assembly were not suitable for use in nickel zinc cells, which needed modification.

The first modification was made by winding the electrode assembly with nylon thread and applying pressure on the face of the electrode assembly. The electrolyte accessability to the interface between nickel and zinc electrode was believed to be restricted. The anticipated prolonged cell cycle life was not attained with this modification alone. It was found the cell failed with semi-shorting caused by dendrite growth. The dendrite formation and growth was related to the electrolyte distribution. More dendrites were formed at the edges of the electrode where the electrolyte had easier access.

The second modification was made by avoiding electrolyte flooding of the electrode assembly. The bulk electrolyte was stored at the cell bottom as a reservoir without touching the electrode assembly. It was found that the cell cycle life was much prolonged. The electrolyte released from both of the nickel and zinc electrodes during charge left the assembly by gravity and was stored at the cell bottom. During discharge, the nickel and zinc electrodes could take in the electrolyte through the capillary attraction along the Perspex walls. By comparison with the flooded cells, the accessability of the electrolyte to the electrode assembly was much restricted, leading to an improved cycle life. The cell, however, also failed with semi-shorting from zinc dendrites that formed along the lower edges of the zinc electrodes where more of electrolyte gathered. These findings indicated that the distribution of the electrolyte needed further improvement.

The third and final structural modification was made to improve the distribution and access restriction of electrolyte in the electrode assembly. The electrode assembly wound with Nylon thread was bagged with a shrinking plastic bag that was open at the top edge and then was shrunk with hot air. The electrode assembly was tightly bagged with minimal space where the electrolyte could remain. In the cell case, the bulk electrolyte was separated from the electrode assembly with the plastic bag. The level of the electrolyte was below the opening of the plastic bag. During charge or discharge the electrolyte could leave or enter the electrode assembly by gravity or by capillary attraction. During charge only a very small amount of released electrolyte was sufficient to fill the plastic bag that tightly enclosed the electrode assembly. The result is shown in Fig. 5.11 (Cell #5.3). The discharge/charge efficiency for Cell #5.4 was over 70% in 500 cycles. It was thought that the cell structure was successfully optimized, and this was used in the cells for zinc active mass modification.

8.6 Zinc active mass modification

Through the optimized cell structure, it was possible to minimize the amount of electrolyte in direct contact with the zinc electrodes while improving the electrolyte distribution and hence restricted the access of the electrolyte to the zinc active mass, leading to prolonged

cycle life. Addition of zinc stearate or calcium stearate in the zinc active mass to make it hydrophobic was a further effort to restrict the electrolyte access. As anticipated, the zinc active mass formed by precipitating zinc stearate on the surface of zinc hydroxide particles became hydrophobic. Its dry powder could not be wetted with water, but it could be gradually wetted with the alkaline electrolyte. The access and diffusion of the electrolyte to zinc active mass was restricted as a consequence. With the optimized cell structure, the effect of zinc stearate and calcium stearate on cell cycle life was investigated.

High concentrations of zinc stearate (38.3% w/w) failed to improve the cycle life of the cells (Cell #6.1 and Cell #6.2). The efficiency declined to 69.1% only in 13 cycles for the Cell #6.1 shown in Fig. 6.1. Cell #6.2 also failed far earlier than anticipated, maintaining better than 80% capacity for only 45 cycles as shown in Fig. 6.4. It was found that zinc active mass was too hydrophobic and was inactive in charge/discharge cycling. High local current densities because of the inactive zinc mass resulted in dendrite growth causing semi-shorting.

In contrast to high concentration, low concentration of zinc stearate(5.8% w/w) in the zinc active mass was unable to retard zinc electrode shape change by restricting the access of the electrolyte to the zinc active mass. The discharge/charge efficiency reduced to 70.6% in 189 cycles. Figure 6.22 shows the result for the cell (Cell #6.6) consisting of 5.8% (w/w) zinc stearate.

An intermediate concentration of zinc stearate (18.9% w/w) resulted in much prolonged cycle life of the cell (Cell #6.3). Over the first 400 cycles the capacity for Cell #6.3 only declined from 94% to 91%. The efficiency remained over 80% in 620 cycles. The result is shown in Fig. 6.5.

Further modification made by using 18.9% (w/w) calcium stearate in place of zinc stearate, adding solid KOH into the zinc active mass and coating the brass mesh with zinc by electroplating prior to pasting further prolonged the cycle life of the cells (Cells #6.4 and #6.5).

Cell #6.4 showed a high, and even slightly increasing discharge capacity from 92% to 94% over the first 560 cycles. The discharge/charge efficiency remained over 84.9% in the 720 cycles. During 720 cycles there were 4 periods of overcharging of the cell due to equipment failure, but no long lasting effects were discernible. The result is shown in Fig. 6.13.

The results for Cell #6.5 (shown in Fig. 6.18) is similar in nature to those for Cell #6.4. After deliberate external shorting, the performance of these two cells was recovered. The discharge/charge efficiency for Cell #6.4 remained over 70.7 % for 1221 cycles while the discharge/charge efficiency for Cell #6.5 remained over 70.2 % for 1112 cycles.

Cells #6.4 and #6.5 exhibit the most prolonged cycle life performance of any other nickel zinc battery described in the open literature.

8.7 Scale up of the cells

It was an important task to identify the possibility of scaling up the cells by size and by the number of electrodes. The commercial 10 Ah nickel zinc cell cases and the electrodes provided by Evercel were taken as the sample for the cells to be scaled up. The size of the zinc electrode in the scaled cells was 8.3 cm × 8.3 cm slightly larger than the nickel electrode (7.8 cm × 7.8 cm). Unlike the 10 Ah Evercel cells consisting of 4 nickel and 5 zinc electrodes, the scaled cells comprised 3 zinc electrodes and 2 nickel electrodes. The structure, electrolyte and the zinc active mass were identical to the cells (Cells #6.4 and #6.5). Two bagged nickel electrodes were interleaved between three bagged zinc electrodes, which was then wound with nylon thread and bagged with a heat-shrink plastic bag. Two duplicate cells (Cells #7.1 and #7.2) were cycled but failed in early cycles as shown in Figs. 7.3 and 7.5 respectively. Zinc dendrites were responsible for the failure of these two cells as shown in Figs. 7.4 and 7.6. Investigation revealed that the zinc dendrites formed and grew preferentially at the central zinc electrode where the current density was higher than that at the side zinc electrodes.

There was an unbalanced mass and current distribution between the central and side zinc electrodes in the scaled cells. In order to improve the mass and current distribution between these zinc electrodes, the structure of the scaled cells was modified.

The modified scaled cell structure shown in Fig. 7.8 consists of two units, each unit identical to the Cells #6.4 and #6.5 except for the size and capacity. The two units were connected in parallel with charge exchange but without distinct mass exchange.

The modified cell structure incorporating with reducing the cutting voltage from 1.3 V to 0.8 V was successful in scaling up the cells. Figure 7.15 shows the results for Cell #7.4, which had cycle life approaching 550 cycles with efficiency over 70%. Its failure was associated with the exhaustion of electrolyte in the cell when no more electrolyte was added. Problems with swelling electrode assembly and hydrogen oxygen recombination still exist. These are beyond this study and could well be another project in the future.

8.8 Future work

i) Further scale up of cells using cell components used in Ni-Cd cells;

ii) Construct practical prototype cells connected as a small energy storage system with potential use in renewable energy development, such as wind power and solar energy;

iii) Using technology already attained, develop cylindrical C-sized cells as a portable power supply by employing cell components used in rechargeable cylindrical Ni-Cd and Ni-MH cells;

iv) Explore catalysts for oxidation of hydrogen and reduction of oxygen to develop sealed nickel zinc cells;

v) Investigate the cause of swelling in the electrode assembly;

vi) Further investigate the interaction between stearate and the zinc active mass; and

vii) The behavour of the zinc active particle surface when soaked in alkaline electrolyte.

References

1. Colin A. Vincent and Bruno Scrosati, Modern Batteries, Second edition, 1997 by Arnold, London.
2. David Linden, Handbook of Batteries, Second edition, 1995 by McGraw-Hill Inc.
3. Mukund R. Patel, Wind and Solar Power Systems, 1999 by CRC Press LLC.
4. T. R. Crompton, Battery Reference Book, 2000 by Reed Educational and Professional Publishing Ltd.
5. H. Bode, Lead-Acid Batteries, 1977 by Wiley, New York.
6. Lazarides, C., Hampson, N.A. and Hedderson. M., J. Appl. Electrochem., 11 (1981) 605.
7. www.evercel.com
8. Sealed Nickel Cadmium Batteries, 1982 by Varta-Batterie-AG.
9. T. R. Cromton, Small Batteries, Volume 1 Secondary Batteries, 1982 by The MacMlillan Press Ltd.
10. James Skelton and Roberto Serenyi, Journal of Power Sources, 65 (1997), 39-45.
11. www.eaglepicher.com.
12. K. Kordesch (ed.), Btteries, Vol. 1, Manganese Dioxide, Dekker, Yew York, 1974.
13. www.rayovac.com
14. Mikhalovskii, Br. Patent 15 370 (1899).
15. J. J. Drumm, British Patent 365, 125 (July 17, 1930).
16. J. J. Drumm, U.S. Patent 1,955,115 (April 17 1934).
17. J. J. Drumm and A. G. Burnell, U.S. Patent 2,227,636 (March 24, 1942).
18. James McBreen. Journal of Power Sources, 51 (1994), 37-44.
19. Dwaine Coasts, Allen Charkey, Proc of the 32nd intersociety, 1997 p857-862.

20. McBreen, James. (Yardney International Corp.). U.S. (1970), 7 pp. CODEN: USXXAM US 3505115 19700407 Application: US 19670511. CAN 73:31058 AN 1970:431058.

21. McBreen, James. (General Motors Corp., USA). U.S. (1976), 5 pp. CODEN: USXXAM US 4000005 19761228 Application: US 76-647624 19760108. CAN 86:124211 AN 1977:124211.

22. McBreen, James. (General Motors Corp., USA). U.S. (1975), 6 pp. CODEN: USXXAM US 3876470 19750408 Application: US 72-310254 19721129. CAN 83:63427 AN 1975:463427.

23. McBreen, James. Electrochem. Dep., Gen. Mot. Corp., Warren, Mich., USA. J. Electrochem. Soc. (1972), 119(12), 1620-8.

24. E. J. Cairns and James McBreen. Ind. Res., 17 (1975) 56.

25. Jiri Jindra. Inst. Chem. Technol., Tech. Univ. Darmstadt, Darmstadt, Germany. J. Power Sources (1992), 37(3), 297-313.

26. Jiri Jindra. Institute of Chemical Technology, Technical University Darmstadt, Petersenstrasse 20, 64287, Darmstadt, Germany. J. Power Sources (1997), 66(1-2), 15-25.

27. Jiri Jindra. Academy of Sciences of the Czech Republic, Prague, Czech Rep. J. Power Sources (2000), 88(2), 202-205.

28. Charkey, Allen; Zhang, Hanlin; Cao, Frank. Evercel Inc., Danbury, CT, USA. Proceedings of the Intersociety Energy Conversion Engineering Conference (2001), 36th(Vol. 2), 917-922.

29. Charkey, Allen; Cao, Frank; Bowling, Glen. Evercel Corporation, Danbury, CT, USA. Proc. Power Sources Conf. (2000), 39th 322-325.

30. Cao, Frank; Charkey, Allen; Williams, Keith. Evercel Inc., Danbury, CT, USA. Proc. Intersoc. Energy Convers. Eng. Conf. (2000), 35th(Vol. 2), 985-994.

31. Martin, Franklin; Charkey, Allen; Handberry, Virgil. (Evercel, Inc., USA). PCT Int. Appl. (2000), 42 pp.

32. Coates, Dwaine; Charkey, Allen. Evercel Corporation, USA. Proc. Intersoc. Energy Convers. Eng. Conf. (1999), 34th 216-219.

33. Charkey, Allen; Coates, Dwaine K. (Energy Research Corp., USA). PCT Int. Appl. (1998), 27 pp.

34. Coates, Dwaine; Charkey, Allen. Energy Res. Corp., Danbury, CT, USA. Proc. Intersoc. Energy Convers. Eng. Conf. (1997), 32nd 857-862.

35. Charkey, Allen. (Energy Research Corp., USA). U.S. (1997), 4 pp.

36. Coates, Dwaine; Ferreira, Elio; Charkey, Allen. Energy Research Corporation, 3 Great Pasture Road, Danbury, CT, USA. J. Power Sources (1997), 65(1-2), 109-115.

37. Coates, D.; Ferreira, E.; Charkey, Allen. Energy Research Corporation, Danbury, CT, USA. Editor(s): Frank, Harvey A.; Seo, Eddie T. Annu. Battery Conf. Appl. Adv., 12th (1997), 23-28.

38. Charkey, Allen. (Energy Research Corporation, USA). U.S. (1996), 8 pp. Cont.-in-part of U.S. 5, 460, 899. CODEN: USXXAM US 5556720 A Application: US 95-431556 19950501. Priority: US 94-292614 19940818

39. Charkey, Allen. (Energy Research Corporation, USA). Eur. Pat. Appl. (1996), 9 pp. CODEN: EPXXDW EP 697746 A1 19960221 Designated States R: DE, FR, GB. Application: EP 95-113014 19950818. Priority: US 94-292614 19940818; US 95-431556 19950501.

40. Charkey, Allen. (Energy Research Corp., USA). U.S. Patent No.5 460 899 (1995)

41. Charkey, Allen. (Energy Research Corp., USA). Eur. Pat. Appl. (1992), 7 pp. CODEN: EPXXDW EP 512417 A1 19921111 Designated States R: DE, FR, GB, IT. Application: EP 92-107399 19920430. Priority: US 91-695437 19910503.

42. Charkey, Allen; Januszkiewicz, Stanley. (Energy Research Corp., USA). Eur. Pat. Appl. (1991), 9 pp. CODEN: EPXXDW EP 427192 A1 19910515 Designated States R: DE, FR, GB. Application: EP 90-121197 19901106. Priority: US 89-431998 19891106.

43. Levy, Isaac; Charkey, Allen. (Energy Research Corp., USA). U.S. (1989), 6 pp. CODEN: USXXAM US 4810598 A 19890307 Patent written in English. Application: US 88-172632 19880324.

44. Viswanathan, S.; Charkey, Allen. Energy Res. Corp., Danbury, CT, USA. Avail. NTIS. Report (1988), (AFWAL-TR-87-2088; Order No. AD-A194979), 184 pp.

45. Leo, Anthony; Charkey, Allen. Energy Res. Corp., Danbury, CT, USA. Proc. Power Sources Symp. (1984), 31st 249-54.

46. Charkey, Allen; Januszkiewicz, Stanley. (Energy Research Corp., USA). US Patent No. 4546058

47. Dodin, Mark G.; Charkey, Allen. (Energy Research Corp., USA). Eur. Pat. Appl. (1983), 18 pp. CODEN: EPXXDW EP 77030 A1 19830420 Designated States R: DE, FR, GB. Application: EP 82-109273 19821007. Priority: US 81-309814 19811008.

48. Charkey, Allen. Lawrence Berkeley Lab., Berkeley, CA, USA. Avail. NTIS. Report (1982), (LBL-14674; Order No. DE82020608), 33 pp

49. Charkey, Allen. (Energy Research Corp., USA). Eur. Pat. Appl. (1982), 15 pp. CODEN: EPXXDW EP 48009 A1 19820324 Designated States R: DE, FR, GB. Patent written in English. Application: EP 81-107216 19810914. Priority: US 80-187335 19800915. CAN 97:9212

50. Dodin, Mark G.; Charkey, Allen. (Energy Research Corp., USA). Eur. Pat. Appl. (1981), 13 pp. CODEN: EPXXDW EP 40826 A1 19811202 Designated States R: DE, FR, GB. Patent written in English. Application: EP 81-103917 19810521. Priority: US 80-152725 19800523

51. Charkey, Allen; Klein, Martin. Energy Res. Corp., Danbury, CT, USA. Proc. - Power Sources Symp. (1978), 28th 145-9

52. Klein, M. G.; Charkey, Allen.; Vaidyanathan, H.; Viswanathan, S. Energy Res. Corp., Danbury, CT, USA. Proc. Intersoc. Energy Convers. Eng. Conf. (1979), 14th(Vol. 1), 646-50.

53. Charkey, Allen. (Energy Research Corp., USA). Ger. Offen. (1978), 21 pp. CODEN: GWXXBX DE 2707051 19780720 Patent written in German. Application: DE 77-2707051 19770218.

54. Charkey, Allen. (Energy Research Corp., USA). U.S. (1977), 6 pp. CODEN: USXXAM US 4022953 19770510 Patent written in English. Application: US 75-606866 19750822.

55. Charkey, Allen. Energy Res. Corp., Danbury, Conn., USA. Proc. - Intersoc. Energy Convers. Eng. Conf. (1976), 11, Vol. 1 452-6.

56. Charkey, Allen. Energy Res. Corp., Danbury, Conn., USA. Avail. NTIS. U. S. NTIS, AD Rep. (1976), (AD-A022467), 21 pp

57. Charkey, Allen. Energy Res. Corp., Danbury, Conn., USA. Rec. Intersoc. Energy Convers. Eng. Conf., 10th (1975), 1126-30.

58. Charkey, Allen. Energy Res. Corp., Bethel, Conn., USA. Intersoc. Energy Convers. Eng. Conf., Conf. Proc. 7th (1972), 110-13

59. Charkey, Allen. Energy Res. Corp., Bethel, Conn., USA. Power Sources Symp., Proc. (1972), 25 64-7.

60. Charkey, Allen. Energy Res. Corp., Bethel, Conn., USA. Avail. NTIS. U. S. Nat. Tech. Inform. Serv., AD Rep. (1972), (No. 748896), 39 pp. From: Govt. Rep. Announce. (U.S.) 1972, 72(21), 92.

61. Charkey, Allen; Brooks-Smith, Derryk. (Yardney International Corp.). U.S. (1972), 4 pp. CODEN: USXXAM US 3652338 19720328 Patent written in English. Application: US 69-852497 19690822. CAN 77:69411

62. Blossom, Raymond W.; Charkey, Allen. (Yardney International Corp.). U.S. (1972), 3 pp. CODEN: USXXAM US 3655451 19720411 Patent written in English. Application: US 69-816077 19690414. CAN 77:13292

63. Kober, Frederick P.; Charkey, Allen. Yardney Electr. Corp., New York, N. Y., USA. Editor(s): Collins, Derek H. Power Sources 3: Res. Develop. Non-Mech. Elec. Power Sources, Proc. Int. Symp., 7th (1971), Meeting Date 1970, 309-26.

64. Charkey, Allen; Kober, Frederick P. (Yardney International Corp.). Fr. Demande (1970), 16 pp. CODEN: FRXXBL FR 2020314 19700710 Patent written in French. Application: FR 69-34551 19691009.

65. Charkey, Allen; Kober, Frederick P. (Yardney International Corp.). Ger. Offen. (1970), 16 pp. CODEN: GWXXBX DE 1950920 19700416 Patent written in German. Priority: US 19681010

66. Charkey, Allen. Yardney Elec. Corp., USA. Proc., Annu. Power Sources Conf. (1969), 23 115-19.

67. Charkey, Allen; Di Pasquale, Renato. (Yardney International Corp.). Fr. (1968), 5 pp. CODEN: FRXXAK FR 1550508 19681220 Patent written in French. Priority: US 19661214. CAN 71:87158

68. Charkey, Allen; Dalin, George A. Yardney Elec. Corp., New York, N. Y., USA. Proc., Annu. Power Sources Conf. (1966), 20 79-83.

69. R. McLarnon and E. J. Cairns, J. electrochem. Soc., 138 (1991) 645.

70. T. C. Adler, F. R. McLarnon and E. J. Cairns. J. Electrochem. Soc., Vol. 140, No. 2, February 1993 289-293

71. P. Dirkse, J. Electrochem. Soc., 101 (1954) 328

72. R. Jain, T. C. Alder, F. R. McLarnon and E. J. Cairns , J. Appl. Electrochem., 22 (1992) 1039.

73. H. Chang and C. Lim, J. Power Sources, 66 (1996) 115.

74. V.V.Romanoff, J. Appl. Chem. (USSR). 35(1962) 1246.

75. N. A. Zhulidov and F. I. Efremov, Vest. Elektroprom. 34 (1971) 74

76. W. J. van der Grinten, No. 38, p. 96, The electrochemical Society Extended Abstracts, Oct. 15-20 (1967).

77. W. J. van der Grinten, No. 38, p. 96, The electrochemical Society Extended Abstracts, Oct. 15-20 (1967).

78. Y. Maki, M. Fujita, H. Takahashi and T. Ino (Hitachi, Ltd. and Tokyo Electric Poer Co.,) U.S. Patent 3816178(1974).

79. R. A. Jones (General Motors Corporation), U.S. Patent 4358517 (1982).

80. Sharma, J. Electrochem. Soc., 133 (1986) 2215.

81. Sharma, J. Electrochem. Soc., 135 (1988) 1875.

82. G. Gagnon, J. Electrochem. Soc., 133 (1986) 1989.

83. G. Gagnon and Y. M. Wang, J. Electrochem. Soc., 134 (1987) 2091

84. G. Gagnon and B. S. Hill, J. Electrochem. Soc., 137 (1990) 377.

85. G. Gagnon, J. Electrochem. Soc., 138 (1991) 3173.

86. Adler, T. C.; McLarnon, F. R.; Cairns, E. J.. Applied Sci. Div., Lawrence Berkeley Lab., Berkeley, CA, USA. Proc. Intersoc. Energy Convers. Eng. Conf. (1987), 22nd(Vol. 2), 1097-101.

87. Jain, R.; McLarnon, F. R.; Cairns, E. J.. Lawrence Berkeley Lab., Berkeley, CA, USA. Avail. NTIS. Report (1989), (LBL-25332; Order No. DE90004040), 151 pp.

88. US Patent No. 5,863,676

89. Dwaine Coates and Allen Charkey, Proc. of the 32-nd Intersociety, 1997, vol. 2, 857-862.

90. C.zhang, J. M. Wang, L. Zhang, J. Q. Zhang and C. N. Cao. Journal of Applied Electrochmistry, 31: 1049-1054, 2001

91. Charkey, Allen. Energy Res. Corp., Bethel, Conn., USA. Power Sources Symp., Proc. (1974), 26 87-90.

92. US Patent No. 4,332,871

93. M. Yano, S. Fujitani, K. Nishio, Y. Akai, M. Kurimura, J. Power Sources, **74** (1998) 129

94. J. Skelton, R. Serenyi, J. Power Sources, **65** (1997) 39

95. James McBreen and E. Gannon, J. Power Sources, **15** (1985) 169

96. C. Biegler, R. L. Deutscher, S. Fletcher, S. Hua and R. Woods, J. Electrochem. Soc. , **130** (1983) 2303

97. Schneider and Z. Dominiczak, in D. H. Collins (ed.), Power Sources, Vol. 4, Oriel, Newcastle upon Tyne, 1973, pp.115-140.

98. Eisenberg, US Patent 4 224 391(1980).

99. Eisenberg, US Patent 5 215 836 (1993)

100. Furukawa, K. Inone and M. Nogami, Jpn. Patent JP 62 165 878(1987); CA, 107(1987), 137752

101. M. Jost, US Patent 3 485 673(1969)

102. Adler, F. R. McLarnon and E. J. Cairns, 176th Electrochem. Soc. Meet., 1989, Ext. Abstr., Vol. 89-2, Abstr. no.5

103. T. C. Adler, F. R. McLarnon and E. J. Cairns. J. Electrochem. Soc., Vol. 140, No. 2, February 1993 289-293

104. Jenn-Shing Chen, Frank R. McLarnon and Elton J. Cairns. J. Power Sources, 39 (1992) 333-348.

105. Anho,Tamiko, Jpn. Patent, Jp 08 329 977 (1996); CA, 126, 120097d.

106. Shivkumar, G. Paruthimal Kalaignam and T. Vasudevan, J. Power Sources, 55, (1995) 53-62

107. Baohong, Ch. Meng, Xu Donggri and W.Yindong, Ext. Abstr., 46th ISE meet., Ximan, P.R. China, 1995, Vol. 2, Abstr. No.5-43

108. Jinrong Liu, Yingxin Lin and Zhiqiang Zhu, Chinese Patent ZL92 2 45225.3.

109. Okabe, Kazuya; Onda, Toshuki; Fujii, Kenkichi; Yamane, Mitsuo; Matoba, Noriko; Nakajima, Sanehiro; Rikihisa, Katsutoshi; Adachi, Kazu yuki, Jpn. Patent, JP 07 161 375(1995). CA., 123, 204393y

110. Doddapaneni and D. Ingersoll, Ext. Abstr., 188th meet. The Electrochem. Soc., 1995, Vol. 92-5, Abstr. No.61-2

111. F. Fauvarque, S. Guinot, N. Bouzin, E. Salmon and J. F. Penneau, et al, Electrochim. Acta, 40, (1995) 2449-2453.

112. Alexandre P. Paqvlov,Ljudmila K. Grigorieva, Semen P. Chizhik and Vitaly Kh. Stankov, et al, J. Power Sources, 62, (1996)113.

113. Itami and Toshio, Jpn. Patent, JP 08 45 539(1996) . CA, 124, 265737f.

114. Tassin, G. Bronoel, J. F.Fauvarque and A. Millot, Proc. Power Sources Conf., 1996, 37th, 378-381.

115. J. McBreen, E. Gannon, D. T. Chin and R. Sethi, J. Electrochem. Soc., 130 (1983) 1641

116. K. Wall, 'Modern Chlor-Alkali Technology', Vol. 3 (Ellis Horwood, Chichester, UK, 1986).

117. S. Sotiropoulos, I. J. Brown, G. Akay and E. Lester, Mater. Lett. 35 (1998) 383.

118. I. J. Brown, D. Clift and S. Sotiropoulos, Mater. Res. Bull. 34 (7) (1999) 1055.

119. I. J. Brown and S. Sotiropoulos, J. Appl. Electrochem. , 31 (2001) 1203-1212.

120. Wu Su Gao, *et al*, Electroless Plating Technology for Plastics (in chinese), Shichuan Science and Technology Press, 1983.

121. David R. Lide. Handbook of Chemistry and Physics. 82nd Edition, 2001-2002, by CRC Press CLC.

122. L. Binder and K. Kordesch, Electochim. Acta, 31 (1986) 255

123. Y. P. Lin and J. R. Selman, J. Electrochem. Soc., 138 (1991) 3525

124. Exide Management and Technology Co., " Annual Report for 1980 on Research, Development and Demonstration of Nickel-Zinc Batteries for Electric Vehicle Propulsion",Argonne National Laboratory Report, ANL/OEPM-80-15, Argonne, IL(1981)

125. Y. Sato, M. Kauda, H. Niki, M. Ueno, K. Murata, T. Shirogami and T. Takamura, J. Power Sources, 9 (1983) 147.

126. David R. Lide. Handbook of Chemistry and Physics. 82nd Edition, 2001-2002, by CRC Press CLC

Appendix A List of apparatus

Name	Model
Computers	486
Monitors	15' PHILIPS
0-30V 5A Lab Power Supplies	Dick Smith Electronics Q1760
Parallel Port Interface	Dick Smith Electronics, K-2805
Relays	2369HP
Multimeters	Dick Smith Electronics, Q-1424
Linear Sweeping Voltammetry	BAS100B/W

Appendix B QBasic program used for cell cycling

The core of this code was written by Dr Simon Brown based upon information supplied with the 8-bit analog to digital convertor by Dick Smith Electronics Ltd. Dr Simon Hall modified this code to operate the relay switching equipment.

```
DECLARE SUB SetTTLDAC (Vapp AS SINGLE)
DECLARE SUB WasteTime ()
DECLARE SUB BatteryCycle ()
DECLARE SUB delay (dt!)
DECLARE SUB BoardOff ()
DECLARE SUB BoardOn ()
DECLARE SUB SetTTL (N%, dout() AS INTEGER)
DECLARE FUNCTION ReadADC! (Channel%)
DECLARE SUB SetDAC (DAC%, V)
DECLARE SUB SetRelay ()
DECLARE FUNCTION BinStr$ (V!)
DECLARE SUB DoCharge ()
DECLARE SUB DoOCC ()
DECLARE SUB DoDischarge ()
DECLARE SUB DoOCD ()
DECLARE SUB Dostring ()
DIM SHARED dout(0 TO 7) AS INTEGER
DIM SHARED Vout(0 TO 1) AS SINGLE
'DIM SHARED Pol(1 TO 10) AS INTEGER
'DIM SHARED CRange(1 TO 10, 6 TO 7) AS INTEGER
'DIM SHARED Cpot(1 TO 10) AS SINGLE
'DIM SHARED CTime(1 TO 10) AS LONG
CONST Base0 = &H378          'Printer port address'
'Plot boundaries'
TMax = 500: TMin = 0
YMax = 6: YMin = 0
dX = TMax - TMin: dY = YMax - YMin
dt = .2
CLS
SCREEN 8
COLOR 15
FOR i = 0 TO 7
    dout(i) = 0
NEXT i
PRINT "Switching power on ... "
CALL BoardOn
PRINT "Power on"
Ans% = 0
WHILE (Ans% <> 6)
  CLS
  LOCATE 1, 1: PRINT "Power on"
  LOCATE 8, 20: PRINT "0.  Set Card TTL and DAC"
  LOCATE 10, 20: PRINT "1.  Continuous recording"
  LOCATE 12, 20: PRINT "2.  Set DACs"
```

```
LOCATE 14, 20: PRINT "3.  Toggle TTLs"
LOCATE 16, 20: PRINT "4.  Test TTLs using DACs"
LOCATE 18, 20: PRINT "5.  Battery Cycle"
LOCATE 20, 20: PRINT "6.  Quit"
LOCATE 22, 20: INPUT "Enter option (1 - 6) : ", Ans%
SELECT CASE Ans%
  CASE 0
    CLS
    WRITE "TTL settings:"
    WRITE "TTL:  Current      New?"
    FOR i% = 0 TO 7
     PRINT i%, dout(i%),
     INPUT dout(i%)
    NEXT i%
    INPUT "Voltage setting for #1", Vapp
    CALL SetTTLDAC(Vapp)
  CASE 1

    TIME$ = "00:00:00"

    INPUT "Enter input channel (0 - 9) : ", Channel%
    INPUT "Duration (s) : ", TMax
    TMin = 0: YMax = 6: YMin = 0
    dX = TMax - TMin: dY = YMax - YMin
    SCREEN 11
    T0 = TIMER
    PSET (0, 0)
    Count = 0
    V = 0
    WHILE (TIMER - T0 < TMax) AND (INKEY$ = "")
        Vout = ReadADC(Channel%)
        y = 440 * (1 - ((Vout - YMin) / dY))
        x = 640 * (TIMER - T0 - TMin) / dX
        LINE -(x, y)
        IF Count < 20 THEN
         Count = Count + 1
        ELSE
         'V = ABS(V - 1)
         'CALL SetDAC(0, ABS(V))
         'CALL SetTTL(0, Dout())
         Count = 0
        END IF
    WEND
    SCREEN 0
  CASE 2

     TIME$ = "00:00:00"

    INPUT "Enter DAC (0 - 1) and voltage (0 - 5) : ", DAC%, V
    IF (DAC% = 0) OR (DAC% = 1) THEN CALL SetDAC(DAC%, V)
  CASE 3

     TIME$ = "00:00:00"

     INPUT "Enter TTL (0 - 7) : ", TTL%
     CALL SetTTL(TTL%, dout())
```

```
    CASE 4
       CLS

       TIME$ = "00:00:00"

       TTL$ = " "
       WHILE (TTL$ <> "")
         INPUT "Enter TTL (0 - 7) : ", TTL$
         IF (INSTR("01234567", LTRIM$(RTRIM$(TTL$))) <> 0) THEN
           FOR i = 0 TO 7
             PRINT USING "####"; i; SPC(4);
           NEXT i
           PRINT
           FOR N% = 0 TO 7
             CALL SetTTL(N%, dout())
             CALL delay(dt)
             PRINT USING "####.###"; ReadADC(N%);
             CALL delay(dt)
           NEXT N%
           PRINT
         END IF
       WEND
    CASE 5

       TIME$ = "00:00:00"
       CALL BatteryCycle
    CASE 7
     CALL Dostring
  END SELECT
WEND
FOR i% = 0 TO 7
  IF (dout(i%) = 1) THEN CALL SetTTL(i%, dout())
NEXT i%
CLS
PRINT "Closing down board ..."
CALL SetDAC(0, 0)
CALL SetDAC(1, 0)
CALL BoardOff
PRINT "Power off"
END

SUB BatteryCycle

CLS
SCREEN 8
COLOR 14
LOCATE 1, 27: PRINT "Battery Cycle Monitoring"
LOCATE 3, 10: PRINT "Pseudo Constant Current Charge - Constant Current Discharge"
COLOR 15
LOCATE 6, 1: PRINT "          General Parameters"

LOCATE 8, 1: INPUT "     Input output filename (no extension):", fileout$
LOCATE 10, 1: INPUT "Input the initial number of battery cycles:", inumber%
LOCATE 12, 1: INPUT " Input the final Number of battery cycles :", CCyc%
totchargetime& = 0
tbefore& = 0
```

```
LOCATE 14, 1: INPUT "        Brief Description of the Battery: ", Special$

CLS
COLOR 14
LOCATE 1, 27: PRINT "Battery Cycle Monitoring"
LOCATE 3, 10: PRINT "Pseudo Constant Current Charge - Constant Current Discharge"
COLOR 13
LOCATE 6, 1: PRINT "Charging Conditions"
COLOR 15
LOCATE 8, 1: PRINT "Charging will terminate either at maximum time"
LOCATE 9, 1: PRINT "or when Ecell approaches a maximum set value"
LOCATE 11, 1: INPUT "Charging Current (mA) : ", ICharge%
LOCATE 13, 1: PRINT "Maximum Charge Duration"
LOCATE 14, 1: INPUT "        hours : ", chargehours%
LOCATE 15, 1: INPUT "      minutes : ", chargemins%
LOCATE 16, 1: INPUT "      seconds : ", chargesecs%
LOCATE 18, 1: INPUT "Input number of seconds between each sample:", CTincr%
LOCATE 20, 1: INPUT "              Termination Ecell Potentil: ", Vcellmax!
Ctime& = chargehours% * (60 ^ 2)
Ctime& = Ctime& + chargemins% * 60
Ctime& = Ctime& + chargesecs%
CQ = ICharge% / 1000 * Ctime& / 3600
CLS
COLOR 14
LOCATE 1, 27: PRINT "Battery Cycle Monitoring"
LOCATE 3, 10: PRINT "Pseudo Constant Current Charge - Constant Current Discharge"
COLOR 13
LOCATE 6, 1: PRINT "Open Circuit Conditions after Charging"
COLOR 15
LOCATE 8, 1: PRINT "Post Charging Open Circuit Duration"
LOCATE 9, 1: INPUT "        hours : ", OCchargehours%
LOCATE 10, 1: INPUT "      minutes : ", OCchargemins%
LOCATE 11, 1: INPUT "      seconds : ", OCchargesecs%
LOCATE 13, 1: INPUT "Input number of seconds between each sample:", OCCTincr%
OCCTime& = OCchargehours% * (60 ^ 2)
OCCTime& = OCCTime& + OCchargemins% * 60
OCCTime& = OCCTime& + OCchargesecs%
CLS
COLOR 14
LOCATE 1, 27: PRINT "Battery Cycle Monitoring"
LOCATE 3, 10: PRINT "Pseudo Constant Current Charge - Constant Current Discharge"
COLOR 10
LOCATE 6, 1: PRINT "Discharge Conditions"
COLOR 15
LOCATE 8, 1: PRINT "Discharge will terminate either at maximum time"
LOCATE 9, 1: PRINT "or when Ecell approaches a minimum set value "
LOCATE 11, 1: INPUT "    Discharge Current (mA): ", Dload
LOCATE 13, 1: PRINT "Maximum Discharge Duration"
LOCATE 14, 1: INPUT "      hours : ", dischargehours%
LOCATE 15, 1: INPUT "    minutes : ", dischargemins%
LOCATE 16, 1: INPUT "    seconds : ", dischargesecs%
LOCATE 18, 1: INPUT "Input number of seconds between each sample:", DTincr%
LOCATE 20, 1: INPUT "              Termination Ecell Potential:", Vcellmin!
DTime& = dischargehours% * (60 ^ 2)
DTime& = DTime& + dischargemins% * 60
```

```
DTime& = DTime& + dischargesecs%
CLS
COLOR 14
LOCATE 1, 27: PRINT "Battery Cycle Monitoring"
LOCATE 3, 10: PRINT "Pseudo Constant Current Charge - Constant Current Discharge"
COLOR 10
LOCATE 6, 1: PRINT "Open Circuit Conditions after Discharge"
COLOR 15
LOCATE 8, 1: PRINT "Post Discharge Open Circuit Duration"
LOCATE 9, 1: INPUT "        hours : ", OCdischargehours%
LOCATE 10, 1: INPUT "       minutes : ", OCdischargemins%
LOCATE 11, 1: INPUT "       seconds : ", OCdischargesecs%
LOCATE 13, 1: INPUT "Input number of seconds between each sample:", OCDTincr%
OCDTime& = OCdischargehours% * (60 ^ 2)
OCDTime& = OCDTime& + OCdischargemins% * 60
OCDTime& = OCDTime& + OCdischargesecs%



CLS
REM Write General Information output file
IF LEN(fileout$) > 8 THEN
  fileout$ = LEFT$(fileout$, 8)
END IF
Genout$ = fileout$ + ".GEN"
OPEN Genout$ FOR APPEND AS #1
PRINT #1, "Date: "; DATE$
PRINT #1, "Battery Cycle Monitoring"
PRINT #1, "Pseudo Constant Current Charge - Constant Current Discharge"
PRINT #1, "General Parameters"
PRINT #1, "Number of battery cycles          : ", CCyc%
PRINT #1, "Brief Description of Battery: "
PRINT #1, Special$
PRINT #1, ""
PRINT #1, "Charging Conditions"
PRINT #1, "Charging Current (mA) = ", ICharge%
PRINT #1, "Maximum Charge Duration"
PRINT #1, chargehours%, " hours"
PRINT #1, chargemins%, " minutes"
PRINT #1, chargesecs%, " seconds"
PRINT #1, "Number of seconds between each sample = ", CTincr%
PRINT #1, "Termination Ecell Potential = ", Vcellmax!
PRINT #1, ""
PRINT #1, "Post Charging Open Circuit Conditions"
PRINT #1, "Open Circuit Duration"
PRINT #1, OCchargehours%, " hours"
PRINT #1, OCchargemins%, " minutes"
PRINT #1, OCchargesecs%, " seconds"
PRINT #1, "Number of seconds between each sample = ", OCCTincr%
PRINT #1, ""
PRINT #1, "Discharge Conditions"
PRINT #1, "Discharge Current (mA) = ", Dload%
PRINT #1, "Maximum Discharge Duration"
PRINT #1, dischargehours%, " hours"
PRINT #1, dischargemins%, " minutes"
PRINT #1, dischargesecs%, " seconds"
```

```
PRINT #1, "Number of seconds between each sample = ", DTincr%
PRINT #1, "Termination Ecell Potential = ", Vcellmin!
PRINT #1, ""
PRINT #1, "Post Discharge Open Circuit Conditions"
PRINT #1, "Open Circuit Duration"
PRINT #1, OCdischargehours%, " hours"
PRINT #1, OCdischargemins%, " minutes"
PRINT #1, OCdischargesecs%, " seconds"
PRINT #1, "Number of seconds between each sample = ", OCDTincr%
CLOSE #1
adriveout$ = "a:\" + Genout$
REM End of writing General Information file

REM Copy to A:
OPEN Genout$ FOR INPUT AS #1
OPEN adriveout$ FOR OUTPUT AS #2
 DO
  LINE INPUT #1, a$
  PRINT #2, a$
 LOOP UNTIL (EOF(1))
CLOSE #1
CLOSE #2

REM Battery is disconnected (Dout(0)=0) and charger is selected (Dout(1)=0)
REM at Board Startup
duration& = Ctime& + OCCTime& + DTime& + OCDTime&
hrsduration = duration& / 3600


FOR j% = inumber% TO CCyc%
 CLS
 tbefore& = 0
 telapsed& = 0
SELECT CASE j%
 CASE 1 TO 9
  dataout$ = fileout$ + ".00"
  dataout$ = dataout$ + LTRIM$(STR$(j%))
 CASE 10 TO 99
  dataout$ = fileout$ + ".0"
  dataout$ = dataout$ + LTRIM$(STR$(j%))
 CASE 100 TO 999
  dataout$ = fileout$ + "."
  dataout$ = dataout$ + LTRIM$(STR$(j%))
 CASE IS > 999
  dataout$ = fileout$ + "XXX"
END SELECT


CLS
SCREEN 12, 5
LINE (10, 0)-(10, 300)
LINE (9, 0)-(9, 300)

LINE (9, 0)-(5, 8)
LINE (9, 0)-(7, 8)
LINE (10, 0)-(14, 8)
```

```
LINE (10, 0)-(12, 8)

LINE (10, 160)-(15, 160)
LINE (10, 120)-(15, 120)
LINE (10, 80)-(15, 80)
LINE (10, 40)-(15, 40)

LINE (10, 200)-(630, 200)
LINE (10, 199)-(630, 199)

LINE (10, 240)-(15, 240)
LINE (10, 280)-(15, 280)

LINE (630, 199)-(622, 196)
LINE (630, 199)-(622, 198)
LINE (630, 200)-(622, 204)
LINE (630, 200)-(622, 202)

FOR S = 1 TO hrsduration - 1
LINE (10 + S * 620 / hrsduration, 200)-(10 + S * 620 / hrsduration, 192)
NEXT S

OPEN dataout$ FOR OUTPUT AS #1
PRINT #1, "Charge/Discharge conditions located in file: "; Genout$
PRINT #1, "Cycle "; j%; " of "; CCyc%
PRINT #1, "Mode 1 = charge,          Mode 2 = open circuit after charge,"
PRINT #1, "Mode 3 = discharge,       Mode 4 = open circuit after discharge."
PRINT #1, ""
PRINT #1, "Time    Total time (hrs.)    mode    Vcell    Vneg    Vpos"

TIME$ = "00:00:00"
T0 = TIMER
tlast = T0
Vneg = ReadADC(0)
Vcell = ReadADC(1)
Vpos = Vcell - Vneg
Vneg = 0 - Vneg
PRINT #1, TIME$, " 1", "0", Vcell, Vneg, Vpos
CLOSE #1

COLOR 14
y = (200 - 200 * Vcell / 5)
x = 10
PSET (x, y)
PSET (x + 1, y)
PSET (x, y + 1)


COLOR 11
y = 200 * (1 - Vneg / 5)
PSET (x, y)
PSET (x + 1, y)
PSET (x, y + 1)


COLOR 12
```

```
y = 200 * (1 - Vpos / 5)
PSET (x, y)
PSET (x + 1, y)
PSET (x, y + 1)


COLOR 15
hrs = FIX(Ctime& / 3600)
mins = FIX((Ctime& - 3600 * hrs) / 60)
secs = FIX(Ctime& - 3600 * hrs - 60 * mins)

LOCATE 1, 4: PRINT "Voltage (V)"
LOCATE 14, 71: PRINT "Time(hrs.)"
LOCATE 1, 25: PRINT "Cycle Number:  "; j%; " of "; CCyc%
LOCATE 28, 32: PRINT "Segment Length: "; hrs; " hrs.  "; mins; " mins   "; secs; " secs"
LOCATE 22, 32: PRINT "Interval: "; CTincr%; " secs"
LOCATE 24, 32: PRINT "Charging at "; ICharge%; " mA   "
T0 = TIMER
tlast = T0

REM Make closed circuit on Relay 0, Relay 1 remains at default charging position
dout(0) = 1
dout(1) = 0
CALL SetRelay
REM CALL DoCharge
REM Starts here
'PRINT "telapsed& = ", telapsed&
'PRINT "tebfore&  = ", tebefore&
'PRINT "CTime&    = ", CTime&
'PRINT "CTincr%   = ", CTincr%
'INPUT tmp%
DO WHILE ((INKEY$ <> "q") AND ((telapsed& < Ctime&) AND (Vcell < Vcellmax)))
  FOR itmp% = 1 TO CTincr%
    CALL delay(1)
    telapsed& = TIMER - T0
    IF telapsed& < 0 THEN
      telapsed& = telapsed& + 86400
    END IF
    hrs = FIX(telapsed& / 3600)
    mins = FIX((telapsed& - 3600 * hrs) / 60)
    secs = FIX(telapsed& - 3600 * hrs - 60 * mins)
    COLOR 10
    LOCATE 22, 62: PRINT "Time: "; TIME$
    COLOR 13
    LOCATE 20, 32: PRINT "Elapsed Time:  "; hrs; " hrs  "; mins; " mins  "; secs; " secs  "
    Vneg = ReadADC(0)
    Vcell = ReadADC(1)
    Vpos = Vcell - Vneg
    Vneg = 0 - Vneg
    Vpos = CINT(100 * Vpos) / 100
    Vneg = CINT(100 * Vneg) / 100
    COLOR 14
    LOCATE 20, 10: PRINT "                "
    LOCATE 20, 10: PRINT "                "
    LOCATE 20, 3: PRINT "Vcell = "; Vcell; " (Volts)"
    COLOR 12
```

```
      LOCATE 22, 10: PRINT "                "
      LOCATE 22, 10: PRINT "                "
      LOCATE 22, 3: PRINT "V(+) = "; Vpos; " (Volts)"
      COLOR 11
      LOCATE 24, 10: PRINT "                "
      LOCATE 24, 10: PRINT "                "
      LOCATE 24, 3: PRINT "V(-) = "; Vneg; " (Volts)"
      COLOR 10
      LOCATE 22, 62: PRINT "Time: "; TIME$
      COLOR 13
      LOCATE 20, 32: PRINT "Elapsed Time:  "; hrs; " hrs  "; mins; " mins  "; secs; " secs  "
    NEXT itmp%
    Vneg = ReadADC(0)
    Vcell = ReadADC(1)
    Vpos = Vcell - Vneg
    Vneg = 0 - Vneg
    Vpos = CINT(100 * Vpos) / 100
    Vneg = CINT(100 * Vneg) / 100
    OPEN dataout$ FOR APPEND AS #1
    PRINT #1, TIME$, "1", Vcell, Vneg, Vpos
    CLOSE #1
    COLOR 14
    LOCATE 20, 10: PRINT "                "
    LOCATE 20, 10: PRINT "                "
    LOCATE 20, 3: PRINT "Vcell = "; Vcell; " (Volts)"
    COLOR 12
    LOCATE 22, 10: PRINT "                "
    LOCATE 22, 10: PRINT "                "
    LOCATE 22, 3: PRINT "V(+) = "; Vpos; " (Volts)"
    COLOR 11
    LOCATE 24, 10: PRINT "                "
    LOCATE 24, 10: PRINT "                "
    LOCATE 24, 3: PRINT "V(-) = "; Vneg; " (Volts)"
    COLOR 14
    y = 200 * (1 - Vcell / 5)
    x = 10 + INT(620 * (tbefore& + telapsed&) / duration&)
    PSET (x, y)
    PSET (x + 1, y)
    PSET (x, y + 1)
    COLOR 11
    y = 200 * (1 - Vneg / 5)
    PSET (x, y)
    PSET (x + 1, y)
    PSET (x, y + 1)
    COLOR 12
    y = 200 * (1 - Vpos / 5)
    PSET (x, y)
    PSET (x + 1, y)
    PSET (x, y + 1)
    COLOR 10
    LOCATE 22, 62: PRINT "Time: "; TIME$
    COLOR 15
LOOP

V1 = Vcell
Vz1 = Vneg
```

```
Vn1 = Vpos


REM DoCharge ends here

LINE (x, 30)-(x, 200)
tbefore& = telapsed&
REM Finished Charging, now go open circuit
REM Set Relay 0 at open circuit, Relay 1 remains at default charging position
dout(0) = 0
dout(1) = 0
CALL SetRelay
telapsed& = 0

COLOR 15
hrs = FIX(OCCTime& / 3600)
mins = FIX((OCCTime& - 3600 * hrs) / 60)
secs = FIX(OCCTime& - 3600 * hrs - 60 * mins)

LOCATE 1, 4: PRINT "Voltage (V)"
LOCATE 14, 71: PRINT "Time(hrs.)"
LOCATE 1, 25: PRINT "Cycle Number:  "; j%; " of "; CCyc%
LOCATE 28, 32: PRINT "Segment Length: "; hrs; " hrs.  "; mins; " mins   "; secs; " secs"
LOCATE 22, 32: PRINT "Interval: "; OCCTincr%; " secs"
LOCATE 24, 32: PRINT "Open Circuit                    "
T0 = TIMER
REM CALL DoOCC
REM Starts here
DO WHILE ((INKEY$ <> "q") AND (telapsed& < OCCTime&))
  FOR itmp% = 1 TO OCCTincr%
    CALL delay(1)
    telapsed& = TIMER - T0
    IF telapsed& < 0 THEN
      telapsed& = telapsed& + 86400
    END IF
    hrs = FIX(telapsed& / 3600)
    mins = FIX((telapsed& - 3600 * hrs) / 60)
    secs = FIX(telapsed& - 3600 * hrs - 60 * mins)
    COLOR 10
    LOCATE 22, 62: PRINT "Time: "; TIME$
    COLOR 13
    LOCATE 20, 32: PRINT "Elapsed Time:  "; hrs; " hrs  "; mins; " mins  "; secs; " secs  "
    Vneg = ReadADC(0)
    Vcell = ReadADC(1)
    Vpos = Vcell - Vneg
    Vneg = 0 - Vneg
    Vpos = CINT(100 * Vpos) / 100
    Vneg = CINT(100 * Vneg) / 100
    COLOR 14
    LOCATE 20, 10: PRINT "                "
    LOCATE 20, 10: PRINT "                "
    LOCATE 20, 3: PRINT "Vcell = "; Vcell; " (Volts)"
    COLOR 12
    LOCATE 22, 10: PRINT "                "
    LOCATE 22, 10: PRINT "                "
    LOCATE 22, 3: PRINT "V(+)  = "; Vpos; " (Volts)"
```

```
      COLOR 11
      LOCATE 24, 10: PRINT "                "
      LOCATE 24, 10: PRINT "                "
      LOCATE 24, 3: PRINT "V(-) = "; Vneg; " (Volts)"
      COLOR 10
      LOCATE 22, 62: PRINT "Time: "; TIME$
      COLOR 13
      LOCATE 20, 32: PRINT "Elapsed Time:  "; hrs; " hrs  "; mins; " mins  "; secs; " secs  "
    NEXT itmp%
    Vneg = ReadADC(0)
    Vcell = ReadADC(1)
    Vpos = Vcell - Vneg
    Vneg = 0 - Vneg
    OPEN dataout$ FOR APPEND AS #1
    PRINT #1, TIME$, "2", Vcell, Vneg, Vpos
    t1 = tbefore& + telapsed&
    CLOSE #1

    Vpos = CINT(100 * Vpos) / 100
    Vneg = CINT(100 * Vneg) / 100
    COLOR 14
    LOCATE 20, 10: PRINT "                "
    LOCATE 20, 10: PRINT "                "
    LOCATE 20, 3: PRINT "Vcell = "; Vcell; " (Volts)"
    COLOR 12
    LOCATE 22, 10: PRINT "                "
    LOCATE 22, 10: PRINT "                "
    LOCATE 22, 3: PRINT "V(+) = "; Vpos; " (Volts)"
    COLOR 11
    LOCATE 24, 10: PRINT "                "
    LOCATE 24, 10: PRINT "                "
    LOCATE 24, 3: PRINT "V(-) = "; Vneg; " (Volts)"
    COLOR 14
    y = 200 * (1 - Vcell / 5)
    x = 10 + INT(620 * (tbefore& + telapsed&) / duration&)
    PSET (x, y)
    PSET (x + 1, y)
    PSET (x, y + 1)
    COLOR 11
    y = 200 * (1 - Vneg / 5)
    PSET (x, y)
    PSET (x + 1, y)
    PSET (x, y + 1)
    COLOR 12
    y = 200 * (1 - Vpos / 5)
    PSET (x, y)
    PSET (x + 1, y)
    PSET (x, y + 1)
    COLOR 10
    LOCATE 22, 62: PRINT "Time: "; TIME$
    COLOR 15
LOOP

V2 = Vcell
Vz2 = Vneg
Vn2 = Vpos
```

```
REM DoOCC ends here

LINE (x, 30)-(x, 200)
tbefore& = tbefore& + telapsed&

REM Finished open cicuit after charging. Next is discharge.
REM Now switch Relay 1 to discharge and then Relay 0 to close circuit
dout(1) = 1
CALL SetRelay
REM do Relay 0 after writing screen stuff
telapsed& = 0

COLOR 15
hrs = FIX(DTime& / 3600)
mins = FIX((DTime& - 3600 * hrs) / 60)
secs = FIX(DTime& - 3600 * hrs - 60 * mins)

LOCATE 1, 4: PRINT "Voltage (V)"
LOCATE 14, 71: PRINT "Time(hrs.)"
LOCATE 1, 25: PRINT "Cycle Number:  "; j%; " of "; CCyc%
LOCATE 28, 32: PRINT "Segment Length: "; hrs; " hrs.  "; mins; " mins   "; secs; " secs"
LOCATE 22, 32: PRINT "Interval: "; DTincr%; " secs"
LOCATE 24, 32: PRINT "Discharging Current "; Dload; " mA"
LOCATE 26, 32: PRINT "    Cutting voltage "; Vcellmin!; " V"
dout(0) = 1
REM Set Relay 0 to close circuit
CALL SetRelay

REM CALL DoDischarge
REM Starts here
T0 = TIMER
DQ = 0
DO WHILE ((INKEY$ <> "q") AND ((telapsed& < DTime&) AND (Vcell > Vcellmin)))
  FOR itmp% = 1 TO DTincr%
    CALL delay(1)
    telapsed& = TIMER - T0
    IF telapsed& < 0 THEN
      telapsed& = telapsed& + 86400
    END IF

    hrs = FIX(telapsed& / 3600)
    mins = FIX((telapsed& - 3600 * hrs) / 60)
    secs = FIX(telapsed& - 3600 * hrs - 60 * mins)
    COLOR 10
    LOCATE 22, 62: PRINT "Time: "; TIME$
    COLOR 13
    LOCATE 20, 32: PRINT "Elapsed Time:  "; hrs; " hrs  "; mins; " mins  "; secs; " secs  "
    Vneg = ReadADC(0)
    Vcell = ReadADC(1)
    Vpos = Vcell - Vneg
    Vneg = 0 - Vneg
    Vpos = CINT(100 * Vpos) / 100
    Vneg = CINT(100 * Vneg) / 100
    COLOR 14
```

```
    LOCATE 20, 10: PRINT "                "
    LOCATE 20, 10: PRINT "                "
    LOCATE 20, 3: PRINT "Vcell = "; Vcell; " (Volts)"
    COLOR 12
    LOCATE 22, 10: PRINT "                "
    LOCATE 22, 10: PRINT "                "
    LOCATE 22, 3: PRINT "V(+)  = "; Vpos; " (Volts)"
    COLOR 11
    LOCATE 24, 10: PRINT "                "
    LOCATE 24, 10: PRINT "                "
    LOCATE 24, 3: PRINT "V(-)  = "; Vneg; " (Volts)"
    COLOR 10
    LOCATE 22, 62: PRINT "Time: "; TIME$
    COLOR 13
    LOCATE 20, 32: PRINT "Elapsed Time:  "; hrs; " hrs  "; mins; " mins  "; secs; " secs  "
  NEXT itmp%
  Vneg = ReadADC(0)
  Vcell = ReadADC(1)
  Vpos = Vcell - Vneg
  Vneg = 0 - Vneg

  OPEN dataout$ FOR APPEND AS #1
  t2 = tbefore& + telapsed&
  DQ1 = (t2 - t1) * Dload / 3600 / 1000
  DQ = DQ + DQ1
  PRINT #1, TIME$, "3", Vcell, Vneg, Vpos
  t1 = tbefore& + telapsed&
  CLOSE #1

  Vpos = CINT(100 * Vpos) / 100
  Vneg = CINT(100 * Vneg) / 100
  COLOR 14

LOCATE 4, 6: PRINT "discharge capacity="; CINT(DQ * 1000) / 1000; "(Ah)"
LOCATE 3, 6: PRINT "      Efficiency="; CINT(DQ * 10000 / CQ) / 100; "%"

  LOCATE 20, 10: PRINT "                "
  LOCATE 20, 10: PRINT "                "
  LOCATE 20, 3: PRINT "Vcell = "; Vcell; " (Volts)"
  COLOR 12
  LOCATE 22, 10: PRINT "                "
  LOCATE 22, 10: PRINT "                "
  LOCATE 22, 3: PRINT "V(+)  = "; Vpos; " (Volts)"
  COLOR 11
  LOCATE 24, 10: PRINT "                "
  LOCATE 24, 10: PRINT "                "
  LOCATE 24, 3: PRINT "V(-)  = "; Vneg; " (Volts)"
  COLOR 14
  y = 200 * (1 - Vcell / 5)
  x = 10 + INT(620 * (tbefore& + telapsed&) / duration&)
  PSET (x, y)
  PSET (x + 1, y)
  PSET (x, y + 1)
  COLOR 11
  y = 200 * (1 - Vneg / 5)
  PSET (x, y)
```

```
    PSET (x + 1, y)
    PSET (x, y + 1)
    COLOR 12
    y = 200 * (1 - Vpos / 5)
    PSET (x, y)
    PSET (x + 1, y)
    PSET (x, y + 1)
    COLOR 10
    LOCATE 22, 62: PRINT "Time: "; TIME$
    COLOR 15
LOOP
LOCATE 4, 6: PRINT "discharge capacity="; CINT(DQ * 1000) / 1000; "(Ah)"
LOCATE 3, 6: PRINT "       Efficiency="; CINT(DQ * 10000 / CQ) / 100; "%"


V3 = Vcell
Vz3 = Vneg
Vn3 = Vpos

REM DoDischarge ends here

LINE (x, 30)-(x, 200)
tbefore& = tbefore& + telapsed&


REM Finished discharge, now do open circuit time to complete cycle
REM Relay 0 needs to go to open cicuit and then Relay 1 to
REM the charging position ready for the next cycle
dout(0) = 0
CALL SetRelay
dout(1) = 0
CALL SetRelay
telapsed& = 0

COLOR 15
hrs = FIX(OCDTime& / 3600)
mins = FIX((OCDTime& - 3600 * hrs) / 60)
secs = FIX(OCDTime& - 3600 * hrs - 60 * mins)

LOCATE 1, 4: PRINT "Voltage (V)"
LOCATE 14, 71: PRINT "Time(hrs.)"
LOCATE 1, 25: PRINT "                                    "
LOCATE 1, 25: PRINT "Cycle Number:  "; j%; " of "; CCyc%
LOCATE 28, 32: PRINT "Segment Length: "; hrs; " hrs.  "; mins; " mins   "; secs; " secs"
LOCATE 22, 32: PRINT "Interval: "; OCDTincr%; " secs"
LOCATE 24, 32: PRINT "Open Circuit after Discharge                "
LOCATE 26, 32: PRINT "                                    "

T0 = TIMER

REM CALL DoOCD
REM Starts here
DO WHILE ((INKEY$ <> "q") AND (telapsed& < OCDTime&))
  FOR itmp% = 1 TO OCDTincr%
    CALL delay(1)
    telapsed& = TIMER - T0
```

```
  IF telapsed& < 0 THEN
    telapsed& = telapsed& + 86400
  END IF
  hrs = FIX(telapsed& / 3600)
  mins = FIX((telapsed& - 3600 * hrs) / 60)
  secs = FIX(telapsed& - 3600 * hrs - 60 * mins)
  COLOR 10
  LOCATE 22, 62: PRINT "Time: "; TIME$
  COLOR 13
  LOCATE 20, 32: PRINT "Elapsed Time:  "; hrs; " hrs  "; mins; " mins  "; secs; " secs  "
  Vneg = ReadADC(0)
  Vcell = ReadADC(1)
  Vpos = Vcell - Vneg
  Vneg = 0 - Vneg
  Vpos = CINT(100 * Vpos) / 100
  Vneg = CINT(100 * Vneg) / 100
  COLOR 14
  LOCATE 20, 10: PRINT "                "
  LOCATE 20, 10: PRINT "                "
  LOCATE 20, 3: PRINT "Vcell = "; Vcell; " (Volts)"
  COLOR 12
  LOCATE 22, 10: PRINT "                "
  LOCATE 22, 10: PRINT "                "
  LOCATE 22, 3: PRINT "V(+)  = "; Vpos; " (Volts)"
  COLOR 11
  LOCATE 24, 10: PRINT "                "
  LOCATE 24, 10: PRINT "                "
  LOCATE 24, 3: PRINT "V(-)  = "; Vneg; " (Volts)"
  COLOR 10
  LOCATE 22, 62: PRINT "Time: "; TIME$
  COLOR 13
  LOCATE 20, 32: PRINT "Elapsed Time:  "; hrs; " hrs  "; mins; " mins  "; secs; " secs  "
NEXT itmp%
Vneg = ReadADC(0)
Vcell = ReadADC(1)
Vpos = Vcell - Vneg
Vneg = 0 - Vneg
OPEN dataout$ FOR APPEND AS #1
PRINT #1, TIME$, "4", Vcell, Vneg, Vpos
CLOSE #1
Vpos = CINT(100 * Vpos) / 100
Vneg = CINT(100 * Vneg) / 100
COLOR 14
LOCATE 20, 10: PRINT "                "
LOCATE 20, 10: PRINT "                "
LOCATE 20, 3: PRINT "Vcell = "; Vcell; " (Volts)"
COLOR 12
LOCATE 22, 10: PRINT "                "
LOCATE 22, 10: PRINT "                "
LOCATE 22, 3: PRINT "V(+)  = "; Vpos; " (Volts)"
COLOR 11
LOCATE 24, 10: PRINT "                "
LOCATE 24, 10: PRINT "                "
LOCATE 24, 3: PRINT "V(-)  = "; Vneg; " (Volts)"
COLOR 14
y = 200 * (1 - Vcell / 5)
```

```
    x = 10 + INT(620 * (tbefore& + telapsed&) / duration&)
    PSET (x, y)
    PSET (x + 1, y)
    PSET (x, y + 1)
    COLOR 11
    y = 200 * (1 - Vneg / 5)
    PSET (x, y)
    PSET (x + 1, y)
    PSET (x, y + 1)
    COLOR 12
    y = 200 * (1 - Vpos / 5)
    PSET (x, y)
    PSET (x + 1, y)
    PSET (x, y + 1)
    COLOR 10
    LOCATE 22, 62: PRINT "Time: "; TIME$
    COLOR 15
LOOP

V4 = Vcell
Vz4 = Vneg
Vn4 = Vpos

 OPEN dataout$ FOR APPEND AS #1
PRINT #1, "End of charge,  End of Discharge,  Discharge capacity,  Efficiency "

PRINT #1, "          "
   PRINT #1, "Charging capacity="; CINT(CQ * 10000) / 10000; " (Ah)   Discharging capacity="; CINT(DQ
* 1000) / 1000; " (Ah)"
   PRINT #1, "Discharge/Charge Efficiency="; CINT(10000 * DQ / CQ) / 100; "%"

PRINT #1, "          "
PRINT #1, " Efficiency, Capacity, End Open Circuit after charge, End Open Circuit atfer discharge"

PRINT #1, CINT(DQ * 10000 / CQ) / 100; "%", CINT(DQ * 10000) / 10000, V1, Vz1, Vn1, V2, Vz2, Vn2,
V3, Vz3, Vn3, V4, Vz4, Vn4

CLOSE #1

REM DOOCD ends here

LINE (x, 30)-(x, 200)
adriveout$ = "a:\" + dataout$

REM End of writing Charge/OC/Discharge/OC Information file
REM Copy to A:
OPEN dataout$ FOR INPUT AS #1
OPEN adriveout$ FOR OUTPUT AS #2
 DO
   LINE INPUT #1, a$
   PRINT #2, a$
 LOOP UNTIL (EOF(1))
CLOSE #1
CLOSE #2
```

```
NEXT j%
LOCATE 29, 1: INPUT tmp
END SUB

FUNCTION BinStr$ (V)
y = INT(256 * V / 5)
y$ = HEX$(y)
i = 1
WHILE (2 ^ i <= y)
    i = i + 1
WEND
i = i - 1
Bin$ = ""
DO
    Z = 2 ^ i
    IF (y - Z) >= 0 THEN
        y = y - Z
        Bin$ = Bin$ + "1"
    ELSE
        Bin$ = Bin$ + "0"
    END IF
    i = i - 1
LOOP UNTIL i = -1
BinStr$ = Bin$
END FUNCTION

SUB BoardOff
OUT Base0, &H0
END SUB

SUB BoardOn
OUT Base0, &H80
END SUB

SUB delay (dt)
T0O = TIMER
DO
 tgoneby# = TIMER - T0O
 IF tgoneby# < 0 THEN
  tgoneby# = tgoneby# + 86400
 END IF
LOOP UNTIL (tgoneby# > dt)
'WHILE (TIMER - T0O < dt)
'WEND
END SUB

SUB DoCharge
PRINT "telapsed& = ", telapsed&
PRINT "tebfore&  = ", tebefore&
PRINT "CTime&    = ", Ctime&
PRINT "CTincr%   = ", CTincr%
INPUT tmp%
DO WHILE ((INKEY$ <> "q") AND ((telapsed& < Ctime&) AND (Vcell < Vcellmax)))
  FOR itmp% = 1 TO CTincr%
```

```
  CALL delay(1)
  telapsed& = TIMER - T0
  IF telapsed& < 0 THEN
    telapsed& = telapsed& + 86400
  END IF
  hrs = FIX(telapsed& / 3600)
  mins = FIX((telapsed& - 3600 * hrs) / 60)
  secs = FIX(telapsed& - 3600 * hrs - 60 * mins)
  COLOR 10
  LOCATE 26, 62: PRINT "Time: "; TIME$
  COLOR 13
  LOCATE 20, 32: PRINT "Elapsed Time:  "; hrs; " hrs  "; mins; " mins  "; secs; " secs  "
  Vneg = ReadADC(0)
  Vcell = ReadADC(1)
  Vpos = Vcell - Vneg
  Vneg = 0 - Vneg
  Vpos = CINT(100 * Vpos) / 100
  Vneg = CINT(100 * Vneg) / 100
  COLOR 14
  LOCATE 20, 10: PRINT "                "
  LOCATE 20, 10: PRINT "                "
  LOCATE 20, 3: PRINT "Vcell = "; Vcell; " (Volts)"
  COLOR 12
  LOCATE 22, 10: PRINT "                "
  LOCATE 22, 10: PRINT "                "
  LOCATE 22, 3: PRINT "V(+)  = "; Vpos; " (Volts)"
  COLOR 11
  LOCATE 24, 10: PRINT "                "
  LOCATE 24, 10: PRINT "                "
  LOCATE 24, 3: PRINT "V(-)  = "; Vneg; " (Volts)"
  COLOR 10
  LOCATE 26, 62: PRINT "Time: "; TIME$
  COLOR 13
  LOCATE 20, 32: PRINT "Elapsed Time:  "; hrs; " hrs  "; mins; " mins  "; secs; " secs  "
NEXT itmp%
Vneg = ReadADC(0)
Vcell = ReadADC(1)
Vpos = Vcell - Vneg
Vneg = 0 - Vneg
Vpos = CINT(100 * Vpos) / 100
Vneg = CINT(100 * Vneg) / 100
COLOR 14
LOCATE 20, 10: PRINT "                "
LOCATE 20, 10: PRINT "                "
LOCATE 20, 3: PRINT "Vcell = "; Vcell; " (Volts)"
COLOR 12
LOCATE 22, 10: PRINT "                "
LOCATE 22, 10: PRINT "                "
LOCATE 22, 3: PRINT "V(+)  = "; Vpos; " (Volts)"
COLOR 11
LOCATE 24, 10: PRINT "                "
LOCATE 24, 10: PRINT "                "
LOCATE 24, 3: PRINT "V(-)  = "; Vneg; " (Volts)"
COLOR 14
y = 200 * (1 - Vcell / 5)
x = 10 + INT(620 * (tbefore& + telapsed&) / duration&)
```

```
    PSET (x, y)
    PSET (x + 1, y)
    PSET (x, y + 1)
    COLOR 11
    y = 200 * (1 - Vneg / 5)
    PSET (x, y)
    PSET (x + 1, y)
    PSET (x, y + 1)
    COLOR 12
    y = 200 * (1 - Vpos / 5)
    PSET (x, y)
    PSET (x + 1, y)
    PSET (x, y + 1)
    COLOR 10
    LOCATE 26, 62: PRINT "Time: "; TIME$
    COLOR 15
LOOP
END SUB

SUB DoDischarge
DO WHILE ((INKEY$ <> "q") AND ((telapsed& < DTime&) AND (Vcell > Vcellmin)))
   FOR itmp% = 1 TO DTincr%
     CALL delay(1)
     telapsed& = TIMER - T0
     IF telapsed& < 0 THEN
       telapsed& = telapsed& + 86400
     END IF
     hrs = FIX(telapsed& / 3600)
     mins = FIX((telapsed& - 3600 * hrs) / 60)
     secs = FIX(telapsed& - 3600 * hrs - 60 * mins)
     COLOR 10
     LOCATE 26, 62: PRINT "Time: "; TIME$
     COLOR 13
     LOCATE 20, 32: PRINT "Elapsed Time:  "; hrs; " hrs  "; mins; " mins  "; secs; " secs  "
     Vneg = ReadADC(0)
     Vcell = ReadADC(1)
     Vpos = Vcell - Vneg
     Vneg = 0 - Vneg
     Vpos = CINT(100 * Vpos) / 100
     Vneg = CINT(100 * Vneg) / 100
     COLOR 14
     LOCATE 20, 10: PRINT "                "
     LOCATE 20, 10: PRINT "                "
     LOCATE 20, 3: PRINT "Vcell = "; Vcell; " (Volts)"
     COLOR 12
     LOCATE 22, 10: PRINT "                "
     LOCATE 22, 10: PRINT "                "
     LOCATE 22, 3: PRINT "V(+)  = "; Vpos; " (Volts)"
     COLOR 11
     LOCATE 24, 10: PRINT "                "
     LOCATE 24, 10: PRINT "                "
     LOCATE 24, 3: PRINT "V(-)  = "; Vneg; " (Volts)"
     COLOR 10
     LOCATE 26, 62: PRINT "Time: "; TIME$
     COLOR 13
     LOCATE 20, 32: PRINT "Elapsed Time:  "; hrs; " hrs  "; mins; " mins  "; secs; " secs  "
```

```
    NEXT itmp%
    Vneg = ReadADC(0)
    Vcell = ReadADC(1)
    Vpos = Vcell - Vneg
    Vneg = 0 - Vneg
    Vpos = CINT(100 * Vpos) / 100
    Vneg = CINT(100 * Vneg) / 100
    COLOR 14
    LOCATE 20, 10: PRINT "                "
    LOCATE 20, 10: PRINT "                "
    LOCATE 20, 3: PRINT "Vcell = "; Vcell; " (Volts)"
    COLOR 12
    LOCATE 22, 10: PRINT "                "
    LOCATE 22, 10: PRINT "                "
    LOCATE 22, 3: PRINT "V(+)  = "; Vpos; " (Volts)"
    COLOR 11
    LOCATE 24, 10: PRINT "                "
    LOCATE 24, 10: PRINT "                "
    LOCATE 24, 3: PRINT "V(-)  = "; Vneg; " (Volts)"
    COLOR 14
    y = 200 * (1 - Vcell / 5)
    x = 10 + INT(620 * (tbefore& + telapsed&) / duration&)
    PSET (x, y)
    PSET (x + 1, y)
    PSET (x, y + 1)
    COLOR 11
    y = 200 * (1 - Vneg / 5)
    PSET (x, y)
    PSET (x + 1, y)
    PSET (x, y + 1)
    COLOR 12
    y = 200 * (1 - Vpos / 5)
    PSET (x, y)
    PSET (x + 1, y)
    PSET (x, y + 1)
    COLOR 10
    LOCATE 26, 62: PRINT "Time: "; TIME$
    COLOR 15
LOOP
END SUB

SUB DoOCC
DO WHILE ((INKEY$ <> "q") AND (telapsed& < OCCTime&))
   FOR itmp% = 1 TO OCCTincr%
     CALL delay(1)
     telapsed& = TIMER - T0
     IF telapsed& < 0 THEN
       telapsed& = telapsed& + 86400
     END IF
     hrs = FIX(telapsed& / 3600)
     mins = FIX((telapsed& - 3600 * hrs) / 60)
     secs = FIX(telapsed& - 3600 * hrs - 60 * mins)
     COLOR 10
     LOCATE 26, 62: PRINT "Time: "; TIME$
     COLOR 13
     LOCATE 20, 32: PRINT "Elapsed Time:  "; hrs; " hrs  "; mins; " mins  "; secs; " secs  "
```

```
  Vneg = ReadADC(0)
  Vcell = ReadADC(1)
  Vpos = Vcell - Vneg
  Vneg = 0 - Vneg
  Vpos = CINT(100 * Vpos) / 100
  Vneg = CINT(100 * Vneg) / 100
  COLOR 14
  LOCATE 20, 10: PRINT "                "
  LOCATE 20, 10: PRINT "                "
  LOCATE 20, 3: PRINT "Vcell = "; Vcell; " (Volts)"
  COLOR 12
  LOCATE 22, 10: PRINT "                "
  LOCATE 22, 10: PRINT "                "
  LOCATE 22, 3: PRINT "V(+) = "; Vpos; " (Volts)"
  COLOR 11
  LOCATE 24, 10: PRINT "                "
  LOCATE 24, 10: PRINT "                "
  LOCATE 24, 3: PRINT "V(-) = "; Vneg; " (Volts)"
  COLOR 10
  LOCATE 26, 62: PRINT "Time: "; TIME$
  COLOR 13
  LOCATE 20, 32: PRINT "Elapsed Time:  "; hrs; " hrs  "; mins; " mins  "; secs; " secs  "
NEXT itmp%
Vneg = ReadADC(0)
Vcell = ReadADC(1)
Vpos = Vcell - Vneg
Vneg = 0 - Vneg
Vpos = CINT(100 * Vpos) / 100
Vneg = CINT(100 * Vneg) / 100
COLOR 14
LOCATE 20, 10: PRINT "                "
LOCATE 20, 10: PRINT "                "
LOCATE 20, 3: PRINT "Vcell = "; Vcell; " (Volts)"
COLOR 12
LOCATE 22, 10: PRINT "                "
LOCATE 22, 10: PRINT "                "
LOCATE 22, 3: PRINT "V(+) = "; Vpos; " (Volts)"
COLOR 11
LOCATE 24, 10: PRINT "                "
LOCATE 24, 10: PRINT "                "
LOCATE 24, 3: PRINT "V(-) = "; Vneg; " (Volts)"
COLOR 14
y = 200 * (1 - Vcell / 5)
x = 10 + INT(620 * (tbefore& + telapsed&) / duration&)
PSET (x, y)
PSET (x + 1, y)
PSET (x, y + 1)
COLOR 11
y = 200 * (1 - Vneg / 5)
PSET (x, y)
PSET (x + 1, y)
PSET (x, y + 1)
COLOR 12
y = 200 * (1 - Vpos / 5)
PSET (x, y)
PSET (x + 1, y)
```

```
    PSET (x, y + 1)
    COLOR 10
    LOCATE 26, 62: PRINT "Time: "; TIME$
    COLOR 15
  LOOP
  END SUB

  SUB DoOCD
  DO WHILE ((INKEY$ <> "q") AND (telapsed& < OCDTime&))
    FOR itmp% = 1 TO OCCTincr%
      CALL delay(1)
      telapsed& = TIMER - T0
      IF telapsed& < 0 THEN
        telapsed& = telapsed& + 86400
      END IF
      hrs = FIX(telapsed& / 3600)
      mins = FIX((telapsed& - 3600 * hrs) / 60)
      secs = FIX(telapsed& - 3600 * hrs - 60 * mins)
      COLOR 10
      LOCATE 26, 62: PRINT "Time: "; TIME$
      COLOR 13
      LOCATE 20, 32: PRINT "Elapsed Time:  "; hrs; " hrs  "; mins; " mins  "; secs; " secs  "
      Vneg = ReadADC(0)
      Vcell = ReadADC(1)
      Vpos = Vcell - Vneg
      Vneg = 0 - Vneg
      Vpos = CINT(100 * Vpos) / 100
      Vneg = CINT(100 * Vneg) / 100
      COLOR 14
      LOCATE 20, 10: PRINT "                "
      LOCATE 20, 10: PRINT "                "
      LOCATE 20, 3: PRINT "Vcell = "; Vcell; " (Volts)"
      COLOR 12
      LOCATE 22, 10: PRINT "                "
      LOCATE 22, 10: PRINT "                "
      LOCATE 22, 3: PRINT "V(+)  = "; Vpos; " (Volts)"
      COLOR 11
      LOCATE 24, 10: PRINT "                "
      LOCATE 24, 10: PRINT "                "
      LOCATE 24, 3: PRINT "V(-)  = "; Vneg; " (Volts)"
      COLOR 10
      LOCATE 26, 62: PRINT "Time: "; TIME$
      COLOR 13
      LOCATE 20, 32: PRINT "Elapsed Time:  "; hrs; " hrs  "; mins; " mins  "; secs; " secs  "
    NEXT itmp%
    Vneg = ReadADC(0)
    Vcell = ReadADC(1)
    Vpos = Vcell - Vneg
    Vneg = 0 - Vneg
    Vpos = CINT(100 * Vpos) / 100
    Vneg = CINT(100 * Vneg) / 100
    COLOR 14
    LOCATE 20, 10: PRINT "                "
    LOCATE 20, 10: PRINT "                "
    LOCATE 20, 3: PRINT "Vcell = "; Vcell; " (Volts)"
    COLOR 12
```

```
    LOCATE 22, 10: PRINT "                "
    LOCATE 22, 10: PRINT "                "
    LOCATE 22, 3: PRINT "V(+) = "; Vpos; " (Volts)"
    COLOR 11
    LOCATE 24, 10: PRINT "                "
    LOCATE 24, 10: PRINT "                "
    LOCATE 24, 3: PRINT "V(-) = "; Vneg; " (Volts)"
    COLOR 14
    y = 200 * (1 - Vcell / 5)
    x = 10 + INT(620 * (tbefore& + telapsed&) / duration&)
    PSET (x, y)
    PSET (x + 1, y)
    PSET (x, y + 1)
    COLOR 11
    y = 200 * (1 - Vneg / 5)
    PSET (x, y)
    PSET (x + 1, y)
    PSET (x, y + 1)
    COLOR 12
    y = 200 * (1 - Vpos / 5)
    PSET (x, y)
    PSET (x + 1, y)
    PSET (x, y + 1)
    COLOR 10
    LOCATE 26, 62: PRINT "Time: "; TIME$
    COLOR 15
LOOP
END SUB

SUB Dostring
    CLS
    INPUT "Filename = ", fstring$
    PRINT fstring$
    fstring$ = fstring$ + ".GEN"
    PRINT fstring$
    MID$(fstring$, 8) = ".gen"
    PRINT fstring$
    INPUT crp%

END SUB

FUNCTION ReadADC (Channel%)
OUT Base0, &HA0
OUT Base0 + 2, 11
IF (Channel% >= 0) AND (Channel% <= 11) THEN
      V = 0
      Cycle = 0
CYCLESTART:
      Cycle = Cycle + 1
      OUT Base0, &H80
      V = V OR (INP(Base0 + 1) AND &H10) * &H8
      FOR clk = 1 TO 4
            ADDRESS = &H80 + &H40 * (Channel% AND (2 ^ (4 - clk))) / (2 ^ (4 - clk))
            V = V OR (INP(Base0 + 1) AND &H10) * (2 ^ (8 - clk)) / &H10
            OUT Base0, ADDRESS
            OUT Base0 + 2, 11
```

```
            OUT Base0, ADDRESS OR &H2
            OUT Base0 + 2, 11
            OUT Base0, ADDRESS AND &HFD
            OUT Base0 + 2, 11
        NEXT clk
        OUT Base0 + 2, 11
        FOR clk = 5 TO 8
            V = V OR (INP(Base0 + 1) AND &H10) * (2 ^ (8 - clk)) / &H10
            OUT Base0, &H82
            OUT Base0 + 2, 11
            OUT Base0, &H80
            OUT Base0 + 2, 11
        NEXT clk
        OUT Base0, &HA0
        OUT Base0 + 2, 11
        DO WHILE Test = 0
            Test = INP(Base0 + 1) AND &H40
            OUT Base0 + 2, 11
        LOOP
        IF (Cycle = 1) THEN
            V = 0
            GOTO CYCLESTART
        ELSEIF (Cycle = 2) THEN
            IF (Channel% < 10) THEN
                ReadADC = CINT(V * 100 * 5 / 256) / 100
            ELSEIF (Channel% = 10) THEN
                ReadADC = V / 10
            ELSEIF (Channel% = 11) THEN
                ReadADC = V
            END IF
        END IF
    END IF
    END FUNCTION

    SUB SetDAC (DAC%, V)

    IF ((DAC% = 0) OR (DAC% = 1)) AND ((V >= 0) AND (V <= 5)) THEN
        IF (V > 4.98) THEN V = 4.98
        V = CINT(V * 256 / 5)
        N = 0
        IF (DAC% = 1) THEN N = 1
        D0 = -V * (N = 0)
        D1 = -V * (N = 1)
        FOR Bit = 1 TO 24
            SELECT CASE Bit
                CASE 1 TO 8
                    OUT Base0, &H82
                    OUT Base0, &H80
                CASE 9 TO 24
                    IF (Bit <= 16) THEN
                        B = 16 - Bit
                        byte = ((D1 AND 2 ^ B) / 2 ^ B) OR &H80
                    ELSE
                        B = 24 - Bit
                        byte = ((D0 AND 2 ^ B) / 2 ^ B) OR &H80
                    END IF
```

```
                OUT Base0, byte
                OUT Base0, byte OR 2
                OUT Base0, byte
        END SELECT
    NEXT Bit
    IF (N = 0) THEN
        OUT Base0, &H84
    ELSEIF (N = 1) THEN
        OUT Base0, &H88
    END IF
    OUT Base0, &H80
    OUT Base0 + 2, 11
END IF
END SUB

SUB SetRelay
OUT Base0 + 2, 11
dout = 0
FOR NN = 0 TO 7
    IF (dout(NN) = 0) THEN
        dout = dout AND NOT 2 ^ NN
    ELSE
        dout = dout OR 2 ^ NN
    END IF

NEXT NN

FOR Bit = 1 TO 8
    B = 8 - Bit
    byte = ((dout AND 2 ^ B) / 2 ^ B) OR &H80
    OUT Base0, byte
    OUT Base0, byte OR 2
    OUT Base0, byte
NEXT Bit
FOR Bit = 9 TO 24
    OUT Base0, &H82
    OUT Base0, &H80
NEXT Bit
OUT Base0, &H90
OUT Base0, &H80
OUT Base0 + 2, &H8
END SUB

SUB SetTTL (N%, dout() AS INTEGER)
OUT Base0 + 2, 11
N% = FIX(N%)
dout(N%) = ABS(NOT (-dout(N%)))
dout = 0
FOR NN = 0 TO 7
    IF (dout(NN) = 0) THEN
        dout = dout AND NOT 2 ^ NN
    ELSE
        dout = dout OR 2 ^ NN
    END IF

NEXT NN
```

```
FOR Bit = 1 TO 8
      B = 8 - Bit
      byte = ((dout AND 2 ^ B) / 2 ^ B) OR &H80
      OUT Base0, byte
      OUT Base0, byte OR 2
      OUT Base0, byte
NEXT Bit

FOR Bit = 9 TO 24
      OUT Base0, &H82
      OUT Base0, &H80
NEXT Bit
OUT Base0, &H90
OUT Base0, &H80
OUT Base0 + 2, &H8
END SUB

SUB SetTTLDAC (Vapp AS SINGLE)
Vout(0) = 0
Vout(1) = Vapp
OUT Base0 + 2, 11
dout = 0
FOR NN = 0 TO 7
      IF (dout(NN) = 0) THEN
            dout = dout AND NOT 2 ^ NN
      ELSE
            dout = dout OR 2 ^ NN
      END IF

NEXT NN

FOR Bit = 1 TO 8
      B = 8 - Bit
      byte = ((dout AND 2 ^ B) / 2 ^ B) OR &H80
      OUT Base0, byte
      OUT Base0, byte OR 2
      OUT Base0, byte
NEXT Bit
REM Now do the setting of potentials
      FOR i% = 0 TO 1
       IF Vout(i%) < 0 THEN Vout(i%) = 0
       IF Vout(i%) > 5 THEN Vout(i%) = 5
      NEXT i%
      V0 = CINT(Vout(0) * 256 / 5)
      V1 = CINT(Vout(1) * 256 / 5)
      N = 0
      D0 = -V0 * (N = 0)
      N = 1
      D1 = -V1 * (N = 1)
      FOR Bit = 9 TO 24
       IF (Bit <= 16) THEN
         B = 16 - Bit
         byte = ((D1 AND 2 ^ B) / 2 ^ B) OR &H80
       ELSE
         B = 24 - Bit
```

```
        byte = ((D0 AND 2 ^ B) / 2 ^ B) OR &H80
      END IF
      OUT Base0, byte
      OUT Base0, byte OR 2
      OUT Base0, byte
    NEXT Bit
    IF (N = 0) THEN
        OUT Base0, &H84
    ELSEIF (N = 1) THEN
        OUT Base0, &H88
    END IF
    OUT Base0, &H90
    OUT Base0, &H80
    OUT Base0 + 2, 11

END SUB

SUB temp
Genout$ = fileout$ + ".GEN"
OPEN fileout$ FOR OUTPUT AS #1
PRINT #1, Special$
PRINT #1, "Date: "; DATE$
PRINT #1, ""
PRINT #1, "Battery Cycle Monitoring"
PRINT #1, "Pseudo Constant Current Charge - Constant Load Discharge"
PRINT #1, "General Parameters"
PRINT #1, "Number of battery cycles          : ", CCyc%
PRINT #1, "Brief Description of Battery: "
PRINT #1, Special$
PRINT #1, ""
PRINT #1, "Charging Conditions"
PRINT #1, "Charging Current (mA) = ", ICharge!
PRINT #1, "Maximum Charge Duration"
PRINT #1, chargehours%, " hours"
PRINT #1, chargemins%, " minutes"
PRINT #1, chargesecs%, " seconds"
PRINT #1, "Number of seconds between each sample = ", CTincr%
PRINT #1, "Termination Ecell Potential = ", Vcellmax!
PRINT #1, ""
PRINT #1, "Post Charging Open Circuit Conditions"
PRINT #1, "Open Circuit Duration"
PRINT #1, OCchargehours%, " hours"
PRINT #1, OCchargemins%, " minutes"
PRINT #1, OCchargesecs%, " seconds"
PRINT #1, "Number of seconds between each sample = ", OCCTincr%
PRINT #1, ""
PRINT #1, "Discharge Conditions"
PRINT #1, "Discharge Load (ê) = ", Dload!
PRINT #1, "Maximum Discharge Duration"
PRINT #1, dischargehours%, " hours"
PRINT #1, dischargemins%, " minutes"
PRINT #1, dischargesecs%, " seconds"
PRINT #1, "Number of seconds between each sample = ", DTincr%
PRINT #1, "Termination Ecell Potential = ", Vcellmin!
PRINT #1, ""
PRINT #1, "Post Discharge Open Circuit Conditions"
```

```
PRINT #1, "Open Circuit Duration"
PRINT #1, OCdischargehours%, " hours"
PRINT #1, OCdischargemins%, " minutes"
PRINT #1, OCdischargesecs%, " seconds"
PRINT #1, "Number of seconds between each sample = ", OCDTincr%
CLOSE #1
END SUB
```